MAREES TERRESTRES

BULLETIN D'INFORMATIONS

1 2 2

15 MAI 1995

Association Internationale de Géodésie

Commission Permanente des Marées Terrestres

Editeur Prof. Paul MELCHIOR
Observatoire Royal de Belgique
Avenue Circulaire 3
1180 Bruxelles

BIM 122

15 mai 1995

Special Issue II

Meeting of the Working Groups on

THEORETICAL TIDAL MODEL, CALIBRATION, and HIGH PRECISION TIDAL DATA PROCESSING

Bonn, August 30 - September 2, 1994

Table des matières

IUGG General Assembly at Boulder

Working Meeting of the Earth Tide Commission
within Symposium G12: Geodynamics

Thursday July 13th 1995, 15:30 - 17:00
Lead-convenor: Jean Dickey
Chairman: Hans-Georg Wenzel

Preliminary agenda (March 19th 1995):

Roosbeek: New tide generating potential at the ngal level

Hartmann: Catalogue HW10391 of the earth tide generating potential

Mathews: Considerations on theoretical modeling of tidal phenomena

Dehant: Working Group on Theoretical Tidal Model

Jentzsch: Working Group on High Precision Tidal Data Processing

N.N.: Election of Vicepresident and Secretary of the Earth Tide Commission

Please circulate the contents of this box to anybody who may be interested!
Please notify to me if you intend to come to the meeting!

H.-G. Wenzel, March 19th 1995
Geodaetisches Institut, Universitaet Karlsruhe

Processing of the data from two superconducting gravimeters, recorded in 1990 - 1991 at Richmond (Miami, Florida). Some problems and results.

Martina Harnisch, Günter Harnisch
Institut für Angewandte Geodäsie, Außenstelle Potsdam
Michendorfer Chaussee 23, PF 600808, D-14408 Potsdam

Summary

Two superconducting gravimeters, the **SGB** and the **TT40**, were run side by side from 1989 to 1991 at Miami (Florida). The data processing was aimed at the investigation of long term phenomena (e.g. the influence of polar motions). Disturbed sections (earthquakes, spikes) and steps are eliminated directly from the raw data. Sections with exponential drift are corrected by fitting one or two exponential functions to the hourly values and subtracting them. Great care has to be taken at this station on the strong influences of hydrological phenomena. The residual gravity signal (after subtraction of tides and meteorological influences) strongly depends on the extent to which steps are eliminated.

1. Introduction

At the end of 1989, two superconducting gravimeters, the **SGB** of the University of California, San Diego (**UCSD**) and the **TT40** of the Institute for Applied Geodesy, Frankfurt a.M., Germany (**IfAG**) were installed at the US Naval Observatory in Richmond (Miami) in the southwestern Florida peninsula. Both gravimeters were under operation till the second half of 1991. The data of both gravimeters was recorded with the data acquisition systems both of **UCSD** and **IfAG**. Serious evaluation of the gravity data could not start before april 1990 when the first groundwater data became available. Unfortunately the data sets are broken by large gaps (**SGB** between 21st July and 7th August, 1990; **TT40** between 21st December, 1990 and 25th January, 1991) into two independent subsets which cannot be joined reliably.

The terrain around the observatory is extremely flat (maximum elevations only a few meters). The underground consists of extended karstic limestones with high porosity (up to about 40%). To the West of the station are the Everglades, the giant outflow area of the Lake Okeechobee. The minimum distance to the Atlantic Ocean to the East is about 10 km.

Based on the **IfAG** recordings of the **SGB** and of the **TT40** the main features of the data processing of both gravimeters are described in the following. Finally the activities are directed at the investigation of long term phenomena (e.g. the influence of polar motions). Therefore the "Restkurve" was constructed, i.e. the known earth tides as well as environmental influences (air pressure, groundwater) were subtracted from the gravity signal. Keeping in mind the cumulative behaviour of steps, greatest care has to be taken in their complete detection and correct elimination. It must be ensured that the final result is falsified neither by unidentified steps nor by spurious ones erroneously corrected.

2. Processing of the raw data

The term "raw data" denotes the untreated output data coming from the data acquisition system. It is influenced by the transfer function of the analogue output filters with time constants of approx. 30 s (**TT40**) and 4 min (**SGB**), measured in voltage units and sampled at intervals of about 10 s (**TT40**) and 1 min (**SGB**). Because in the case of the **IfAG** equipment this data is not exactly equidistant, the corresponding times must also be recorded and taken into account in all further steps of the raw data processing. In this way, gaps do not disturb the data processing if they are not too large.

In the past at the **IfAG** at first the raw data were decimated to equidistant hourly values by fitting a parabola of fifth (**TT40**) or fourth (**SGB**) order over intervals of three hours overlapping by one hour. Only the greatest disturbances were eliminated together with the data decimation. An example of this

kind of processing is the excellent data set published by *B. Richter* [1] for the first observation period at Bad Homburg (1981-1984), clearly showing the influence of polar motions.

A great disadvantage of the early change to hourly values is that the transfer function of the decimation process changes the shape of the disturbances considerably. This makes the exact detection of steps and the exact determination of their heights at least more difficult, if not impossible. Therefore, the preprocessing is now done directly on the raw data. The software for this purpose must be developed in the **IfAG**, equiped with HP workstations and X-terminals based on the UNIX operation system. PHIGS was used for terminal graphics to enable interactive data processing.

To correct disturbed sections of the data, the original values are replaced by interpolated ones. The parameters of the interpolation polynomials are estimated by fitting the observed values on both sides of the disturbances. As a rule of thumb, the width of the marginal sections should be in the same order as the disturbed section itself. In the same manner, steps are corrected by fitting polynomials to the marginal values in the region of interest, taking into account the step height as an additional unknown. The time of the step is determined visually on the terminal screen.

Keeping in mind that during one month about 260000 gravity values are sampled at a rate of 10 s, it was attempted to minimize the size of the files and to restrict them to gravity data and the corresponding synthetic tides. Also to minimize the number of constants included in the data processing (e.g. scale factors, regression coefficients), an approximated tide free gravity signal was derived by local fitting of the observed gravity values to the synthetic tides. This approximated "Restkurve" is represented in a fixed scale on the terminal screen. It is used only as a help for the inspection of the data and the tracing of disturbed sections and steps. The corrections themselves (replacing of disturbed sections by interpolated values, destepping) are computed directly from the measured gravity data. In so doing, polynomials up to the fifth degree must be used to avoid interpolation errors. This procedure may be applied to disturbed sections of up to one or two hours. The more extended the disturbances the higher must be the degree of the polynomials. The decision on the appropriate degree is facilitated by the interactive technique because the success of the corrections may be monitored on the screen. Disturbances extending over more than one or two hours must be corrected in the hourly data.

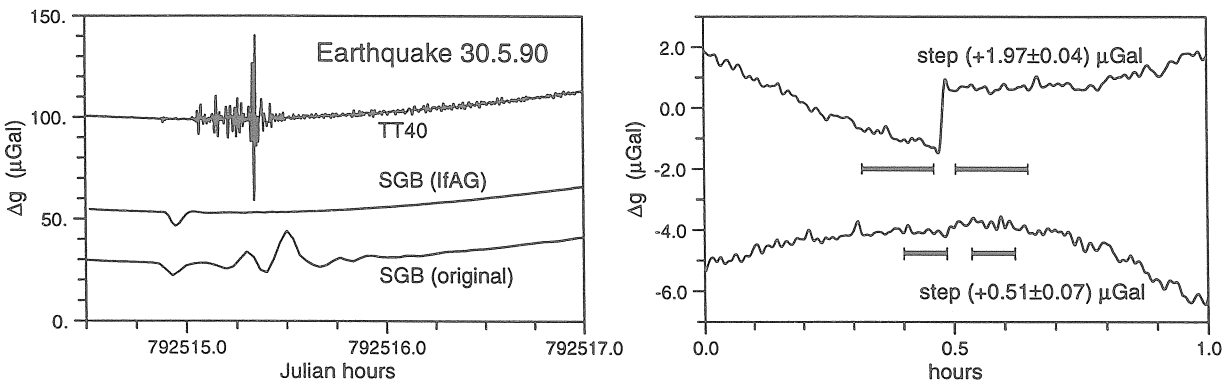

Fig. 1: Disturbed sections and steps recorded by the gravimeters **SGB** (original), **SGB (IfAG)** and **TT40**. *Left side*: Reflection of one and the same earthquake by the three data sets. Due to the different transfer functions the shape of the curves is very different. *Right side*: Clear step of about 2 μGal at Julian hour 792638 (4.6.1990) and week step of about 0.5 μGal at Julian hour 793003 (19.6.1990) in the data of **TT40**. The horizontal bars indicate the marginal sections around the step used to derive the step height together with the parameters of the best fitting polynomial.

As an example of disturbances, fig. 1 shows the reflection of one and the same earthquake in the data of the **SGB** and of the **TT40** on its left side. Clearly the influence of the different transfer functions is expressed and it becomes evident that systematic errors may occur, if the disturbances are not

eliminated carefully. On the right side, there are two examples of steps, the one of about 2 µGal and the other of about 0.5 µGal; both are significant from the statistical point of view. The chance to detect small steps is limited by the noise, but there is also the risk of interpreting random variations falsely as steps. In the Miami data of the **TT40**, steps smaller then about 0.3 µGal are not detectable. Difficulties may arise if a disturbed section in the data set ("gap") is connected with a step. Though the developed software may also solve this problem directly, in individual practical cases only an iterative treatment can achieve plausible corrections.

Altogether the great number of 448 steps was detected in the **TT40** data set, the greatest part of them less than 1 µGal. This corresponds to observations of other authors, e.g. [3].

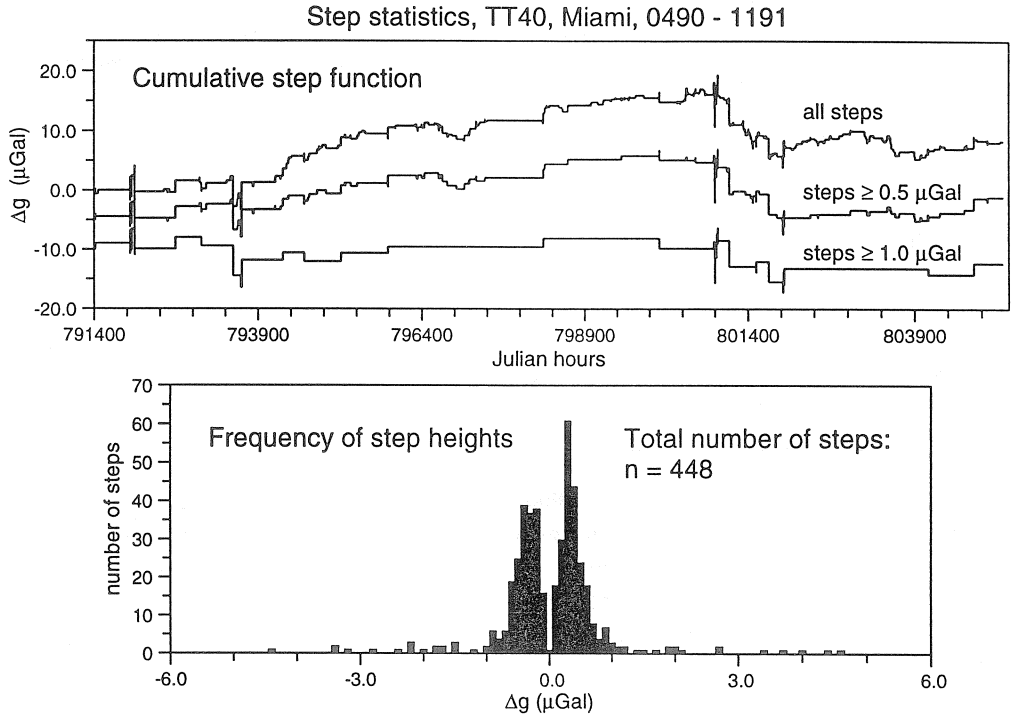

Fig. 2: Cumulative step function (at the top) and frequency of step heights (at the bottom) of all the 448 steps detected in the data of the **TT40**. In addition cumulative step functions are given for subsets containing only the steps > 0.5 µGal (140 values) and > 1.0 µGal (41 values).

To estimate the influence of step corrections on the residual gravity signal cumulative step functions and the corresponding distributions of the step heights were calculated (fig. 2). Due to the fact that the detection of small steps is limited by the noise level, the frequency distribution is bimodal. The higher the threshold determined by the noise level, the wider the gap between both maxima. Changing the threshold numerically, not only the general (linear) trend but also the bulge (nonlinear trend) and single details of the cumulative step function are influenced. In this way, incorrect step corrections may simulate false instrumental drift as well as the existence or false magnitudes of long term gravity variations.

3. Processing of the hourly data

The hourly values were deduced from the raw data by fitting a polynomial of fourth or fifth degree in a similar manner as has been done in the **IfAG** up to now. Because the raw data are not exactly equidistant, filtering techniques can not be applied. If the raw data are processed successfully, the hourly data have to be corrected only for some larger gaps and for exponential drift (if required).

Preprocessing of hourly values is applied on the residual gravity signal after elimination of tides and environmental influences ("Restkurve"). ETERNA-30 [4] is used for multichannel analyses to get the tidal parameters and regression coefficients needed for this purpose. The elimination of disturbed sections of the data set ("correction of gaps") is done in the same way as in the case of raw data.

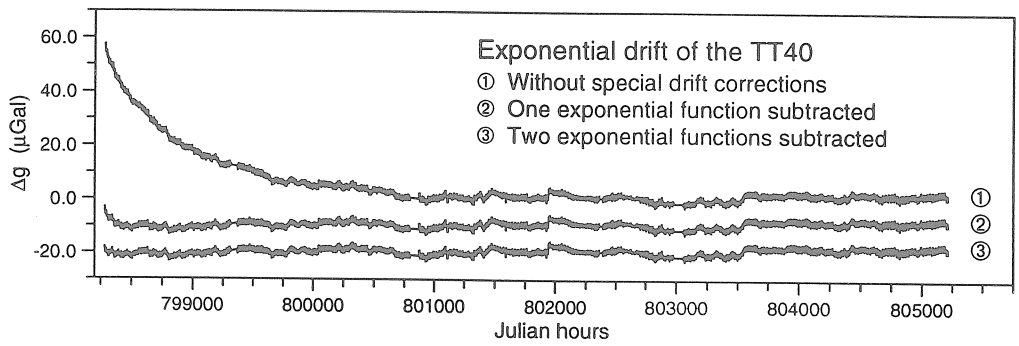

Fig. 3: Exponential drift behaviour of the **TT40** after re-initialization (upper curve). The effect may be eliminated by fitting and subtracting two exponential functions overlaying a linear drift. - For better presentation a linear trend of -0.012 μGal/hour was subtracted from the three curves.

Exponential drift occurs if the gravimeter must be re-initialized after serious technical disturbances. If this part of the drift is not eliminated, the influenced section of the data would have to be rejected. To correct exponential drift an exponential function is fitted together with a linear trend:

$$\Delta g = a + b \cdot x + c \cdot \exp(-d \cdot x)$$

The parameters *a*, *b*, *c*, *d* are calculated iteratively. Starting values are estimated from sections at the beginning and at the end of the data set. As an example, fig. 3 and tab. 1 show the exponential drift of the **TT40** after the large gap at the end of 1990 (35 days). The decay time is about 30 days (I). Fitting a second exponential function, a decay time of approx. 3 days results and the approximation improves (II). A similar behaviour was found by *Goodkind* [2] who used the first section of the **TT40** data (November 1989 to July 1990).

Tab. 1: Exponential behaviour of the gravimeters **TT40** and **SGB (IfAG)**

	TT40	**SGB (IfAG)**	
	January-February 1991	April 1990	August 1990
amplitude *c* (μGal)	I 50.64983 II 4.88023	-17.96640	-4.85913
decay constant *d* (hours^{-1})	I 0.001394 II 0.013512	0.002820	0.007853

4. Influences of air pressure and groundwater

Caused by heavy rainfalls and the high porosity of the underground, variations of soil moisture and groundwater have a strong influence on the tidal gravity measurements at Miami. Therefore, four groundwater gauges were installed in the neighbourhood of the station (distances between 10 and 100 m). The water level varied between about -3.0 and -4.0 m during the whole observation period (fig. 5, at the bottom). The differences between the four gauges are very small (in the order of 1 cm). The gravity signal must follow the groundwater variations immediately, but really it seems to react faster (fig. 4). This effect is due to the influence of the soil moisture, increasing suddenly after rainfall and

seeping downward until it reaches and influences the groundwater after several hours. The influence of the groundwater was eliminated in the usual way by empirical linear regression using the coefficients from the multichannel tidal analysis. The influence of soil moisture was not taken into account. However, at least to some extent it is included in the regression coefficient of the groundwater.

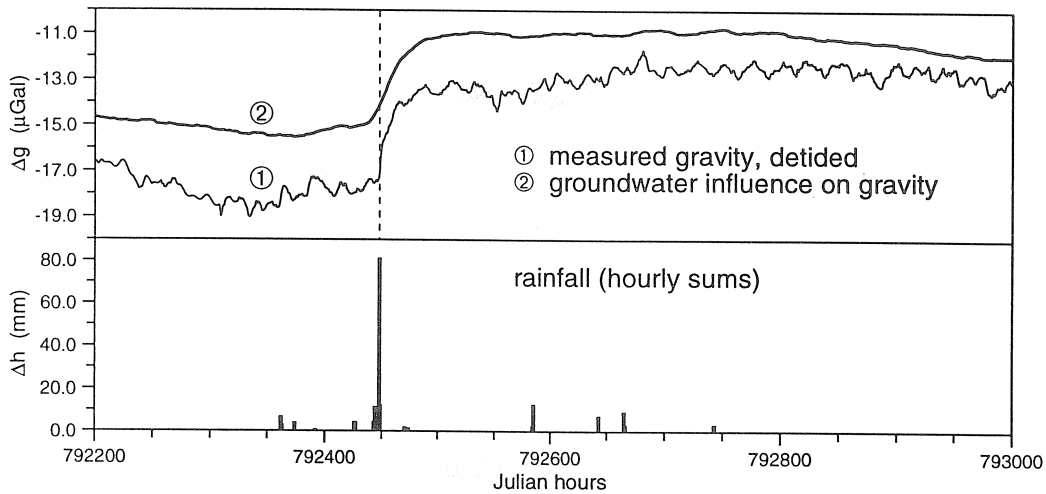

Fig. 4: Gravity effect of the observed variations of the groundwater level, cumulative hourly rainfall and the measured gravity variations.

In a corresponding manner, the air pressure influence was corrected. Also there the greatest part may be represented by linear regression between the gravity signal and the local air pressure at the earth's surface.

In tab. 2 the regression coefficients for the influences of air pressure and groundwater are shown, derived from separate multichannel analyses for each subset of the data. While the values of the air pressure influence are in good agreement, the groundwater values show greater discrepancies between both gravimeters as well as between the observation periods. Obviously the result of the regression analysis is influenced by the long term trend of the groundwater signal (fig. 5, at the bottom).

Tab. 2: Regression coefficients of air pressure and groundwater, derived from the data of **TT40** and **SGB (IfAG)** by multichannel analysis using ETERNA-30

	TT40		SGB (IfAG)	
	April - December 1990	January - November 1991	April - July 1990	August 1990 - June 1991
air pressure (μGal/hPa)	- 0.3414 ± 0.0083	- 0.3416 ± 0.0424	- 0.3162 ± 0.0058	- 0.3073 ± 0.0034
groundwater [1] (μGal/cm)	- 0.0998 ± 0.0026	- 0.1422 ± 0.0082	- 0.1061 ± 0.0019	- 0.0721 ± 0.0013

[1] Because in the original data the depth of the groundwater is counted positive in downward direction the regression coefficients of the groundwater are negative.

5. Discussion of some results

The main result of the data processing reported here should be the residual curves represented in fig. 5. It was expected, that these curves would reflect the gravity effect of the polar motions. The **SGB (IfAG)** data shows the best correlation concerning the amplitude as well as the phase. The

corresponding TT40 curve (lowest of the curves), however, including corrections for all the 448 detected steps, shows little or no similarities, even if it is taken into consideration that the two parts of each curve may be shifted in the vertical direction by arbitrary amounts relative to each other.

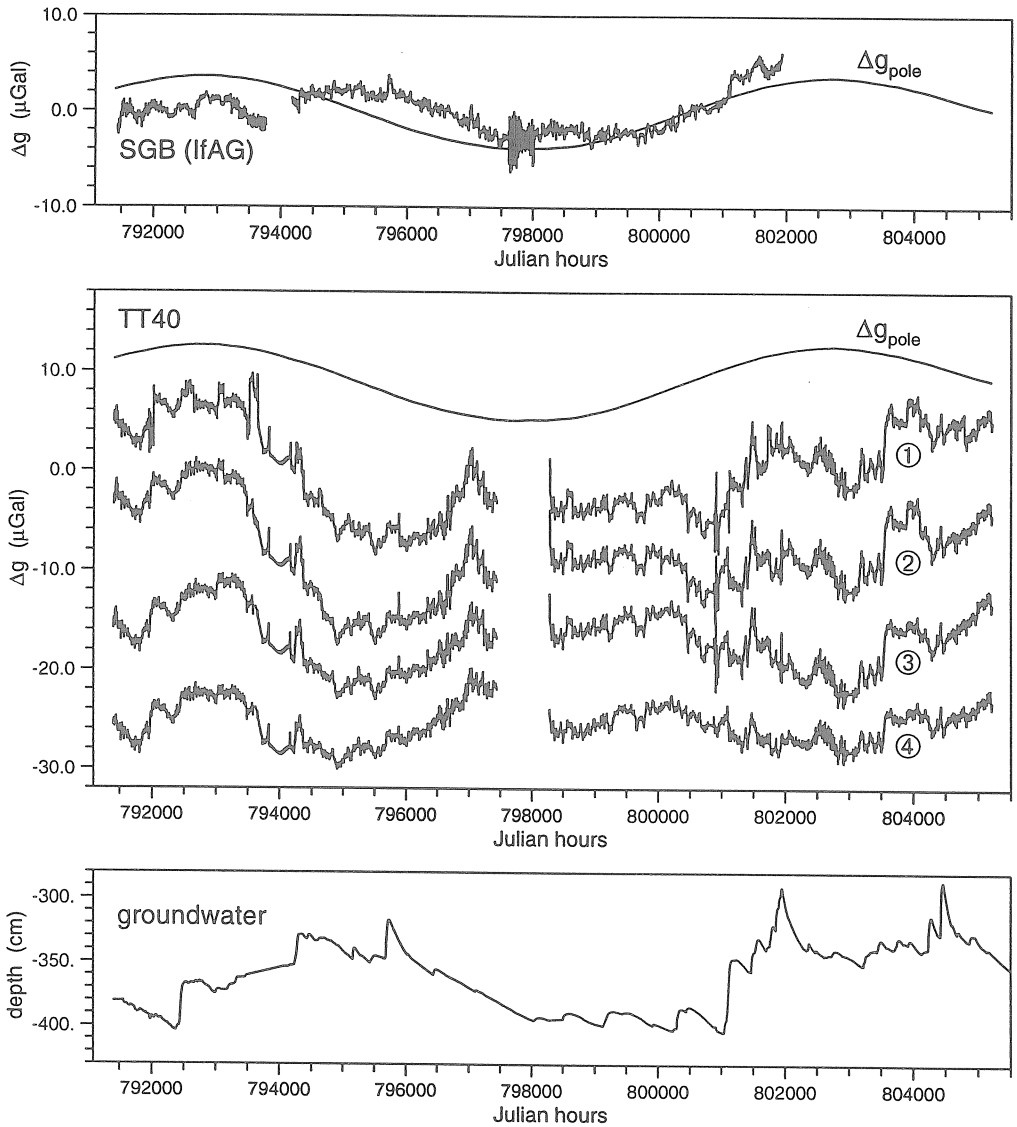

Fig. 5: Residual gravity signal of **SGB (IfAG)** and **TT40**. All curves represented in this figure and parts of them may be shifted in the vertical direction by arbitrary distances. The **TT40** data was corrected for steps exceeding various thresholds: 1 - without step corrections, 2 - steps ≥ 1.0 μGal eliminated, 3 - steps ≥ 0.5 μGal eliminated, 4 - all steps eliminated. For comparison the gravity effect of the observed polar motions and the groundwater variations (depth beneath the earth's surface) are shown.

Looking for reasons for these disappointing results, the step corrections were examined in more detail. On the one hand, fig. 4 shows that in the special case of Miami, heavy rainfall may create sudden step-like variations in the measured gravity. A comparison of the groundwater series with the cumulative step function and the residual gravity signal shows a large number of steps during periods of frequent rainfall. It cannot be excluded that some such rainfall events are falsely interpreted to be steps. On the other hand, fig. 2 and fig. 5 show the influence of step corrections on the cumulative step function and the resulting changes of the residual gravity signal. If only steps above a certain threshold are

considered, the mean linear part of the drift is changed as well as its nonlinear part (see section 2). Even if all steps are neglected (uppermost of the **TT40** curves), no satisfying result is attained. Processing the **SGB** data, a step characteristic is found similar to that of the **TT40** (fig. 2). However, due to the different transfer function, in the data set of the **SGB** noticeably fewer steps could be detected and therefore, the influence of the cumulative step function on the "Restkurve" of this instrument is less important.

The treatment of the data was done as accurately as possible, without looking at an expected result. The current state of processing the **SGB** and **TT40** data shall not be the final one. Further improvements may be achieved, if the influences of rainfall, soil moisture and groundwater are taken into consideration in more detail. As these influences act on **SGB** and **TT40** in the same manner, corresponding corrections may reduce the disagreement between both gravimeters only then, when the discrepances are produced by the different response of the gravimeters (e.g. due to different transfer functions, fig. 1).

6. Acknowledgements

We thank *B. Richter* for numerous hints, advice and friendly discussions concerning the data processing of superconducting gravimeters in general, the treatment of the Miami **SGB** and **TT40** data and the compilation of this paper in particular.

References

[1] *Richter, B.*: Das supraleitende Gravimeter. Anwendung, Eichung und Überlegungen zur Weiterentwicklung.
Dt. geod. Komm. R. C, H. 329. Verl. Inst. Angew. Geodäsie, Frankfurt a.M., 1987, 126 S.

[2] *Goodkind, J. M., Young, C., Richter, B., Peter, G., Klopping, F.*: Comparison of two superconducting gravimeters and an absolute meter at Richmond Florida.
Proc. Workshop: Non Tidal Gravity Changes: Intercomparison between absolute and superconducting gravimeters. Walferdange (Luxembourg), September, 5th to 7th, 1990. Luxembourg 1991, pp. 91 - 98

[3] *Richter, B., Wolf, P., Otto, G., Wenzel, H.-G., Zürn, W.*: Comparison of a cryogenic and a spring gravimeter between 0.2 and 96 cpd at BFO Schiltach.
Paper, presented on the Meeting of the Working Group ˝High Precision Tidal Data Processing˝, Bonn 1994

[4] *Wenzel, H.-G.:* ETERNA - an Earth tide analysis program package for the personal computer.
Bull. géodésique, Paris 1994

SG record at Cantley, Canada: the short period part of the spectrum

D. Banka [1], D. Crossley [2]

Abstract

The usual used tidal band of the recordings of Superconducting Gravimeters is extended to higher frequencies. 1s-data of the Canadian Superconducting Gravimeter (GWR12) are used to show the average-signal in the short-period-band below 20s, which contains several kinds of noise. The 1s-data record after the Guam earthquake of 8 Aug 1993 (M_S = 8.2) is used for a simple analysis in respect to free modes and Q-Factors. A few suggestions for improvements of the data acquisition systems are made to accept the challenge of the spring-gravimeters.

Introduction

In the last years we heard a lot about investigations of Superconducting Gravimeters and their recordings in the tidal band and lower frequencies as one can see in the list:

- Richter (1987): Tidal band, parallelrecord of two superconducting gravimeters.
- Hsu et al. (1991): Tidal band, superconducting gravimeter at Wuhan/China.
- Hinderer et al. (1993): Hourly values, gravity noise levels of two SG's.
- Defraigne et al. (1993): SG data around the 50 day and the 14hr periods.
- Flach et al. (1993): Long-term and aperiodic signals, movable SG in a salt mine.
- Neumeyer & Dittfeld (1993): Tidal band, superconducting gravimeter at Potsdam.

These analysises have their justification in respect to the high sensitivity, long term stability and low drift rates of Superconducting Gravimeters.

The next step might be the extension to higher frequencies. All Superconducting Gravimeter record with sampling rates between one (Cantley, Canada) and twenty seconds (Asse or Wuhan, China). Until now there are a few papers, which deal with the high frequencies in connection with Superconducting Gravimeters, for example: Zürn et al. (1991) analysed high quality data from LaCoste-Romberg Gravimeters with electrostatic feedback and challenged the working groups of the Superconducting Gravimeters. Other works on the short period part of the spectrum were done by Japanese working groups (e.g. Imanishi et al., 1991) and Kamal & Mansinha (1992). They used the Superconducting Gravimeter in Cantley as a long-period seismometer, analysed the Minhassa Earthquake of 18 Apr 1990 (M_S = 7.5) and found a good agreement of the normal mode frequencies and Q values obtained with the Superconducting Gravimeter and earlier reported values from spring-gravimeters and -seismometers.

Our idea is to continue and to extend their work in respect to other earthquakes and methods, but first we would like to present two power spectral densities, to show the quality of the data.

1: Institut für Geophysik, Technische Universität Clausthal, Arnold-Sommerfeld-Straße 1, 38678 Clausthal-Zellerfeld, Germany

2: Department of Earth and Planetary Sciences, McGill University, 3450 University Street, Montreal, Quebec, H3A-2A7, Canada

Extension to higher frequencies

In Fig. 1. we can see the power spectral density of a one-year-time series sampled to one minute. The diurnal, semidiurnal and ter-diurnal tides are obvious, we can see an increasing noise level to lower frequencies and the influence of the decimating filter at high frequencies. Likewise the peak of the fortnightly tide is visible. For the short-period part of the spectrum it is not possible to calculate a spectrum of a one-year time series sampled to one second. To get an average of several days we calculated the spectra of 30 days, which were nearly earthquake-free and stacked them. The result is shown in Fig. 2: Because of the shortness of the single time series, the part below two cycles per hour is not liable for a statement. Beside the aspect of smoothing, the medium part fits to Fig. 1 and above 4.11 log cpd we have the influence of the anti-aliasing filter, but at this part we see broad peaks (at about 6s, 7.5s, 14s, 15s) in the spectrum. These might be generated by the microseismic and the ocean noise, possibly in combination with the resonance of the gravimeter and its feedback system. Thus, for analysis of these signals it is necessary to have the transfer function of the gravimeter.

The frequencies of free modes

The strongest earthquake during the recording period of the Superconducting Gravimeter in Cantley took place near Guam at 8 Aug 1993 (M_S = 8.2). The data of nine days after the earthquake are available; they are shown in Fig. 3. The initial earthquake occured at 8:34:25 UTC, and it was followed by earthquakes at other locations. The high-frequent noise becomes much more significant after subtracting the tides (Tamura potential; 1987; constant values for each group) (Fig. 4): It has an amplitude between 2.5 and 10μgal and it covers nearly every signal. Especially after 130h the noise increases. We assume meterological influences or ocean noise. After the removals of the influence of the air pressure and the initial earthquake, which brought the sphere in the Superconducting Gravimeter to its limits, and the subtraction of the linear drift, we get a spectrum with high amplitudes at high frequencies - up to 50 nanogal at 100 ... 120cph -, especially in comparison with the free modes, and no zone separates these two frequency bands. Fig. 5 shows a part of the free modes band: One can see the fundamental spheroidal modes with a signal-to noise-ratio less than 6, a noise level of about 1 nanogal and an apparent splitting resulting from the overlong time series (Dahlen, 1982).

For free mode analysis it would not make any sense to eliminate the initial earthquake - at least the part, which is in the limits of the gravimeter - but the following earthquakes might disturb the spectra in the same way, so much the more because the stronger ones generate free modes by themselves, but with a different phase, surface pattern and shorter periods. On the other hand the gravimeter might run out of limits; this would add non-harmonic signals from the instrument. Fig. 6 shows the spectrum after this processing step: The high amplitudes at the high freuquencies are much lower. They are only a little bit higher than the peaks of the free modes and in Fig. 8 we can see much lower noise levels, while the signal decreases only slightly. At this step we can identify a few modes in respect to PREM (Dziewonski & Anderson, 1981): In Fig. 7 ${}_0S_7$ and ${}_0S_6$ are significant above the noise level, but there is not any mode fitting to 4.0993cph and so we can't do a serious fitting to ${}_2S_4$, ${}_0S_5$ and all the other small peaks. Only ${}_0S_2$ and ${}_0S_3$ seem to be visible. Fig. 8 and Fig. 9 show the fundamental modes between ${}_0S_8$ and ${}_0S_{29}$ depending on the surface pattern. Also one can recognize a few radial overto-

nes with low amplitudes. The next part of the spectrum (Fig. 10) also shows a few fundamental modes and one can notice the problem with strong damped modes in long time series: the peaks become broad and short, they split, so it is more difficult to identify them in the noise.

The Q-Factors

The other aspect of free modes is their loss of energy, expressed in the Q-factor, which can be calculated from the parameters of an exponential regression function through the peaks of one mode in a shifting window. The window length is given by 0.5 Q cycles (Dahlen, 1982) and so in every calculation one can only consider one mode. For the first we choose ${}_0S_{15}$, and to reduce the computing time 1-min-data were used with a time shift of 5min (Fig. 11). We see a non-monotonous exponential decay up to 30 hours and nearly a constant for the following time. So one can say this mode is down in the noise after 30h and only this part should be used for Q-calculations. In Fig. 12 we can see the fitting af the regression to the data and the Q-factor is 289. This result fits well to the findings of other authors: 342 (Widmer et al., 1991), 318 (Masters et al., 1983), 293 (Roult & Romanowicz, 1984), 296 (Kamal & Mansinha, 1992), 290 (Dziewonski & Anderson, 1981 (PREM)), 227 (Sailor & Dziewonski, 1978).

Conclusions

The frequencies and Q values obtained from the Superconducting Gravimeter agree to those reported in earlier papers and we can confirm Kamal & Mansinha (1992). We see a lot of normal mode peaks significant above the noise level. But we saw a strong influence of the high-frequent noise, which covers the interesting part of the signal. So there are a few suggestions to improve the situation:

- Application of the transfer function to get true amplitudes for comparison with other (spring-) gravimeters.
- Reduction of the sampling rate to 10s or 20s to get true amplitudes from 1min on: This would reduce the needed storage and the computing time, and the interesting part of the spectrum becomes more visible.
- Shifting the dynamic range to higher amplitudes: At present the high dynamic range is used to look at the noise, but to look for free oscillations we have to start the analysis after the gravimeter signal is stable again. To study the excitation and the increasing oscillation it is necessary to start earlier, but this is only possible with wider limits of the gravimeter.

We can expect to identify much more frequencies and Q values of free oscillations after the improvement of the analysis exceeding the simple Fourier-analysis of one long time-series, especially in connection with other sites.

Acknowledgements

We acknowledge the support of the Canadian Superconducting Gravimeter Installation by the National Science and Engineering Research Council of Canada. Co-author D. Banka was supported by the German Academic Exchange Service. Thanks to G. Jentzsch for several interesting discussions, suggestions and ideas.

References

Dahlen, F. A.: The effect of data windows on the estimation of free oscillation parameters; The Geophysical Journal of the Royal Astronomical Society, Vol. 69, p. 537, 1982

Defraigne, P.; Billiau, A.; Collin, F.; Ducarme, B.; Dehant, V.: Analysis of the superconducting gravimeter data outside the tidal frequency band: Around the 50 day and the 14hr periods; Bulletin d'Information Marées Terrestres, Volume 116, p. 8590, 1993

Dziewonski, A. M.; Anderson, D. L.: Preliminary Reference Earth Model (PREM). Physics of the Earth and Planetary Interiors, Volume 25, p. 297, 1981

Flach, D.; Gommlich, G.; Jentzsch, G.: Three years of experiences with a movable superconducting gravimeter at the underground installation site in the salt mine ASSE in northern Germany; Bulletin d'Information Marées Terrestres, Vol. 117, p. 8639, 1993

Hinderer, J.; Crossley, D.; Xu, H.: Gravity noise levels from a two-year comparison of two superconducting gravimeter data.
Bulletin d'Information Marées Terrestres, Volume 116, p. 8612, 1993

Hinderer, J.; Crossley, D.; Xu, H.: A two-year comparison between the French and Canadian superconducting gravimeter data.
Geophysical Journal International, Volume 116, p. 252, 1994

Hsu, H. T.; Jahr, T.; Jentzsch, G.; Tao, G. X.: Some results from the superconducting gravimeter in Wuhan/China.
Bulletin d'Information Marées Terrestres, Volume 110, p. 7973, 1991

Kamal; Mansinha, L.: A test of the superconducting gravimeter as a long-period seismometer; Physics of the Earth and Planetary Interiors, Volume 71, p. 52, 1992

Masters, G.; Park, J.; Gilbert, F.: Observations of coupled spheroidal and toroidal modes. Journal of Geophysical Research, Volume 88, No. B12, p. 10285, 1983

Neumeyer, J.; Dittfeld, H.-J.: First results of the registration with the superconducting gravimeter installed at gravimetric observatory Potsdam.
Bulletin d'Information Marées Terrestres, Volume 117, p. 8649, 1993

Preliminary determination of epicenters (PDE), U. S. Department of the Interior, Geological Survey

Richter, B.: Parallelregistration with two superconducting gravimeters.
Bulletin d'Information Marées Terrestres, Volume 99, p. 6757, 1987

Sailor, R. V.; Dziewonski, A. M.: Measurements and interpretation of normal mode attenuation. The Geophysical Journal of the Royal Astronomical Society, Vol. 53, p. 559, 1978

Tamura, Y.: An harmonic development of the tide generating potential
Bulletin d'Information Marées Terrestres, Volume 99, p. 6813, 1987

Widmer, R.; Zürn, W.; Masters, G.: Observation of low order toroidal modes from the 1989 Macquarie rise event.
Berichtsband 1990-1992 des Sonderforschungsbereichs 108: „Spannung und Spannungsumwandlung in der Lithosphäre" an der Universität Karlsruhe, p. 1413
also: Geophysical Journal International, Volume 111, p. 226, 1992

Zürn, W.; Wenzel, H.-G.; Laske, G.: High quality data from LaCoste-Romberg Gravimeters with electrostatic feedback: A challenge for superconducting gravimeters.
Bulletin d'Information Marées Terrestres, Volume 110, p. 7940, 1991

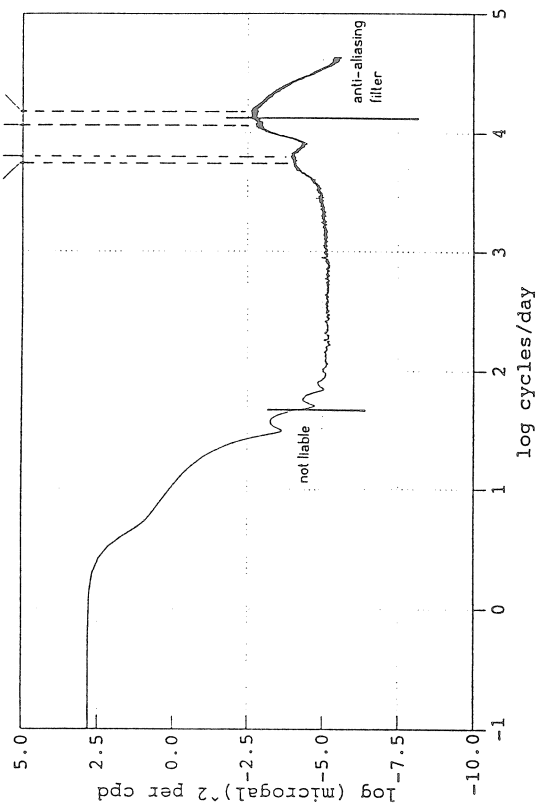

Fig. 2: Stacked power spectral density of 30 gravimeter time series of one day, 1-sec-sampling, no gaps, no large earthquakes, linear drift subtracted

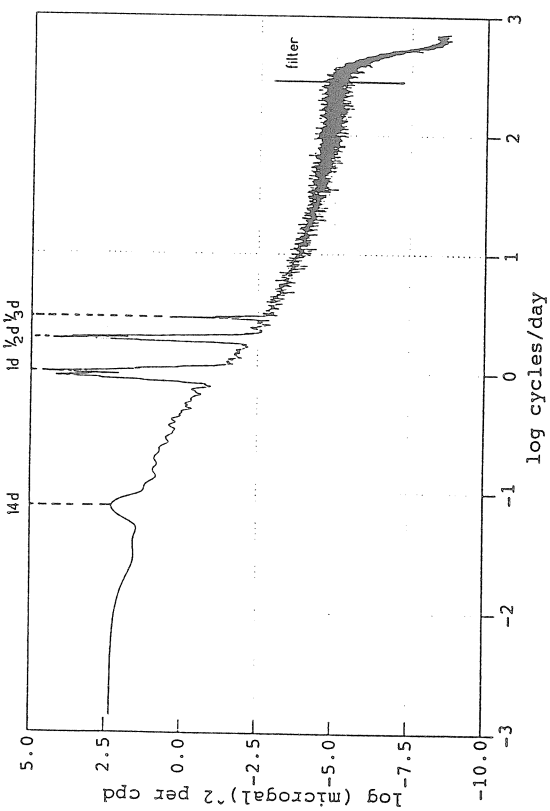

Fig. 1: Power spectral density of a gravimeter time series of one year, 1-min-sampling, gaps interpolated, linear drift subtracted

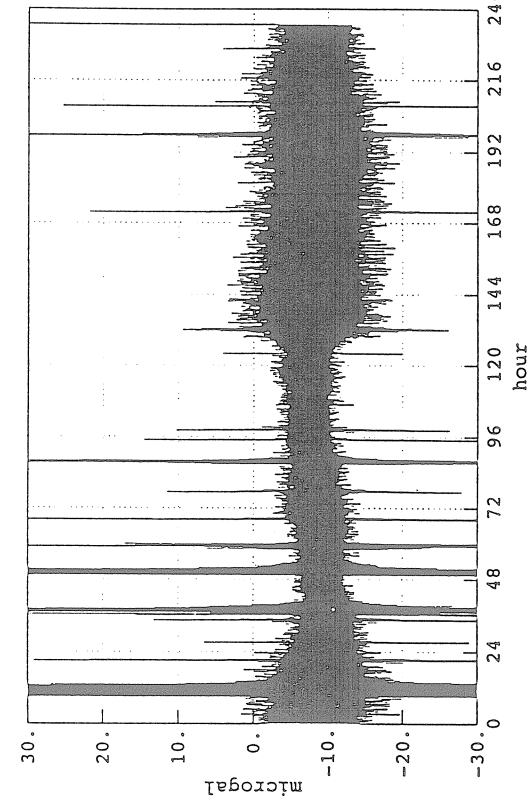

Fig. 4: Gravimeter time series from 8 Aug 1993 to 17 Aug 1993, 1-sec-sampling, no gaps,

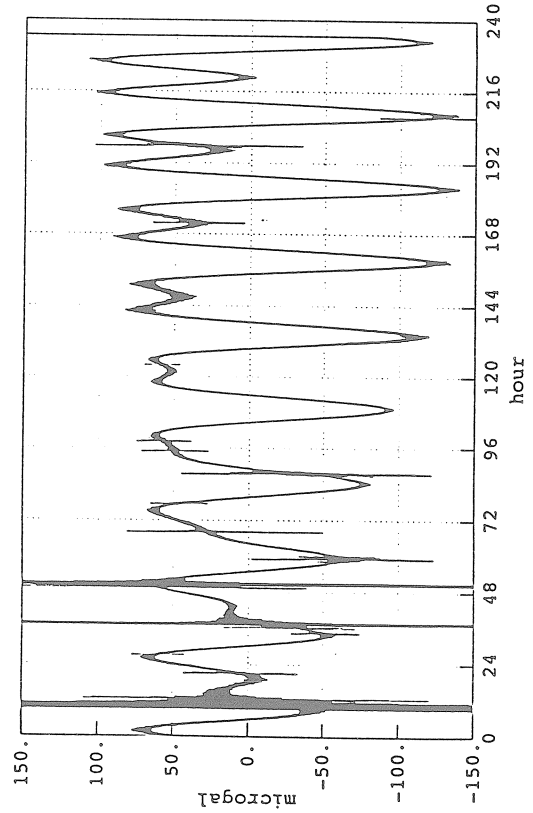

Fig. 3: Gravimeter time series from 8 Aug 1993 to 17 Aug 1993, 1-sec-sampling, no gaps

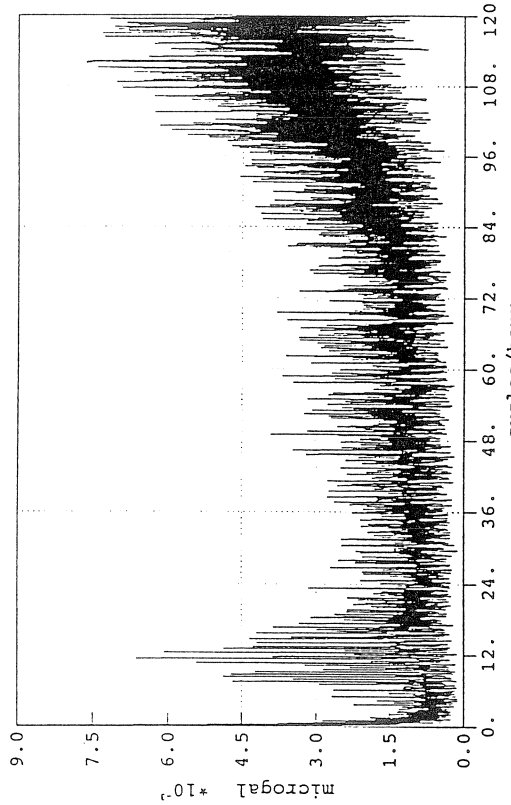

Fig. 6: Amplitude spectrum of a gravimeter time series from 8 Aug 1993 to 17 Aug 1993, 1-sec-sampling, large earthquakes eliminated, tides and influence of air-pressure subtracted, initial earthquake cutted, linear drift removed

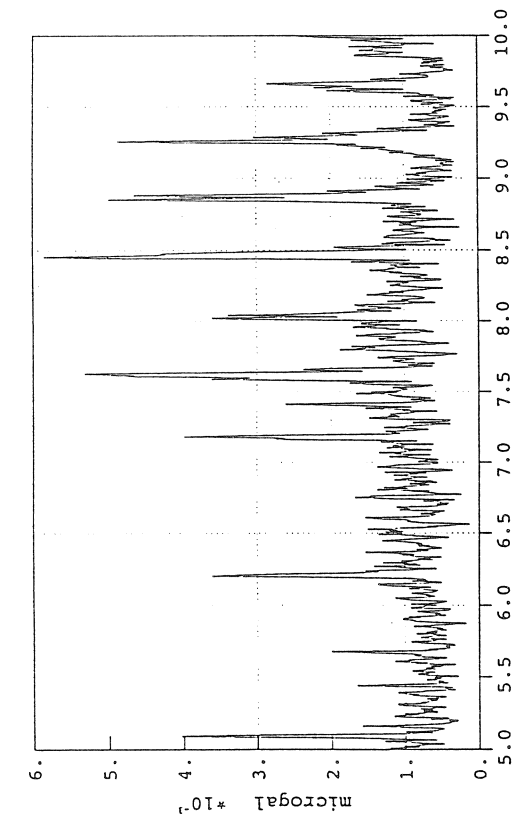

Fig. 5: Amplitude spectrum of a gravimeter time series from 8 Aug 1993 to 17 Aug 1993, 1-sec-sampling, no gaps, tides and influence of air-pressure subtracted, initial earthquake cutted, linear drift removed

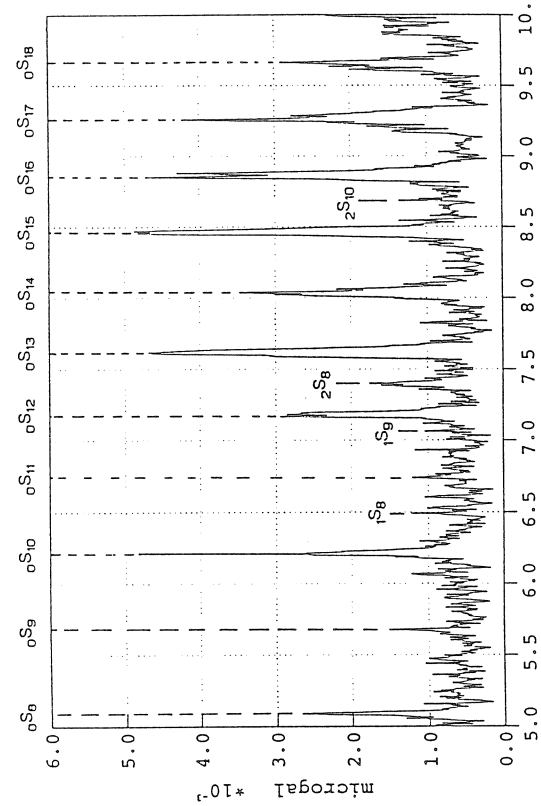

Fig. 8: Amplitude spectrum of a gravimeter time series from 8 Aug 1993 to 17 Aug 1993, 1-sec-sampling, large earthquakes eliminated, tides and influence of air-pressure subtracted, initial earthquake cutted, linear drift removed

Fig. 7: Amplitude spectrum of a gravimeter time series from 8 Aug 1993 to 17 Aug 1993, 1-sec-sampling, large earthquakes eliminated, tides and influence of air-pressure subtracted, initial earthquake cutted, linear drift removed

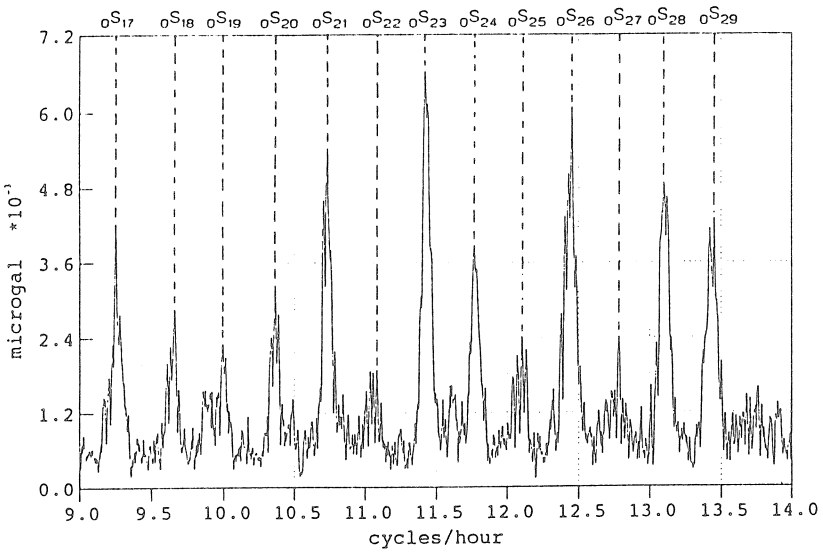

Fig. 9: Amplitude spectrum of a gravimeter time series from 8 Aug 1993 to 17 Aug 1993, 1-sec-sampling, large earthquakes eliminated, tides and influence of air-pressure subtracted, initial earthquake cutted, linear drift removed

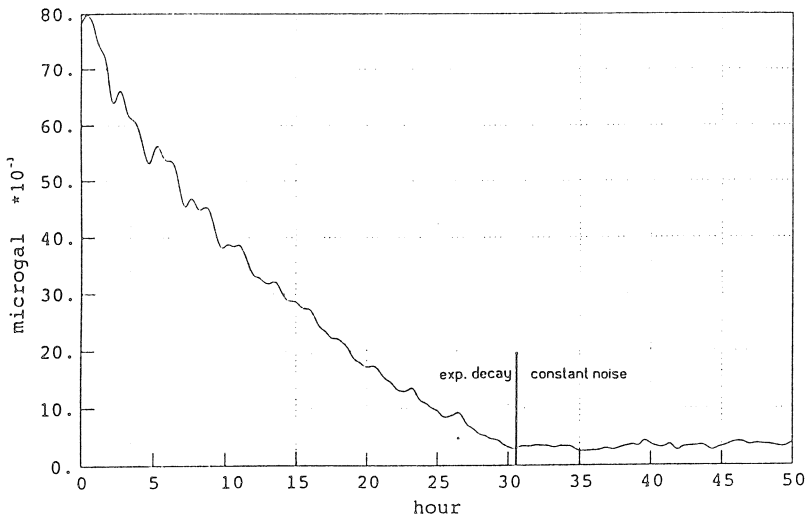

Fig. 11: Amplitudes of the 8.4577cph peak ($_0S_{15}$) in spectra of gravimeter time series from 8 Aug 1993, window length: 1027min, 5-min-sampling

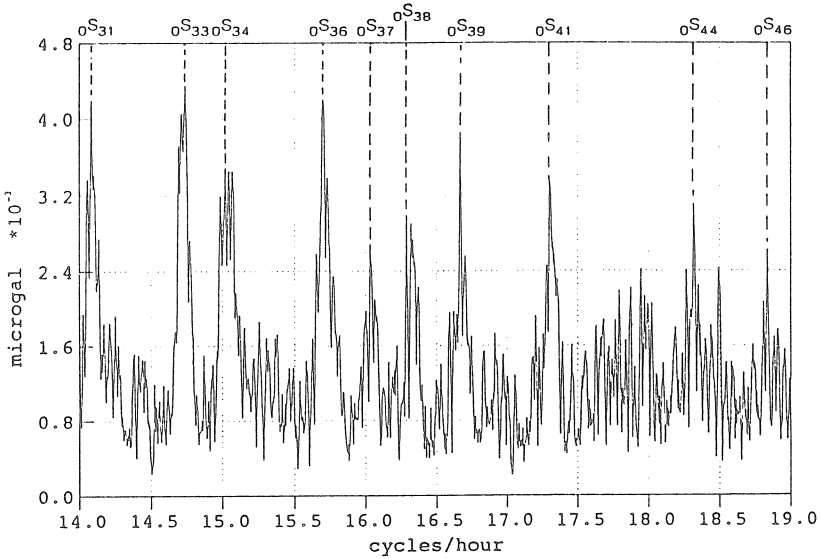

Fig. 10: Amplitude spectrum of a gravimeter time series from 8 Aug 1993 to 17 Aug 1993, 1-sec-sampling, large earthquakes eliminated, tides and influence of air-pressure subtracted, initial earthquake cutted, linear drift removed

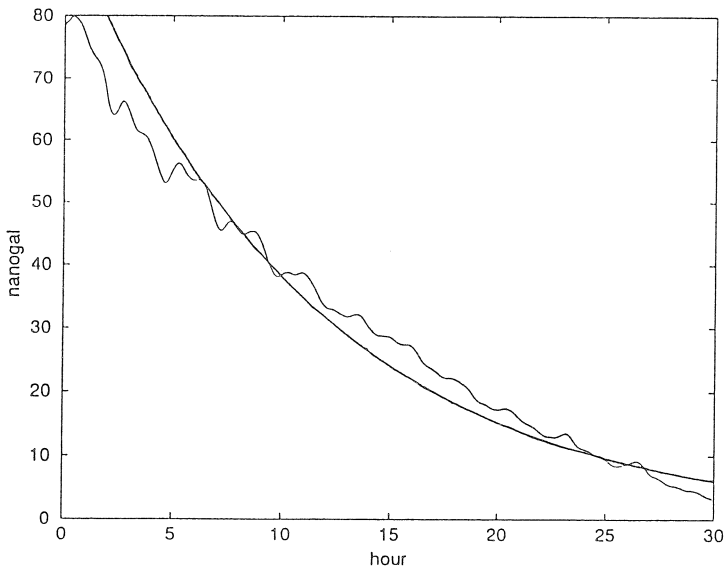

Fig. 12: Amplitudes of the 8.4577cph peak ($_0S_{15}$) in spectra of gravimeter time series from 8 Aug 1993, window length: 1027min, 5-min-sampling
Regression function: Q = 289

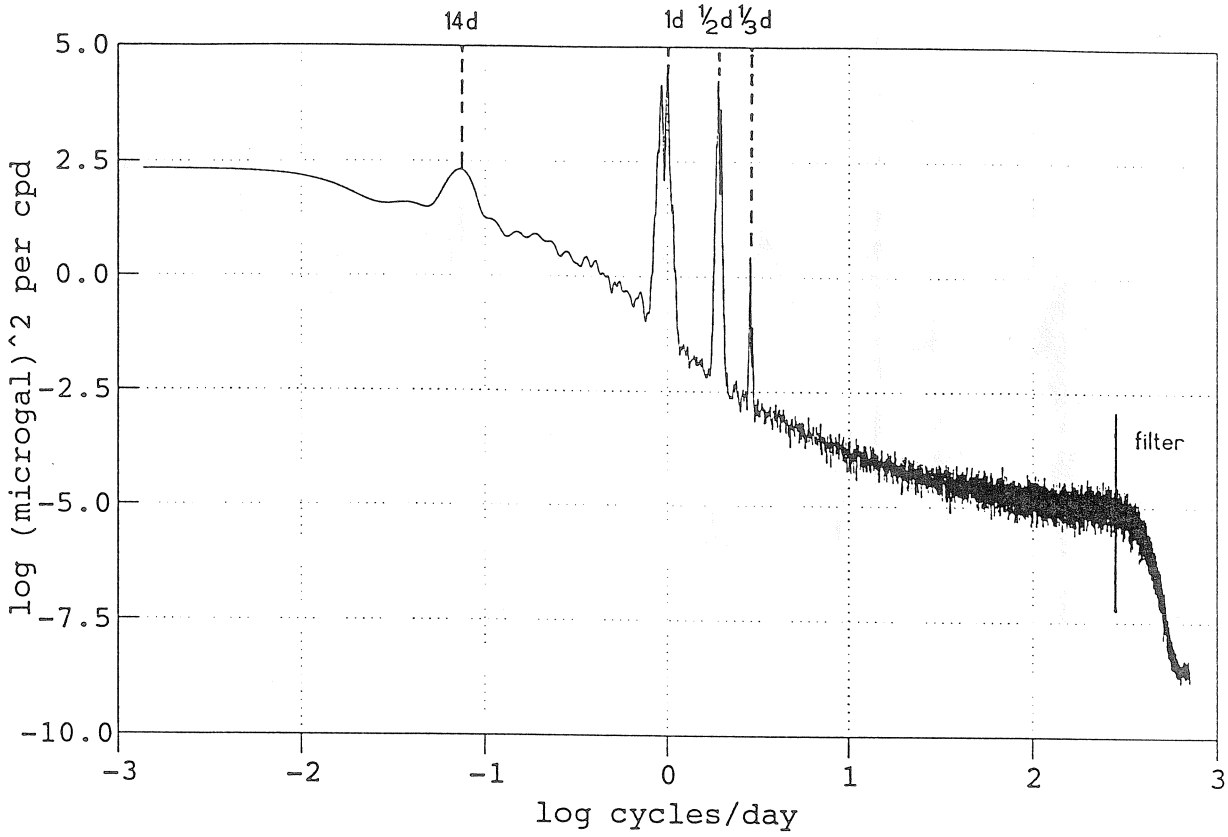

Fig. 1: Power spectral density of a gravimeter time series of **one year**, 1-min-sampling, gaps interpolated, linear drift subtracted

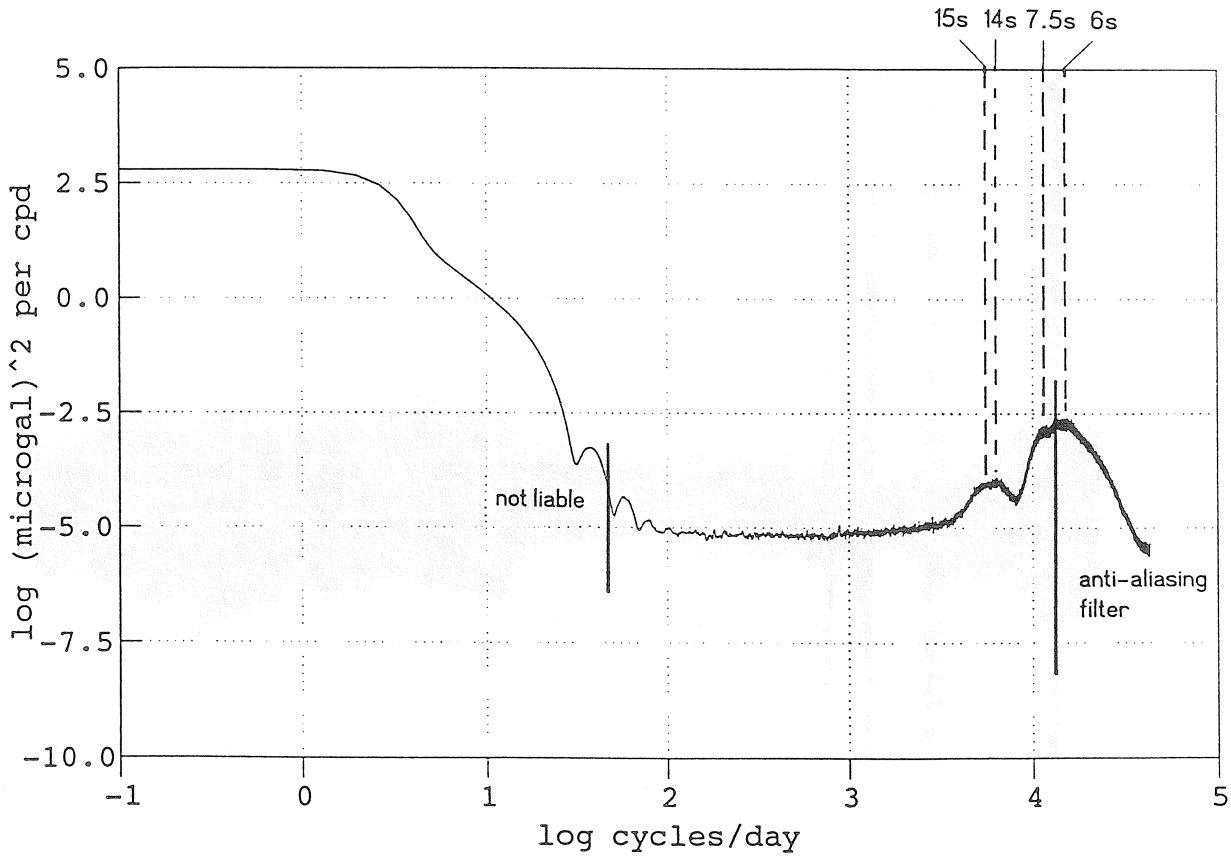

Fig. 2: Stacked power spectral density of 30 gravimeter time series of **one day**, 1-sec-sampling, no gaps, no large earthquakes, linear drift subtracted

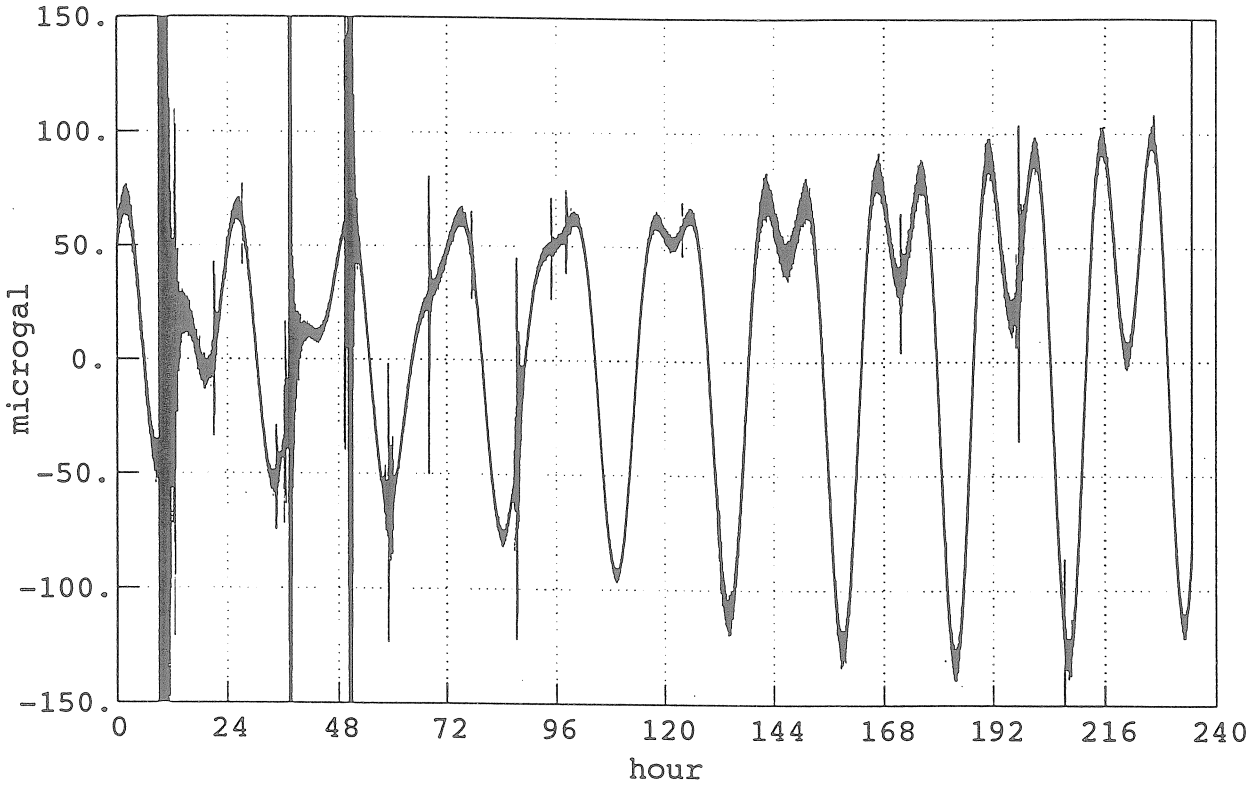

Fig. 3: Gravimeter time series from 8 Aug 1993 to 17 Aug 1993, 1-sec-sampling, no gaps

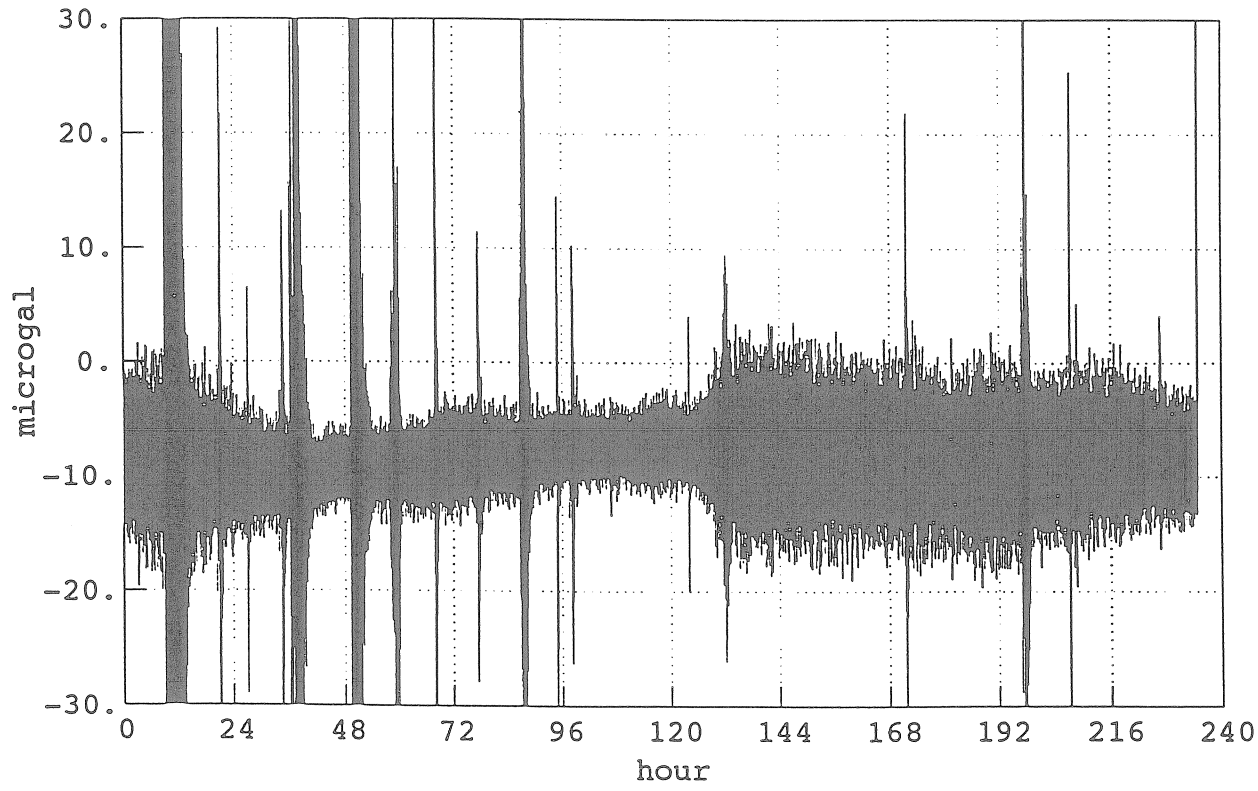

Fig. 4: Gravimeter time series from 8 Aug 1993 to 17 Aug 1993, 1-sec-sampling, no gaps, tides subtracted

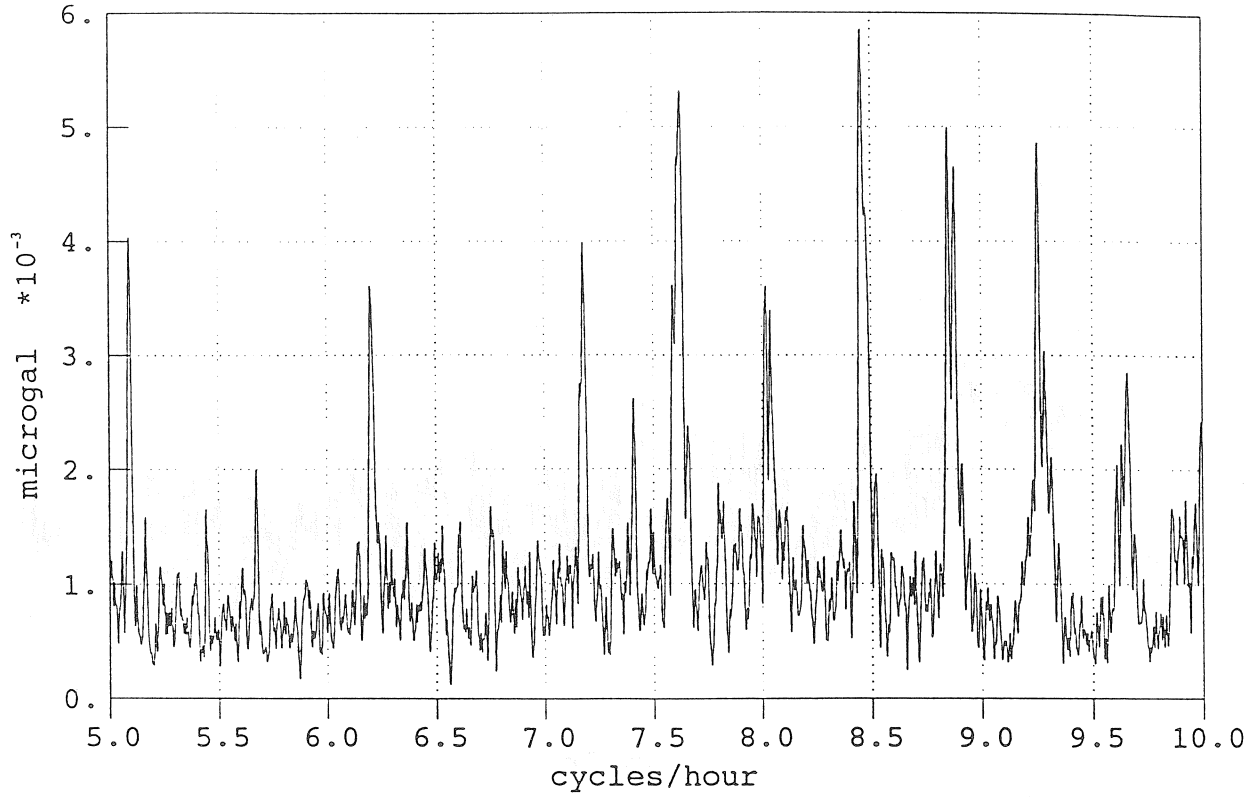

Fig. 5: Amplitude spectrum of a gravimeter time series from 8 Aug 1993 to 17 Aug 1993, 1-sec-sampling, no gaps, tides and influence of air-pressure subtracted, initial earthquake cutted, linear drift removed

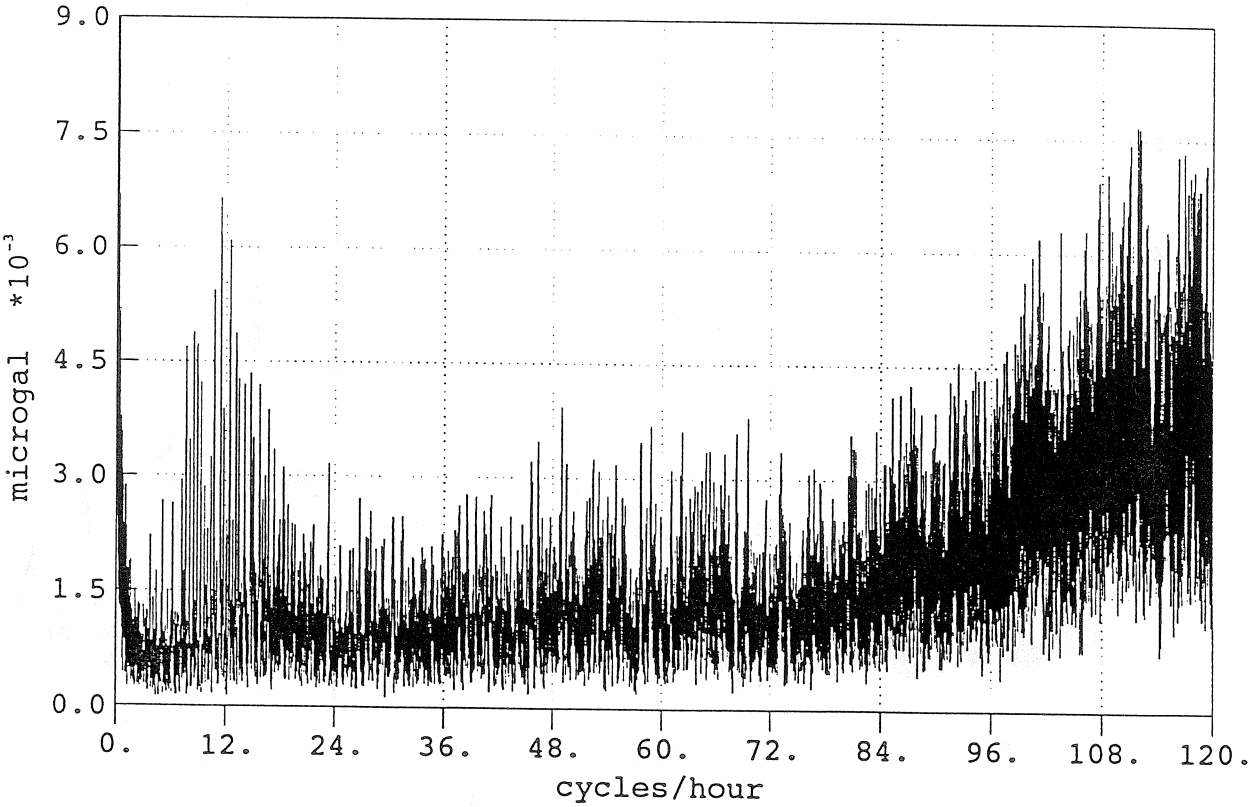

Fig. 6: Amplitude spectrum of a gravimeter time series from 8 Aug 1993 to 17 Aug 1993, 1-sec-sampling, **large earthquakes eliminated**, tides and influence of air-pressure subtracted, initial earthquake cutted, linear drift removed

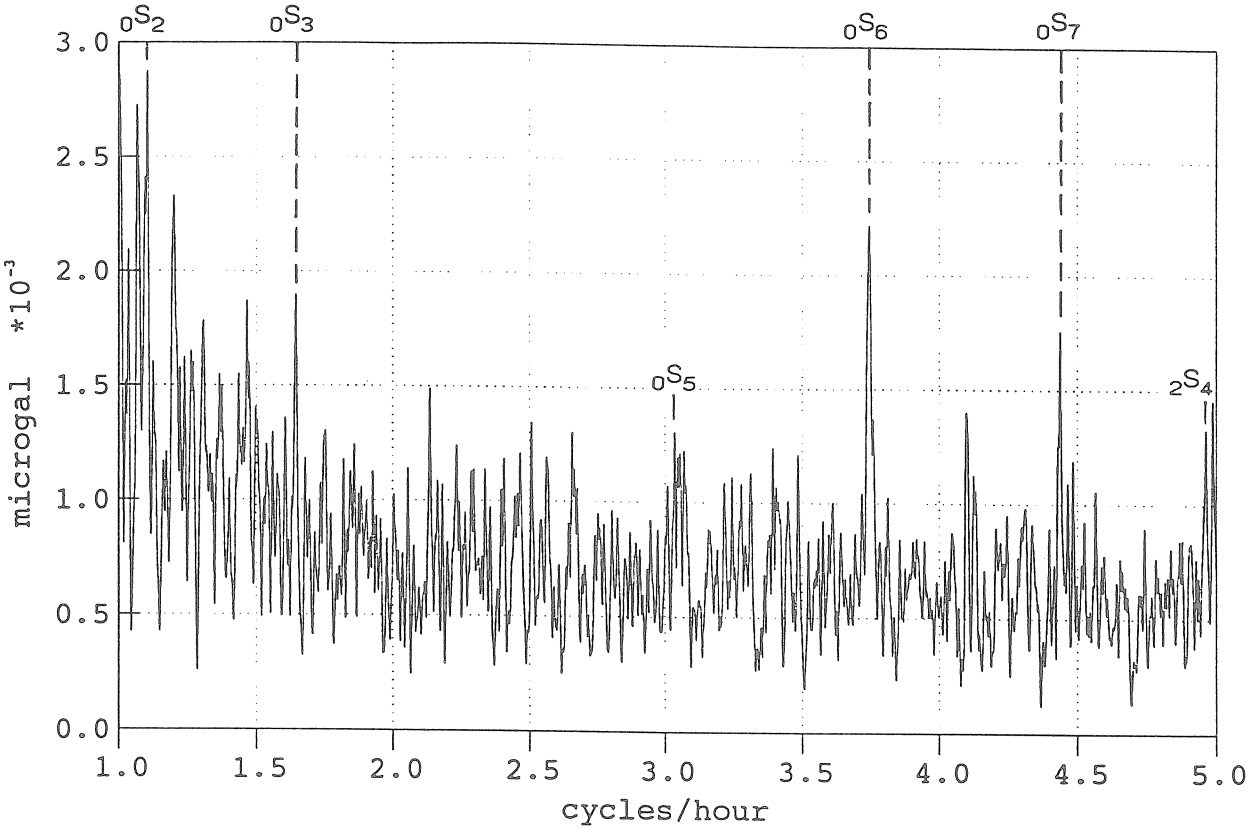

Fig. 7: Amplitude spectrum of a gravimeter time series from 8 Aug 1993 to 17 Aug 1993, 1-sec-sampling, large earthquakes eliminated, tides and influence of air-pressure subtracted, initial earthquake cutted, linear drift removed

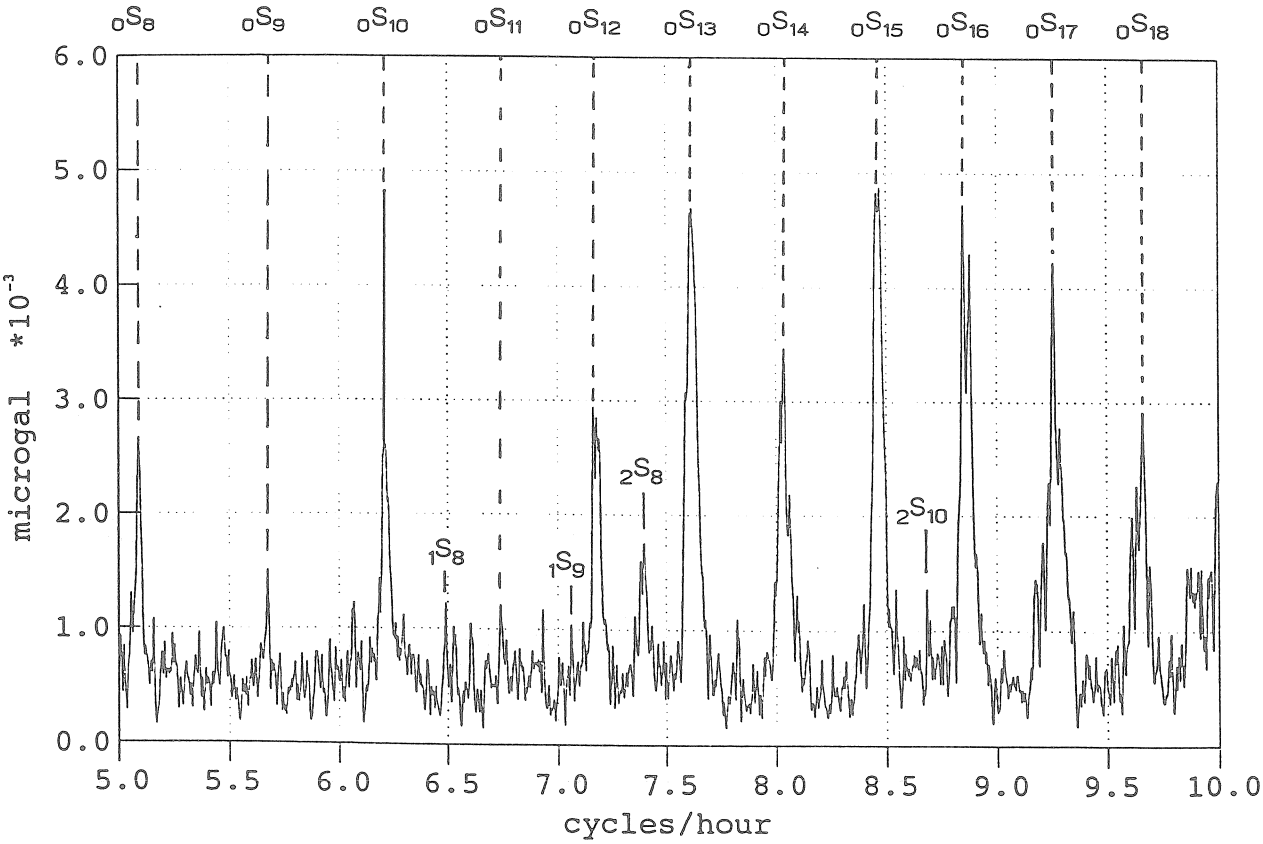

Fig. 8: Amplitude spectrum of a gravimeter time series from 8 Aug 1993 to 17 Aug 1993, 1-sec-sampling, large earthquakes eliminated, tides and influence of air-pressure subtracted, initial earthquake cutted, linear drift removed

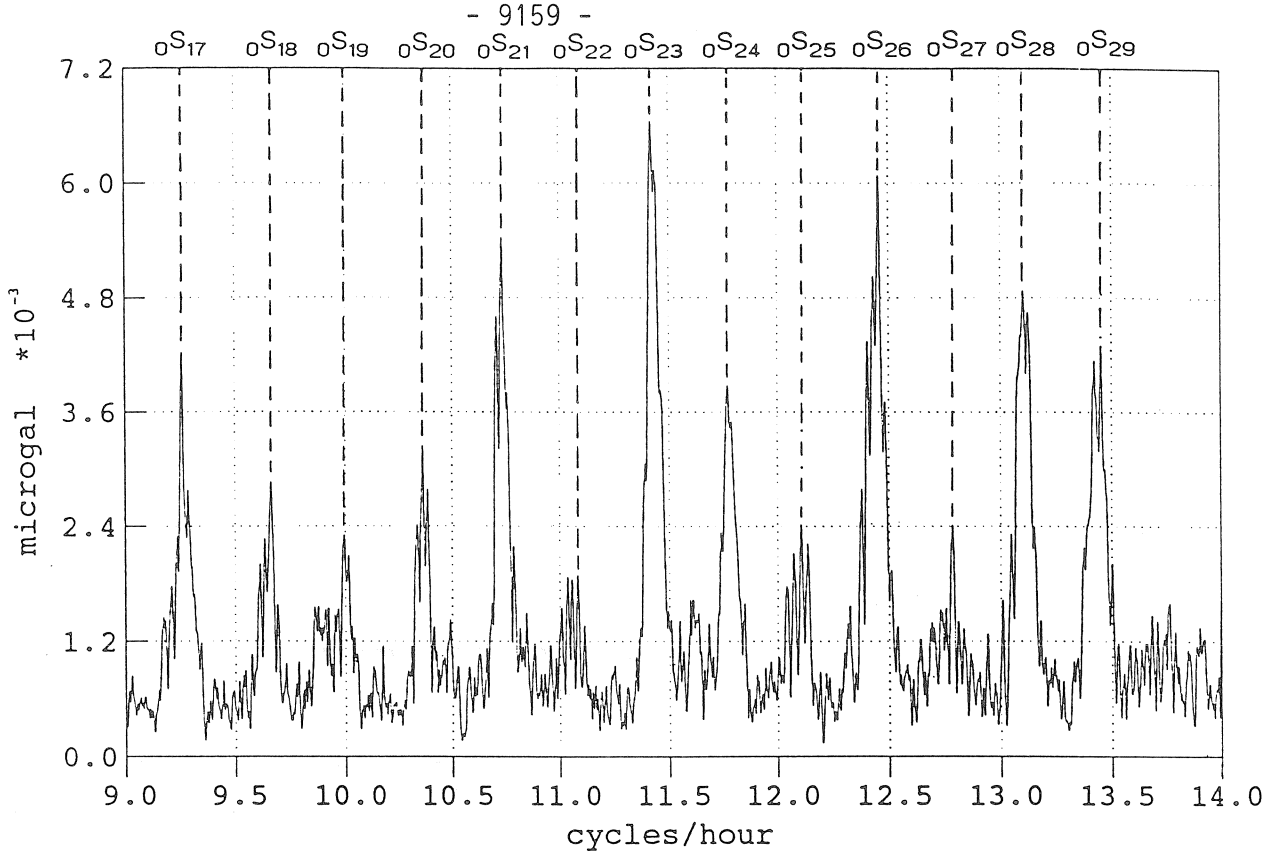

Fig. 9: Amplitude spectrum of a gravimeter time series from 8 Aug 1993 to 17 Aug 1993, 1-sec-sampling, large earthquakes eliminated, tides and influence of air-pressure subtracted, initial earthquake cutted, linear drift removed

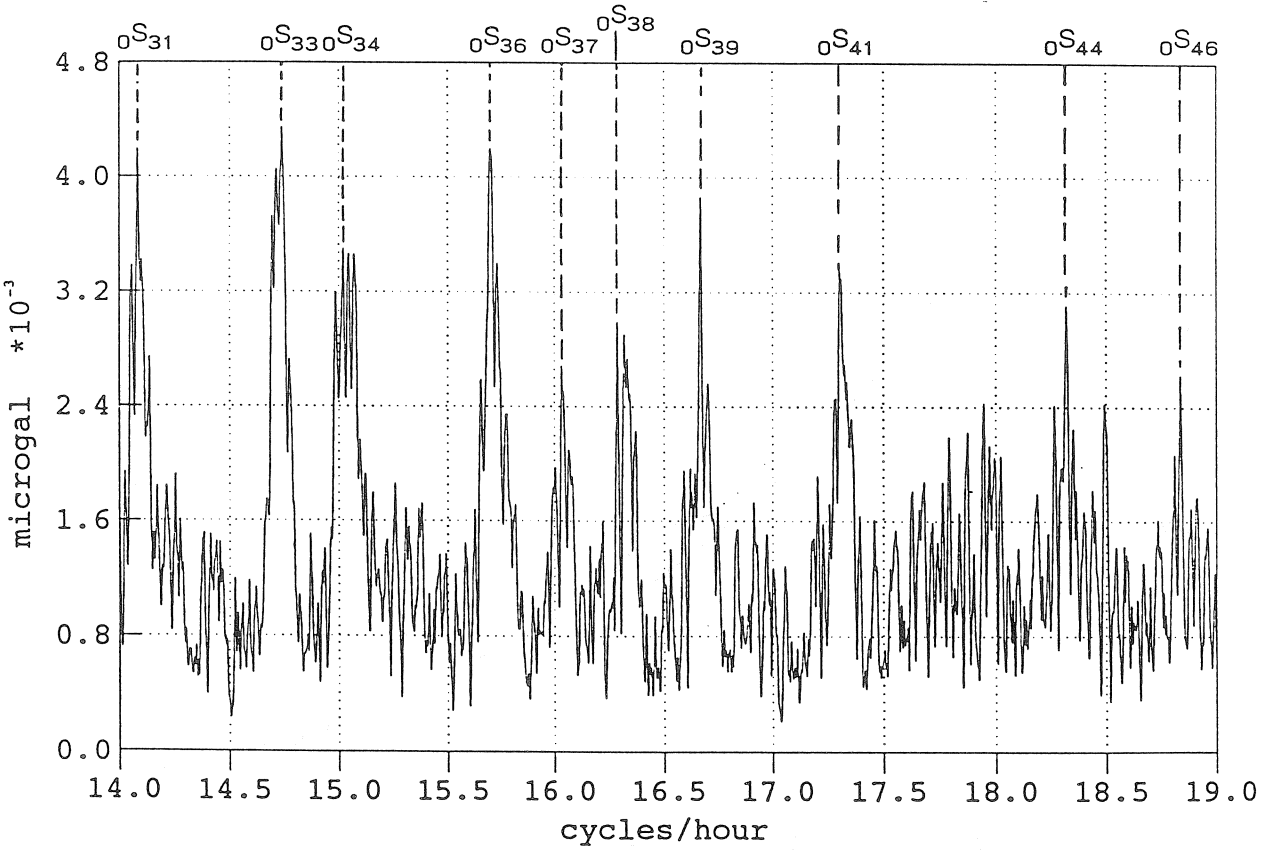

Fig. 10: Amplitude spectrum of a gravimeter time series from 8 Aug 1993 to 17 Aug 1993, 1-sec-sampling, large earthquakes eliminated, tides and influence of air-pressure subtracted, initial earthquake cutted, linear drift removed

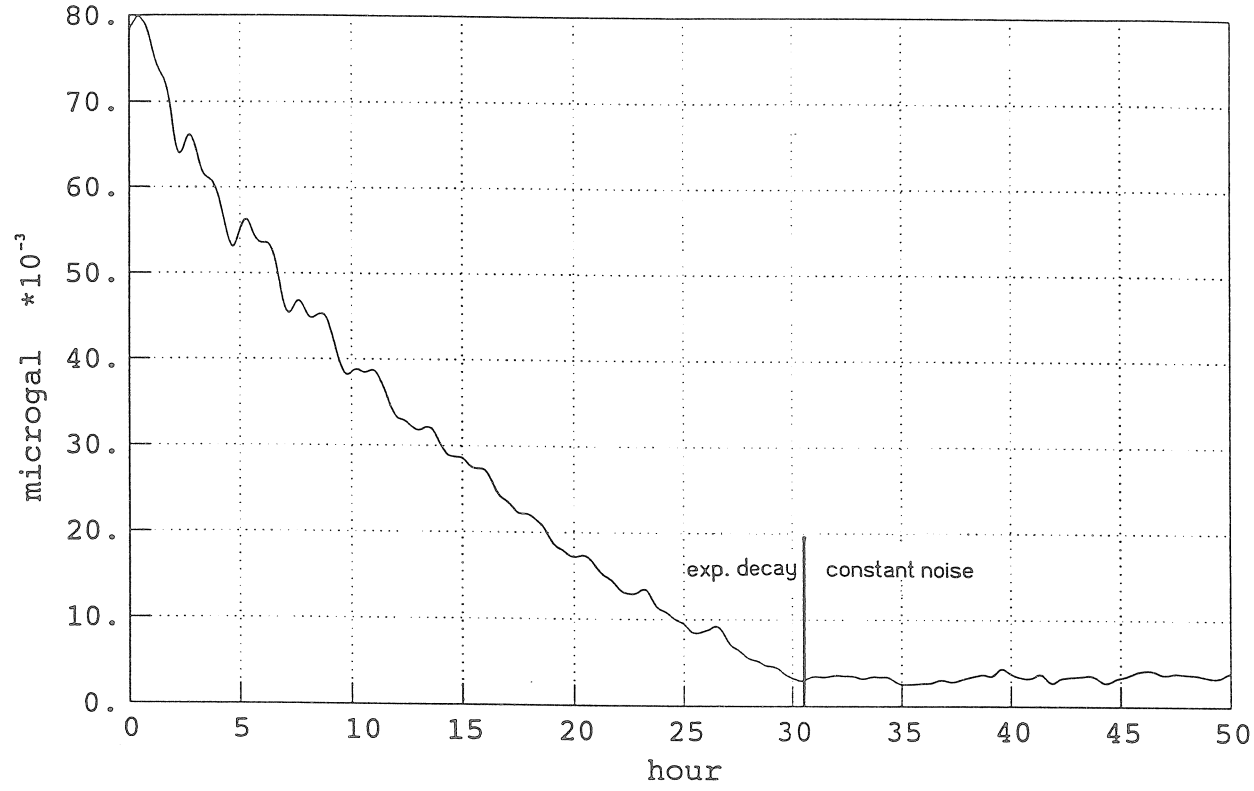

Fig. 11: Amplitudes of the 8.4577cph peak ($_0S_{15}$) in spectra of gravimeter time series from 8 Aug 1993, window length: 1027min, 5-min-sampling

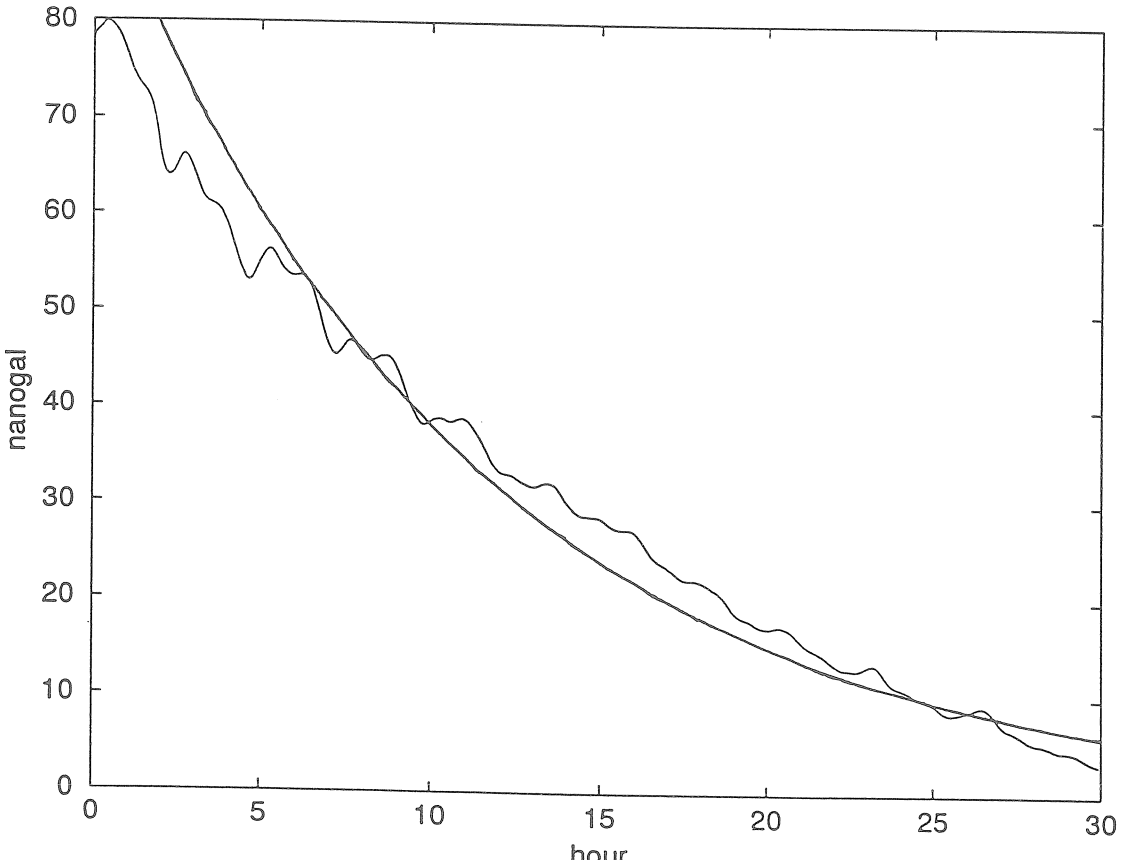

Fig. 12: Amplitudes of the 8.4577cph peak ($_0S_{15}$) in spectra of gravimeter time series from 8 Aug 1993, window length: 1027min, 5-min-sampling
Regression function: Q = 289

The Slichter Triplet - Why Have We Not Seen It ?

D. Crossley[1], O. Jensen[1], M. G. Rochester[2] and W. Wu[2]

[1] *Department of Earth & Planetary Sciences, McGill University, Montreal*
[2] *Department of Earth Sciences, Memorial University, St. John's, Newfoundland*

Despite the recent flurry of activity in the literature concerning the possible detection of the Slichter triplet (e.g. Smylie, 1992; Crossley et al., 1992; Rochester and Peng, 1993; Hinderer et al., 1994), a number of issues are still unresolved. We do not know the period because it depends critically on the ICB density contrast and we know neither the excitation nor damping mechansims. Furthermore, thermodynamic phase changes may occur at the ICB due to the motion of the inner core. With such uncertainty it is not suprising that any observations would be more than welcome. In this paper we review the current status and then attempt to answer some of the possible reasons why the triplet has so far eluded surface detection.

Is the IC Sufficiently Excited ?

The inner core could be induced to move by earthquake excitation from the upper mantle or by direct mechanical (e.g. fluid motions in the liquid core) or thermodynamic excitation near the inner core boundary (ICB), impulsive reactions in the chemical BL associated with decending or ascending blobs. To date only the first possibility has been modelled. Smith (1976) estimated the level of excitation to be at about the 1 nangal level for a large Chilean-type earthquake. Here we extend similar calculations of Crossley (1992) to fully account for rotation in the excitation which we show spreads the energy over several harmonics of the motion but does not substantially alter the non-rotating results.

The excitation is checked using seismic normal modes observed with the Canadian superconducting gravimeter (SG). We thus can be fairly confident that this mechanism yields gravity variations at the surface that would be seen only by a global stack of SGs following a large (in seismic moment) earthquake.

Is the Damping Light Enough ?

Coherent oscillations of the IC can only be detected at the nanogal level using superconducting gravimeters if we use either (a) long records and assume the excitation is at worst incoherent and intermittent or at best continuous and phase coherent or (b) short records following a large earthquake where we can stack using a known earthquake excitation model.

Option (a) assumes the Q is high, otherwise a highly damped, randomly excited motion will not be seen. Option (b) allows for lower Q's so that each seismic event can be considered in isolation. Naturally a combination of (a) and (b) is possible. To date seismic (anelastic) Q estimates are high (> 1000), but almost totally unconstrained by conventional seismology. Both magnetic and viscous damping (e.g. Buffet and Goertz, 1995) fail to provide definitive answers, largely because other parameters are poorly known. An alternative damping mechanism is considered below.

Is the ICB a Phase Boundary ?

Conventional seismic theory, used to date, treats the Slichter triplet as a mechanical, adiabatic oscillation. But if the ICB is at the melting point, the thermodynamics of the phase transition have to be considered. As the inner core translates, the leading edge moves into a region of reduced ambient, hydrostatic, pressure (modified only slightly by the flow pressure in the surrounding fluid): similarly the trailing edge moves into a region of increased hydrostatic pressure. Thus the local temperatures ΔT of the leading and trailing edges are respectively reduced/increased with respect to the surrounding material. At the same time the change in freezing temperature ΔT_f can be calculated from the Clausius-Clapeyron equation. The net supercooling is thus $\Delta T_f - \Delta T$ at the trailing edge and there is a similar heating at the leading edge. The overall growth/destruction of solid material at the ICB is dependent on the extent to which heat can be transported compared to the mechanical speed of the boundary.

We estimate (e.g. Wu and Rochester, 1994), using extrapolations of the pertinent parameters, that the amount of material melted and frozen onto the inner core is likely to be small enough to be negligible and thus the phase boundary moves with the material boundary. On the other hand the net heat dissipated thermodynamically can be substantial and thus may lead to considerable damping of the translational motion. If confirmed, this fact would be sufficient to eliminate the possibility of the Slichter vibration being detected at the Earth's surface.

References

Buffet, B.A. and Goertz, D.E., 1995., Magnetic Damping of the Translational Oscillations of the Inner Core, SEDI 94 Symposium, Geophys. J. Int., 120, 103-110.

Crossley, D.J., 1992, Eigensolutions and seismic excitation of the Slichter mode triplet for a fully rotating Earth model, *EOS*, 73, 60.

Crossley, D.J., Rochester, M.G. & Peng, Z.R., 1992, Slichter modes and Love numbers, *Geophys. Res. Lett.*, 19, 1679-1682.

Hinderer, J., Crossley, D.J. and Jensen, O., 1994, A search for the Slichter triplet in superconducting gravimeter data, *accepted for publication in Phys. Earth Planet. Int.*.

Rochester, M.G. & Peng, Z.R., 1993, The Slichter modes of the rotating Earth : a test of the subseismic approximation. *Geophys. J. Int.* 113, 575-585.

Smith, M.L., 1976, Translational inner core oscillations of a rotating, slightly elliptical Earth, *JGR*, 81, 3055-3065.

Smylie, D. E., 1992, The inner core translational triplet and the density near Earth's center, *Science*, 255, 1678-1682.

Wu, W.-J. & Rochester, M.G., 1994, Gravity and Slichter modes of the rotating Earth, *Phys. Earth Planet. Int. (in press).*

Comparison of a cryogenic and a spring gravimeter between 0.2 and 96 cpd at BFO Schiltach

B. Richter and P. Wolf, Institut für Angewandte Geodäsie, Richard-Strauss-Allee 11, D-60598 Frankfurt a.M.,
and
H. Otto, H.-G. Wenzel, W. Zürn, Black Forest Observatory Schiltach, Heubach 206, D-77709 Wolfach.

Abstract

The cryogenic gravimeter SG102 of GWR company has been operated for about half a year at the underground Black Forest Observatory (BFO) Schiltach in parallel to the permanently installed LaCoste and Romberg spring gravimeter ET19 with electrostatic feedback. The purpose of this experiment was to compare a cryogenic and a spring gravimeter directly at a very low noise site. The tide channels and free mode channels of both instruments were recorded using the same data acquisition system with 21 bit resolution and 5 s sampling interval, after apropriate anti-alias filtering. In this paper, we describe the recording, processing and analysis of the tidal signals for both instruments and compare the recorded signals and analysis results between 0.2 and 96 cpd. The data processing has been carried out with the same programs using the same options for both instruments. The analysis and comparison of recorded free oscillations with both instruments will be presented in (Zürn, Widmer, Richter and Wenzel 1994).

The processing of the first 62^d of the tidal record has shown a number of small steps (about 10 nm/s^2 magnitude) of unknown origin in the record of the cryogenic gravimeter, and large steps (about 200 nm/s^2 magnitude) connected with several hours anomalous drift in case of Helium refilling. After editing of these steps, the noise level of the cryogenic gravimeter was slightly higher than that of the spring gravimeter in the frequency range of 1 to 96 cpd. For frequencies below 0.2 cpd, the cryogenic gravimeter SG102 is superior to the spring gravimeter ET19. The earth tide analysis of the first 62^d with program ETERNA (Wenzel 1994b) using highpass filtering option gave standard deviations of 0.737 and 0.556 nm/s^2 for the cryogenic and the spring gravimeter respectively. A regression analysis of the residuals yielded a correlation of 0.82 between the residuals of both gravimeters, an rms model noise (unmodelled gravity signals of the earth, atmosphere and hydrosphere) of about 0.61 nm/s^2 and an rms instrumental noise of 0.21 nm/s^2.

1 Introduction

With the invention of superconducting gravimeters (SG), the long period frequency band (periods of up to 432^d) has been made available for studies of gravity variations on the surface of the earth (e.g. Prothero and Goodkind 1968, Richter 1987, Richter and Zürn 1988). This frequency band cannot be reached even by the best spring gravimeters, because the stable "magnetic spring" is far superior to the metal alloy springs for long periods. However, at present it is not clear at which frequency the SG becomes superior to a good spring gravimeter at a low noise site.

It has been demonstrated in a recent paper by Zürn et al. (1992), that some of the best spring gravimeters, operated under favorable conditions and with extreme care, could provide signal-to-noise ratios comparable to those achieved with superconducting gravimeters for periods of 14 days

and shorter. The gravimeters were LaCoste-Romberg gravimeters equipped with electrostatic feedback and the data were recorded digitally. It was not clear at which periods the instrumentally caused noise becomes larger than the earth noise (including unavoidable gravity signals from the atmosphere and hydrosphere) at quiet sites. Since the magnetic spring of the superconducting gravimeter is more stable than the metal alloy spring of the LaCoste-Romberg gravimeters, it was expected that better signal-to-noise ratios can be obtained with the superconducting gravimeters. This has not been demonstrated at present except for periods of one month and longer. Because the data used by Zürn et al. (1992) were obtained at different sites, there were also site effects included in the comparison. Additionally, most of the SG stations cannot be considered as low noise sites. Therefore we have operated the superconducting gravimeter SG102 for about half a year at the low noise site BFO Schiltach in parallel to the permantly operating LaCoste-Romberg gravimeter ET19. Both gravimeters were operated under the same conditions, the signals from both gravimeters were recorded on the same data acquisition system, and the data processing and data analysis has been carried out with the same programs using identical options. Thus, the differences between both recorded signals should be of instrumental origin only.

2 Data recording

The La-Coste and Romberg earth tide gravity meter ET19, equipped with a Weber-Larson electrostatic feedback (Weber and Larson 1966, Larson 1968) is operating continously since 1979 at BFO Schiltach for earth tide and free oscillation recording. The gravimeter has two outputs, named tide and mode channel. The gravimeter is installed in the gravimeter vault behind the air lock with about 150 m rock coverage (Fig. 1). The temperature in the gravimeter vault is about 12^0 C, the humidity is about 100% . The gravimeter vault is not thermostatized, but the temperature is stable to a few mK. The gravimeter is protected against humidity by installation in a box in which dried air is continously pumped in.

The superconducting gravimeter SG102 of GWR Instruments is a small size instrument with a half-inch sphere, a 50 l dewar and without refrigeration system. The gravimeter has been installed on a concrete pillar in the BFO tiltmeter vault at a distance of about 20 m to the gravimeter vault (Fig. 1). The temperature and humidity conditions of the tiltmeter vault were very similar to the gravimeter vault. The gravimeter was shielded against humidity by a tent of thin plastic film, automatically filled by the outgazing dry Helium. Helium had to be refilled at a rate of about 20 days, which caused large steps in the recorded gravity signal. One of these steps was so large, that the feedback of the gravimeter was out of range and the instrument had to be re-initialized. The maintenance of the gravimeter SG102 caused small disturbances to all other sensors (including the gravimeter ET19) installed behind the air lock.

The analog signals of both gravimeters (tide and free mode channels for gravimeter ET19, tide channel, free mode channel and two tilt channels for gravimeter SG102) and of an air pressure sensor named BMG6, installed in front of the air lock, were send via analog cables to the electronic vault (Fig. 1). After anti-alias filtering by 8 pole Butterworth filters with 25 s cutoff period, these signals were digitized at the electronic vault by a 20 channel 21 bit resolution data acquisition system Hewlett Packard HP3852s at 5 s interval. The epoch of the samples was given to about 50μs by a DCF77 radio controlled clock operating in the laboratory building. The digitized data were send via optical fibre to the laboratory building, where they have been stored on optical discs.

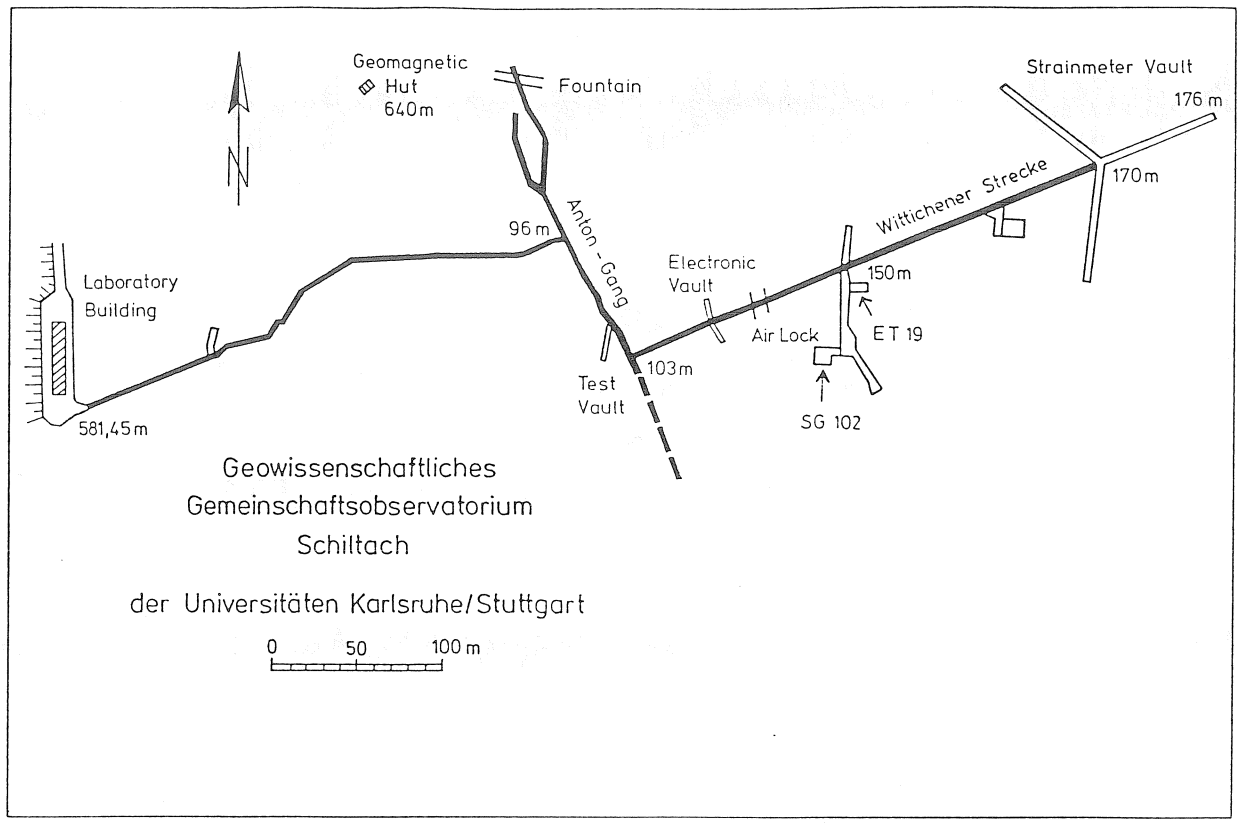

Figure 1: Sketch of the Black Forest underground observatory.

3 Data preprocessing

After numerical filtering and decimation from 5 s to 1 min interval, the data of both gravimeters have been preprocessed using the PRETERNA software package (Wenzel 1994a) assisted by a graphical editor named PREGRED (Vetter and Wenzel 1994). The data have been calibrated using approximate calibration parameters, detided using approximate tidal parameters, and depressured using approximate airpressure regression parameters. Steps have been removed and small gaps have been interpolated. Finally, the data have been decimated to 5 min and hourly interval after apropriate numerical filtering. As an example, the detided and depressured 1 min data are shown for both gravimeters at March 20th, 1994 in Fig. 2. The numerically differentiated 1 min data (differences between subsequent samples) are displayed additionally in Fig. 2. They show a larger short periodic noise of the SG of about 0.14 nm/s^2 rms compared to the ET19 of about 0.06 nm/s^2 rms. During the data preprocessing, a number of small steps in the order of a few nm/s^2 have been found in the detided signal of the SG, whereas no step could be seen in the record of the ET19 (Fig. 2). The origin of these steps is unknown, but these steps have been removed using the graphical editor. Helium refill at a rate of about 20^d produced large steps and significant disturbances for several hours (Fig. 3).

Using the preprocessed 5 min data (16384 samples = 56.9^d starting at $17^h\ 00^{min}$ March 16th, 1994), Fourier amplitude spectra of the detided and depressured data are given in Fig. 4 and 5. In Fig. 5, we find a significant peak of 0.006 nm/s^2 at 48 cpd (half an hour period), which is unexplained yet. For the removal of the airpressure influence to the recorded signal, adjusted regression parameters from the ETERNA analysis (see section 4) have been used. There can be seen significant residual signals caused by the errors of the approximate tidal model used for the detiding at about 2 cpd. In Fig. 6 and 7 are zoomed the Fourier spectra of gravimeters SG102 and

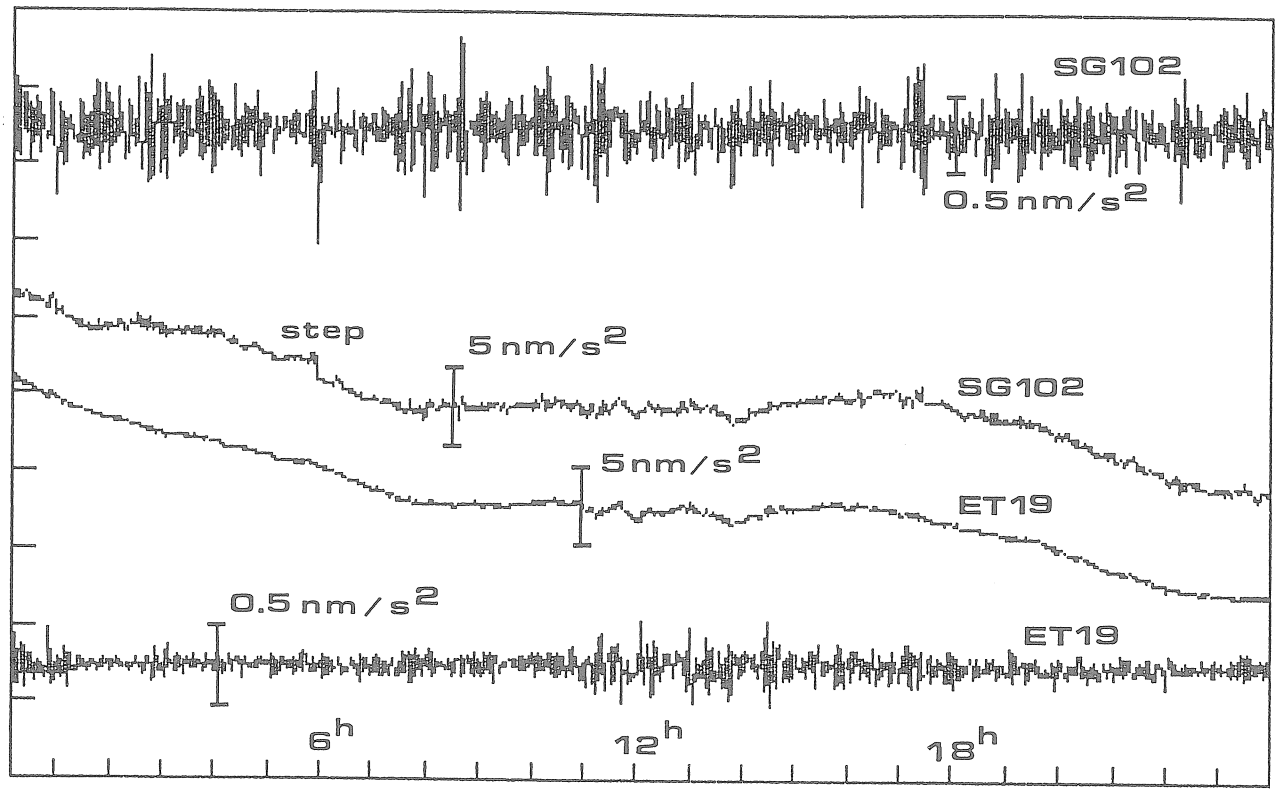

Figure 2: Detided and depressured 1 min data of gravimeter SG102 and ET19, and numerically differentiated data at March 20th, 1994.

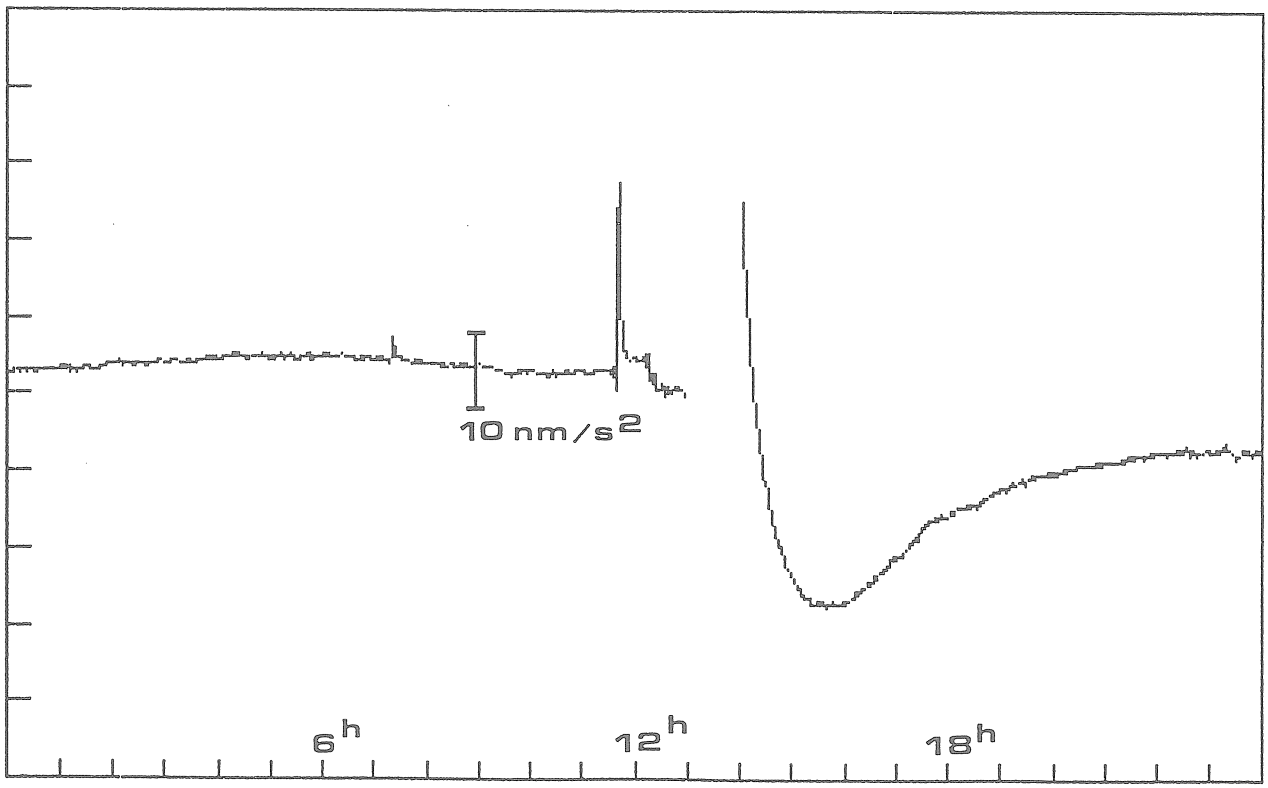

Figure 3: Detided and depressured 1 min data of gravimeter SG102 during Helium refill at March 29th. Step of 200 nm/s^2 has already been removed.

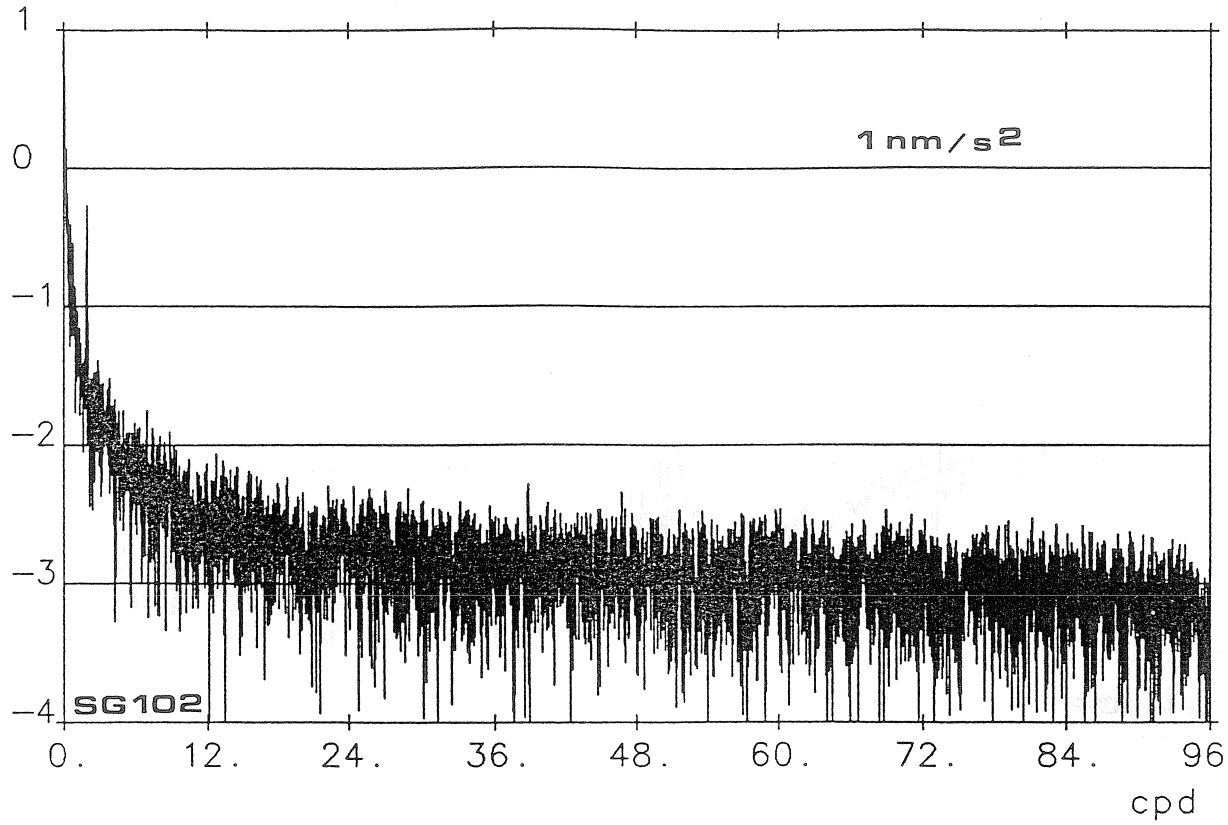

Figure 4: Logarithmic Fourier amplitude spectrum in nm/s^2 of detided and depressured preprocessed 5 min data of gravimeter SG102.

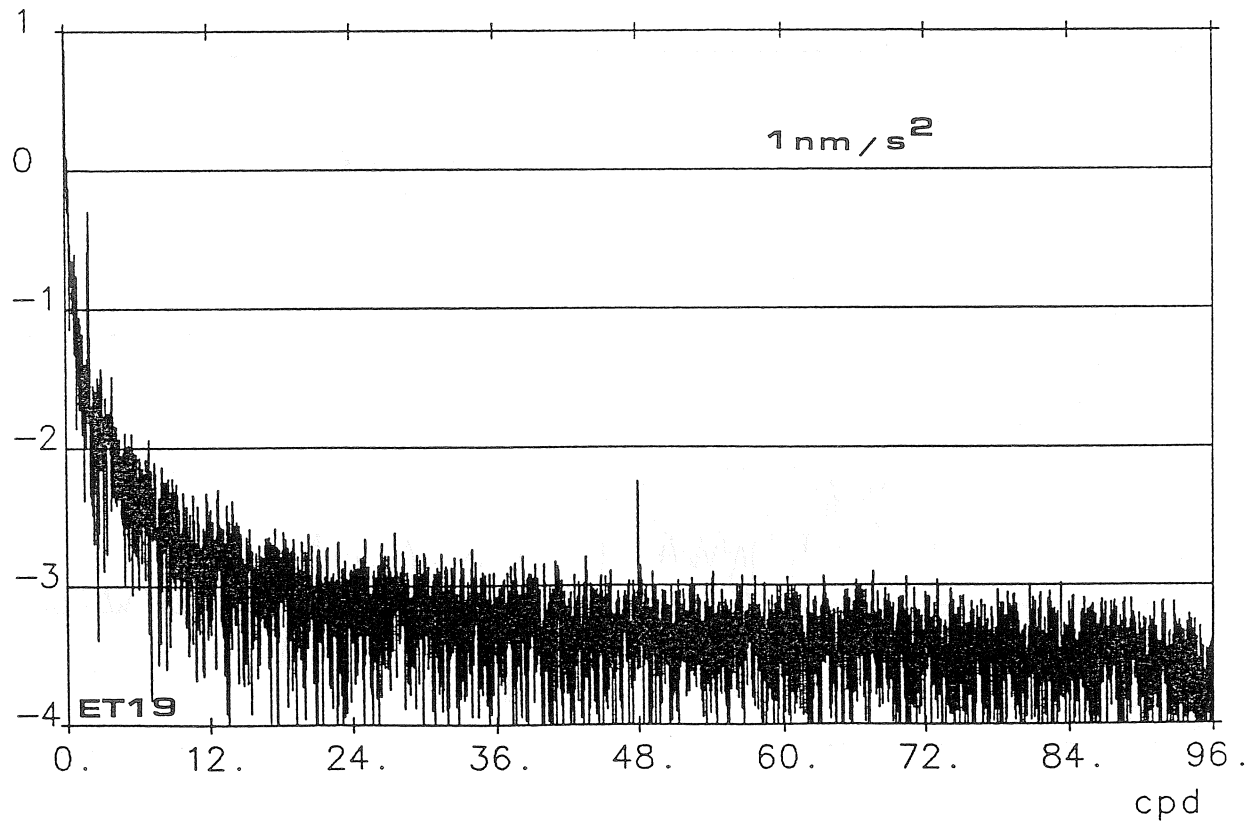

Figure 5: Logarithmic Fourier amplitude spectrum in nm/s^2 of detided and depressured preprocessed 5 min data of gravimeter ET19.

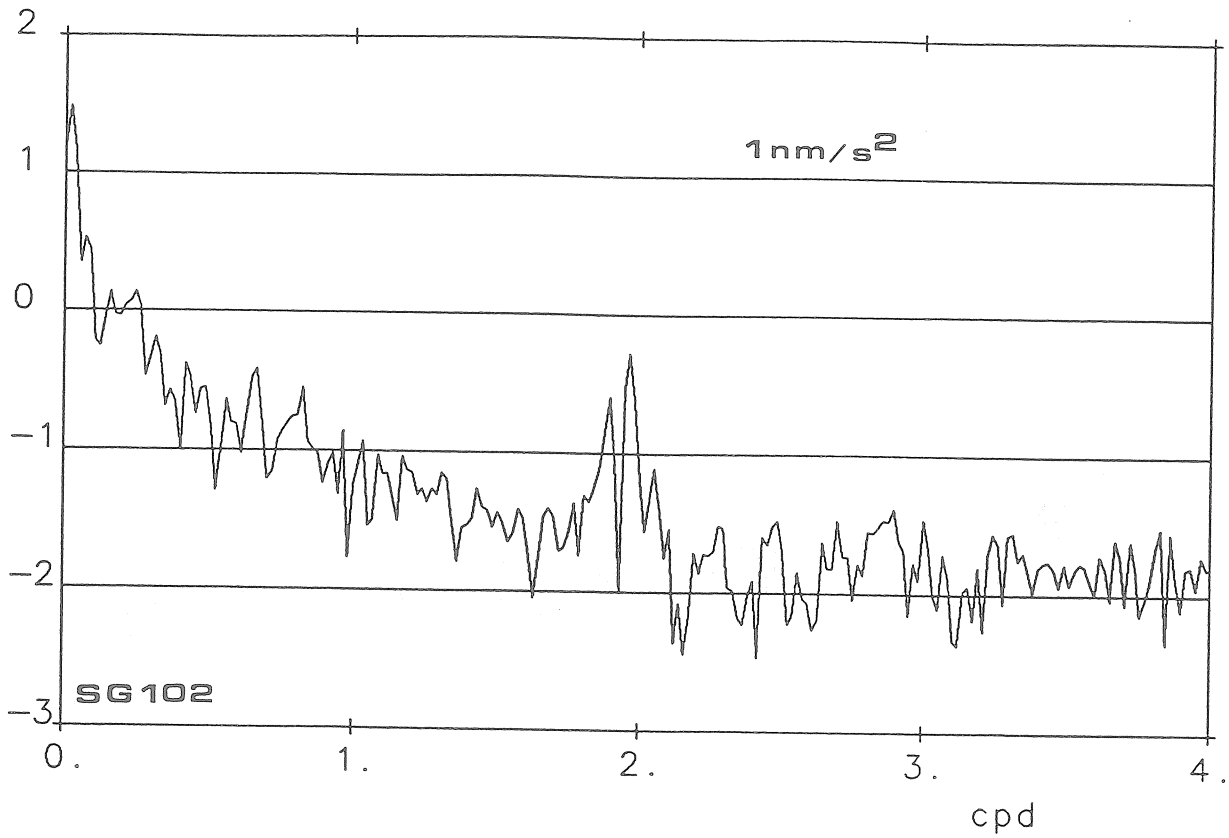

Figure 6: Fourier amplitude spectrum in nm/s^2 between 0 and 4 cpd of detided and depressured preprocessed 5 min data of gravimeter SG102.

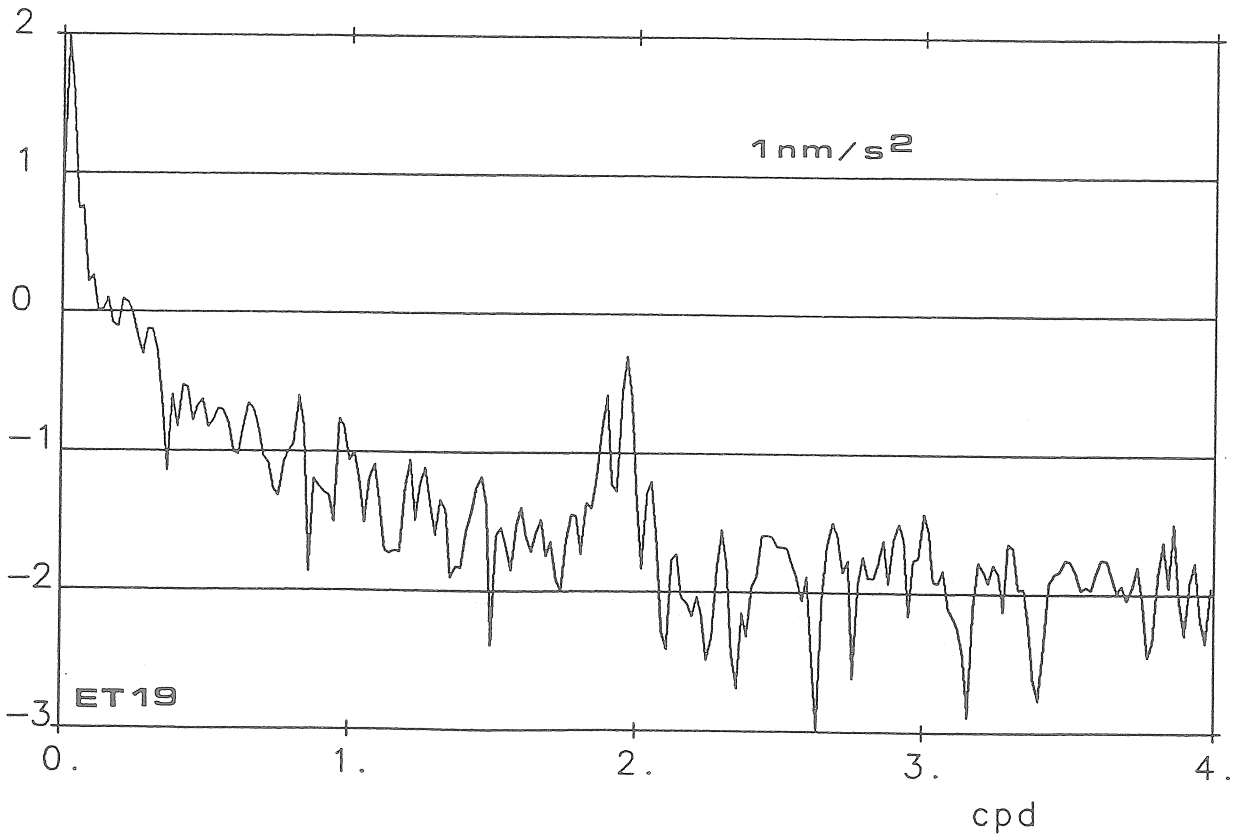

Figure 7: Fourier amplitude spectrum in nm/s^2 between 0 and 4 cpd of detided and depressured preprocessed 5 min data of gravimeter ET19.

ET19 between 0 and 4 cpd. For frequencies between 0.5 and 4 cpd, there can hardly be seen any difference between both spectra. For frequencies above 4 cpd, the noise level of the SG102 is about two times that of the ET19. In Tab. 1 is given the rms Fourier amplitude spectrum for both gravimeters at different frequency ranges. We can see that the SG102 is superior below 0.2 cpd, whereas the ET19 is superior above 0.2 cpd.

Table 1: Rms noise level for gravimeters SG102 and ET19

frequency [*cpd*]	SG102 [nm/s^2]	ET19 [nm/s^2]	relation SG102/E19
0.05 ... 0.10	2.80200	4.67300	0.60
0.10 ... 0.20	0.93100	1.17800	0.79
0.20 ... 6.00	0.16300	0.15000	1.08
6.00 ... 12.0	0.00553	0.00343	1.61
12.0 ... 24.0	0.00268	0.00130	2.06
24.0 ... 36.0	0.00193	0.00101	1.91
36.0 ... 48.0	0.00166	0.00064	2.59
48.0 ... 60.0	0.00144	0.00059	2.44
60.0 ... 72.0	0.00135	0.00049	2.76
72.0 ... 84.0	0.00116	0.00041	2.83
84.0 ... 96.0	0.00100	0.00036	2.78

4 Data analysis and comparison

The preprocessed hourly data for both gravimeters are given in Fig. 8; there can hardly be seen any difference except that there might exist a larger drift of gravimeter ET19. The hourly data were analyzed using the ETERNA 3.0 earth tide analysis program (Wenzel 1994b) applying highpass filtering, the tidal potential development of Tamura (1987), and a linear regression with airpressure. The standard deviations were 0.737 nm/s^2 for gravimeter SG102 and 0.556 nm/s^2 for gravimeter ET19. The adjusted airpressure regression coefficients were -3.28 and - 3.37 nm/s^2 per hPa for the SG 102 and ET19 resp. The residuals are given for both gravimeters in Fig. 9, showing slightly larger residuals for gravimeter SG102. There obviously exist a high correlation between the residuals of both gravimeters. A correlation analysis of the residuals of both gravimeters (Fig. 10) yields a correlation of 0.82.

Because the residuals of both gravimeters are highly correlated, we believe that they reflect to a large extend the so-called gravity model noise (unmodelled gravity signals from the earth, atmosphere and hydrosphere). We have computed an approximation to the gravity model noise by taking the average of both residuals at the same instant. An approximation to the instrumental noise is then given by the difference of the individual residual to the average. Because we had only two gravimeters running in parallel, we cannot decide from this simple approximation which gravimeter has larger instrumental noise. Both model noise and instrumental noise (average of both instruments) is shown in Fig. 11. The rms model noise was estimated to 0.61 nm/s^2 and the rms average instrumental noise was estimated to 0.21 nm/s^2. This demonstrates that both gravimeters have a very low instrumental noise of about $2 \cdot 10^{-11}$ g in the frequency range 1 ... 12 cpd, whereas the gravity model noise is about three times larger. We have also given in Fig. 11 the highpass filtered air pressure, which seems to be in some way correlated with the model noise. But naturally the linear correlation coefficient between highpass

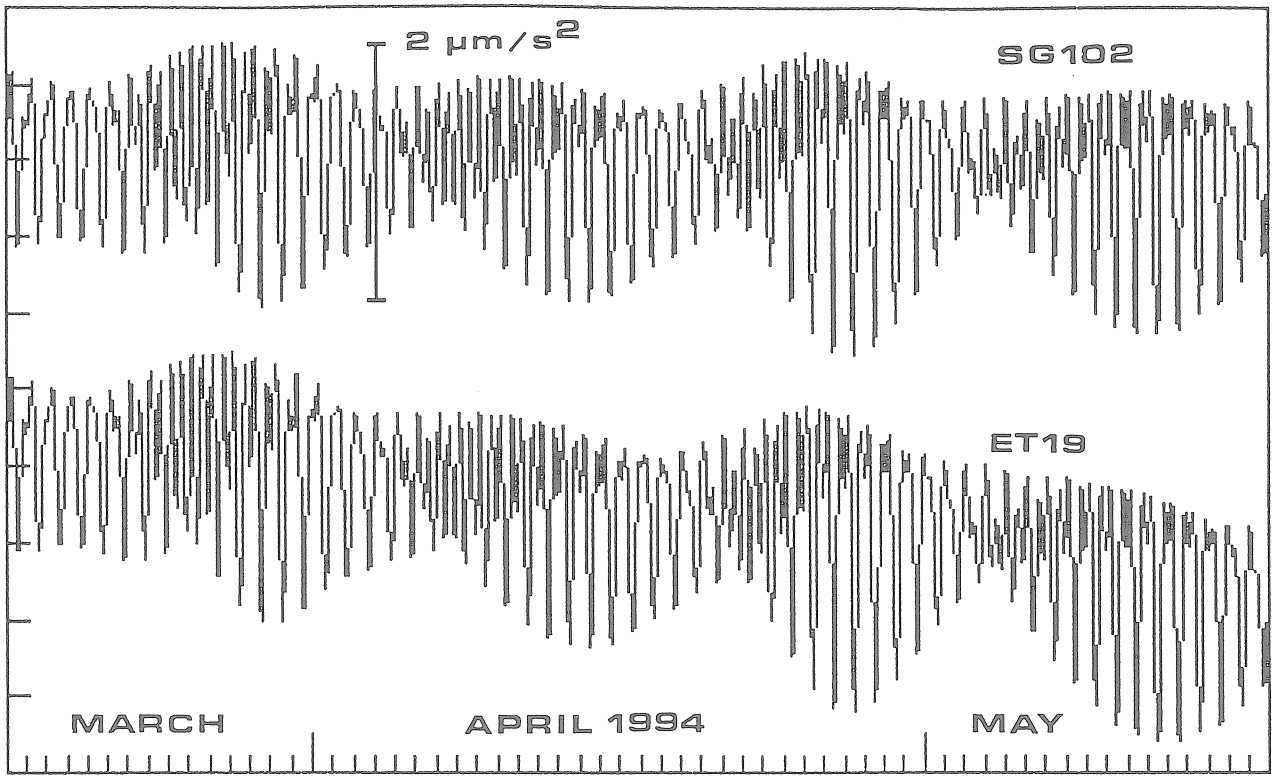

Figure 8: Hourly data of gravimeters SG102 and ET19, March 17th to May 17th, 1994.

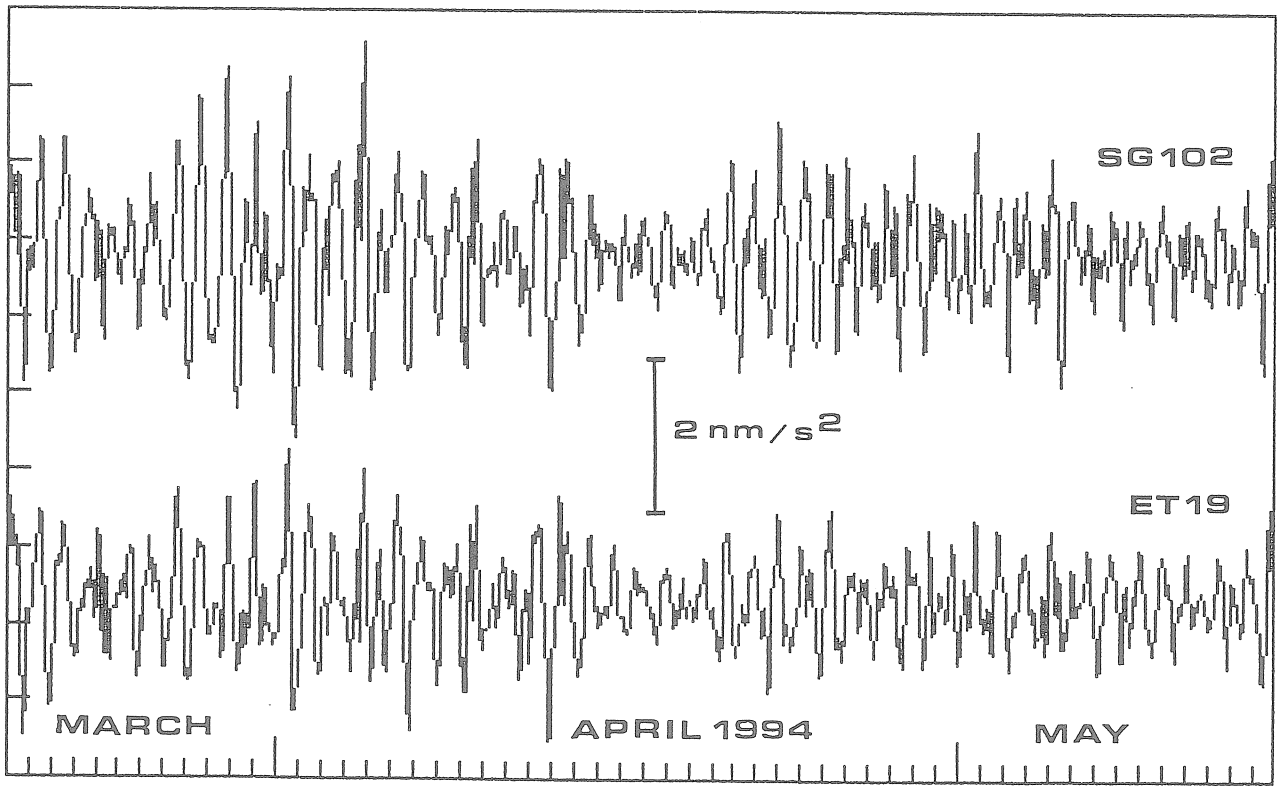

Figure 9: Residuals of gravimeters SG102 and ET19, March 17th to May 17th, 1994.

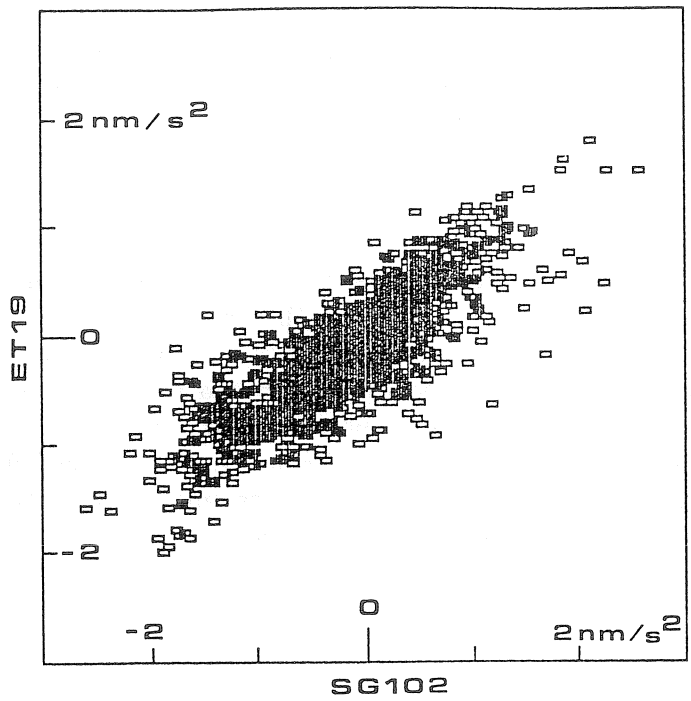

Figure 10: Regression of residuals of gravimeters SG102 and ET19.

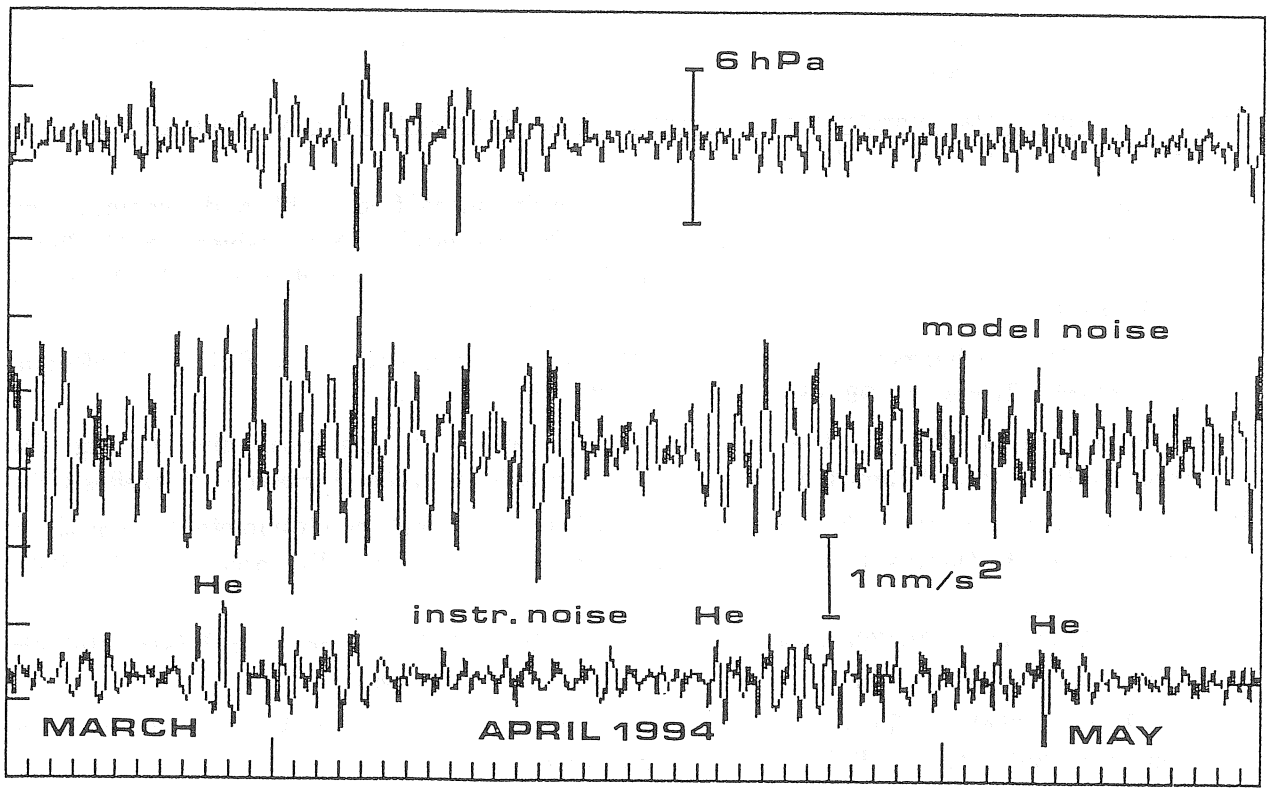

Figure 11: Bandpass filtered air pressure (top), model noise (middle) and instrumental noise (bottom) from gravimeters SG102 and ET19.

filtered air pressure and residuals is zero, because the linear regression between highpass filtered air pressure and highpass filtered gravity has been taken out by the adjustment with ETERNA. The time dependent correlation function between highpass filtered air pressure and residuals shows only weak correlations of about ± 0.2 within $\pm 24^h$ time lag.

5 Conclusions

From the analysis of the first 62^d of gravity recorded with the superconducting gravimeter SG102 and the LaCoste-Romberg spring gravimeter ET19 at the low noise site BFO Schiltach, we can conclude that both gravimeters have a very low instrumental noise of about $2 \cdot 10^{-11}$ g in the frequency range 1 to 12 cpd. The gravity model noise (unmodelled gravity signals generated by the earth, atmosphere or hydrosphere) is about three times larger (about $6 \cdot 10^{-11}$ g) than the instrumental noise in the frequency range from 1 to 12 cpd. For frequencies below 0.2 cpd, the superconducting gravimeter SG102 is superior to the spring gravimeter ET19. For frequencies above 0.2 cpd, the spring gravimeter ET19 shows about two times less noise than the superconducting gravimeter SG102. The last conclusion is supported by comparisons of the free mode channels of both gravimeters (Zürn et al. 1994).

References

Larson, J. (1968): A cross correlation study of the noise performance of electrostatically controlled LaCoste and Romberg Gravimeters. PhD. Thesis, Maryland University, 1968.

Prothero, W.A. and J.M. Goodkind (1968): A superconducting gravimeter. The Review of Scientific Instrumnets, 39, no. 9, 1257-1262, 1968.

Richter, B. (1987): Das supraleitende Gravimeter. Deutsche Geodätische Kommission, Reihe C, Heft Nr. 329, Frankfurt a.M. 1987.

Richter, B. and W. Zürn (1988): Chandler effect and nearly diurnal free wobble as determined from observations with a superconducting gravimeter. Proceedings IAU Symposium 128, Coolfont, Virgina 1986: The Earth's Rotation and Reference Frames for Geodesy and Geodynamics (A.K. Babcock and G.A. Wilkins, Eds.), IAU, 309-315.

Tamura, Y. (1987): A harmonic development of the tide generating potential. Bulletin d'Informations Marées Terrestres, 99, 6813-6855, Bruxelles 1987.

Vetter, M. and H.-G. Wenzel (1994): PREGRED - an interactive graphical editor for digitally recorded tidal data. Submitted to Bulletin d'Informations Marées Terrestres, Bruxelles 1994.

Weber, J. and J.V. Larson (1966): Operating of LaCoste and Romberg Gravimeter at sensitivity approaching the thermal fluctuation limits. Journal of Geophysical Research, 71, 6006-6009, 1966.

Wenzel, H.-G. (1994a): PRETERNA - a preprocessor for digitally recorded tidal data. Bulletin d'Informations Marées Terrestres, 118, 8722-8734, Bruxelles 1994.

Wenzel, H.-G. (1994b): ETERNA - an earth tide analysis program package for the personal computer. Submitted to Bulletin Geodesique, 1994.

Zürn, W., H.-G. Wenzel and G. Laske (1991): High quality data from LaCoste-Romberg gravimeters with electrostatic feedback: A challenge for superconducting gravimeters. Bulletin d'Informations Marées Terrestres, 110, 7940-7952, Bruxelles 1991.

Zürn, W., R. Widmer, B. Richter and H.-G. Wenzel (1994): Comparison of free oscillation spectra from different instruments. Submitted to Bulletin d'Informations Marées Terrestres, Bruxelles 1994.

Comparison of free oscillation spectra from different instruments

W. Zürn, R. Widmer
Black Forest Observatory Schiltach, Heubach 206, D - 77709 Wolfach, Germany

B. Richter
Institute for Applied Geodesy, Richard Strauss-Allee 11, D - 60598 Frankfurt, Germany

and

H.-G. Wenzel
Geodetic Institute, University of Karlsruhe, D - 76128 Karlsruhe, Germany

1 Instrument comparison

Free oscillations of the earth have been very well observed by the LaCoste-Romberg gravimeters with electrostatic feedback of the IDA - network (Agnew et al., 1986), which was scientifically extremely successful. Zürn et al. (1991) list a series of achievements which became only possible after its installation. The operators of superconducting gravimeters have so far failed to demonstrate conclusively that their devices have lower instrumental noise in the frequency band of the free oscillations of the earth than the spring gravimeters of IDA or other high-performance modern long-period seismographs.

At the Schiltach underground observatory (BFO) in SW-Germany a superconducting gravimeter GWR-102 (half-inch sphere, 50 l Dewar and no refrigeration) was temporarily installed in 1994 (Richter et al.: Comparison of a Cryogenic and a Spring Gravimeter between 0.2 and 96 cpd at BFO Schiltach, this volume). This provided the opportunity of recording simultaneously with several instruments at the same station under identical conditions the free oscillations of the earth and comparing signal-to-noise ratios (SNR). The transfer functions of the different sensors need not be corrected for in such a comparison. However, it should be noted that whatever the conclusions are, they rigorously apply only to the individual sensors tested and not necessarily to the whole sets of their kind.

We conducted a comparison between four long period vertical seismometers: the mode channel of the superconducting gravimeter GWR-102, the mode channel of LCR - ET-19 (electrostatic feedback), the very long period (VLP) channel of an STS-1 vertical seismometer and the LP channel of the vertical component of an STS-2 triaxial seismometer. The broadband STS-1 leaf spring seismometer was described by Wielandt and Streckeisen (1982) and is deployed in a large percentage of the stations of the global digital seismic networks, like GEOSCOPE

(Romanowicz et al., 1984), IRIS/IDA (e. g. Given, 1990) and others. The three-component, very broadband leaf-spring seismometer STS-2 by the same manufacturer is also deployed in global and regional seismic networks, for example in the German Regional Seismic Network (GRSN). This seismometer has not been described in the literature as yet, so we have to refer to the manufacturer's manual (Streckeisen, G., 1990: Portable Very-Broad-Band Triaxial Seismometer STS-2, Pfungen, Switzerland).

For BFO it has been demonstrated that it is a low noise site in a wide frequency band (Wenzel et al., 1991; Zürn et al., 1991; Widmer et al., 1992). All four instruments were located behind the air-lock, where ambient temperature stability is a few mK (unless disturbed by man) and the distances to the surface are 150 m vertically and 450 to 550 m horizontally. The data from the gravimeters and the STS-1/Z were recorded with a 5 s sampling interval defined with an accuracy better than 0.1 ms and a resolution of 21 bit on the same data acquisition system. The data from the STS-2/Z were digitized with a sampling rate of 1 Hz and a resolution of 24-bit directly at the seismometer, while the signals from the other three instruments had to be brought to the digitizer through analog cables over distances between 70 and 350 m. As a critical frequency range for comparison we chose the band between 0.25 and 1.3 mHz, where the lowest order free modes of the earth have their eigenfrequencies. It is very hard to observe these gravest modes of the earth, because even by very large earthquakes these are not excited to large amplitudes and because of their very low frequencies.

The deep earthquake in Northern Bolivia (641 km) on June 9, 1994 was selected for a comparison here, but the results were confirmed by similar analyses for other very large seismic events. Both seismometers stayed within their dynamic range during the first Rayleigh-wave arrivals, while both gravimeters did not. A necessary liquid Helium refill for the GWR-102 could not be delayed by more than about 3.5 days after the quake and caused a severe disturbance of this gravimeter. Therefore two 80 hour long windows from about 5 to 85 (window 1) and 87 to 167 hrs (window 2) after the earthquake were selected for the comparison. For the purpose of comparing the SNRs of different instruments at their best the actual window or quake used is not an important issue, provided there is a large signal present and none of the instruments is perturbed. Both conditions were satisfied for all sensors in these two windows. All 8 records were decimated from their original sampling rates to sampling intervals of 40 s after low-pass filtering for prevention of aliassing. The records were multiplied by identical Hanning windows and Fourier transforms computed. The spectra for both windows were normalized to have the same peak amplitude for the overtone ${}_3S_1$ (0.94256 mHz), which happened to be very strongly excited by this quake.

Window 1 is a normal time window for free oscillation analyses starting only a few hours after the quake and lasting more than three days. The gravest mode ${}_0S_2$ is not above the noise but ${}_0S_3$ can be detected in all four data sets. The

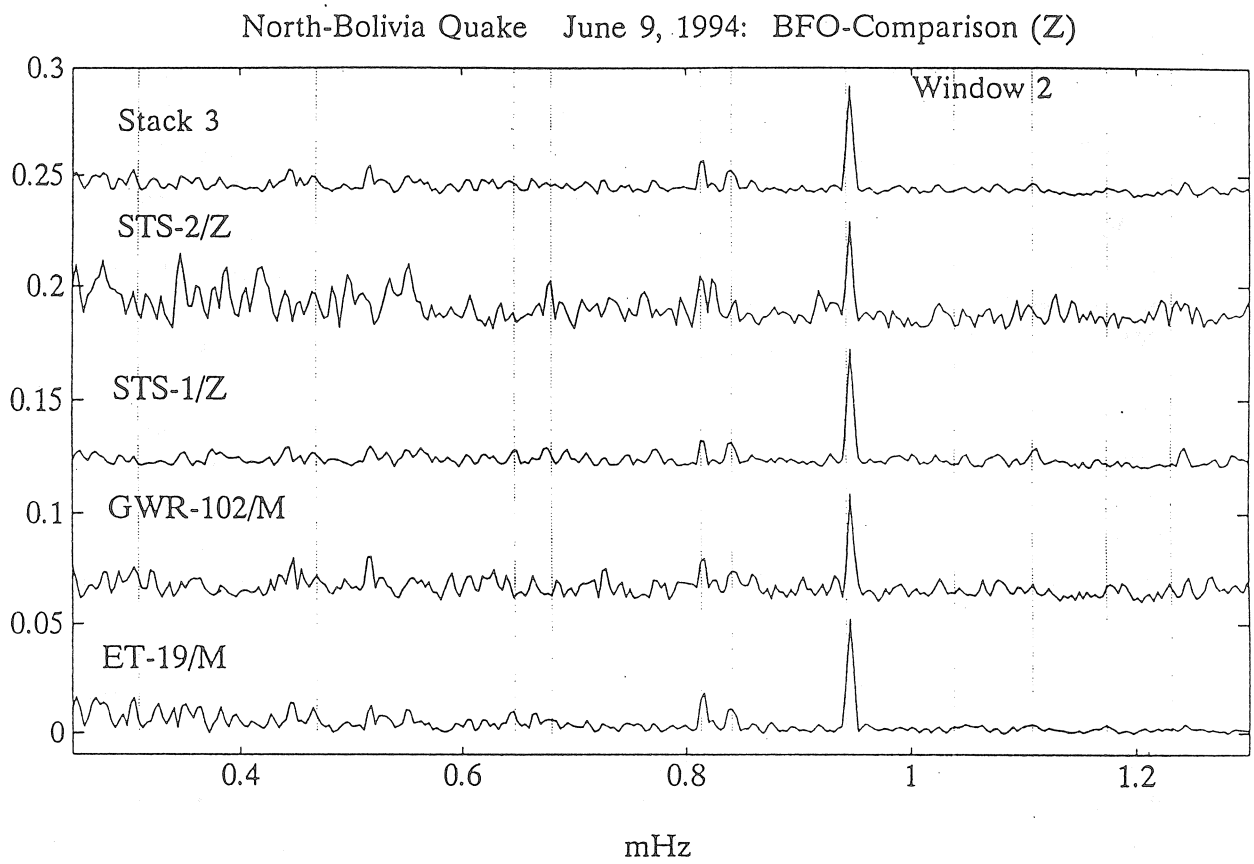

Fig. 1: Amplitude spectra for time window 2 from about 87 to 167 hrs after the Northern Bolivia 641 km deep earthquake of June 9, 1994. Sensors are indicated at left. Top trace (Stack 3) is average of lowermost three. All amplitudes normalized to maximum spectral amplitude (Mode 3S1). Vertical dotted lines indicate theoretical degenerate eigenfrequencies from earth model 1066A (Gilbert and Dziewonski, 1975), from the left for the modes: ${}_0S_2$, ${}_0S_3$, ${}_0S_4$, ${}_1S_2$, ${}_0S_0$, ${}_0S_5$, ${}_3S_1$, ${}_0S_6$, ${}_3S_2$, ${}_1S_4$ and ${}_0S_7$.

higher mode ${}_3S_1$ was the strongest mode in this frequency window. ${}_1S_2$ and ${}_0S_0$ are barely above the noise levels, but can clearly be seen. The first observation was that the STS-2/Z has smaller SNRs for all peaks in this band. For all modes the differences between the three other sensors are very tiny, but it appears that the GWR-102 has very slightly inferior SNRs compared with the other two.

Window 2 starts after most fundamental spheroidal modes have died out because of their lower Qs caused by high fractions of shear energy. The only modes visible (Fig. 1) above the noise are ${}_0S_0$, ${}_0S_5$ and ${}_3S_1$. As in window 1 the SNR of the STS-2/Z is obviously lower than for the other three sensors. It is much clearer here that the GWR-102 is slightly inferior to the ET-19 and STS-1/Z, as far as SNRs go. The fundamental mode ${}_0S_5$ cannot be distinguished from the noise in the GWR-102 spectrum, while it is above the noise floor for the ET-19 and STS-1/Z. No clear decision can be made which one of the two latter instruments is the better one in this respect. It is interesting to compare similarities in the spectral structure of the noise between 0.4 and 0.8 mHz for the two best instruments, however there are also some distinct differences.

The conclusions from the evidence presented (and additional results not shown here) are the following. Clearly the STS-2/Z cannot compete in this frequency band with the other three instruments at a very low noise site. However, one has to keep in mind, that in window 1 the mode ${}_0S_3$ was well above the noise and this places this instrument at this station also into the upper class of the global digital seismic network at very long periods (many seismograms were inspected). The other three sensors, the STS-1/Z and the mode channels of the two gravimeters, are very excellent long period seismometers. However, the GWR-102 appears to be very slightly, but clearly more noisy than the other two. The source of this additional noise must be of instrumental origin, while we cannot easily decide if there are instrumental contributions to the noise for ET-19 and STS-1/Z. However, some differences in spectral structure, not in absolute levels, of the noise from these two sensors appear to indicate instrumental noise sources in one or both of the two.

2 The parasitic mode of the superconducting gravimeter

Every owner of a superconducting gravimeter is familiar with a high Q parasitic mode of these instruments, which is believed to be a rotational oscillation of the suspended sphere coupling into the vertical force - balance. No publication exists on this mode to the knowledge of the authors. The eigenfrequency of this mode differs from instrument to instrument, but is always (to our knowledge) located in the free oscillation band of frequencies. For the GWR-TT40

at Bad Homburg (1983/84) this eigenmode had an eigenfrequency of 5.11 mHz (corresponding to 3.26 min period) and a Q of about 40. This mode is to our experience never excited by teleseismic or regional events. However, every time the instrument is touched, for example during the refilling with liquid Helium, strong excitations occur and due to the small damping this mode persists for several hours. This was regularly observed after the refills in GWR-102. The mode channel data were used to study this mode in some detail and interesting properties were found. The average frequency found from 9 individual excitations is 36.186 ± 0.147 mHz and the Q was determined to be 250. However, there might be systematic influences involved in this estimate because of a special observation. This special case concerned an excitation to very large amplitude by a liquid Helium-refill on May 5, 1994. Results of a detailed analysis of this data are shown in Fig. 2. The upper left panel shows the digital time series from the mode channel of GWR-102 after high-pass filtering with a cutoff-period of 50 s. The modulation of the mode in amplitude occurs simultaneously with a slow return of the tide-signal to a stable position, well after the refilling was finished. Part of the spectrum of this record is shown in the upper right panel. While the peak of the spectral line is very near to the normal eigenfrequency, the line shape is highly asymmetric. Since it was not expected that the amplitude-modulation in the time series would cause such an asymmetric line-shape, further investigations were in order. The lower left panel shows a plot of the 'instantaneous frequency' vs. time of these oscillations determined by first calculating the Hilbert-transform of the signal and then determining, unwrapping and differentiating its phase as a function of time. The frequency of the parasitic mode increases slowly from about 25 mHz to its small-amplitude value near 36 mHz. This is the reason for the large asymmetry of the spectral peak. The time series in this panel is shortened at the end, because the 'instantaneous frequency' becomes very unstable, when the mode amplitude approaches the noise level. Another method to depict the frequency change is the phasor-walkout method (Zürn and Rydelek, 1994). The walkout for a test frequency of 36.000 mHz is shown in the lower right panel. At the origin of the complex plane, corresponding to the beginning of the time series, the frequency of the mode obviously is lower than the test-frequency as seen from the strong curvature to the left. This curvature then slowly decreases as the mode-frequency approaches the test-frequency. The walkout straightens out, when the mode-frequency equals the test-frequency and then curves to the right with continuously increasing curvature. Note that at the end of the time series the mode frequency is only about .2 mHz higher than the test-frequency in this walkout. Zürn and Rydelek (1994) show a synthetic example very similar to this real observation in a physical instrument. All this means, that the eigenfrequency of the parasitic mode obviously depends on amplitude, indicating nonlinear properties of the physics of this mode.

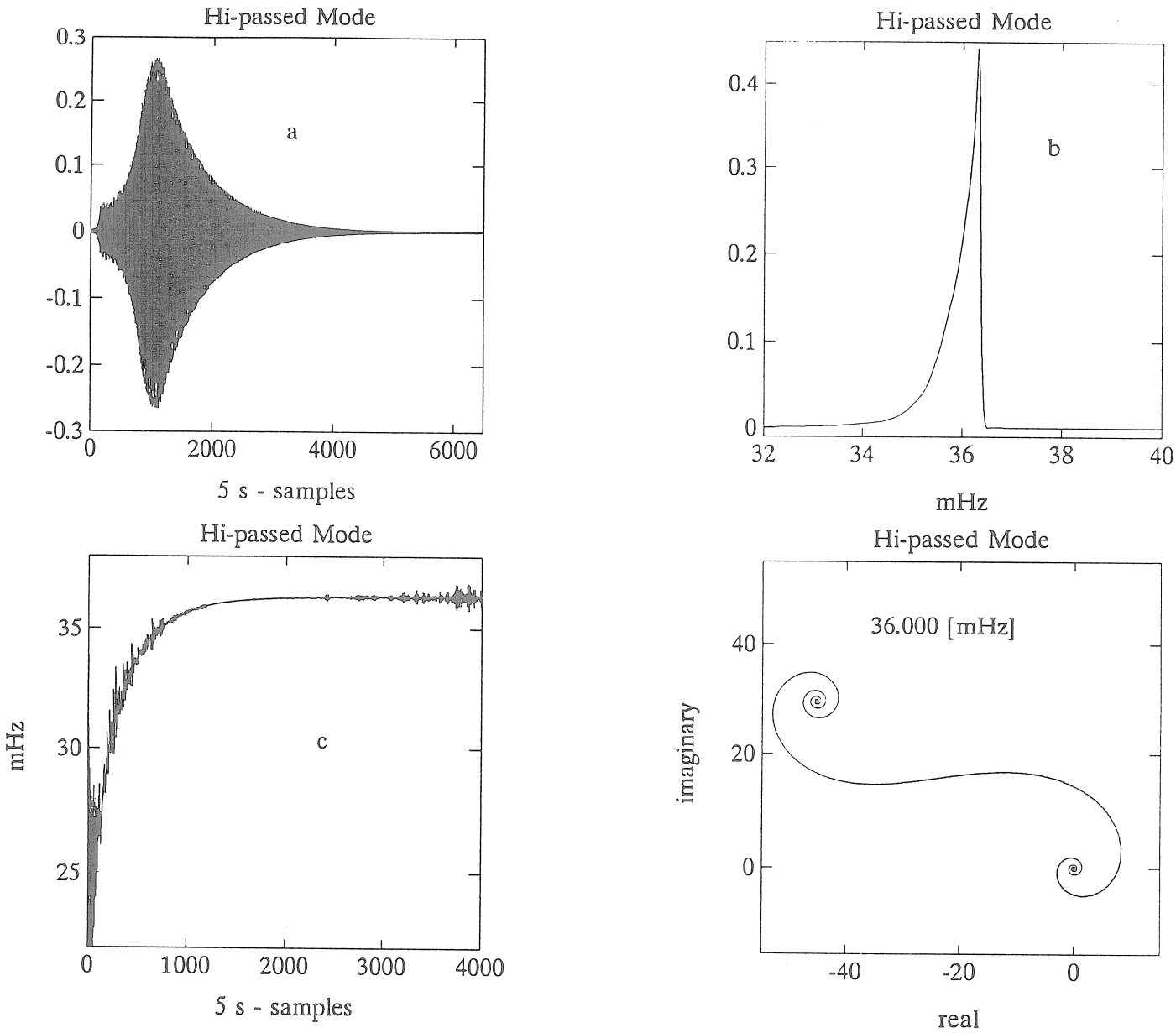

Fig. 2: Sphere rotational mode of GWR-102 after Liquid Helium refill on May 5, 1994. Data from mode-channel of the instrument. a) Time series after high-pass filtering with cutoff-frequency of 20 mHz. b) Section of amplitude spectrum of this time series after application of Hanning window. Not asymmetry of spectral line. c) Instantaneous frequency of the parasitic mode versus time for first part of the time series in a). d) Phasor-walkout of this time series for test-frequency of 36.000 mHz, slightly to the left of maximum spectral amplitude in b). Curvatures to the left or right indicate positive or negative frequency-difference between test- and actual oscillation-frequency in time series.

Acknowledgements

Special thanks are extended to Heinz Otto (BFO), Peter Wolf (IfaG) and Walter Grossmann (BFO) for their enthusiasm during this experiment. We also thank Dirk Ansorge for maintaining the air quality in the vault during several liquid Helium refills.

References:

Agnew, D.C., Berger, J., Farrell, W.E., Gilbert, J.F., Masters, G., Miller, D., 1986 : Project IDA: A Decade in Review.
EOS (Trans. AGU) 67, 16, 203 - 211

Gilbert, F., Dziewonski, A. M., 1975: An Application of Normal Mode Theory to the Retrieval of Structural Parameters and Source Mechanisms from Seismic Spectra.
Phil. Trans. R. Soc. Lond., A278, 187 - 269

Given, H. K., 1990: Variations in broadband seismic noise at IRIS/IDA stations in the USSR with implications for event detection.
Bull. seismol. Soc. Am., 80, Part B, 2072 - 2088.

Romanowizc, B., Cara, M., Fels, J.F.and Rouland D., 1984. GEOSCOPE: A French initiative in long period three component global seismic network.
E.O.S., Trans. Am. Geophys. Union, 65: 753-754.

Wenzel, H.-G., Zürn, W., Baker, T.F., 1991: In Situ Calibration of LaCoste-Romberg Earth Tide Gravity Meter ET19 at BFO Schiltach.
Bull. Inf. Marees Terrestres, 109, 7849 - 7863

Widmer, R., Zürn, W., Masters, G., 1992: Observation of Low-order Toroidal Modes from the 1989 Macquarie Rise Event.
Geophys. J. Int., 111, 226 - 236

Wielandt, E., Streckeisen, G., 1982: The Leaf-Spring Seismometer: Design and Performance
Bull. Seism. Soc. Am. 72A, 6, 2349 - 2368

Zürn, W., Rydelek, P. A., 1994: Revisiting the Phasor-Walkout Method for Detailed Investigation of Harmonic Signals in Time Series.
Surveys in Geophysics, 15, 409 - 431

Zürn,W., Wenzel,H.-G., Laske, G., 1991: High quality data from LaCoste-Romberg gravimeters with electrostatic feedback: A challenge for superconducting gravimeters
Bull. Inf. Marees Terrestres 110, 7940 - 7952

Underground SG–gravity record at the Asse/Northern Germany: Air pressure effects and long–term drift

Jentzsch[1], G., C.Kroner[1], D. Flach[2], G.Gommlich[2]

Extended Abstract

These investigations are a co–operation of the GSF–Forschungszentrum für Umwelt und Gesundheit, GmbH, and the Institute for Geophysics of the TU Clausthal.
Since April 1989 a superconducting gravimeter basing on the gravimeter type TT70 is recording at the 750 m level in the salt mine Asse in Northern Germany. The instrument was conceived by GWR as a movable system. It turned out that moving the gravimeter caused more disturbances than initially expected. The period of time that had to be waited for until the gravimeter became stable was also longer than intended. The gravimeter therefore was used stationarily. The goal of the gravity measurements is to get information about the vertical component of the strain tensor.
For the first three years, from April 1989 until March 1992, only an analog record is available. The installation in the mine and the results of this first period are given by Flach et al. (1993). In March 1992 the gravimeter started recording with a digital recording system. The digital time series is processed until September 1993.
The effects of air pressure in the gravity data were eliminated by applying admittance functions, a method suggested in Beijing by Crossley & Jensen (1993).
As a result of the larger data gaps and the seasonal variations in the correlation between gravity and air pressure admittance functions were calculated for different parts of the digital data. The functions finally used for the air pressure reduction contained in the longer periods (periods $\geq$ 1 week) an admittance function calculated for the entire data set, and in the shorter periods the seasonal admittance functions.
With regard to the strong dèpendence of the admittance function on the data quality the analog data were handled in a something different way. In this case the air pressure reduction was carried out applying only the admittance function calculated for the whole data set. In this way it could be guaranteed that at least part of the noise did not influence the correlation between gravity and air pressure and that the frequency dependence of the regression coefficient was taken into account.
For the tidal analysis there is practically no difference in the results between using a single regression coefficient and applying frequency dependent admittance functions. However, the application of these functions leads to an improvement visible in the Fourier–spectrum of the digital data (fig. 1). The improvement is evident for periods longer than one day.

[1] Institut für Geophysik, TU Clausthal, Arnold–Sommerfeld–Str.1,
D–38678 Clausthal–Zellerfeld

[2] GSF–Forschungszentrum für Umwelt und Gesundheit, Postfach 2163,
D–38011 Braunschweig

After removing tides, annual and semi-annual tides were eliminated by using the theoretical amplitude factor of 1.16, and after the elimination of air pressure effects the long-period residuals are dominated by two effects: on the one hand there is a periodic signal and on the other hand the data contain a long-term drift. The periodic signal can be correlated with the effect of polar motion for the entire data set. The long-term drift consists of a strongly increasing part over the first 9 months which is followed by a nearly linear component. The linear drift is about 13 μGal/year. The analysis of the observed long-term drift will be subject to further investigations.

Further results as well as the discussion of the admittance functions are given by Jentzsch et al. (1994).

References

Crossley, D.J. & Jensen, O.G., 1993: Effective barometric admittance and gravity residuals.– Proc. 12th Symposium on Earth Tides, Beijing, Aug. 1993

Flach, D., Gommlich, G. , and Jentzsch, G., 1993: Three years of experiences with a movable superconducting gravimeter at the underground installation site in the salt mine Asse in Northern Germany.– Bull. Inf. Marées Terrestres, 117, 8639–8648

Jentzsch, G., Kroner, C., Flach, D. , and Gommlich, G., 1994: Long– and aperiodic effects in the recording of the superconducting gravimeter in the Asse salt mine in Northern Germany.– Proc. Second Workshop on 'Non Tidal Gravity Changes' at Walferdange, Luxembourg, Sept. 1994

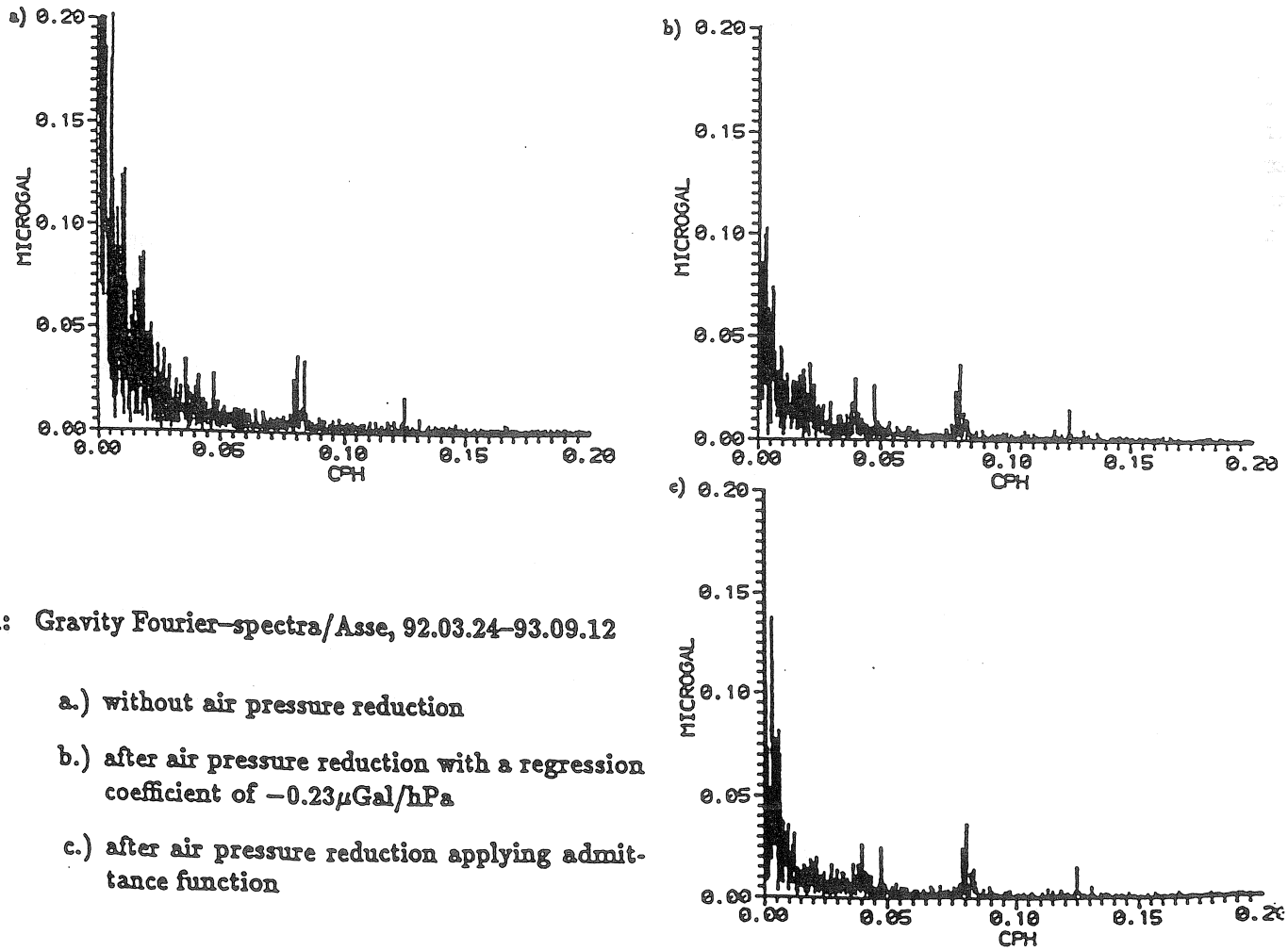

Fig. 1: Gravity Fourier–spectra/Asse, 92.03.24–93.09.12

a.) without air pressure reduction

b.) after air pressure reduction with a regression coefficient of −0.23μGal/hPa

c.) after air pressure reduction applying admittance function

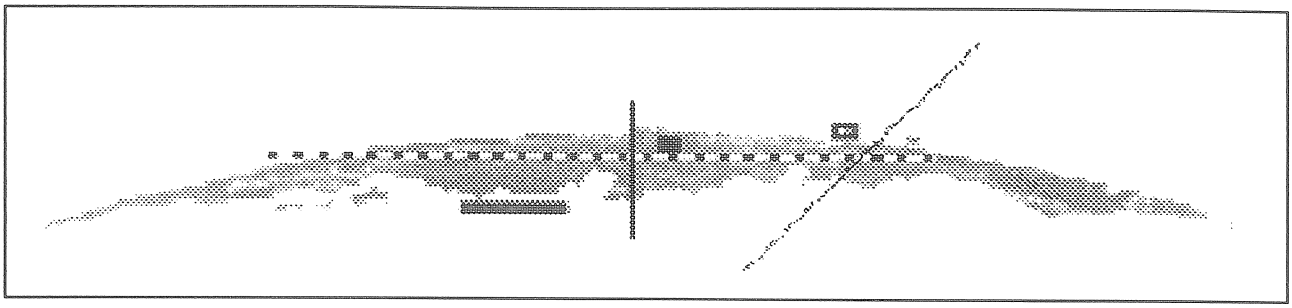

GeoForschungsZentrum Potsdam
Stiftung des öffentlichen Rechts

Telegrafenberg A17
D-14473 Potsdam

Proposal for an Information System and Data Centre for GGP-Data (GGP-ISDC)

B. Ritschel, J. Neumeyer, J. Wächter

Contents

Abstract

In cooperation with the project group Gravity Field and Figure of the Earth, the Data and Computing Centre (DCC) of the GFZ Potsdam plans to realize an Information System and Data Center (ISDC) for Superconducting Gravimeter (SG) data. This paper presents the ideas and the concept for a realisation of the ISDC and shall serve a proposal for a Global Geodynamics Project - Information System and Data Centre (GGP-ISDC).

The planned GGP-ISDC is an advancement of other GGP-Data Centre proposals, e.g. presented to the SEDI meeting in Vienna 1991 (Aldridge, Crossley, Mansinha, Smylie 1991). It will offer an easy and comfortable data access using special created data retrieval and data exchange software. The incoming GGP-data will

be checked for plausibility and format compatibility, to get harmonised and stable data archives. All data will be access protected and only on the demand of the project participants distributed. The GGP-ISDC will collect all relevant information and data presenting a consistent view of the up-to-date project state. To communicate with the GGP-ISDC a PC or workstation, access to the Internet and free WWW software (World Wide Web) is needed, e.g. the tool MOSAIC.

1. The Data and Computing Centre (DCC) of the GFZ Potsdam

The Data and Computing Centre (DCC) is a staff section of the GFZ Potsdam. Main tasks of the DCC are planning, installation and operation of an efficient infrastructure for the management and distribution of data in the field of geoscientific research. The DCC designs, develops and operates open information systems and database applications created with special database and hypermedia tools (RDBMS Sybase, 4GL Uniface, Gainmomentum, Mosaic) in cooperation with other project groups. It provides commercial and public information systems and databases.

The DCC administrates a heterogenious network linked to the Internet integrating PCs, workstations (SUN, HP, IBM) and mainframes (CONVEX 3820/3420). The data storage archive subsystem is based on a Metrum RSP-2150 using VHS cassettes.

The DCC itself is organized in a layered structure. The information layer offers the fields of information services, information systems, system analysis and data standards. The application layer covers the branches 4GL-software, hypermedia, Geographic Information Systems (GIS) and databases. The base layer offers file services, archive services and batch services.

2. Advantages of an Information System and Data Centre for GGP-Data (GGP-ISDC)

Modern information systems are sophisticated data management tools and powerful user interfaces integrated into conventional data centres. These information systems offer an online, flexibel and fast access to the ever increasing amount of data. To create and operate information systems, special knowledge about storage of data is necessary. This knowledge is concentrated in accessible meta data. Meta data are descriptions and documentations about data, covering the internal data structure and relations as well as the availability of data.

Our proposal for a GGP-ISDC is based on the concept for integrated information systems using meta data. Because of the consideration of the logical unit of exchange data and meta data the planned GGP-ISDC will offer not only the exchange data itself but also exchange data descriptions and methods about the measurement and data extraction processes. In addition, all

further relevant project accompanying data will be stored and offered as meta data too.

All project participants will have the same convenient access on desired meta and exchange data using easy to handle meta data retrieving and exchange data transfer tools linked to a graphic user interface (GUI).

All received data will be checked for plausibility, integrity and format compatibility, to create harmonized and complete databases and exchange data sets. The data access protection is realized by user and password dependent system rights.

A high degree of data disposal will be achieved using an up-to date relational database management system (RDBMS) and special file management and archive techniques. The data archives will be based on VHS cassettes and CD-ROM.

An important precondition to achieve a high benefit of the GGP-ISDC consists in a regulary receiving of project and exchange data from all participants.

3. GGP-data management (messages, meta data and exchange data)

Before explaining the data management in the GGP-ISDC it's necessary to clarify the meaning and the contents of the terms messages, meta data and exchange data regarding to the GGP. Messages contains short project accompainying data, e.g. project status meta data. Important meta data about exchange data are gravimeter site locations and geological structures, industrial noise, technical arrangements and parameters about the instrument, measurement conditions, the preprocessing and the environment (table 1). Exchange data are preprocessed and formated superconducting gravimeter (SG) measurement data, physically stored on files using the PRETERNA format including a header containing important meta data (Neumeyer 1993, Wenzel 1994a, Wenzel 1994b).

To understand the GGP-ISDC data management it's usefull to consider the different types of data and data flows as well as the data access interfaces. Figure 1 shows the data flows labelled by arrows from the data input (left side) to the data output (right side). Input and output data are messages, meta data and exchange data. The data exchange tools and communication ways are electronic mail (e-mail), File Transfer Protocol (FTP), World Wide Web (WWW), client server communication and Telnet. Generally the data transport medium is the Internet, but telephon lines and floppy disc will be supported too.

The central part of figure 1 describes the internal data flows between the different servers. The meta data (received by FTP or e-mail and extracted from messages and from the header of the exchange data) will be transformed into relational structures and loaded into the database. The checked exchange data (received by

Site location	-Longitude -Latitude -Height
Geological structure of the site	-Brief description
Industrial noise	-Brief description
Technical arrangement	-Brief description
Instrumental parameters	-Gradient of the SG -Tilting of the instrument
Measurement room or chamber parameters	-Temperature -Humidity
Data acquisition parameters	-Frequency response function (corner frequency and damping) of anti-aliasing filter -ADC-resolution -Sampling rate (hardware or software trigger) -Time base (accuracy)
Preprocessing parameters	-Frequency response function of the filter -Threshold of spike elimination -Number and size of corrected data steps -Time interval of data gaps (correction yes or no)
Environmental parameters	-Atmospheric pressure -Ground water level -Rainfall -Snow -Humidity

Table 1: Meta data regarding exchange data

FTP or floppy disc) will be compressed and stored within archives on VHS cassettes and CD-ROM. To preserve the logical connection between meta data and exchange data all necessary links will be managed by the RDBMS.

Figure 2 shows the Internet communication tools to deliver or receive GGP-data. In addition to the common used tools e-mail and FTP to exchange messages and data the GGP-ISDC will offer special meta data retrieval applications with a graphical user interface. The retrieval software designed with the 4GL Uniface will be based on a connection to the GGP-RDBMS server using the RDBMS client server communication. The Mosaic Internet browser connected to the GGP-ISDC WWW server offers hypermedia pages

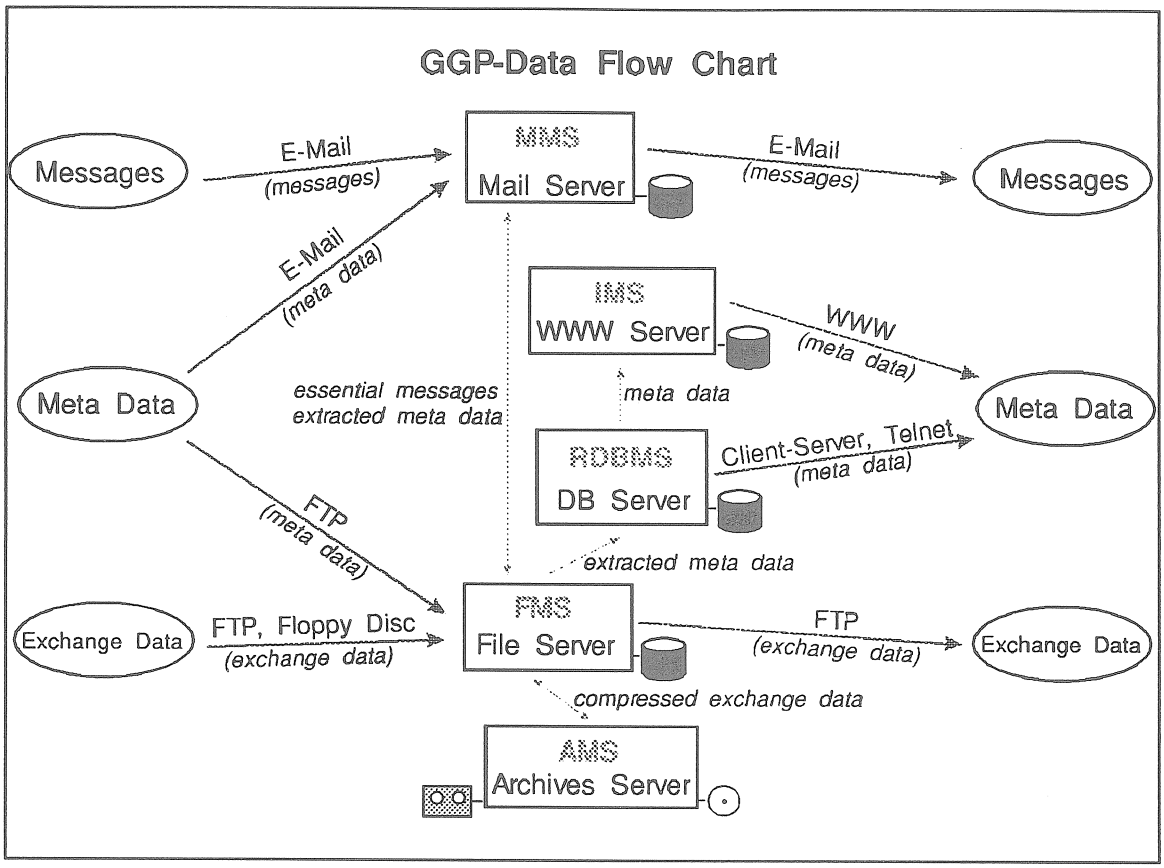

MMS: Mail Management System
IMS: Information Management System
RDBMS: Relational Database Management System
FMS: File Management System
AMS: Archive Management System

Figure 1: GGP-data flow chart

integrating meta data retrieval abilities using a special WWW-RDBMS interface. Mosaic also allows to start e-mail or FTP tools. In the case of slow data transfer rates the usage of the simple Telnet tool to communicate with the GGP-ISDC will be supported too.

To protect meta data and exchange data against improper use, only the data owner (person who delivered the data) will decide on the access rights and every access to the GGP-ISDC will be checked regarding user rights.

A data replication mechanism is essential to increase data safety and access speed for participants all over the world. Complete GGP-data set files containing meta and exchange data should be regulary exchanged with other data centres.

After achieving special project phases and setting up complete GGP-databases and archives, the GGP-ISDC will offer GGP-data set files on CD-ROM.

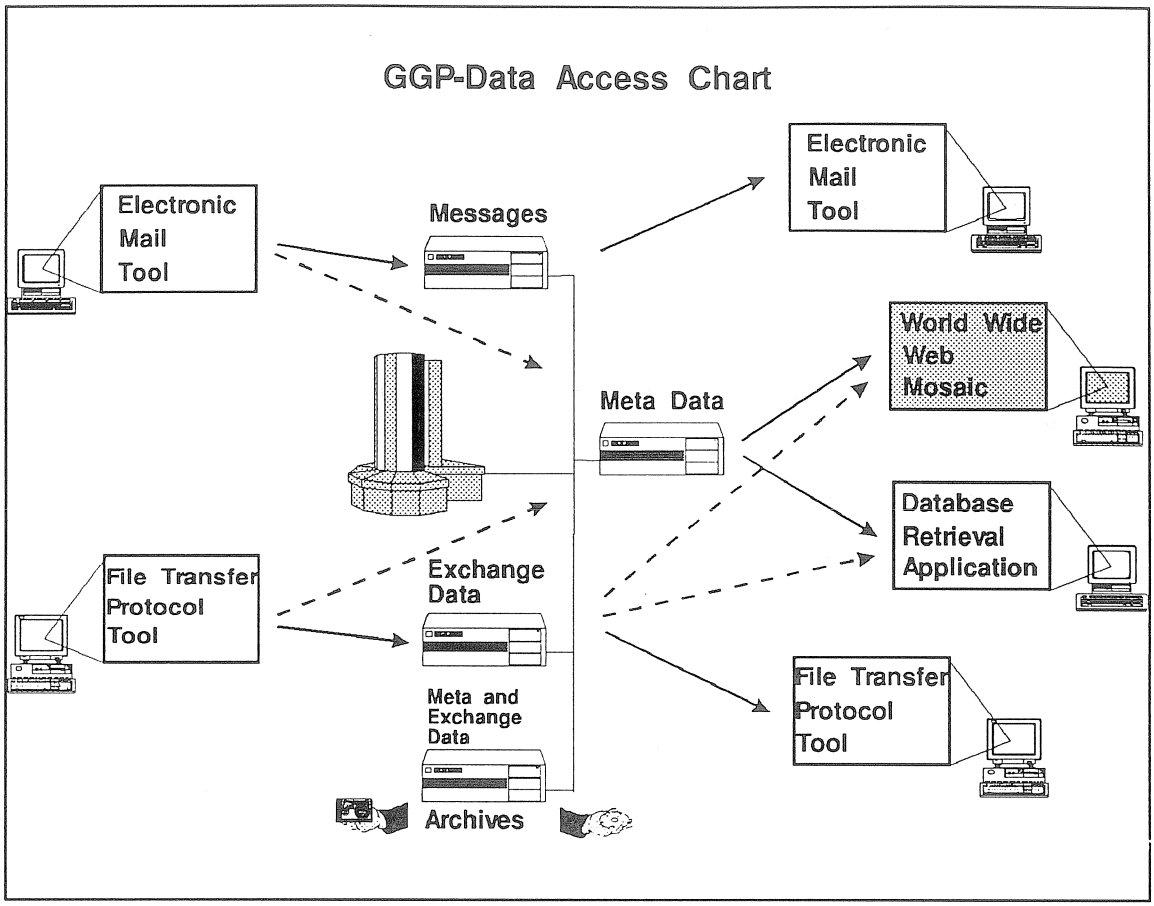

Figure 2: GGP-data access chart

4. User requirements for participation in GGP-data exchange

To take part in data exchange with the GGP-ISDC the project participant only needs a workstation or PC and access to the Internet.

A WWW client and the Internet browser Mosaic are the only necessary software. Both software products are freeware. The installation of a Sybase client on the remote workstation or PC allows using special Uniface retrieval programs to communicate with the GGP-ISDC.

The communication program Telnet can be used to set up an ASCII terminal connection.

Even with no Internet access data exchange is possible using modem or floppy disc.

5. Concrete tasks for the realisation of the GGP-ISDC

To realize the GGP-ISDC in the GFZ Potsdam following steps are planned:

- All GGP-participants are invited to, take part in GGP-data exchange.

- To create an exact and complete GGP-data flow model, knowledge is necessary about the amount and the structure of exchange data as well as accumulation, processing, storage, archiving and distribution of data. The meta data and exchange data file format must be defined and fixed.

- A special meta data model must be designed for the RDBMS in consideration of links to the matching exchange data. It will be used to create all necessary database objects.

- Both, the data flow model and the data model are required to design Uniface and Mosaic based database retrieval applications.

- Extensive live communication and data exchange tests have to be carried out in cooperation with partners, e.g. other data centres to check and to improve the GGP-ISDC applications.

References

Aldridge, K., Crossley D.J., Mansinha L., Smylie D.E. (1991): GGP: The Global Geodynamics Project (Working Version, April 15, 1991). Tiré à des Cahiers du Centre Européen de Géodynamique et de Séismologie. Volume 3 - 1991

Neumeyer, J. (1993): Acquisition, preprocessing and evaluation of GFZ Potsdam SCG data. Presented at the meeting of the Working Group on High Precision Tidal Data Processing, 1993

Wenzel, H.-G. (1994a): PRETERNA - a preprocessor for digitally recorded tidal data. Bulletin d'Informations Marées Terrestres, 118, 8722-8734, Bruxelles 1994

Wenzel, H.-G. (1994b): Format and structure for the exchange of high precision tidal data. To be presented at the meeting of the Working Group on High Precision Tidal Data Processing, August 30 - September 2, Bonn, Germany

Identification of quarter-diurnal tidal waves in Superconducting Gravimeter Data

Nicolas Florsch, Jacques Hinderer* & Hilaire Legros*

Laboratoire de Géophysique Appliquée, Université P. et M. Curie, Paris, France
* Ecole et Observatoire de Physique du Globe, Strasbourg, France

Abstract

We show here that quarter-diurnal tidal waves of lunisolar origin can be identified in high quality Superconducting Gravimeter data However a number of numerical treatments (filtering, degapping, despiking) has to be applied to raw gravity data corrected for local pressure changes in order to lower significantly the residual noise level. This level allows then to detect weak gravity changes of a few nanogal amplitude in the period range of some hours.

Introduction

When considering the spherical harmonic expansion of the tidal potential, the dominant terms are those arising from the second and third degree, which involve a large spectral range from 1/18.6 years to diurnal, semi-diurnal and ter-diurnal frequencies (Cartwright and Tayler, 1971; Cartwright and Edden, 1973). Numerous studies were devoted to the observation of these tidal components (see e.g. Melchior, 1983 for a review). More recently, theoretical expansions have been provided including the 4th degree tidal terms (Tamura, 1987; Xi QinWen, 1989). A first study using Lacoste-Romberg spring gravimeters (Wenzel and Zürn, 1990), has shown than accurate observations allow to point out, in the range from 1 to 3 cycle/day, specific terms of these recent potentials. We show here than the Superconducting Gravimeter records from Strasbourg (France) and Cantley (Canada) exhibit waves of the 4th order with periods close to 6 hours (quarter-diurnal waves) having amplitudes of a few nanogal (1 nanogal $\approx 10^{-12}$g = 1 pico-g). These observations also confirm the potentiality of the cryogenic gravimeters in the search for very weak signals due to the dynamics of the deep Earth, which are of great interest for global dynamics understanding (Hinderer et al., 1991a).

Data processing

The electrical signal provided by the gravimeter, which is the feedback voltage maintaining the sphere in levitation, is first filtered by an anti-aliasing filter, then sampled and digitized every 2 seconds. A second anti-aliasing filter is applied (numerically) to further decimate the gravity signal to a final sampling interval of 5 minutes. The next step consists in multiplying this signal by the calibration factor and to correct it for atmospheric effects. The calibration factor has been obtained by comparison with absolute gravity measurements at the same location (Hinderer et al., 1991b). Its accuracy is about 1%. The correction for the atmospheric influence involves two effects: the Newtonian attraction by air masses and the loading effects. Classically the local correction is a rough estimate similar to the Bouguer correction, which is constant in time. Practically, the coefficient of influence on gravity is determined by a least squares procedure during the tidal analysis. It is very close to - 0.3microgal/millibar. Gravity decreases when the pressure increases: the direct attraction effect is larger than the indirect loading effect.

Removal of disturbances

Unfortunately, the resulting record is not continuous: it contains gaps. One could think that this does not lead to a great trouble in further analyses, since the gaps only concern a small amount of the whole record (no more than a few per cent). In fact, these interruptions disturb tremendously the analysis and the search for weak signals. Indeed, the presence of a gap is equivalent to the multiplication of the signal by a function equal to 1 outside the gap and 0 inside. Hence, the computed spectrum is the convolution between the spectrum of this function and that of the real signal.

These gaps may correspond to earthquakes (which saturate the instrument) or to instrumental maintenance operations like helium refills. They are generally short (a few hours) but, exceptionally, may exceed a day (breakdown due to lightening for instance). The gaps are replaced by a synthetic tide taking into account local gravimetric amplitude and phase factors. The error introduced by this correction is negligible with respect to the one we would have in keeping the gap itself .

Other disturbances similar to spikes also do exist. In the spectral domain, a spike spreads noise over the whole band (see for instance Florsch et al., 1991). To remove these spikes a simple thresholding is applied to the time signal, provided that main tides are first modelled out.

This despiking procedure which is a non linear process leads to a spectacular reduction of the noise. Since this operation is really of primary importance for the quality of the final results, we detail it hereafter in the case where it is applied to the quarter-diurnal frequency band.

Despiking procedure before spectral analysis

The raw signal (filled by synthetic tides in the gaps) is mainly composed of diurnal and half-diurnal waves. It reaches typically a hundred of microgal. The first step consists in a band-pass filtering which isolates the spectral band of interest and eliminates the main tides. We use here a convolutive filter (FIR) rather then a recursive one (IIR) because of a better control. After this filtering, the residual signal looks random with the presence of more or less numerous impulsive disturbances, as shown on Figure 1a (time unit is 5 min). Then, the histogram of this signal is computed. Figure 2 shows the one obtained for the Strasbourg record which looks like a Gaussian curve. The threshold level can be chosen for each signal in such a way that only a small part of the signal is removed. The signal after despiking is plotted on Figure 1b. One finds in the choice of the threshold level a first control on the importance of the unavoidable perturbations introduced by this process. The threshold is taken here so that no more than 1% of the signal is modified. A second control can be achieved after spectral analysis. The despiking being a non-linear procedure, it re-introduces some noise in the spectral area where the band-pass filtering had previously eliminated any energy. The reduction of the noise in the selected band is strongly reduced. Since the noise generated by the despiking is practically white, its level in the band we are interested in has a level identical to the one generated outside the band and remains small with respect to the residual noise in the selected band. Figure 3 illustrates all these considerations.

The final residuals are mainly due to atmospheric effects. To reduce them, a regional map of hourly pressure data would be necessary. This work has still to be done and would lead, according to current modelling studies (Merriam 1992a) to a noticeable reduction of the noise.

After all these treatments (elementary correction for local atmospheric effects, filling of the gaps, despiking), the residual noise is about the nanogal level. This is an extremely small gravity change (1 nanogal roughly means 1 pico-g) and shows the excellent performance of Superconducting Gravimeters in detecting weak gravity signals of a few hour periodicity. In terms of altitude change, one nanogal corresponds to 3 mm. In terms of Newtonian attraction, it is equivalent to the direct attraction of a 100 kg mass located at 25 meters from the instrument. Finally notice that these results are obtained here from a signal which is not yet perfectly corrected for pressure contributions.

Results and analysis of the spectrum

The band-pass filter is centered on the quarter-diurnal band. It allows to observe the spectrum between 0.14 and 0.18 cycle/hour. On Figure 4 and 5, the normalised spectra of the gravity (in microgal) and pressure (in millibar) are plotted as well as the spectrum of the synthetic tide computed for Strasbourg for the same period (the Canadian spectrum is close to the later). The French spectrum comes from a 5.2 year record and the Canadian one from a 2 year record. The synthetic tide is computed from an astronomical ephemeris tide due to Merriam (1992b). The potential is calculated directly from the Sun and the Moon locations,

meaning that all the tidal waves are included by construction.

One first can notice on the gravity spectrum a group of peaks close to 6 hours (0.1667 cycle/hour) and a corresponding peak in the pressure spectrum. It concerns an harmonic signal coming from the pressure diurnal variation of world-wide origin.

The main expected peak with the largest amplitude in the synthetic spectrum is the wave M4. It appears clearly in the Canadian data but seems to have a reduced amplitude in the Strasbourg data. Such an amplitude is not in contradiction with the variations created by the noise itself. In other terms, it could be that the noise relative to the observation period considered in this study has a frequency component in phase opposition with the wave M4 hence reducing the total amplitude at the same frequency (see for instance Florsch et al., 1994). It is of course not reasonable, taking into account the level of the residual noise, to try to estimate the gravimetric amplitude and phase factors for this 4th degree wave.

A curious phenomenon exists in the Strasbourg data close to the wave at 0.164 cycle/hour. This wave does not appear in the Strasbourg spectrum at the expected frequency. But, very close to this frequency, one can distinguish a double peak the nature of which is unknown. In spite of the proximity of the frequencies, this result should not be due to an artefact of the process described above. Indeed, this process cannot shift nor split the frequency of any phenomenon, and moreover, the processes experienced by the Strasbourg and Cantley data were exactly the same. One can imagine that this double peak is actually triple, the third (and missing) peak being in phase opposition with the tide. Such a triplet can be viewed as a modulation due to a resonant and/or dispersive process. A similar phenomenon has already been encountered in the North Sea level changes, but we did not investigate further this hypothesis which still remains highly speculative. Let us notice that, from a statistical view point (Florsch et al., 1994), such an event has neither a weak probability of occurence by pure chance nor a high one (it can be estimated to a few per cent).

On the Canadian spectrum, a peak of amplitude close to 2 nanogal exists at the frequency of 0.1556 cycle/hour (6 hours and 26 minutes) which is not in relation with a lunisolar tidal wave. Notice that this frequency is very close to the one predicted for the central peak of the Slichter mode of translation of the solid inner core (Crossley et al., 1992).

Conclusion

The observation of very weak signals in the spectrum obtained from Superconducting Gravimeter records is possible because of the quality of these instruments provided that the residual noise has been reduced by appropriate numerical (sometimes non-linear) procedures. On one hand, the observation of spectral peaks close to 6 hour period, corresponding to the 4th degree tidal potential, is clearly an additional verification of the tidal theory but is not

surprising in itself. On the other hand, the level reached by the analyses illustrates the strong potentiality of the Superconducting Gravimeters and opens new perspectives in the detection of weak gravity signals like the Slichter modes or other possible oscillations originating in the Earth's deep interior.

Acknowledgment

We kindly thank David Crossley for having provided the data from the Canadian Superconducting Gravimeter at Cantley (Québec).

References

Cartwright, D. E. & Tayler, R. J., 1971. New computations of the tide-generating potential, Geophys. J. R. astr. Soc., **23**, 45-74.

Cartwright, D. E. & Edden, A. C., 1973. Corrected tables of tidal harmonics, Geophys. J. R. astr. Soc., **33**, 253-264.

Crossley, D., Rochester, M. & Peng, Z., 1992. Slichter modes and Love numbers, Geophys. Res. Lett., **19**, 1679-1682.

Florsch, N., Hinderer, J., Crossley, D., Legros, H. & Valette, B., 1991. Preliminary spectral analysis of the residual signal of a superconducting gravimeter for periods shorter than one day, Phys. Earth Planet. Int., **68**, 85-96.

Florsch, N., Legros, H. & Hinderer, J., 1994. The search for weak harmonic signals in a spectrum with applications to gravity data, Phys. Earth Planet. Int. , sous presse.

Hinderer, J., Legros, H. & Crossley, D., 1991a. Global Earth dynamics and induced gravity changes, J. Geophys. Res., **96**, 20257-20265.

Hinderer, J., Florsch, N., Mäkinen, J., Legros, H. & Faller, J., 1991b. On the calibration of a superconducting gravimeter using absolute gravity measurements, Geophys. J. Int., **106**, 491-497.

Melchior, P., 1983. The tides of the planet Earth, 2nd edn., Pergamon Press, Oxford.

Merriam, J. B., 1992a. Atmospheric pressure and gravity, Geophys. J. Int., **109**, 488-500.

Merriam, J. B., 1992b. An ephemeris for gravity tide predictions at the nanogal level, Geophys. J. Int, **108**, 415-422.

Tamura, Y., 1987. An harmonic development of the tide generating potential, Bull. Inf. Mar. Terr., **99**, 6813-6855.

Wenzel, H. G. & Zürn, W., 1990. Errors of the Cartwright-Tayler-Edden 1973 tidal potential displayed by gravimetric Earth tide observations at BFO Schiltach, Bull. Inf. Mar. Terr., 107, 7555-7574.

Xi Qinwen, 1989. The precision of the development of the tidal generating potential and some explanatory notes, Bull. Inf. Mar. Terr., 105, 7396-7404.

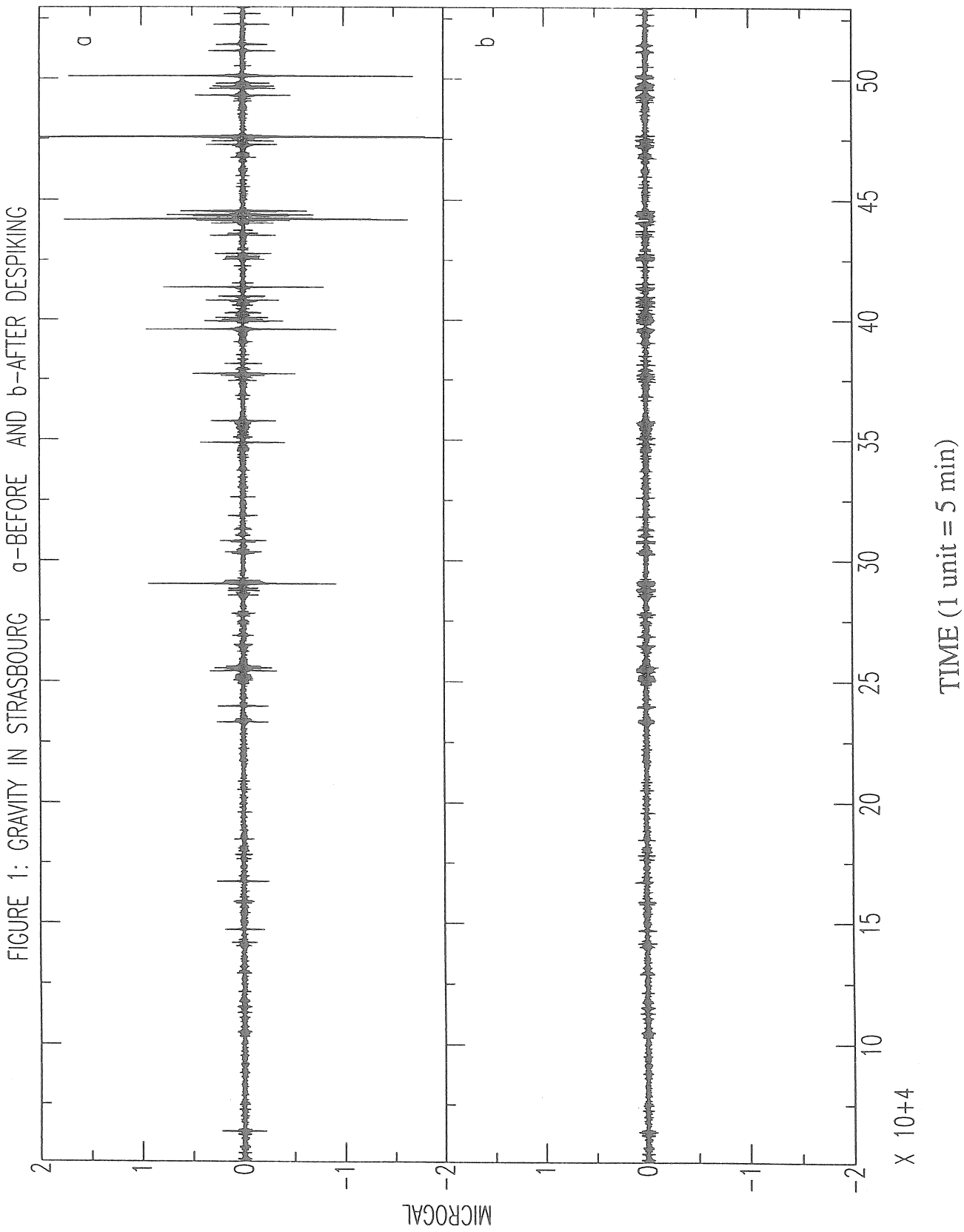

FIGURE 1: GRAVITY IN STRASBOURG a-BEFORE AND b-AFTER DESPIKING

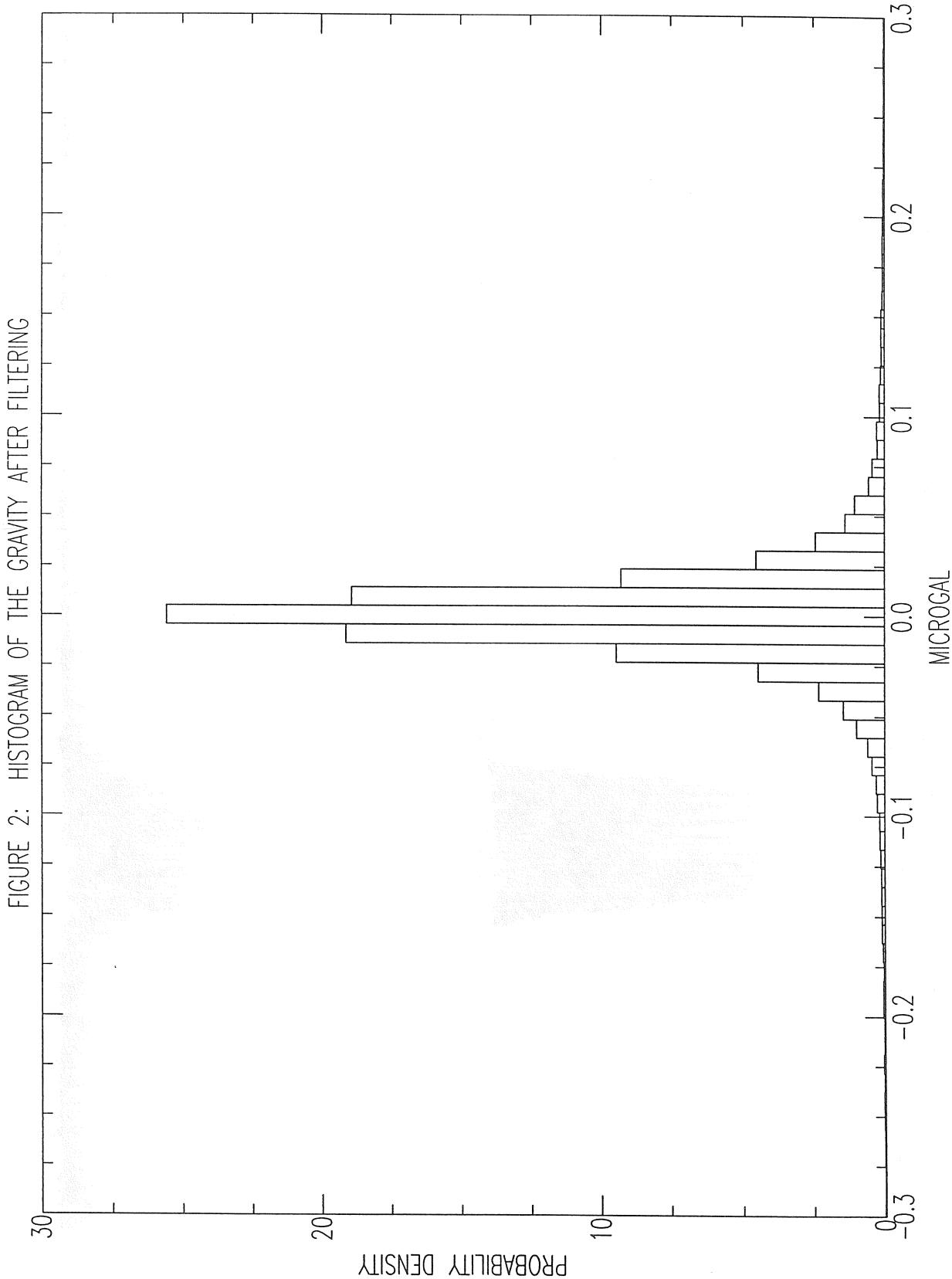

FIGURE 2: HISTOGRAM OF THE GRAVITY AFTER FILTERING

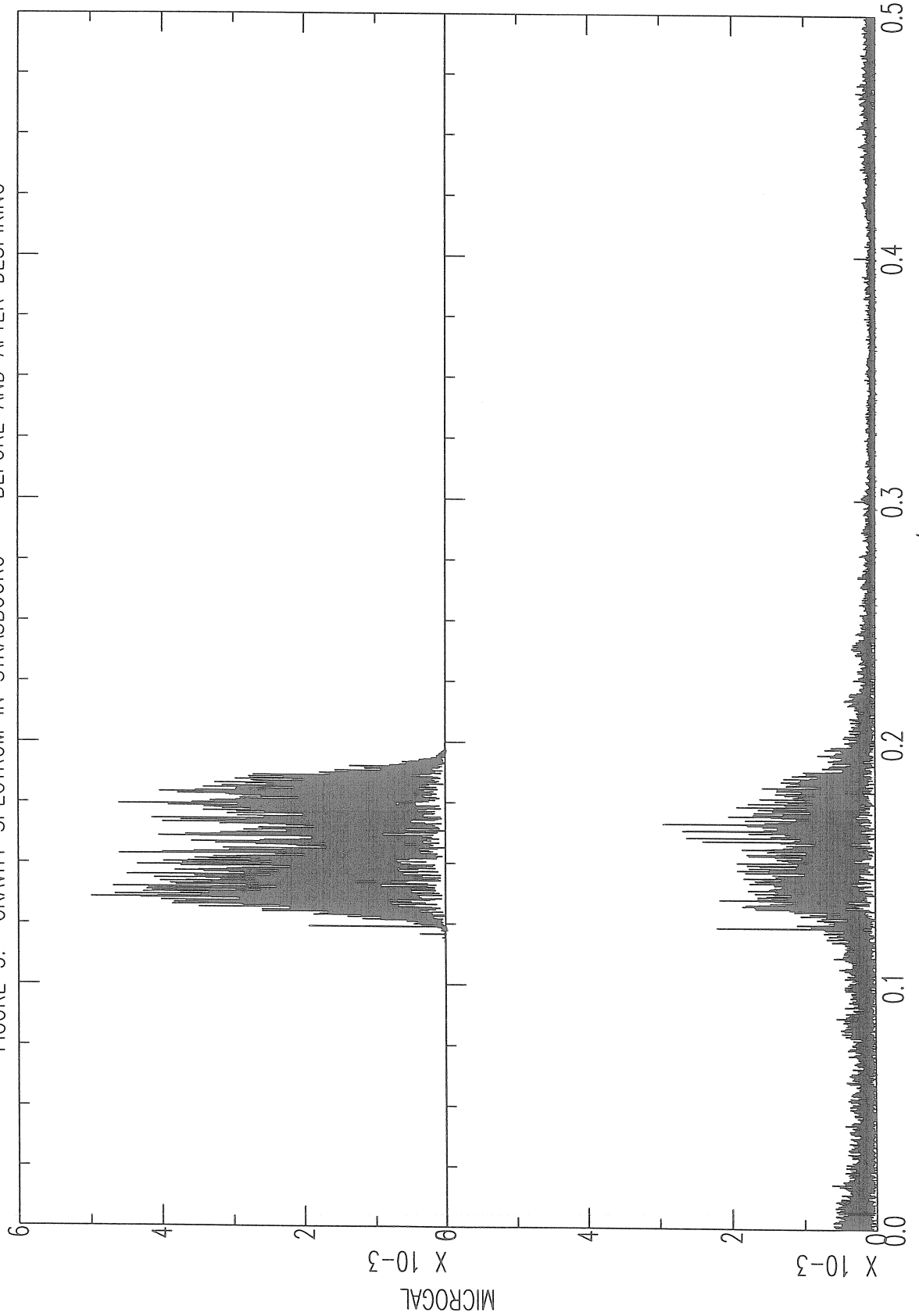

FIGURE 3: GRAVITY SPECTRUM IN STRASBOURG BEFORE AND AFTER DESPIKING

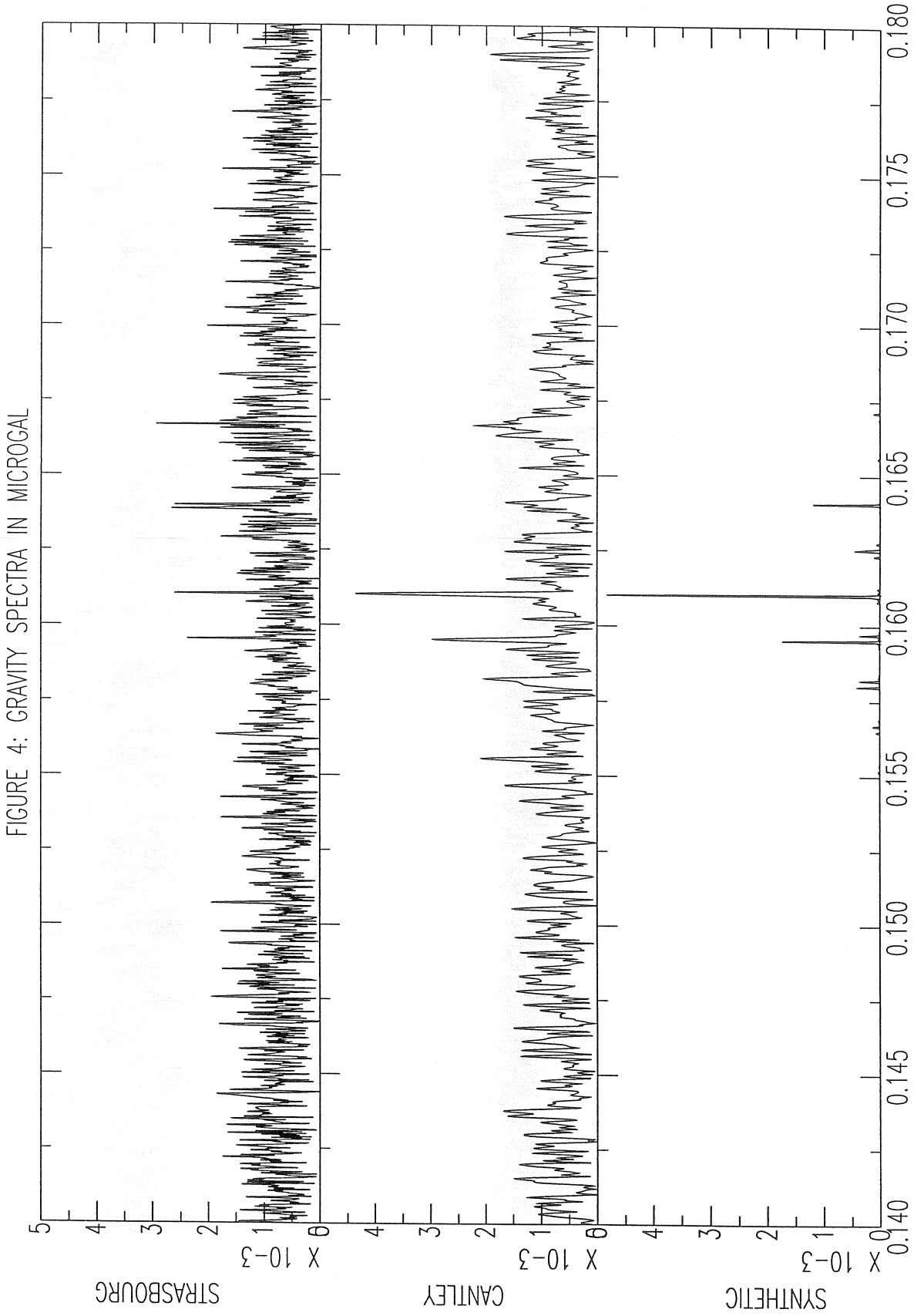

FIGURE 4: GRAVITY SPECTRA IN MICROGAL

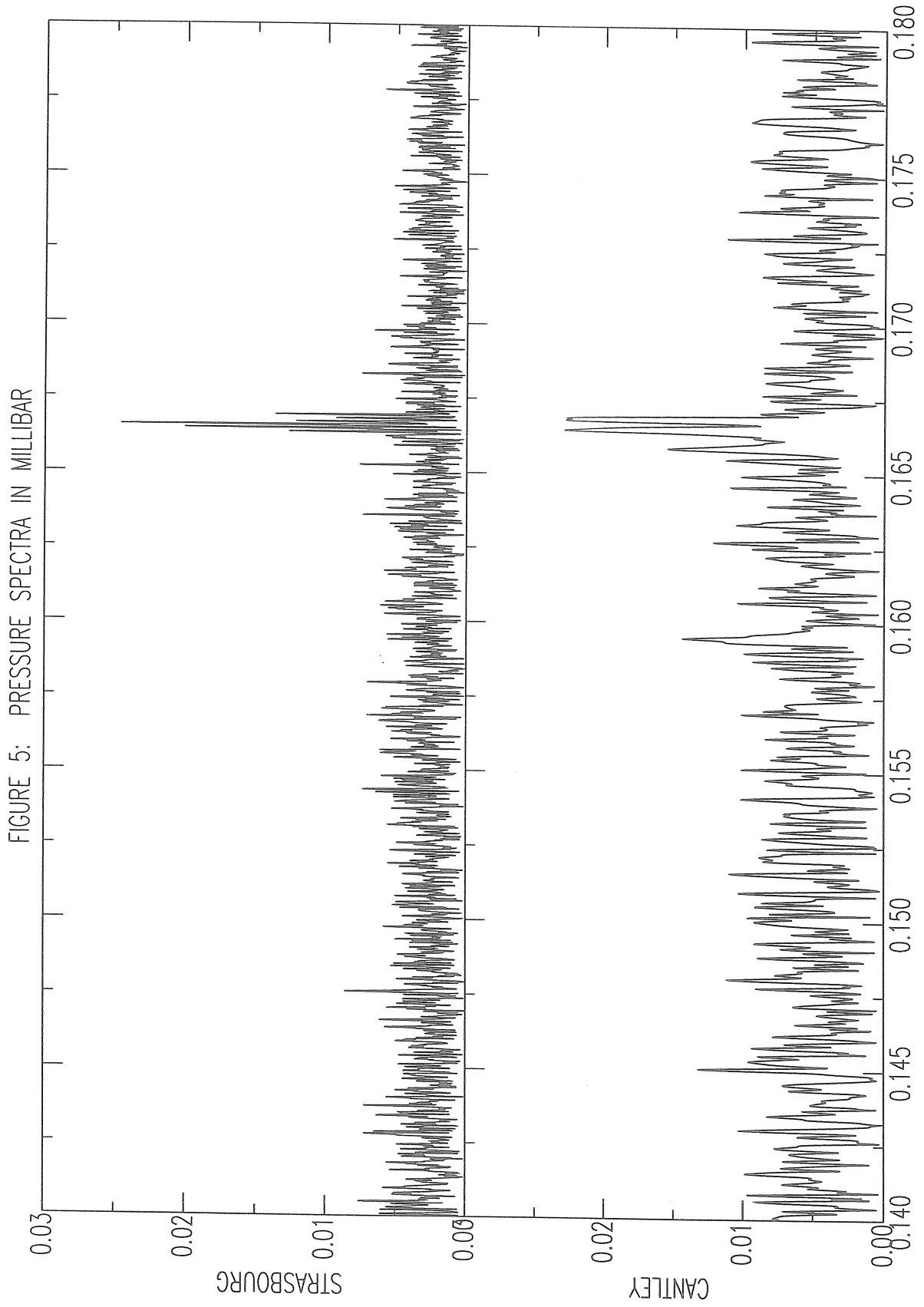

FIGURE 5: PRESSURE SPECTRA IN MILLIBAR

Atmospheric Gravity Green Functions

(Extended Abstract[1])

He-Ping Sun, Bernard Ducarme, Véronique Dehant

Royal Observatory of Belgium
Avenue Circulaire 3
B-1180 Brussels
Belgium
E-mail: heping@astro.oma.ac.be

1 Introduction

For the study of the tidal as well as the non-tidal deformation of the solid Earth, the high sensitivity of the superconducting gravimeters has many advantages. However the observations recorded by such a high precision instrument are simultaneously influenced by the local and regional atmospheric pressure variations. Considering the synoptic storms, the effect can reach 10% of the total signal due to the astronomical forces. Therefore this atmospheric pressure signal must be very carefully removed before taking full advantages of the instrument in study of the geophysical and geodynamical problems of the solid Earth.

The influence of the atmospheric pressure on gravity usually takes three forms: (1) the direct attraction of the atmospheric masses, causing the vertical to deviate and g intensity to vary; (2) a variable flexure of the Earth's crust under the loading effect and (3) a variation of the Earth's potential due to the mass redistribution induced by the deformation of the crust and upper mantle. Farrell (1972) introduced the gravity Green functions under the action of a point mass loading on the Earth's surface. However, when the load is distributed throughout a considerable scale height, we must reconsider the calculation of the Newtonian attraction, because the atmosphere is not simply one single layer distribution as in the case of the ocean tides.

In recent years, a great deal of efforts have been devoted by scientists in geophysics and geodesy to perform atmospheric pressure corrections. In most of those researches, the main subject was how to remove the effect of the atmospheric pressure considered as a noise. It is well known that the Newtonian attraction of the air masses near the gravity station is dominantly upwards and very large, and for the mass far from the gravimeter, it is dominantly downwards and small. A more appropriate calculation introduces corrections which are a function of the scale height of the atmosphere and of the size of the air pressure region.

We model a column load of atmosphere as a function of the angular distance of the gravity station, by using a numerical integration from the surface up to a truncation height z_0 above the Earth's surface. Consequently the effect of such column on gravity can be interpreted as a Green function. In order to distinguish these column Green functions from the more familiar point mass load Green functions given by Farrell (1972), we call them here the atmospheric gravity Green functions. The integration of these functions over the pressure and temperature fields around the gravity station then gives the gravity signal from the atmosphere above this considered area.

[1]Paper presented on the Working Group on High Precision Tidal Data Processing, Calibration, Theoretical Tidal Model, August 30 - September 2, 1994, Bonn, Germany.

2 Techniques

The Newtonian attraction at the gravity station, caused by atmosphere above the Earth's surface (positive downward) can be computed by

$$g(\psi) = -G \int\int\int_V \frac{\rho \cdot sin\alpha}{r^2} dv \tag{1}$$

where G is the gravitational constant, r is the distance between the mass and the gravity station, α is the angle between the attracting direction and the local horizon at the station, ψ is angular distance, ρ represents the density of the mass and dv a small volume occupied by the mass. The above integration covers the whole Earth's surface.

Following the atmospheric theory, the pressure, density and temperature must satisfy the ideal gas law (Triplet and Roche, 1971)

$$\rho(z) = \frac{P(z)}{R \cdot T(z)} \quad (kg/m^3) \tag{2}$$

where $P(z)$ is the air pressure in Pascals, $T(z)$ is the temperature in degrees K and R is the specific gas constant. Assuming hydrostatic equilibrium, and a certain temperature structure and in the case of an isothermal atmosphere, the pressure decreases exponentially with altitude

$$P(z) = P_0 \, exp(-z/\lambda) \tag{3}$$

where P_0 is the surface value, λ represents the atmospheric scale height.

An analytic function of the temperature which approximates six commonly used standard temperature profiles (the Air Force Geoph. Lab. (AFGL) set, and the 1976 U.S. standard) is introduced (Fels, 1986)

$$T(z) = T_0 + C_1 \frac{z}{2} + \frac{1}{2} \sum_{i=1}^{n} \delta_i (C_{i+1} - C_i) log \left[\frac{cosh(z - z_i/\delta_i)}{cosh(z_i/\delta_i)} \right] \tag{4}$$

with $C_{n+1} = 0$ and $z_{i-1} < z < z_i$. T_0 is the surface value, z and z_i are the height, δ_i the measured sharpness of the corner at z_i, and C_i are the discontinuities in dT/dz.

The elastic deformation induced by the atmospheric loading is relatively small and can be considered as in the case of surface mass loads. Farrell (1972) introduced the calculation of the contribution of the elastic deformation and tabulated the loading Green functions. The details of the Earth model are unimportant, the resulting error in gravity due to the uncertainty in the Earth model is only a few tens of $ngals$.

The model mentioned above is valid at sea level only, as most of the gravimeters are located above the sea level, the results can not be directly used to infer the atmospheric pressure correction in the gravity measurement. The effect of a change in the station height should be introduced. In order to solve this problem we must consider a Taylor expansion around a zero height and consequently we need the derivative of the gravity Green functions with respect to the station height.

In addition to the effect of the station height, the topography outside the station is also significant. Thus, if the gravimeter sits on a hill, there is some local atmosphere around the station which is below the height of the instrument horizon and increases gravity. Similarly if the gravimeter is in a valley or below the sea level, there are some local ground fluctuations around the station, which are above the gravimeter horizon. Therefore, the topography corrections must be taken into account. To solve this problem, it is sufficient to consider the effect of the column base height on the atmospheric gravity Green function as a function of the angular distance.

The temperature and pressure appearing in the integration are normalised to their surface values, so that the integration is nominally independent of the surface temperature and pressure. Additionally $g(\psi)$ has an implicit dependence on temperature $T(z)$, which in turn depends on T_0, because the defined thickness of the troposphere and the isothermal part of the stratosphere depend on T_0. As a result, $g(\psi)$ has a weak dependence on T_0. In order to consider the effect of the temperature, it is necessary to compute the derivative of the $g(\psi)$ values with respect to the temperature T.

3 Main results

(1) The atmospheric gravity Green functions for a spherical, radially stratified, inhomogeneous and elastic Earth, can be theoretically calculated as a function of angular distance ψ, for a column model of the atmosphere, by using a numerical integration from the Earth's surface up to a certain truncation height z_0;

(2) The results are relatively insensitive to the details of the atmosphere model, however, a discrepancy of about 10% is found for the two extreme cases of a dry air model and a water-vapour-saturated model;

(3) A truncation height in atmosphere larger than 40 km is necessary, e.g., a height of 60 km can ensure an accuracy better than 1% at all the angular distance ψ;

(4) As the model is valid only at sea level, the effect of the station height and the topography around station should be taken into accound. If the topography within the local zone fluctuates by no more than one km, then topography effects on gravity are probably less than a few tens of $ngals$;

(5) There is a small temperature dependence of the gravity for both the local and regional zones, arising from the expansion and contraction of the atmosphere as the temperature rises and falls. An increase in temperature raises the centre of masses of the column of air; the upward pull of a column of air will be reduced by an increase in temperature. The admittance gives a value of $+0.014(T_c - 15°)\ \mu gal/C°$;

(6) About 90% of the gravity signal (including to the elastic deformation) produced by atmosphere are from the local zone for $\psi < 0.5°$. The signal from the regional zone for $0.5° < \psi < 10°$ is small, and is of the same order as the contribution from the global zone for $\psi > 10°$, i.e., an admittance from the regional zone is of $+0.059\ \mu gal/mbar$;

(7) The results show that the largest discrepancy between our results and those of Merriam appears to be about 10%, but this occurs when the Green functions are themselves small; where the Green functions are large, they differ one another by less than 2%. The difference is probably due to different atmosphere models used;

(8) Integrating the gravity effect at the centre of a spherical cap of uniform pressure of an angle of 0.5° provides an admittance of -0.3603 $\mu gal/mbar$. This indicates that the atmosphere influences the local gravity at about 20 μgal level for a change in the pressure of about 50 $mbar$ at the station. The discrepancy with the value of -0.3560 $\mu gal/mbar$ obtained by Merriam (1992) is less than 1.5%. This result corresponds also to the admittance obtained in our previous study, i.e., -0.395 and -0.333 $\mu gal/mbar$ for local and regional zones respectively, calculated by using the *ECMRWF* pressure data and a direct convolution method (Sun et al, 1993).

Seasonal Variations of the Planetary Solar Air Pressure Waves

Claus Elstner
Institut für Angewandte Geodäsie, Frankfurt/Main
Außenstelle Potsdam

Abstract

The mean seasonal variations of the planetary solar air pressure waves are examined by means of the Potsdam air pressure series existing since 1893. The outcomes of investigations performed by BARTELS (1927) for the period 1893-1922 are compared with results from the period 1974-90, partly already published by ELSTNER, HARNISCH, SCHWAHN (1993). The main features of the seasonal variations of the diurnal and subdiurnal air pressure waves S1, S2, S3 and S4 are the same in both the periods. Significance is tested by the aid of signal-noise ratios of Fourier amplitude spectra.

Introduction

The amplitude spectra of local air pressure and tide free gravity data[1] derived from series of continuous registrations of a few months or more clearly show the existence of diurnal, semi-, ter- and quarterdiurnal waves (Figs. 1,2,3). By current tidal analysis procedures these periods and also a linear gravity-air pressure regression should be eliminated. But several authors [4-6,9-12] found, that the parameters of the S-type waves are more or less dependent on time and their regressions to air pressure deviate significantly from the corresponding mean value determined inside the tidal analysis.

Furthermore the amplitude spectra of the local air pressure show that pressure variations connected with the weather processes seem to be randomly distributed with a noise level increasing with the periods at least inside the shown region up to 30 hours. That means air pressure amplitudes of 10 hPa or more are mutually cancelled. On the other hand the examples display the sharp marked lines of the S-type waves. Their global distribution and characteristic seasonal variations are described in different textbooks and papers [2,3,7,8,13].

The following considerations refer to the temporal stability of the S-type air pressure waves.

Some Features of Solar-type Air Pressure Waves

This type of air pressure waves with amplitudes less than 1 hPa is generated by solar radiation and the connected energy transformation processes inside the

---

[1] Gravity units used: 1 microgal = 10 $nm \cdot s^{-2}$, 1 nanogal = 10 $pm \cdot s^{-2}$

atmosphere and at the surface of the Earth differing oceanic from continental areas.

The diurnal wave S1 is more variable than the other ones and shows in its global changes a clear correlation to the continent-ocean distribution. Both the day-night effect of air temperature and the different thermal and thermodynamic qualities of land and water masses are reflected by this wave.

The semidiurnal wave S2 is the most stable one. It is composed from two parts: one depends on the position of the sun, while the other considerabely smaller part corresponds to a standing wave depending on universal time and is especially affecting the polar regions, where the other component is very small. The global distribution of S2 amplitudes shows distinguished zonal structures with high values in the equatorial regions and descending values to the poles. As causes for the existence of this wave absorption processes in the middle and higher atmospheric regions are supposed (water vapour, ozon). The influences from the surface of the Earth seem to be less important. Therefore the vertical extension is significantly higher than that of S1 for instance.

The terdiurnal air pressure wave already described by J. v. HANN (1918) remains in its amplitudes below 0.2 hPa and shows a very clear seasonal behaviour with fast phase transitions of about 180° in spring and autumn times.

The quarterdiurnal wave with amplitudes of a few Pa offers the strongest seasonal spelling and is in spite of its smallness clearly detectable in extended air pressure series.

For the description of the geographical distribution CHAPMAN and LINDZEN (1970) gave analytical expressions for the first three S-type air pressure waves, which were derived by BARTELS, KERTZ, HAURWITZ & COWLEY and others. Rawly the following formulas may be used with

Φ: geogr. latitude, t: mean local time (MLT), t_U: universal time (UT):

$$S1(p) = 0.593 \cos^3\Phi \sin(15t+12°) \quad (1)$$

$$S2(p) = 1.16 \cos^3\Phi \sin(30t+158°) + 0.042 (3\sin^2\Phi - 1) (\sin 30t_U+118°) \quad (2)$$

$$S3(p) = 0.306 \cos^2\Phi \sin 2\Phi \sin(45t+\sigma_3) \quad (3)$$

$$\sigma_3 = \begin{matrix} 149° & \text{summer} \\ 335° & \text{winter} \end{matrix}$$

The maxima of amplitudes are situated at latitudes:

S1, S2: 0°; S3: ± 30°.

Seasonal variations of amplitudes and phases of S-type air pressure waves at Potsdam for the periods 1893-1922 and 1974-1990

For the first period J. BARTELS determined the parameters of S-type airpressure waves up to the fourth order from hourly air pressure data of the Meteorological Observatory Potsdam [2, S.44, Tab.6]. His results are compared with the corresponding ones of the second period received by an adjustment procedure for

the common determination of the parameters of all four waves. More than 166000 hourly air pressure values were used for the calculation of mean monthly amplitudes A and phases ψ in the form:

$$Si(p) = A_i \cos(\omega_i t - \psi_i) \quad (4)$$

ω_i means the angular frequency of the i-th wave given in degrees per hour. Instead of ψ the time of the occurance of the maximum of the wave:

$$t_{MAX} = (360 + \psi)/\omega \quad (5)$$

is applied in the figures.

The monthly mean values of A and t_{MAX} for the four waves in both the time intervals are referred to the middles of the months and represented in Figs. 4-11. The temporal stability of the seasonal variations of the solar air pressure waves in the course of eighty years clearly is to be seen.

Furthermore these variations increase with ascending order of the waves. The alterations of mean yearly amplitudes inside the decadic intervals are the biggest at S1 [5,6] and may reach relative values of about 100%. In the higher orders amplitudes are more stable, possibly caused by a decreasing influence of the surface of the Earth.

The sources for the significant difference of 0.7 to 0.8 hours in t_{MAX} between both periods are not known at present. Therefore further investigations are needed.

On the reliability of the results

Because of the small amplitudes of the S-type air pressure waves, which are one or two orders of magnitude less than the air pressure variations caused by weather processes, an error estimation via the least square fitting of the wave parameters is not useful. From this reason the Fourier amplitude spectra (Figs.12-15) were used for the detection of the signal-noise relations or the standard deviations of amplitudes $\pm m_A$ and phases $\pm m_\psi = \pm m_A/A$ respectively.

The estimated standard deviations of amplitudes and phases are given in table 1.

Table 1: Amplitudes and Phases of S-type Main Air Pressure Waves from Fourier Spectra

Wave	Amplitude [hPa]	Phase [°]	Period [h]
S1	0.129 ± 0.020	73 ± 9	24
S2	0.279 ± 0.009	-112 ± 2	12
S3	0.035 ± 0.006	0.7 ± 10	8
S4	0.014 ± 0.002	80 ± 8	6

Besides S2 the amplitudes are determined with an relative mean error of about 15%. The higher stability of S2 generates an essential smaller relative error of only 3%.

The reliability of the seasonal variations may be checked too by addition of the symmetric modulation waves to the main wave. The period T_S represents the seasonal variations of the main wave:

$$T_S = T/|T_{MOD}-T| \qquad (6)$$

T, T_{MOD} design the periods of main and modulation waves.

The sign of the denominator ΔT indicates the direction of the movement of the phase with respect to the unmodulated main wave. $\Delta T>0$ means phase delay.

The comparison of mean monthly wave parameters derived from adjustments (ADM) and from Fourier analysis (FA) was performed for S1 (Figs. 16,17).

Conclusions

Decadic means of the S-type air pressure wave parameters at Potsdam do not change its seasonal variations outside the limits of errors of determination in the course of nearly a century. The reasons of the specific seasonal behaviour and included annual variations are situated in the energy transformation processes of solar radiation inside the atmosphere and at the surface of the Earth. The higher modes, especially S2, might be influenced also by seperate sources and not only by irregularities of the diurnal processes. BAKER and ALCOCK [1] reported on seasonal sea level variations of S2 period detected in the data of tide gauges from Iceland, Portugal and around the British Isles, which could be connected with S2 air pressure variations by dynamical coupling and/or by air pressure induced crustal deformations.

With respect to the interpretation of gravity variations occuring in the frequency ranges of the S-waves disturbances of a few hundred nanogal may be produced, while the spectral noise levels remain generally below twenty nanogal.

Acknowledgements

To my colleagues Martina and Günter HARNISCH, Potsdam and to Dr. Wolfgang SCHWAHN, Frankfurt/Main I am indebted for several valuable discussions and helpful calculations in the course of this work.

References

[1] BAKER, T. F.; ALCOCK, G. A. 1983
Time Variation of Ocean Tides
Proc. Ninth Internat. Symp. Earth Tides, New-York 1981, Schweizerbart'sche Verlagsbuchh. Stuttgart, S. 341-350

[2] BARTELS, J. 1927
Über atmosphärische Gezeiten
Abh. Preuss. Meteorolog. Inst., Springer, Berlin VIII, H.9, 52 S.

[3] CHAPMAN, S.; LINDZEN, R. S. 1970
Atmospheric Tides - Thermal and Gravitational
Reidel, Dordrecht

[4] CROSSLEY, D. J.; JENSEN, O. G. 1993
Effective Barometric Admittance and Gravity Residuals
XII. Int. Symp. Earth Tides, Beijing, Aug. 1993

[5] ELSTNER, Cl.; HARNISCH, M.; SCHWAHN, W. 1993a
Planetary Waves in the Spectra of Air Pressure and Gravity Variations
Geodesy and Physics of the Earth, Ed. Montag, Reigber, IAG Symp. 112,
Springer, Berlin, S. 194-199

[6] ELSTNER, CL.; HARNISCH, M.; SCHWAHN, W. 1993b
Annual and Semiannual Modulations of Planetary Waves in the Spectra
of Air Pressure and Some Consequences on Gravity Variations
Bull. Inf. Marées Terrestres, Brüssel, 117, p. 8664-8674

[7] HAURWITZ, B.; COWLEY, A. D. 1973
The Diurnal and Semidiurnal Barometric Oscillations, Global Distribution,
and Annual Variation
PAGEOPH, Basel, 102, 1, S. 193-222

[8] KERTZ, W. 1957
Atmosphärische Gezeiten
Handb. der Physik, Hg. Flügge, Springer, Berlin, 48, S. 928-981

[9] MERRIAM, J. B. 1993
Atmospheric Pressure and Gravity
Geophys. Journ. Int., 109, S. 488-500

[10] SPRATT. R. S. 1982
Modelling the effect of atmospheric pressure variations on gravity
Geophys. Journ. Roy. astr. Soc., 71, p. 173-186

[11] WARBURTON, R. J.; GOODKIND, J. M. 1977
The influence of barometric pressure variations on gravity
Geophys. Journ. Roy. astr. Soc., 48, p. 281-292

[12] WARBURTON, R. J.; GOODKIND, J. M. 1978
Detailed gravity tide spectrum between one and four cycles per day
Geophys. Journ. Roy. astr. Soc., 52, p. 117-136

[13] VOLLAND, H. 1988
Atmospheric Tidal and Planetary Waves
Klüwer Acad. Publ. Dordrecht

Fig 1

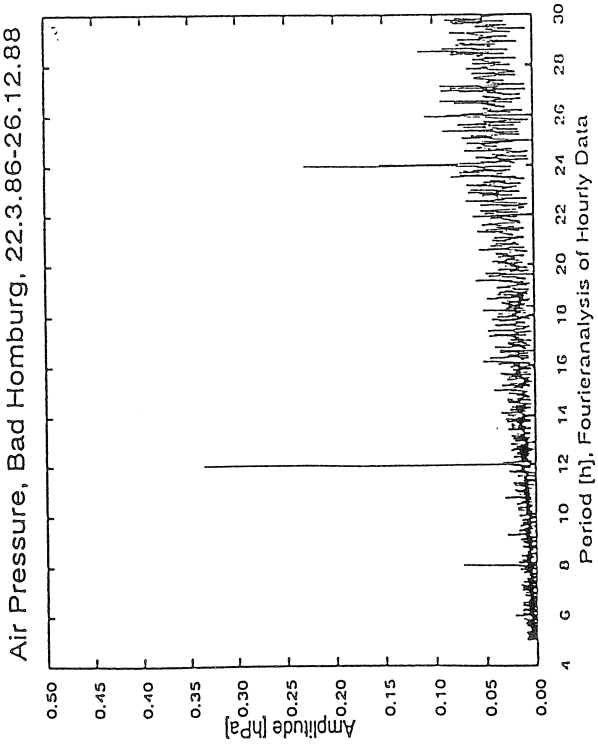

Fig 2

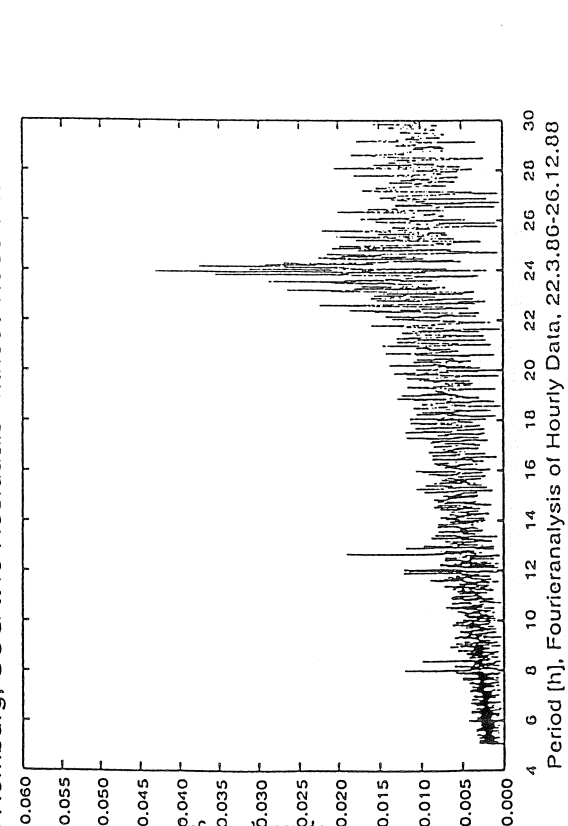

Fig 3

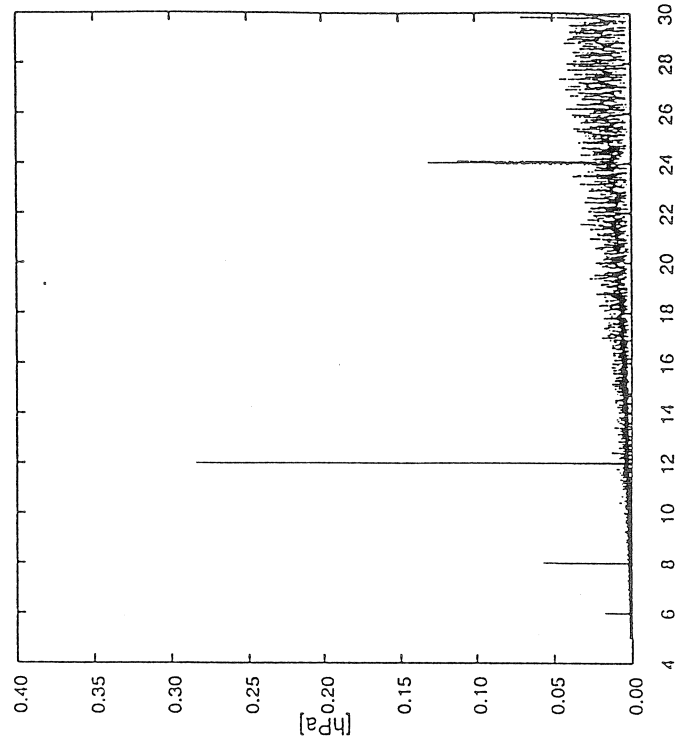

Fig 4

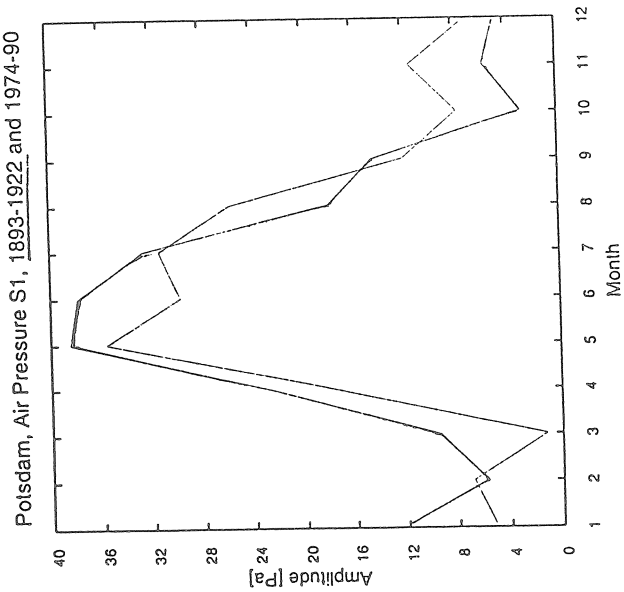

Fig 5

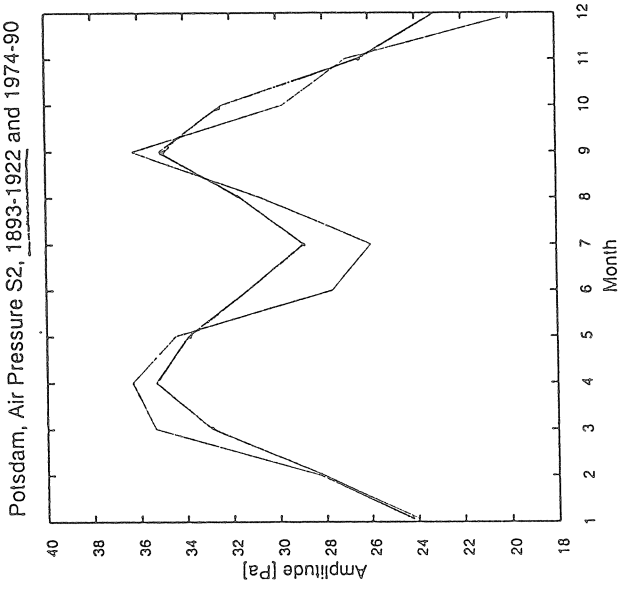

Fig 6

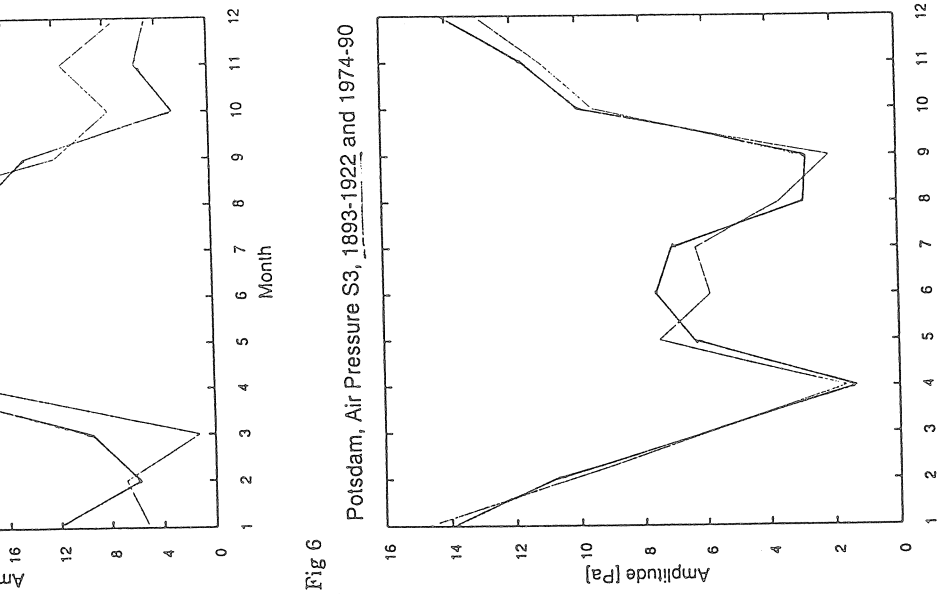

Fig 7

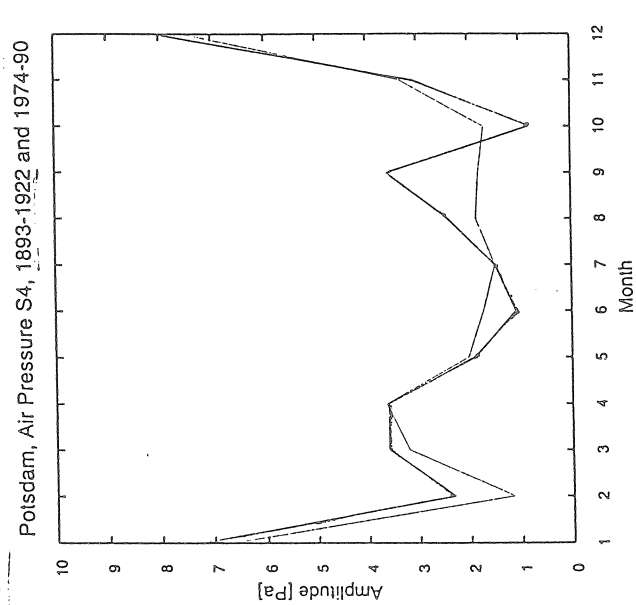

Fig 8

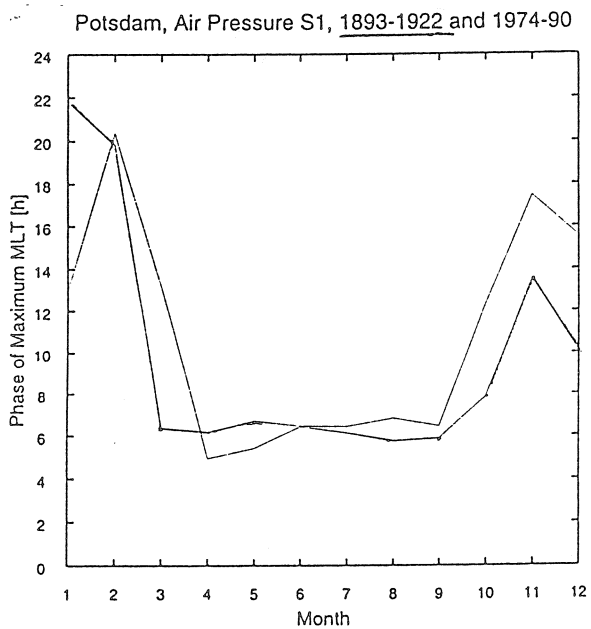

Fig 9

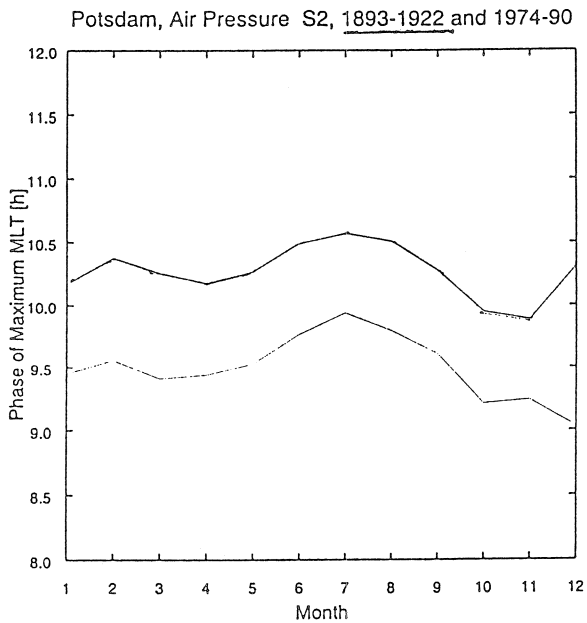

Fig 10

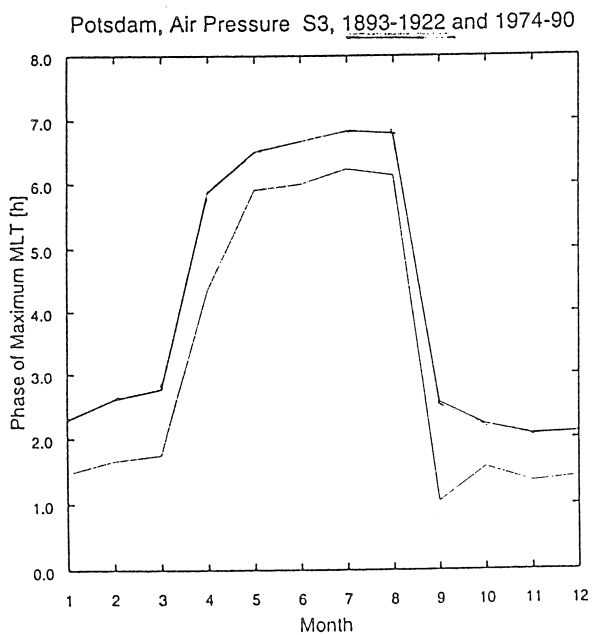

Fig 11

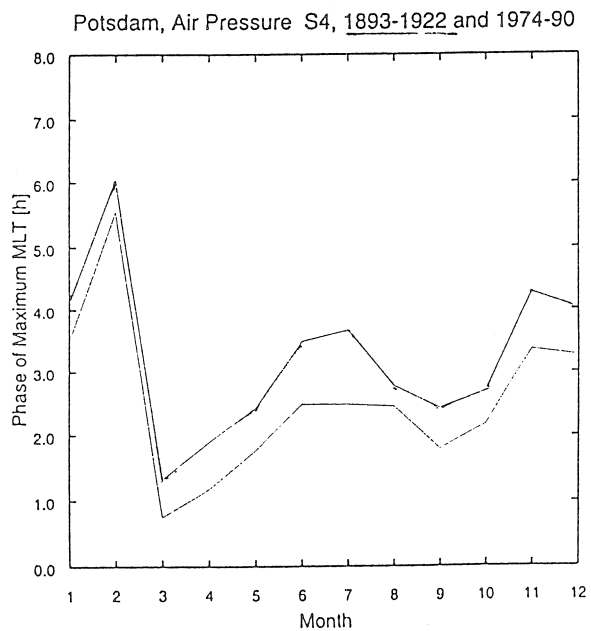

Fig 12

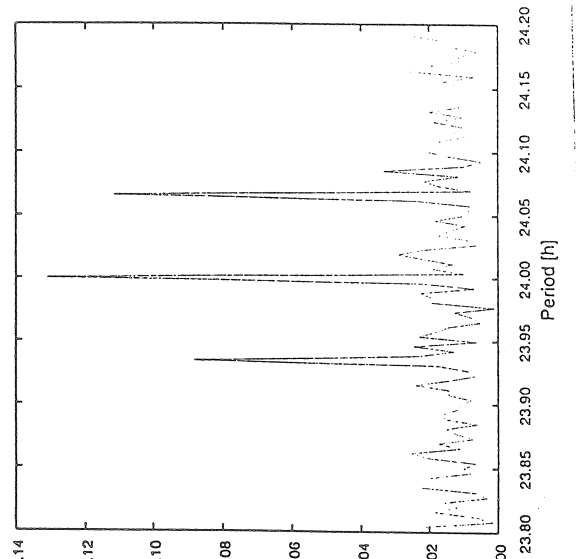

Fig 13

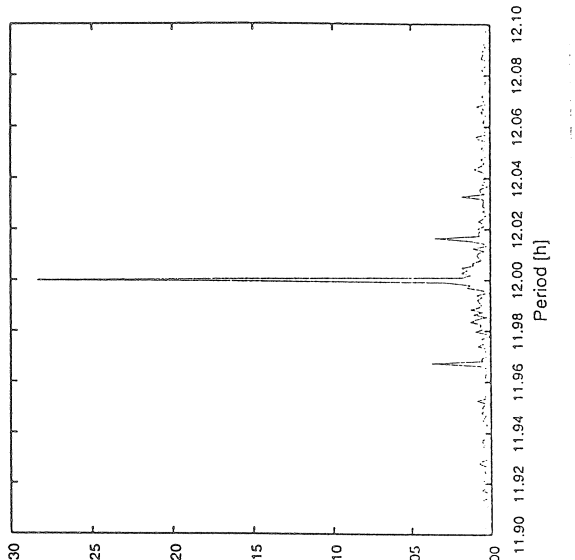

Fig 14

Fig 15

Fig 16

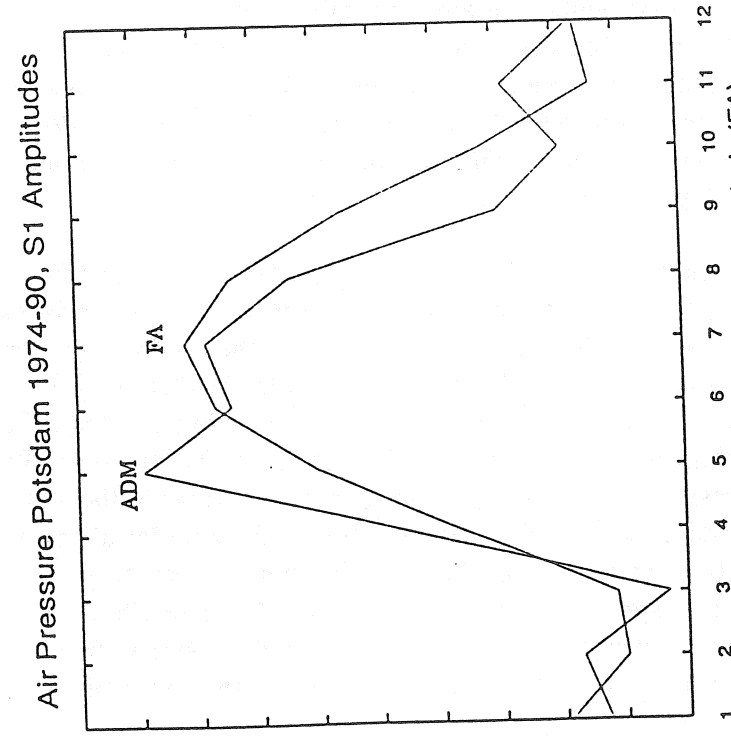
Air Pressure Potsdam 1974-90, S1 Amplitudes
[Pa]
ADM
FA
Month, Adjustment (ADM), Fourieranalysis (FA)

Fig 17

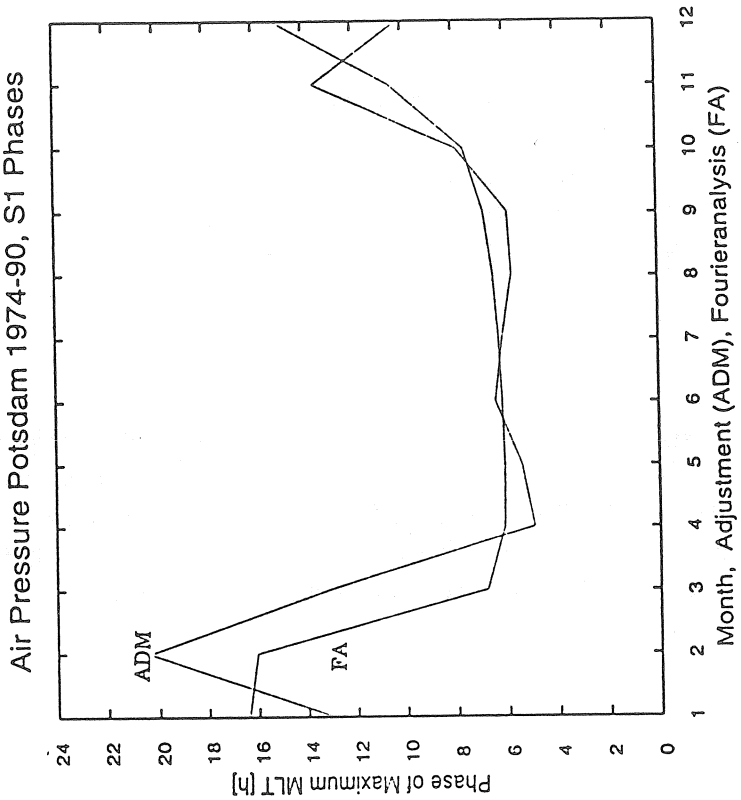
Air Pressure Potsdam 1974-90, S1 Phases
Phase of Maximum MLT [h]
ADM
FA
Month, Adjustment (ADM), Fourieranalysis (FA)

Frequency Dependent Atmospheric Pressure Correction on Gravity Variations by Means of Cross Spectral Analysis

Jürgen Neumeyer

GeoForschungsZentrum Potsdam
Department 1 'Recent Kinematics and Dynamics of the Earth'
Telegrafenberg A17, D-14473 Potsdam, Germany

Summary

The cross spectral analysis is used to determine a frequency dependent atmospheric pressure correction. A method to evaluate the complex admittance and to correct the gravity data is derived. The gravity data of the GFZ Potsdam Superconducting Gravimeter were corrected for atmospheric pressure influences by using the complex admittance before tidal fitting inside the frequency domain. The obtained improvement of the signal to noise ratio in the tidal and non - tidal band is shown.

1. Introduction

The gravimeter is an integrating sensor measuring local gravity variations caused in the near and distant part of its surrounding. The recordings include non-tidal gravitational effects of different sources. A correction of these effects must be done precisely for the interpretation of the time behaviour of the gravity field.

Continuous registrations of gravity variations with the Superconducting Gravimeter and the registration of the environmental parameters allow the improvement of the existing correction models. The linear regression analysis is the usual method to determine correction coefficients, not depending on frequency and phase. Utilizing the cross spectral analysis a frequency dependent correction can be carried out, which should decrease the residual gravity signal level in the non-tidal band and increase the signal to noise ratio in the tidal band. The atmospheric pressure is used to display this.

Atmospheric pressure causes three effects: (1) the gravitational effect (direct attraction of the atmospheric mass), (2) the deformation effect (change in gravity due to vertical displacement of the gravimeter on the deformed Earth) and (3) the change in gravity due to the redistribution of the masses inside the deformed Earth (Melchior [1]). The deformation effect acts in opposite direction to the dominant gravitational effect. The gravimeter is measuring the sum of these effects as well in the near as in the far field. Therefore, the size of the atmospheric pressure region acting on the gravimeter around the station is divided into three zones: (1) the local zone within an area of about 0.5° angular distance, (2) the regional zone between about 0.5° and 10° and (3) the global zone for an angular distance $>10°$ by Sun et al. [2]. The atmospheric models of Merriam [3] and Shi et al. [4] have similar zones. In all three atmospheric models 90% of the total signal that global atmospheric pressure systems contribute to gravity are produced by the atmosphere within an area of about 0.5° angular distance.

---

presented at the meeting of the Working Group on High Precision Tidal Data Processing, August 30 - September 2, Bonn, Germany

The remaining 10% are caused by the regional and global zones. It follows that the atmospheric pressure correction on gravity using the local atmospheric pressure takes into consideration in best case 90% of the whole effect only. Assuming atmospheric pressure changes of ± 50 hPa and a single admittance of -3 nm/s² per hPa cause gravity changes of ± 150 nm/s². The frequency range of the atmospheric pressure effect can be traced from periods of hours to years. Atmospheric pressure models of Warburton and Goodkind [5] and Merriam [6] give explanations of the frequency dependency of the atmospheric pressure admittance. The gravitational and the loading effect are dependent on the square of the horizontal scale. The admittance drops from 4.3 nm/s² per hPa for a circular cell of uniform pressure of $<<$100km to 2.8 nm/s² per hPa for a cell of 1000 km in radius. This can be expressed as frequency dependency of atmospheric pressure effect.

2. Mathematical background

The linear regression analysis determinates a single correction coefficient for the selected frequency band only. A frequency dependent correction coefficient can be estimated by the cross spectral analysis. It is a method to determinate the frequency response function for a single input - single output model as well as a multiple input - single output model.

2.1 Frequency response function (complex admittance) for a single input - single output model

For a single input - single output model the frequency response function H(f) can be calculated after Bendat and Piersol [7] by

$$\hat{H}(f) = \frac{\hat{G}xy(f)}{\hat{G}xx(f)} \qquad (1)$$

where Gxx is the auto spectral density and Gxy the cross spectral density of the input series x_n and the output series y_n, sampled at equally spaced time intervals δt and n = 0,1,...N-1. For evaluation of Gxx and Gxy the data records x_n and y_n must be divided into nb blocks each consisting of N data values (window). The block length N should be a power of 2, then one can use the faster Cooley - Tukey procedure of Fast Fourier Tranformation (FFT) calculation. If needed to suppress side - lobe leakage, the data values in each block can be tapered with an appropriate window (e.g. Hanning).

The averaged one - sided raw auto spectral density estimates from the nb blocks of data can be calculated by the Fast Fourier Transformation according to the formula

$$\hat{G}xx_k = \frac{2}{nb \cdot N} \sum_i |FFT(x_{k,i})|^2 \qquad (2)$$

with i = 0,1,...,nb-1 and k = 0,1,...N/2. The frequency is calculated by

$$f_k = \frac{k}{N \cdot \delta t} \tag{3}$$

The averaged raw cross spectral density estimates from the nb blocks of data can be calculated by the formula

$$\hat{G}xy_k = \frac{2}{nb \cdot N \cdot} \sum_i (FFT(x_{k,i}))^* \cdot FFT(y_{k,i}) \tag{4}$$

The Fourier transformation of two real valued records may be computed simultaneously by inserting the record x_n as the real part and the record y_n as the imaginary part of the complex record $z_n = x_n + iy_n$ by the Complex Fast Fourier Transformation. For determination of the cross spectral density the Fourier transforms of the record y_n and the complex conjugate of the record x_n are used.

The gain factor $H(f_k)$ and the phase factor $\phi(f_k)$ of the frequency response function can be estimated by

$$|\hat{H}(f_k)| = \frac{\sqrt{Re\ \hat{G}xy(f_k)^2 + Im\ \hat{G}xy(f_k)^2}}{\hat{G}xx(f_k)} \tag{5}$$

$$\phi(f_k) = \arctan\left(\frac{Im\ \hat{G}xy(f_k)}{Re\ \hat{G}xy(f_k)}\right) \tag{6}$$

The ordinary coherence function between two records is estimated by

$$\hat{\gamma}^2_{xy}(f_k) = \frac{|\hat{G}xy(f_k)|^2}{\hat{G}xx(f_k) \cdot \hat{G}yy(f_k)} \tag{7}$$

2.2 Correction of the output signal

After determination of the frequency response function (complex admittance cadm) the frequency dependent atmospheric pressure correction can be carried out for the gravity data. This is possible in the frequency domain using FFT techniques or time domain using convolution techniques. The FFT transforms the output series y_n and the input series x_n into frequency domain, where the correction is done according to the complex admittance. After that the Inverse Fast Fourier Transformation(IFFT) retransforms corrected data back into the time domain. This can be done by the following formula.

$$(y_n)_{corr} = IFFT\ [FFT(y_n) - (FFT(x_n) \cdot cadm)] \qquad (8)$$

It must be considered that all frequency domain functions have the same number of elements, to do the correction at the right frequency. With the used FFT and IFFT algorithms the difference between original data and non manipulated retransformed data is 10^{-10}, a neglectable figure.

3. Example of use

The correction of the gravity signal can be considered as a multiple input - single output system. Figure 1 shows different input signals, which affect the gravity signal. If the input signals are known, the frequency response function can be evaluated between input signal and tide free output signal tfo (calibrated gravity minus modelled earth tides values). The following calculations are carried out for a single input - single output model with atmospheric pressure as the input signal.

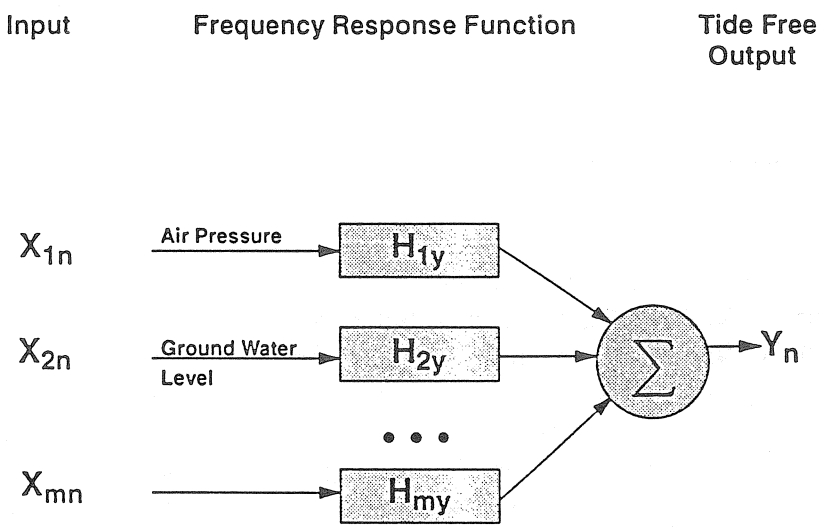

Figure 1 Gravity correction as multiple input single output model

3.1 Complex atmospheric pressure admittance

With the above equations the complex atmospheric pressure admittance is calculated using as input and output time series of 9600 hourly values (start at July 1, 1992) of GFZ Potsdam Superconducting Gravimeter, the atmospheric pressure (ap) and the tide free output (tfo), calculated after processing of gravity raw data with the programs BETA[8] and PRETERNA[9]. The spectrums of tfo and atmospheric pressure are depicted in figure 2. They show the typical harmonics of the S - waves (Elstner et al. [10]).

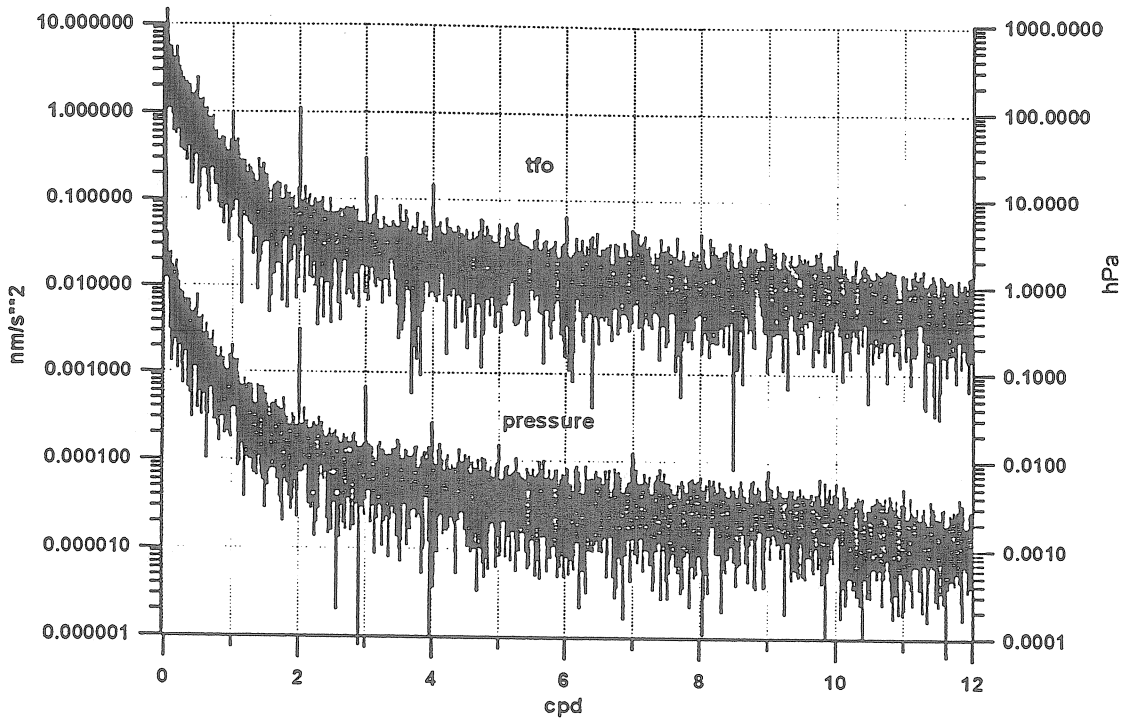

Figure 2 Amplitude spectrum of tide free output and atmospheric pressure

The complex admittance is calculated for different block length N. With N = 1.5 ... 0.5 cpd no S - wave peaks are in the complex admittance but at N = 0.1 ... 0.05 cpd they occur. The complex admittance, figure 3 amplitude spectrum and figure 4 phase spectrum, is calculated at N = 0.1 cpd (10 days) with a sampling rate of 1 hour. With respect to a higher resolution of the complex admittance a higher sampling rate is recommended. After Merriam [6] the S - waves should have smaller coefficients. Crossley [10] also showed smaller coefficients for the S - waves. The opposite direction of the S - waves can be explained by disturbing accelerations at S - wave frequencies or seasonal variations of the S - waves. Figure 5 shows the diurnal oscillation (24 hours stacking) of the atmospheric pressure (ap) and the atmospheric pressure corrected tide free output (tfoc). They have a phase shift of about 180°. The diurnal oscillation of tfoc mainly caused by man made and industrial noise is the reason of the opposite direction of peaks at S - wave frequencies in the complex admittance.

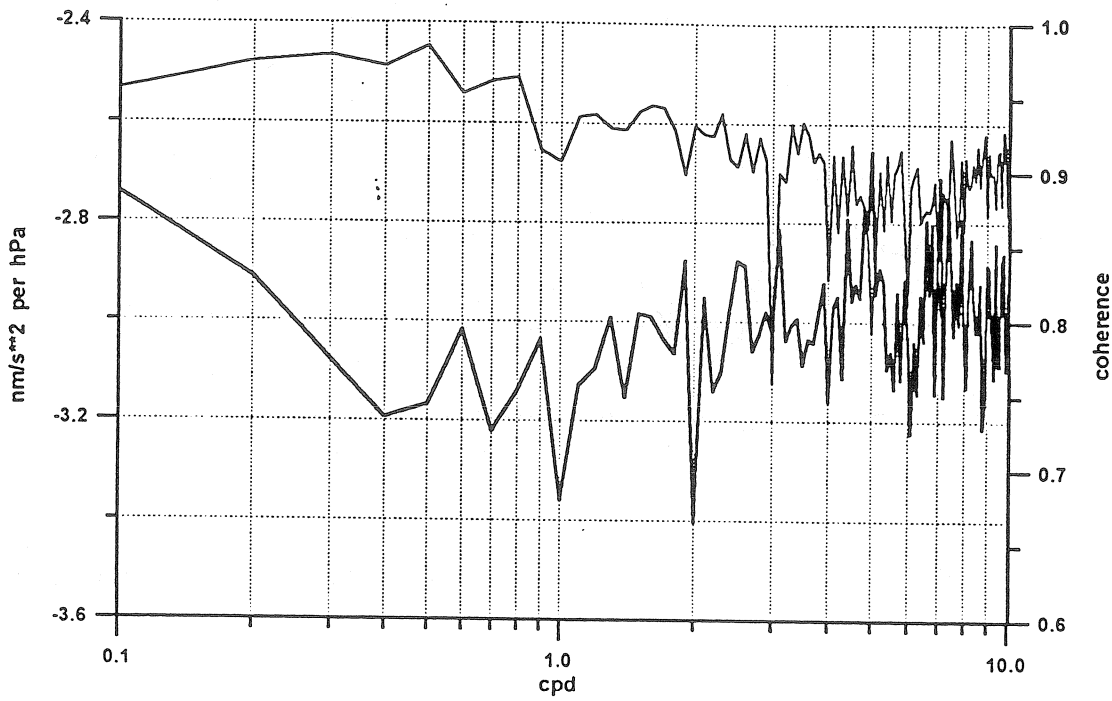

Figure 3 Amplitude spectrum of complex admittance and coherence (upper curve)

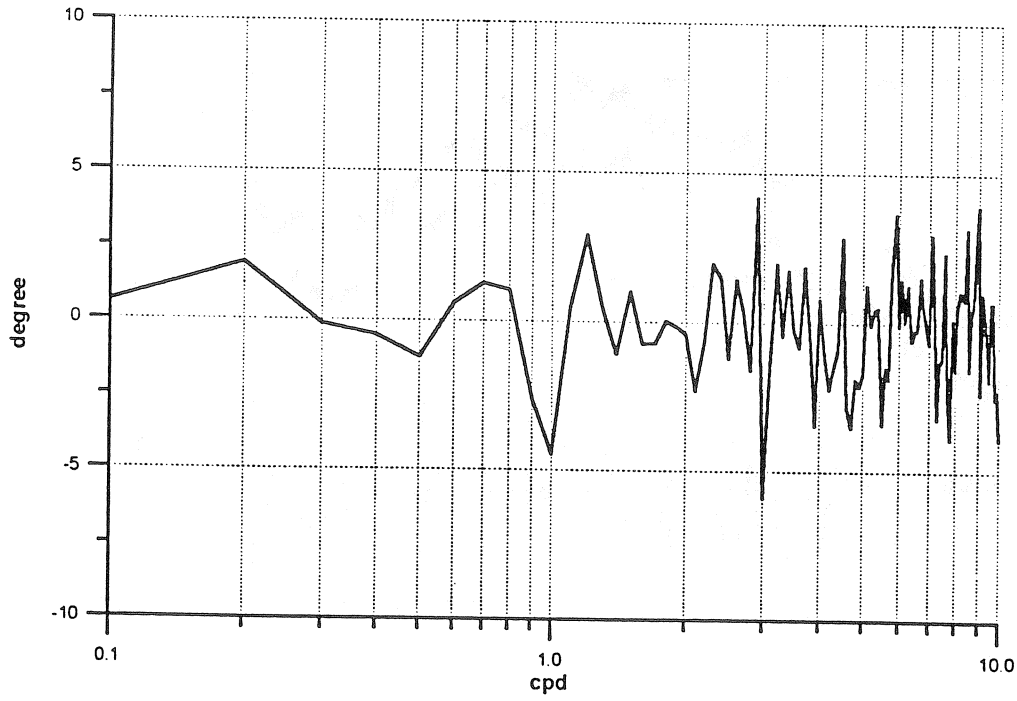

Figure 4 Phase spectrum of complex admittance

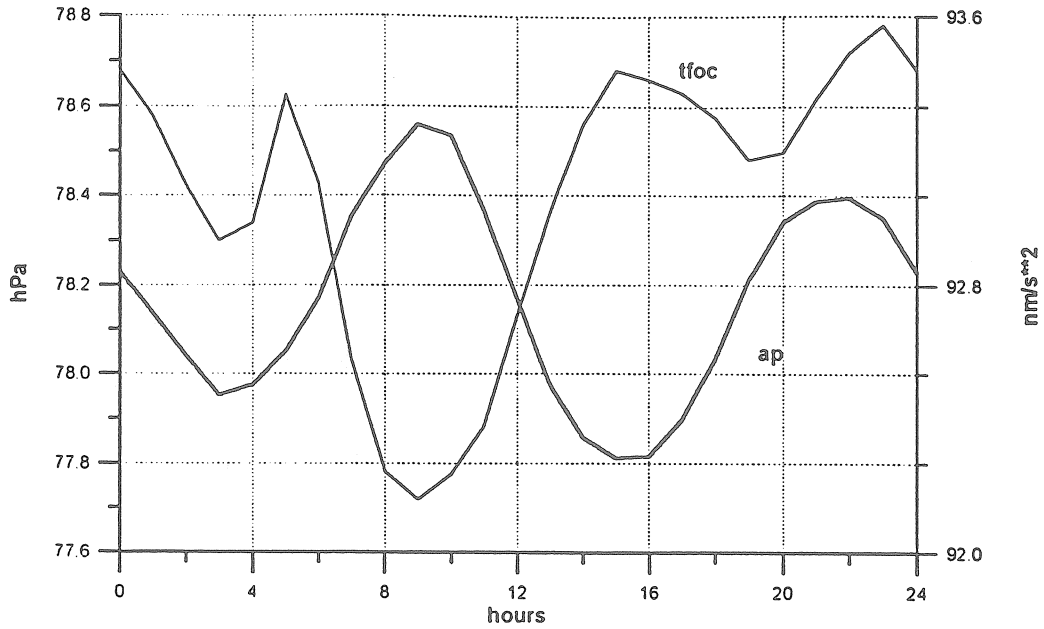

Figure 5 Diurnal oscillation of the atmospheric pressure (ap) and the tide free output (tfoc)

3.2 Correction results in the tide free output

Figure 6 depicts two atmospheric pressure correction results in the tide free output (complex admittance and regression coefficient correction). One can realize a small improvement by the complex admittance correction expressed by the difference of both curves. Some peaks became smaller or disappeared.

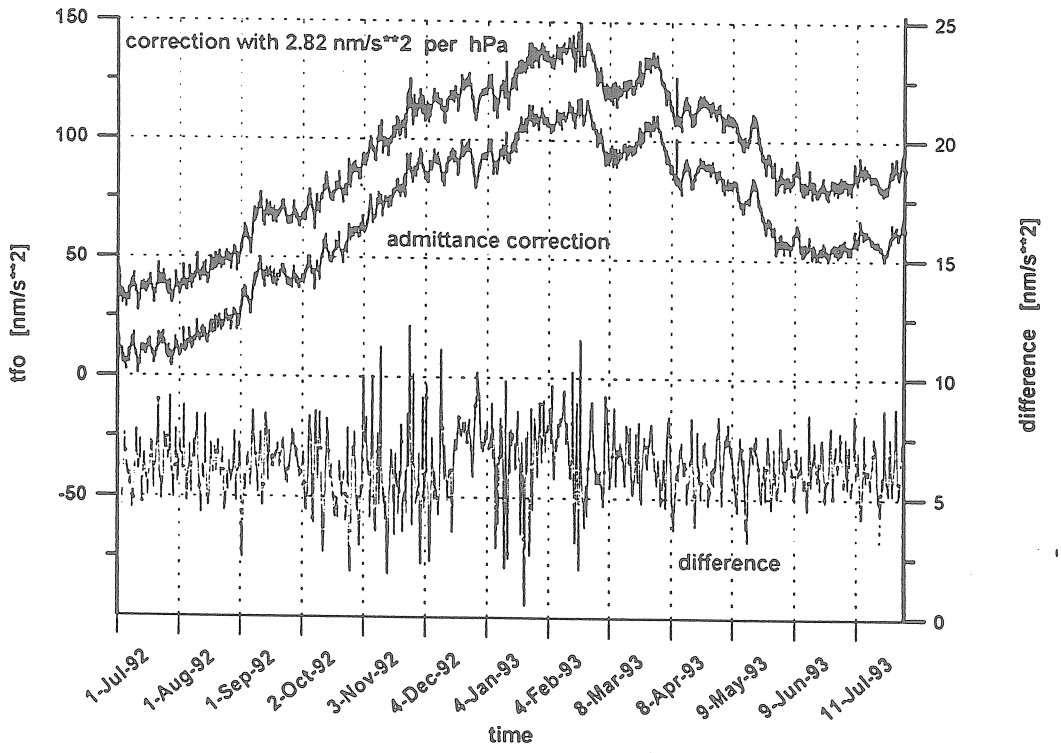

Figure 6 Tide free output (tfo) atmospheric pressure corrected

3.3 Correction results in the tidal band

A suitable method to use local atmospheric pressure is the determination of the complex admittance between tide free output and atmospheric pressure. The correction of the atmospheric pressure should be performed in the gravity data in the frequency domain before tidal fitting. This corrects better for the atmospheric pressure influence. The analysis results of both ways determination of the regression coefficient with the ETERNA program [12] (method B) and the atmospheric pressure correction before tidal fitting (method A) were compared. The ETERNA analysis was done with 38 wave groups and a Chebyshev polynomial bias parameter of second order. The standard deviation for method A results in s_{0adm} = +/-4.85 nm/s^2 and for method B in s_0 = +/-4.97 nm/s^2 This is a small improvement only.

A comparison of the signal to noise ratio between both methods yields however an improvement of about 10% by the complex admittance correction. Figure 7 shows the quotient of the signal to noise ratio of method A and B for the tidal band. For the diurnal and semi diurnal band the improvement factor is about 1.1. This leads especially to a better detection of wave groups of small amplitudes. The long periodic waves have the same or a little bit smaller signal to noise ratio.

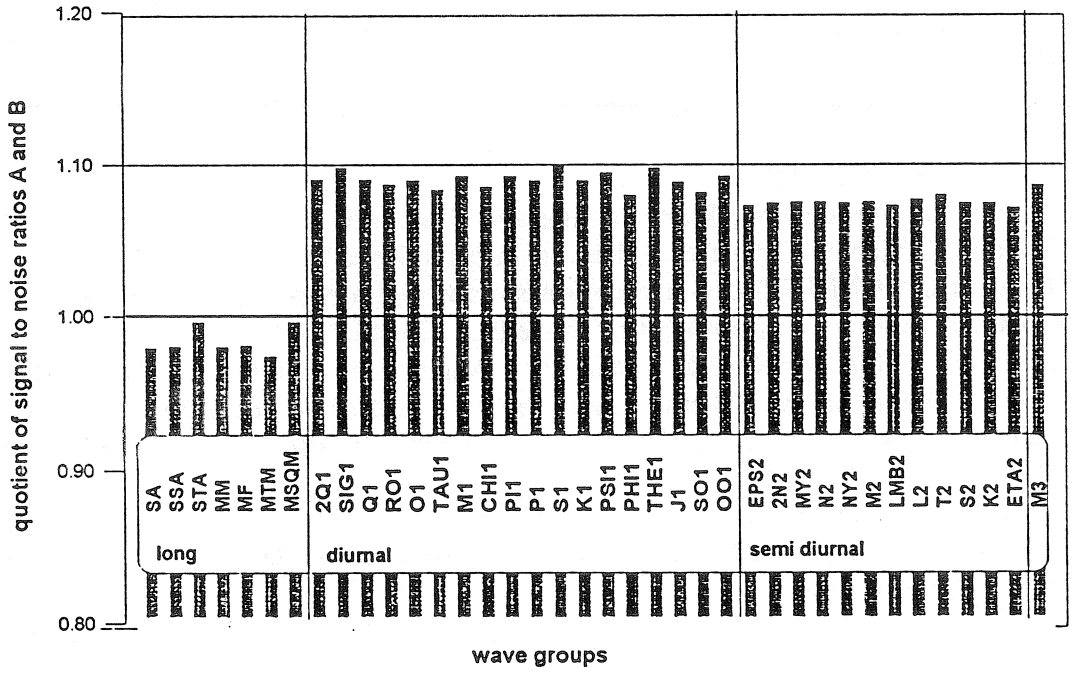

Figure 7 Improvement of the signal to noise ratio for the tidal band

4. Conclusions

For correction of the atmospheric pressure effect the complex admittance should be calculated from tide free output and atmospheric pressure. The block length can be variable between 1.5 and 0.05 cpd depending on the study. Before tidal fitting the atmospheric pressure correction should be done in frequency domain or time domain.

5. Acknowledgements

I thank Cl. Elstner Institut für Angewandte Geodäsie (Potsdam) for helpful discussions and H-.J. Dittfeld GFZ Potsdam for preprocessing of gravity data.

6. References

[1] Melchior P. : The Tides of the Planet Earth, Oxford, Pergamon Press, 1966

[2] Sun H.-P., Ducarme B., Dehant V.: Theoretical Calculation of the Atmospheric Gravity Green Functions. Paper presented on the Working Group on High Precision Tidal Processing, Calibration, Theoretical Tidal Model, Bonn, Germany August 30 - Sept. 2, 1994.

[3] Merriam J.B.: Atmospheric pressure and gravity. Geophys. J. Int. (1992) 109, 488 - 500.

[4] Shi P., Segava J., Fokuda Y.: Effects of Atmospheric Pressure on the Gravity Changes Measured by a Superconducting Gravimeter. Journal of the Geodetic Society of Japan, No. 3, (1993), 39, 293-311.

[5] Warburton R. J., Good kind J.M.: The influence of barometric - pressure variations on gravity. Geophys. J. R. astr. Soc. (1977) 48, 281-292.

[6] Merriam J. B.: The Atmospheric Pressure Correction in Gravity at Cantley Quebec. Paper presented on the 12th International Symposium on Earth Tides August 4.- 7., 1993, Beijing, China.

[7] Bendat J. S., Piersol A. G.: Random Data - Analysis and Measurement Procedures. A Wiley-Interscience Publication JOHN WILEY & SONS New York Chichester Brisbane Toronto Singapore, 1986.

[8] Neumeyer J.: Acquisition, Preprocessing and Evaluation of GFZ Potsdam SCG Data. submitted to Marees Terrestres Bulletin d'Informationes Bruxelles, 1994.

[9] Wenzel H.G.: PRETERNA - a preprocessor for digitally recorded tidal data. Marees Terrestres Bulletin d´Informationes Bruxelles, 118, 8724 - 8734, 1994.

[10] Elstner Cl., Harnisch M., Schwahn W.: Annual and Semiannual Modulations of Planetary Waves in the Spectra of Air Pressure and some consequences on Gravity Variations. Marees Terrestres Bulletin d´Informationes Bruxelles, 117, 8664 - 8674, 1993.

[11] Crossley D. J., Jensen O.G.: Effective Barometric Admittance and Gravity Residuals. Paper presented on the 12th International Symposium on Earth Tides August 4.- 7. 1993, Beijing, China.

[12] Wenzel H.G.: ETERNA - an earth tide analysis program package for the personal computer. submitted to Bulletin Geodesique, 1994.

TIDAL VARIATIONS OF UNDERGROUND WATERLEVEL.

Varga T.,
Eötvös L. Geophysical Institute of Hungary, Budapest

Chojnicki T.,
Space Research Centre, Polish Academy of Sciences, Warsaw

I. Introduction

We introduce the beginning of such research the aim of which is practical usage of research results of earth tide including method of analysis in the field of hydrogeology. Hydrogeology as an application field is promising because the monitoring hydrogeological boreholes already exsist worldwide, thus they are in operation in a great number also in Hungary and the recording of waterlevel has been going on for years.
Our research is divided into two groups:

1. Separation of the earth tide from the recorded data of waterlevel monitoring boreholes.
   Lunisolar variations experienced in waterlevel monitoring boreholes contain information on strain state of undersurface reservoire, their amplitudes and amplituderatios of tidal waves should reflect these.

2. Separation of the waterlevel variations which depends only on hydrogeological factors.
   The elimination of factors resulting the so called additional waterlevel variation (earth tide, temperature, airpressure etc) from data observed in monitoring boreholes.

II. Separation of the earth tide from the recorded data of waterlevel monitoring boreholes.

During our study we have looked at the data set of 5 (Bábolna, Zalacsány, Pilisvörösvár, Szarvas 1 and 3) waterlevel monitoring boreholes (the map of the boreholes is shown by the Figure 1).
The boreholes are of small diameter, they are equipped with non-uniform waterlevel recording devices, where time-signal sample was taken every 1-3 hours. The observations were carried out by the Hungarian State Geological Institute (MÁFI). The recorded data sets were compiled by Z. Kuhen and Gy. Tóth (MÁFI).

As an example we are showing a part of the recorded waterlevel curve of the Bábolna borehole.It can be seen (Figure 2) that from 28th November 1984 for 1440 hours the triassic karstic reservoir's static waterlevel was between 66,5m and 67,2m deep under the surface (the depth of the filtered section is 1266-1273 m).

As the analysis method of the records of the mentioned boreholes the Chojnicki procedure was chosen. It is based on the least-squares principle (Chojnicki, 1977)
To meet the aims of the present study the tidal wave theoretic model has been divided into two wave groups: diurnal-waves O1 and semidiurnal-waves M2.

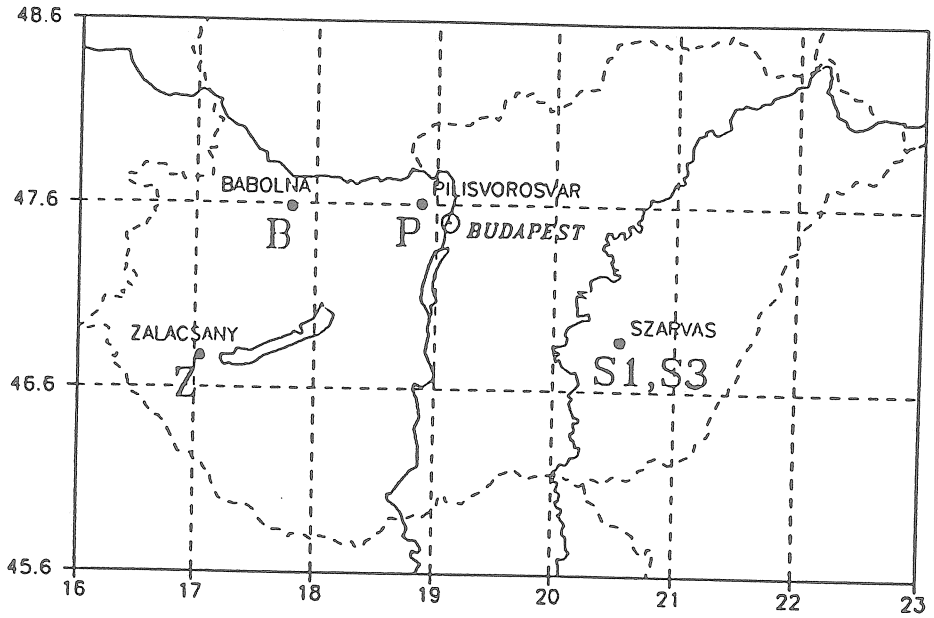

Fig. 1 Map of the observed waterlevel monitoring boreholes.

Main data of the studied monitoring boreholes:

Name of the borehole	Z Zalacsány	B Bábolna	P Pilisvörösvár	S1 Szarvas1	S3 Szarvas3
Surface height in meters	120.5	144.9	183.0	84.7	84.7
Depth of filtered section from surface in meters	206-239	1266-1273	188-225	870-884	192-210
Undersurface reservoir	Triassic karstic limestone dolomite	Triassic karstic limestone dolomite	Triassic karstic limestone dolomite	Pannonian sediment of Pliocene (changing of sandy, clay-like formations)	Pannonian sediment of Pliocene (changing of sandy, clay-like formations)
Studied epoch	1992-1993	1984-1988	1977-1991	1982-1988	1982-1988

During calculations everywhere the same reference epoch was adopted in order to facilitate the comparison of the amplitude values recorded on certain monitoring boreholes. The following results reflect the analysis of tidal waves of the mentioned 5 boreholes (Table 1).At the Pilisvörösvár borehole the 171-day-long data set was analysed also separately,because meteorological data were available only for this period.

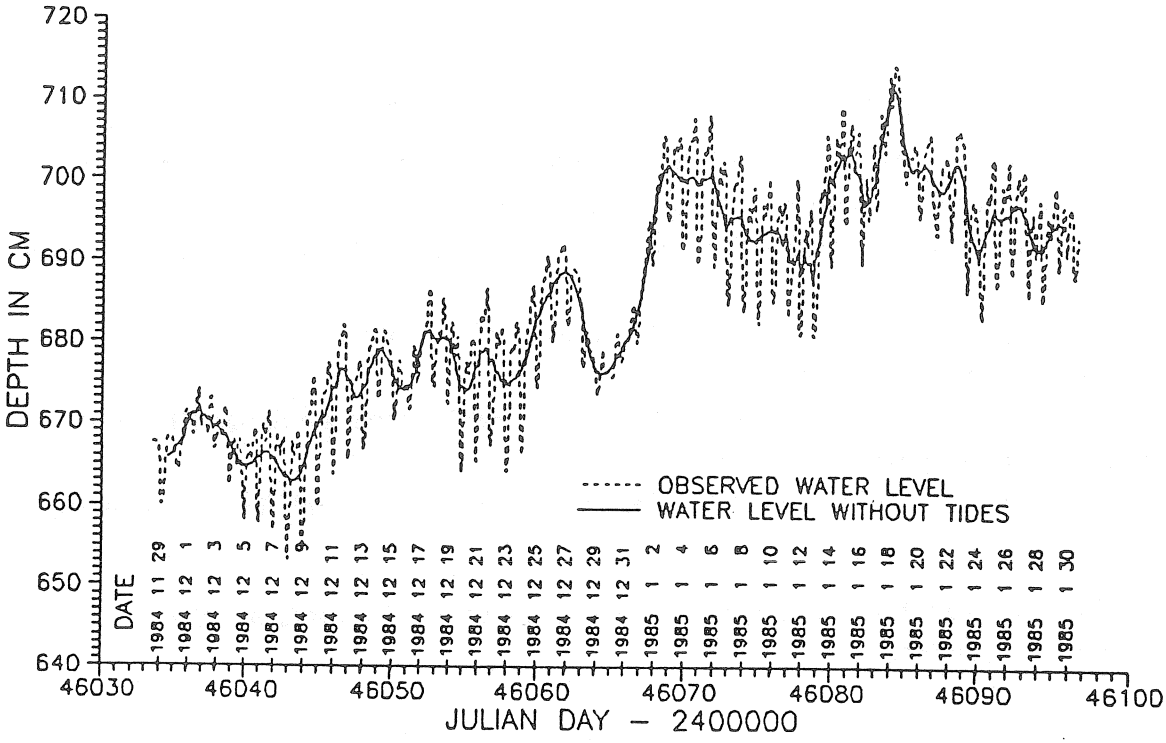

Fig. 2 Observed data at the Babolna borehole.
(to the depth scale value-60 m must be added)

Table 1 Tidal waves of the borehole water level.

Station	Lenght of series *day*	mo *cm*	O1			M2		
			Amplit. factor *cm/μgal*	Phase diff. *degree*	Ampl. *cm*	Amplit. factor *cm/μgal*	Phase diff. *degree*	Ampl. *cm*
B Babolna	1163	2.37	0.0628 .0030	-13.7 2.8	6.59 .32	0.0500 .0054	-11.2 6.3	2.62 .29
Z Zalacsany	345	0.69	0.0349 .0007	-29.5 1.2	3.67 .08	0.0288 .0004	-32.9 .8	1.56 .02
P Pilisvoros.	5210	0.46	0.0038 .0002	-62.7 2.5	0.37 .02	0.0015 .0001	-45.42 3.7	0.09 .01
P Pilisvoros.	171	0.05	0.0013 .0002	-49.8 6.6	0.14 .02	0.0009 .0001	-35.7 5.8	0.05 .00
S1 Szarvas 1	2478	0.28	0.0010 .0001	-11.4 5.8	0.11 .01	0.0007 .0001	-10.2 7.3	0.04 .00
S3 Szarvas 3	971	0.09	0.0004 .0001	-16.9 11.1	0.04 .01	0.0002 .0000	0.1 10.9	0.01 .00

As a supplement what was mentioned above - without detailing the hydrogeology and tectonics of Hungary - we would like to mention the following as an information on Pannonian formations influencing not the least the stressfields:

- the undersurface reservoir belonging to Pilisvörösvár karst borehole can be practically traced up to the surface;
- over the undersurface reservoir belonging to Zalacsány karst borehole an approximately 200m thick Pannonian formation is settled;
- over the undersurface reservoir belonging to Bábolna karst borehole a more as 1000 m thick Pannonian formation is settled;
-the depth of the Pannonian reservoir belonging to Szarvas 1 and 3 borcholes is even deeper than -3500m.

As a summary we can say about the Bábolna, Zalacsány, Pilisvörösvár, Szarvas1 and Szarvas3 boreholes that (Figure 3):

1.

- all earth tide vawes defined in the monitoring boreholes were shown with great certainty because their average least-square error were at least ten times smaller than the amplitude value;
- in accordance with the geophysical and hydrogeological considerations in all monitoring boreholes the observed lunisolar effects are delayed compared to the tide wave generating effect;

2

- the tide waves amplitude values of Zalacsány and Pilisvörösvár in almost equally shallow karst boreholes are essentially different.The greatest amplitude values can be experienced at Bábolna deep karst borehole;
- in case of Szarvas boreholes settled onto Pannonian undersurface reservoir the increase of amplitude values can be experienced depending on the depth, their value is smaller than those experienced in karst boreholes;

3.

- at karst monitoring boreholes the O1 and M2 ratio became 2.20-2.35-2.50 (exception is the Pilisvörösvár borehole 5210-day-long recorded data with 4.11 value). At Pannonian formation monitoring boreholes the O1 and M2 ratio was 4.0 and 5.5.

On the basis of the analysis carried out in 5 boreholes we cannot draw far-reaching conclusions. But we have several hundred such waterlevel monitoring boreholes the recorded data of which are suitable for analysis with Chojnicki method. On the basis of our experiences it seems to be promising to compile maps of amplitudes of O1 and M2 waves and respectively their ratios in order to characterize stressfields of undersurface reservoir.

III. Separation of the waterlevel variations which depends only on hydrogeological factors.

The recorded waterlevel variation W is a function of the following variables:

$$W = f (HG, T, Pr, Ti, I)$$

where:

HG - hydrogeological factors

T - temperature

Pr - airpressure

Ti - earth tide

I - instrumental factors of monitoring boreholes (the filter-packing etc), in the present state of our study in case of monitoring boreholes I=0.

We have tried the application of Chojnicki method for the exclusion of not only the earth tide also the temperature and airpressure, i.e. to reach the W = f (HG) state.

We studied correlation in case of Bábolna deep karst borehole at first between earth tide-free waterlevel and airpressure and at second between the tide- and airpressurefree and temperature (Figures 4a, 4b). In both cases correlation is provable, in case of airpressure correlation it is even better. At the first approximation through first order polinome the defined correlation connection is:

$$W = -0.26\ T + 1.23$$

$$W = -0.62\ P - 2.56$$

where:

W - waterlevel variation (cm)

T - temperature (°C)

P - airpressure (HP)

The situation is similar in the case of Zalacsány karst borehole (Figure 5a, 5b.). The correlation connection here is:

$$W = 0.14\ T + 18.82$$

$$W = -0.64\ P + 128.95$$

In the case of Pilisvörösvár borehole (Figure 6a, 6b.):

$$W = -0.02\ T + 0.23$$

$$W = -0.08\ P - 0.19$$

In case of the Pilisvörösvár Pannonian sedimentsfree borehole this surplus makes 7 cm under 171 day (Figure 10).

Correlation connection in case of Szarvas1 and Szarvas3 Pannonian boreholes are under processing.

As a summary: the curve W = f (HG) determined through Chojnicki method as a function of only hydrogeologic factors is very important for hydrogeologists because it includes also effect of human activity:e.g. waterlevel lowering caused by mining, by watersupplying etc., respectively it can lead to the solution of waterlevel recultivation i.e. environmental protection problems connected with it.

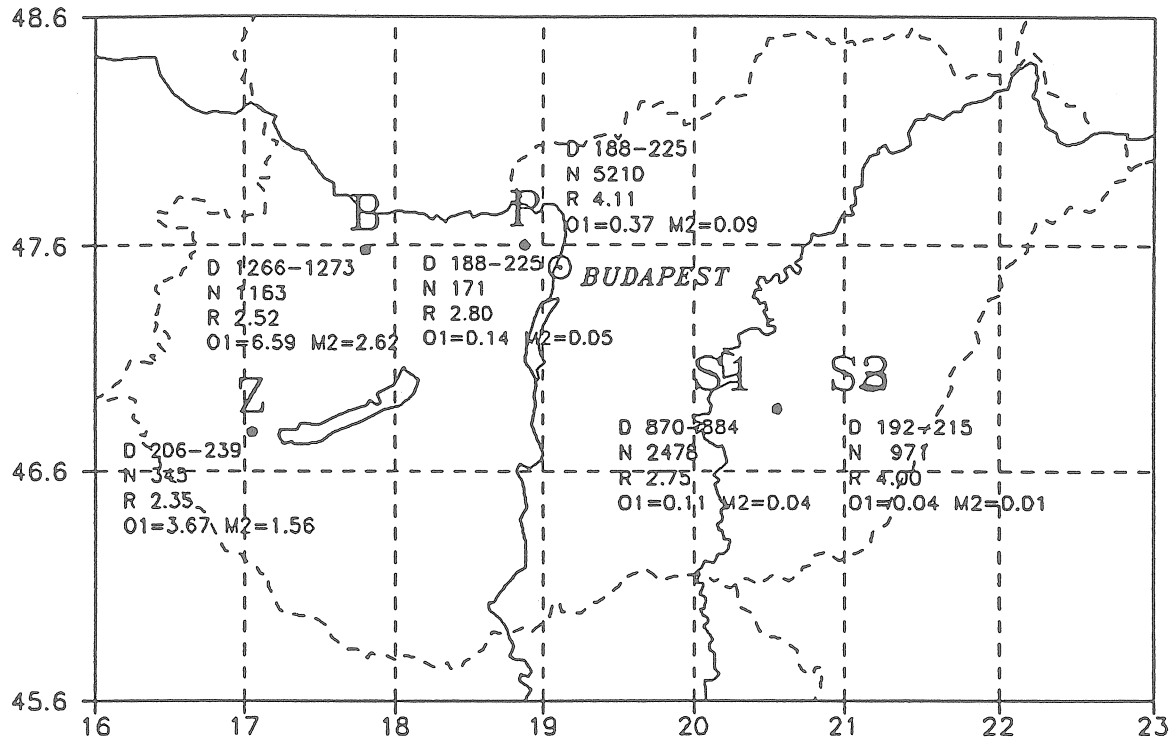

Fig. 3 Map of the studied waterlevel monitoring boreholes with the analyse results.

D – Depth of filtered sections
R – Ratio of the amplitude of O1 and M2
N – Number of studied days
O1,M2 – Amplitude values in cm

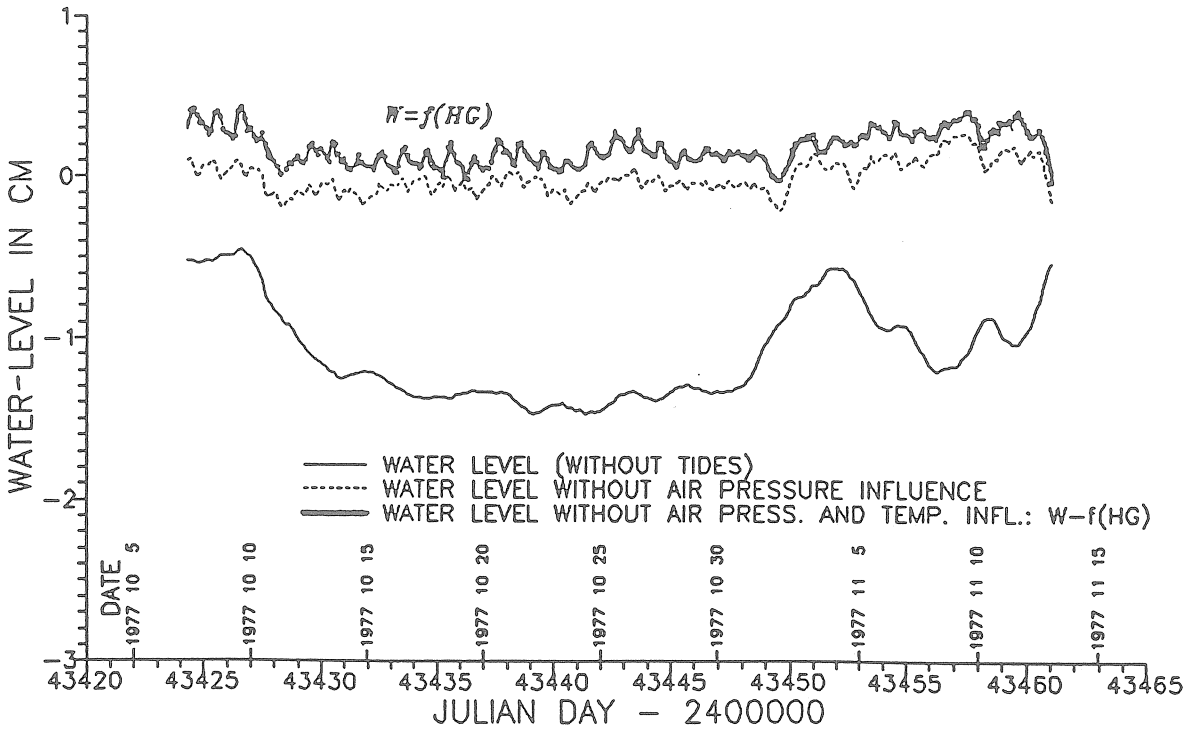

Fig. 10 The curve of hydrogeologic factors W=f(HG) at the Pilisvorosvar borehole.

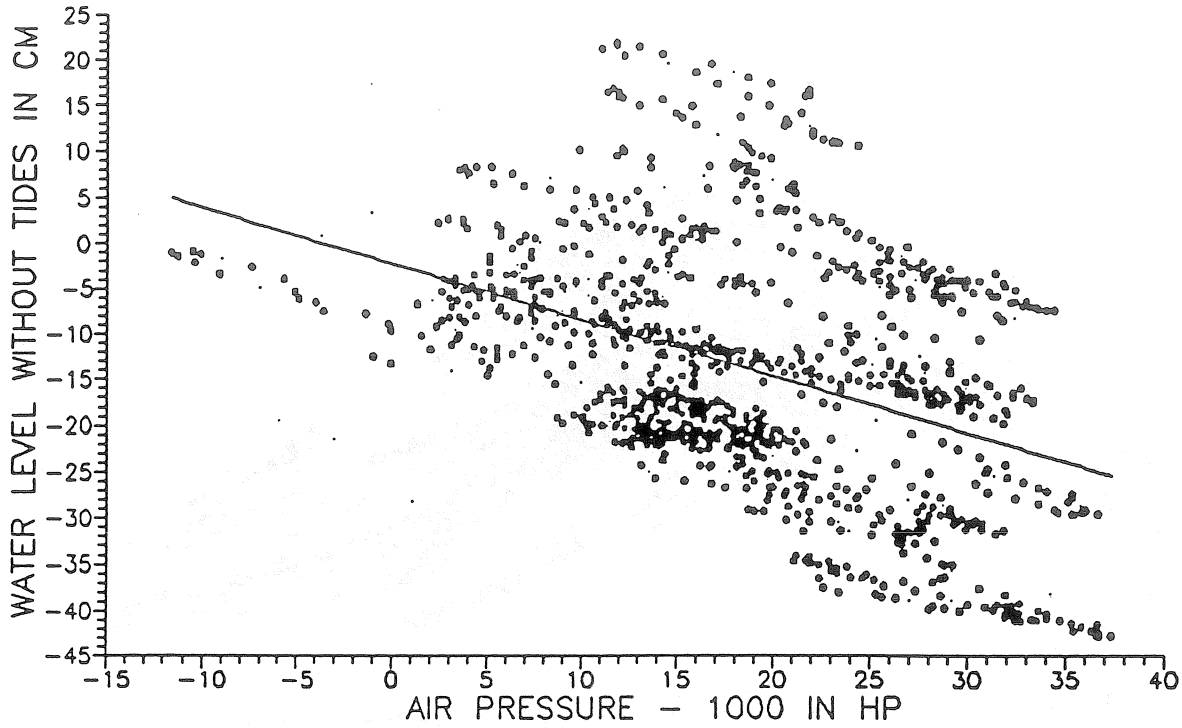

Fig. 4a Correlation of tidal free water level with air-pressure at the Babolna borehole.

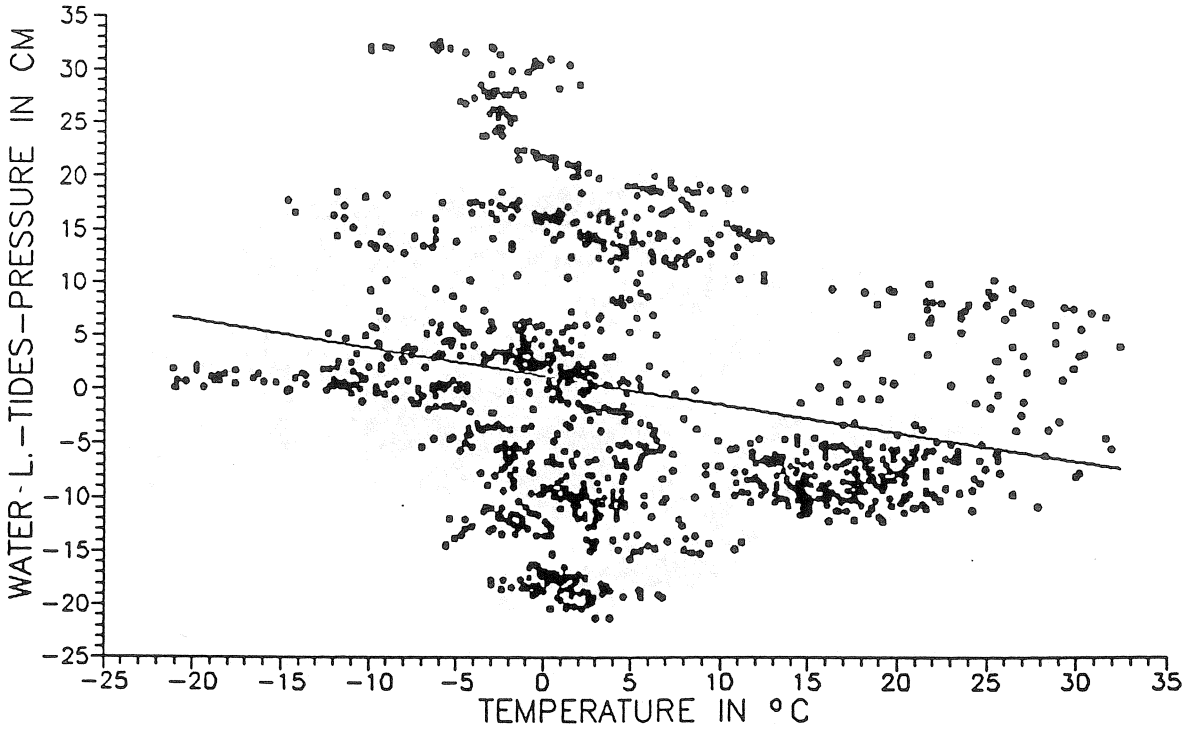

Fig. 4b Correlation of tidal free and air pressure free water level with temperature at the Babolna borehole.

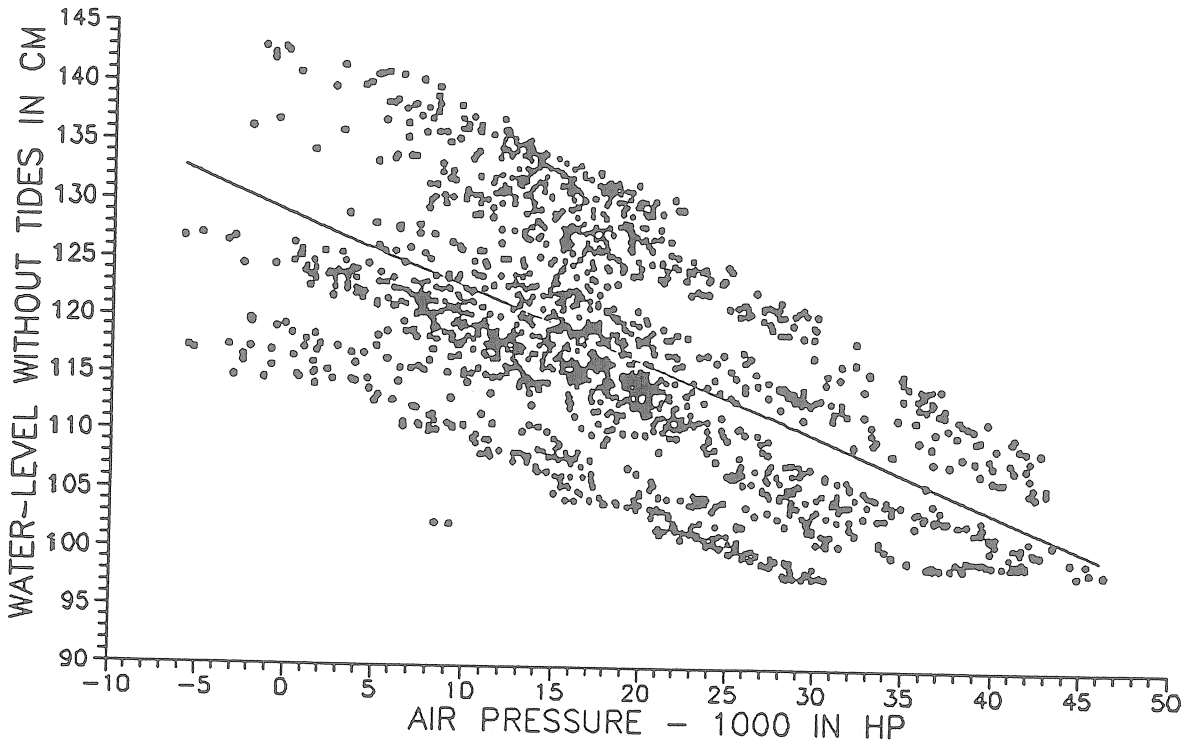

Fig. 5a Correlation of tidal free water level with air pressure at the Zalacsany borehole.

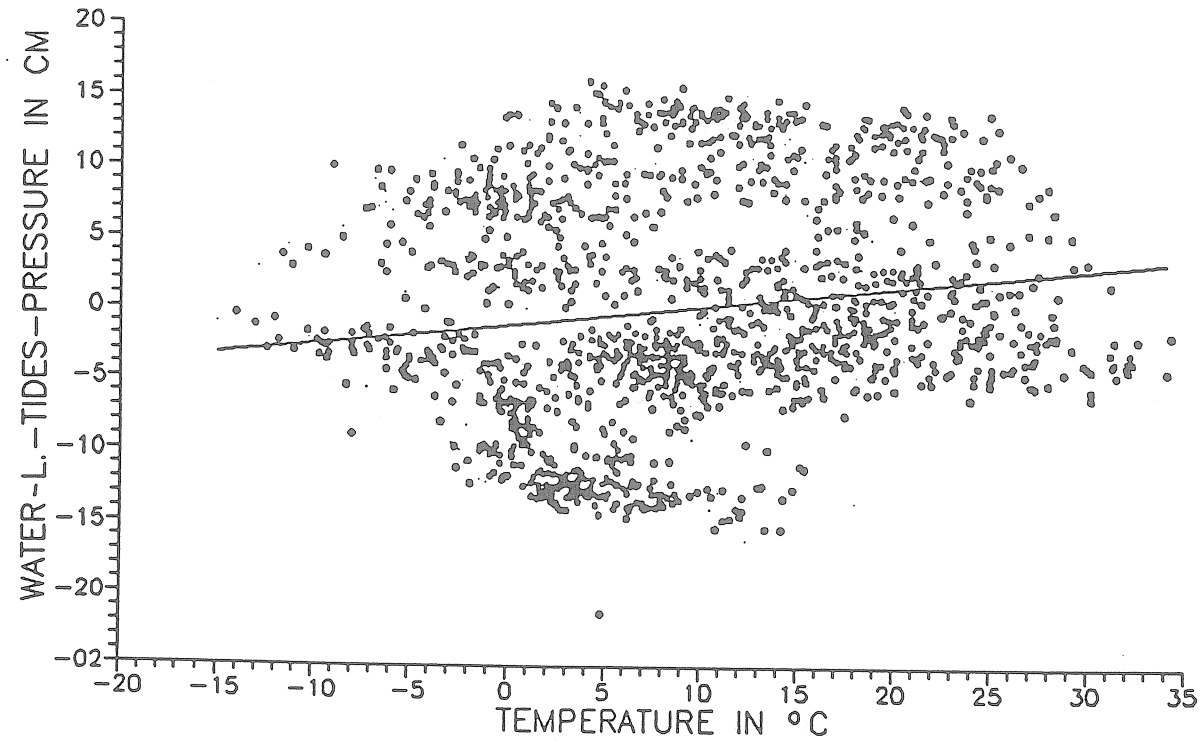

Fig. 5b Correlation of tidal free and air pressure free water level with temperature at the Zalacsany borehole.

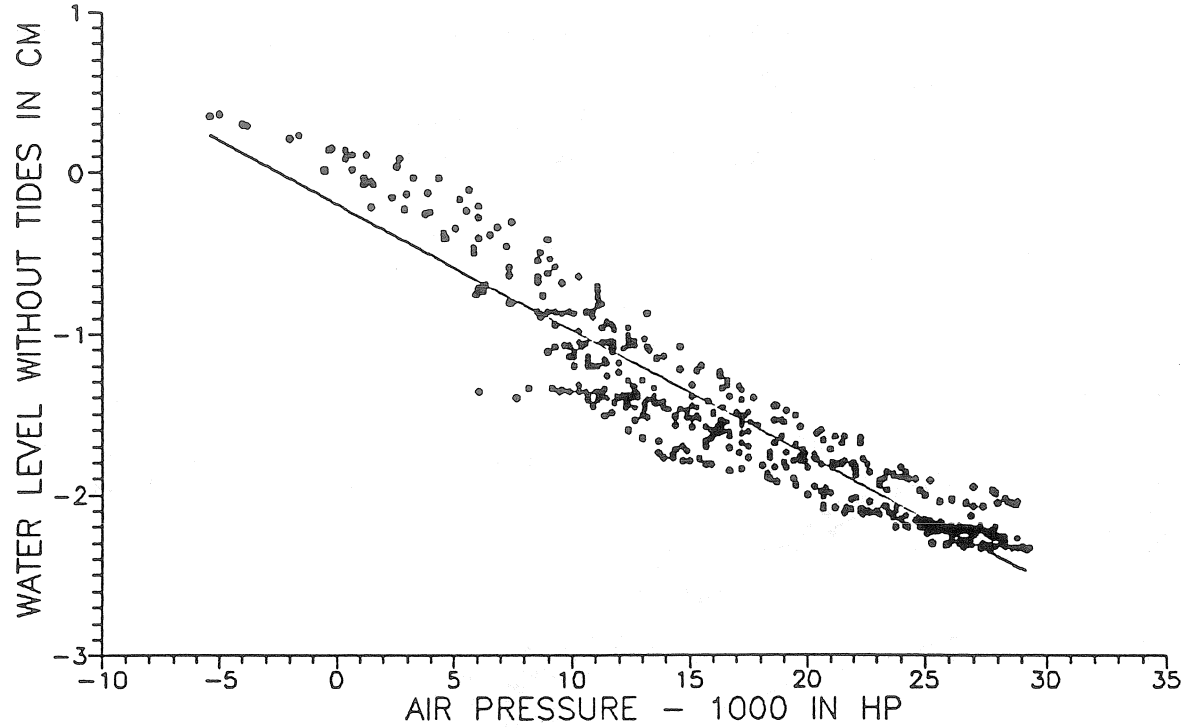

Fig. 6a Correlation of tidal free water level with air pressure at the Pilisvorosvar borehole.

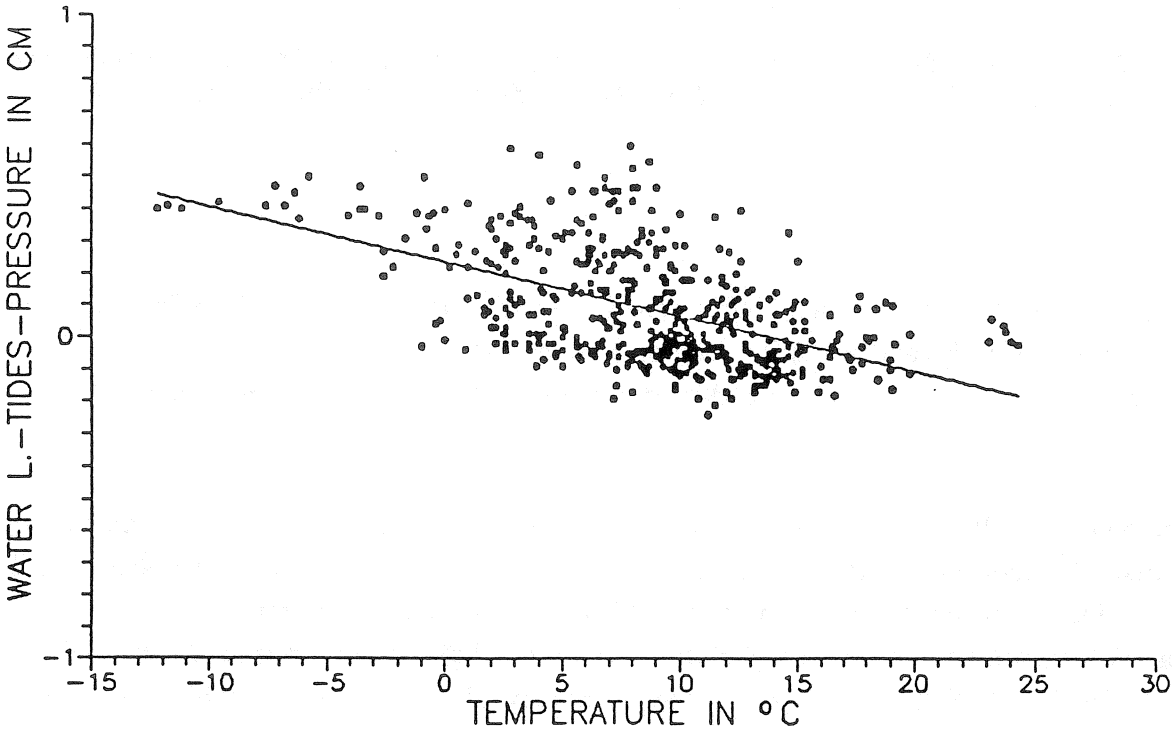

Fig. 6b Correlation of tidal free and air pressure free water level at the Pilisvorosvar borehole.

The results of correlation analysis between the tidefree waterlevel and airpressure which was carried out at different times on the data of this borehole are the following (Figure 7):

$W = -0.05\ P - 0.87$ (5.10.1977 - 15.11.1977)

$W = -0.09\ P + 0.00$ (20.2.1978 - 30.7.1978)

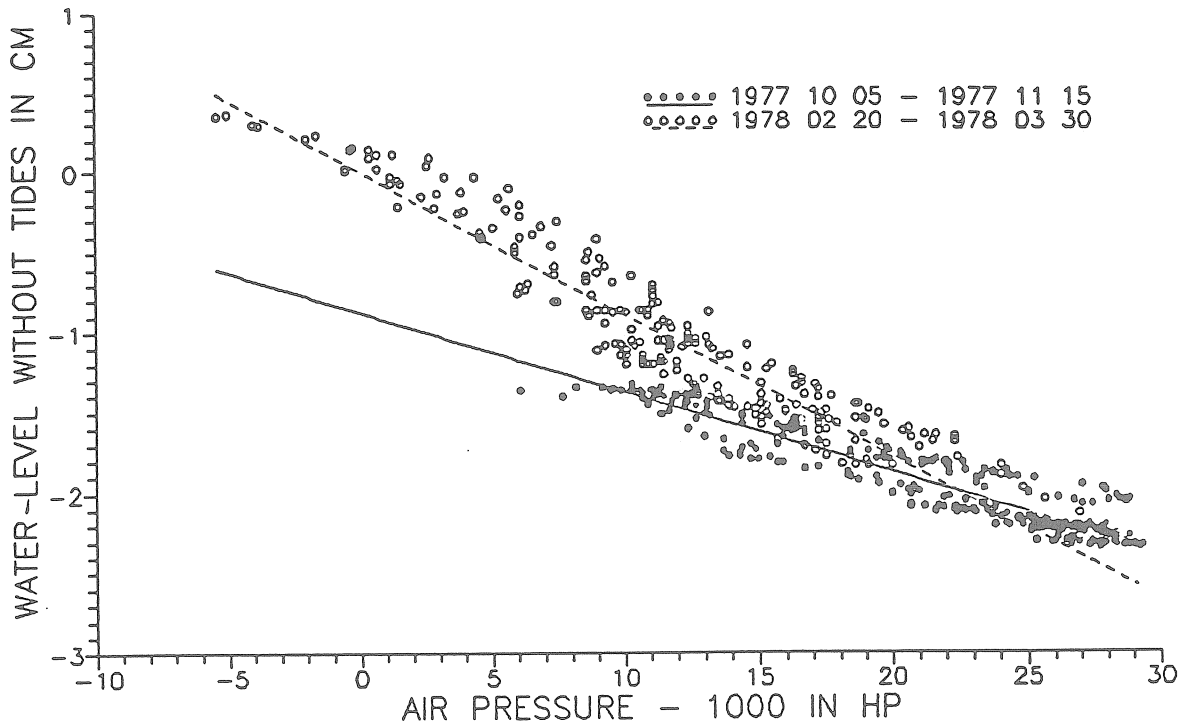

Fig. 7 Correlation of tidal free water level with air pressure at the Pilisvorosvar borehole for different time intervals.

Earth-, temperature- and airpressurefree waterlevel variation in case of the Bábolna, Zalacsány and Pilisvörösvár boreholes can be seen on Figures 8-10.
On these figures the vertical scale does not regard the real depth/height values.

The bold curve W = f (HG) is the function of hydrogeological factors. If we compare this e.g. in case of Bábolna deep karst borehole to the recorded waterlevel curve we can state that the earth tide, airpressure and temperature altogether resulted approximately 25 cm surplus waterlevel variation under two months (Figure 8). This surplus makes 21 cm between 15.10.1992 - 15.9.1993 in case of the Zalacsány shallow karst borehole only due to temperature and airpressure (Figure 9).

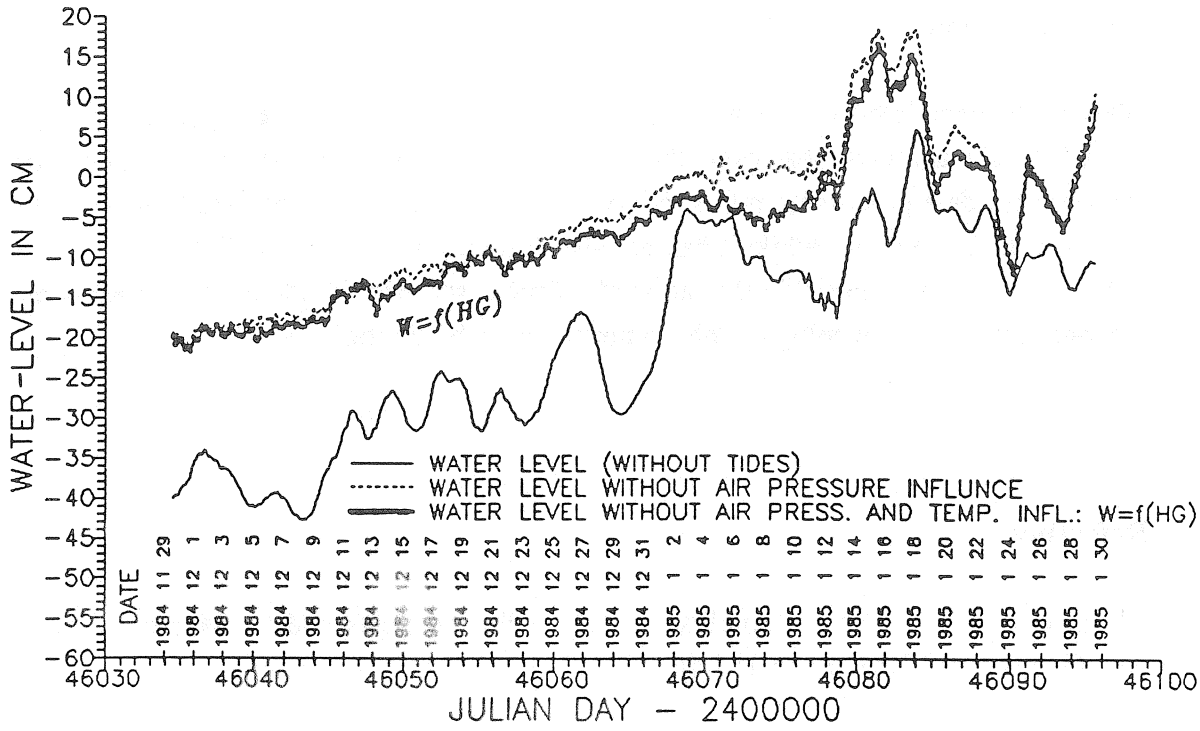

Fig. 8. The curve of the hydrogeologicfactors W=f(HG) at the Babolna borehole.

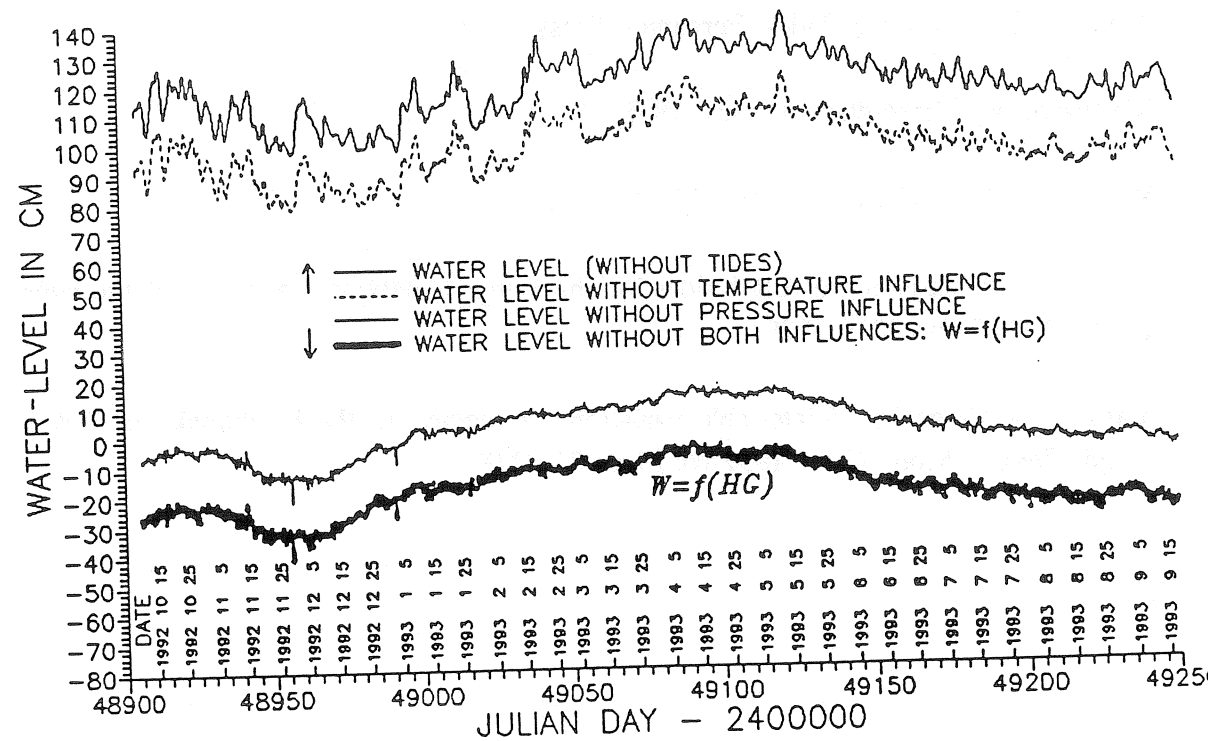

Fig. 9. The curve of hydrogeologic factors W=f(HG) at the Zalacsany borehole.

IV. Conclutions.

During the completed studies we proved at the same time through applying the manyfoldness of Chojnicki analysis, that even the fraction of waterlevel monitoring borehole data sets brought for data processing refers to how useful the recognition and study of earth tide is in regional hydrogeology, while it has got also further developing possibilities.
Moreover it is also possible that at geodynamical stations for the earth tide registration the recognition of hydrogeological phenomena cannot be disregarded.

References:

Chojnicki T.: Sur l'Analyse des Observations de Marees Terrestres. Ann.Geophys.1977.33.1/2.pp.157-160.

Csaba L. - Varga P.: Untersuchung von Schichtenwasser- Spiegelschwankungen in den Schichten-Beobachtungsbrunnen des Ungarischen Staatlichen Geologischen Instituts. Hidrogeológiai Közlöny. 1977. 5. pp.220-224.

A Magyar Állami Földtani Intézet mélységi vízfigyelő kutjainak észlelési adatai.1982.

Melchior P. :The Earth Tides, Pergamon Press. 1966.

Magyarorszag Vízföldtani Atlasza. 1968.

Roeloffs E.A.: PAGEOPH. 1988. 126. pp.177-209.

Varga P. : Investigation of Earth tides by observing dilatational variations of the watertable. B.I.M. 1976.74.pp.4319-4329.

Varga T. - Varga P. : Watertable variations connected to the Earthquake in Bekes. Acta Geod.,Geoph., Mont. Hung.1992.vol.27.pp.231-239.

ANALYSIS OF TIDE GRAVITY STUDIES IN RUSSIA DURING 1960s-1990s

by A.Kopaev
Astronomical Institute of Moscow University
Universitetski prosp. 13, V-234 Moscow, 119899 Russia
fax:+7-095-9390126, e-mail:kopaev@sai.msk.su

1. Abstract

Difficulties of recording gravimeters calibration and ocean tides correction still prevent to use tide gravity data for investigation of the Earth mantle heterogeneities. Territory of Russia is very interesting in this context because of small oceanic influence and suspected δ-factors anomalies, but the russian tide gravity network suffers from insufficient territory coverage and low quality of data obtained with Askania gravimeters only. Further development of tide gravity studies in Russia should be carried out in the framework of international cooperation.

1. Introduction

The interest to the tide gravity observations today is slowly decreasing because of two main reasons:

- difficulties of calibration of recording gravimeters with an accuracy better than 0.1 % [RICHTER, 1991] that is necessary simply to detect spatial variations of δ-factors that could reach of about 0.5 % only [MOLODENSKII, KRAMER, 1980],
- difficulties of ocean tides correction [BAKER et al, 1989].

Both factors still prevent to use tide gravity for investigation of elastic-viscous properties of the heterogeneous Earth mantle that should be the natural aim of tide gravimetry.

Russian territory seems attractive in this context because of small oceanic influence and suspected anomalies of δ-factors of up to 0.7 % in Siberia, according to [MOLODENSKII, KRAMER, 1980] (**fig. 1**).

2. Tide gravity data in Russia

Unfortunately russian tide gravity stations network (**fig. 1**) suffers from both low quality of data obtained with Askania gravimeters only and from insufficient territory coverage - only 5 stations from the former soviet tide gravity network [PARIISKII, 1977] are located on russian territory today:

- Pulkovo (Sanct-Petersburg);
- Obninsk (Moscow);
- Krasnaya Pakhra (Moscow);
- Novosibirsk:
- Irkutsk.

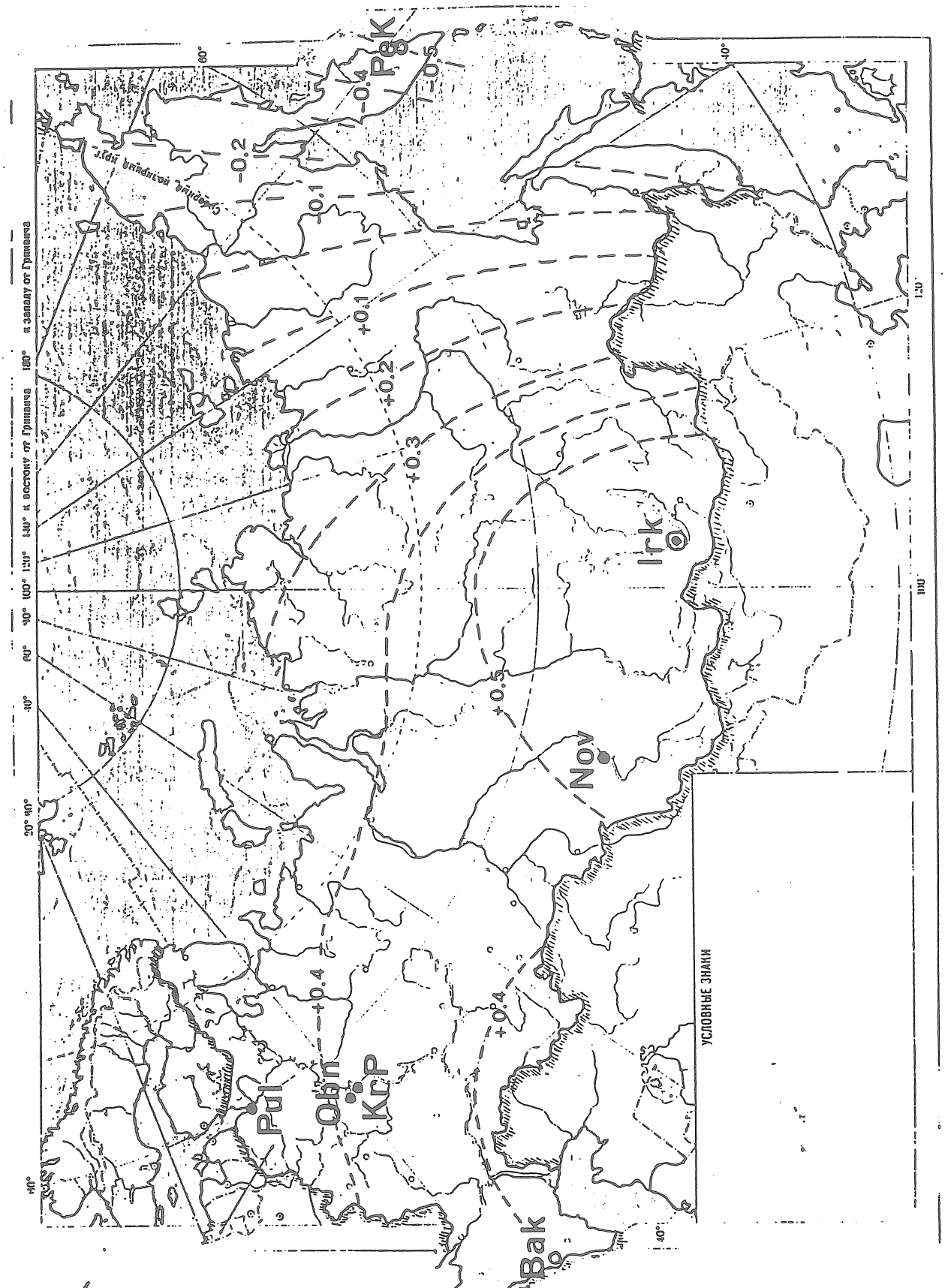

Fig. 1 Tidal gravity network of Russia
- existing stations: Pul = Pulkovo (Sanct-Petersburg)
Obn = Obninsk (Moscow)
KrP = Krasnaya Pakhra (Moscow)
Nov = Novosibirsk
Irk = Irkutsk
- planned stations: Bak = Baksan (Central Caucasus)
Irk = Irkutsk
PeK = Petropavlovsk-Kamtchatskii
- isolines of delta-factor (M2) anomalies (in %)
according to [HOLODENSKII, KRAMER, 1980]

Ocean corrected δ-factors for M_2 and O_1 at russian stations taken from ICET data bank [MELCHIOR, 1994] are represented on Table 1 and fig. 2. They exhibit a large scatter up to 2 % in 'Irkutsk' (for M_2), excluding only 'Obninsk' station, where latest Askania gravimeters ##220, 221 and 224 have been used. Dashed lines represent the average values of ocean corrected δ-factors obtained from most precise recent tide gravity experiments [BAKER ET AL, 1989; TIMMEN, WENZEL, 1994] (inertial correction applied).

Statistical analisys of russian data gives accuracy of $\delta(M_2)$ and $\delta(O_1)$ for single station of about 1 % with mean values:

$$\overline{\delta(M_2)} = 1.163 \mp 0.005 \; ; \; \overline{\Delta\phi(M_2)} = -0.3^{\circ} \mp 0.4^{\circ};$$

$$\overline{\delta(O_1)} = 1.157 \mp 0.003 \; ; \; \overline{\Delta\phi(O_1)} = -0.4^{\circ} \mp 0.2^{\circ},$$

that is about 0.5 % larger than corresponding values in [TIMMEN, WENZEL, 1994].

3. Discussion

Current situation with tide gravity studies in Russia is unsatisfactory because it is a most suitable area for testing modern body tide models, especially for detecting spatial anomalies of δ-factors connected with mantle heterogeneities. The best places for new observations could be Baksan (Central Caucasus), Irkutsk (Baikal rift) and Petropavlovsk-Kamtchatskii (Kamtchtaka) (fig. 1) that are located in tectonically active areas and tide gravity observations there could contribute to the testing the prof. Melchior hypothesis [MELCHIOR, DUCARME, 1989; RYDELEK ET AL, 1991].

4. Conclusion

An international geodynamical project consisting on precise tide gravity recording at least at three stations in tectonically active regions of Russia (Caucasus, Baikal rift, Kamtchatka) with a set of 3-5 tide gravimeters during at least 1 year at each station could give fundamental results concerning spatial variations of δ-factors caused by mantle heterogeneities.

5. Acknowledgements

Author is very indebted to Profs. P.Melchior and B.Ducarme for their attention, valuable help and fruitful discussions.

Table 1

Ocean corrected tide parameters at the stations of russian tidal gravity network

Station	O_1	M_2
Obninsk	δ = 1.1540±0.0012 $\Delta\phi$ = -0.08 ±0.03	δ = 1.1617±0.0026 $\Delta\phi$ = -0.01 ±0.05
Krasnaya Pakhra	δ = 1.1612±0.0076 $\Delta\phi$ = -0.25 ±0.19	δ = 1.1678±0.0050 $\Delta\phi$ = -0.24 ±0.10
Pulkovo	δ = 1.1643±0.0022 $\Delta\phi$ = -0.59 ±0.02	δ = 1.1501±0.0025 $\Delta\phi$ = -0.99 ±0.04
Novosibirsk	δ = 1.1464±0.0073 $\Delta\phi$ = -0.50 ±0.37	δ = 1.1613±0.0044 $\Delta\phi$ = -0.46 ±0.22
Irkutsk	δ = 1.1596±0.0015 $\Delta\phi$ = -0.37 ±0.11	δ = 1.1754±0.0013 $\Delta\phi$ = -0.07 ±0.07

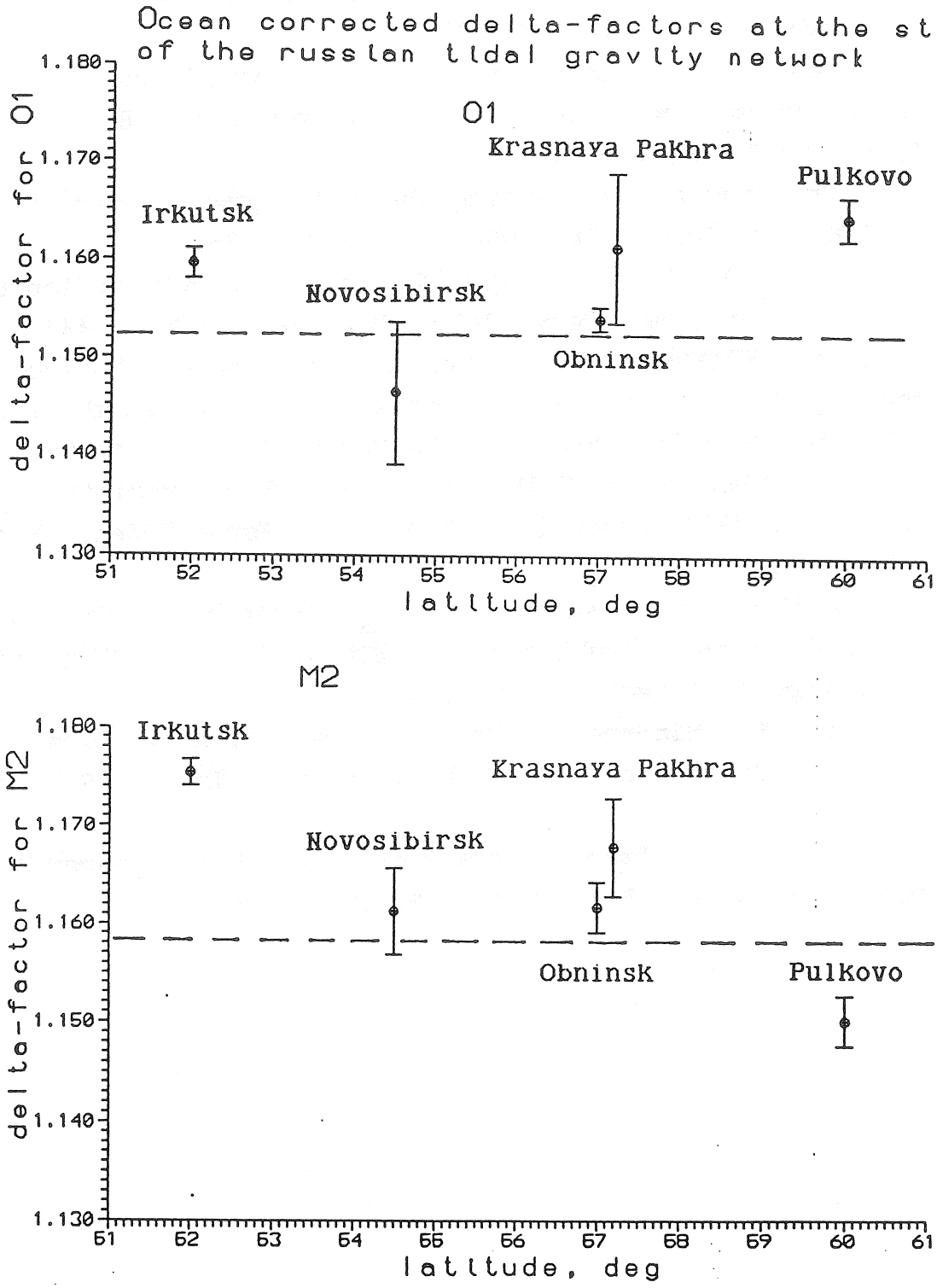
Ocean corrected delta-factors at the stations of the russian tidal gravity network
O1
Krasnaya Pakhra
Pulkovo
Irkutsk
Novosibirsk
Obninsk
delta-factor for O1
1.180
1.170
1.160
1.150
1.140
1.130
51
52
53
54
55
56
57
58
59
60
61
latitude, deg
M2
Irkutsk
Krasnaya Pakhra
Novosibirsk
Obninsk
Pulkovo
delta-factor for M2
1.180
1.170
1.160
1.150
1.140
1.130
51
52
53
54
55
56
57
58
59
60
61
latitude, deg

Fig. 2

6. References

BAKER T., Edge R., Jeffries G. Tide gravity in Europe: better agreement between models and observations. Geophys. Res. Letters, 1989, 16, N 10, 1109-1112.

KOPAEV A., Yushkin V., Leontyev I. First experience of tide recording using modified quartz gravimeter. BGI Bull. d'Inform., 1993, 72, 41-45.

MELCHIOR P. Checking and correcting the tidal gravity parameters of the ICET Data Bank. BIM, 1994, 119, 8899-8935.

MELCHIOR P., DUCARME B. Tidal gravity anomalies and tectonics. Proc. 11th Inter. Symp. Earth Tides, Helsinki, 1989, 445-454.

MOLODENSKII S., KRAMER M. Influence of large-scale horizontal inhomogeneities of the earth mantle on the earth tides. Izvestiya Akademii Nauk SSSR. Fizika Zemli, 1980, 1, 14-25.

PARIISKII N., Barsenkov S., Volkov V. et al. Tidal variations of gravity in the USSR. Proc. 8th Inter. Symp. Earth Tides, Bonn, 1977, 561-579.

RICHTER B. Calibration of superconducting gravimeters. Cah. Cen. Europ. Geod. Seism. (published by ECGS), Vol. 3 "Non-tidal gravity changes", Luxemburg, 1991, 99-107.

RYDELEK P., Zurn W., Hinderer J. On tidal gravity, heat flow and lateral heterogeneities. Phys. Earth Planet. Inter. 1991, 68, 215-218.

TIMMEN L., WENZEL H.-G. Improved gravimetric earth tide parameters for station Hannover. BIM, 1994, 119, 8834-8846.

Tidal gravity measurements on Greenland

by

G. Jentzsch[1], M. Ramatschi[1], and F. Madsen[2]

Abstract

Tidal gravity measurements were started at fiducial sites around the Norwegian-Greenland Sea in order to provide corrections for the dynamic part of the coordinates of the sites. The measurements with our LaCoste & Romberg tidal gravimeter ET 18 started in summer 1993 at Scoresbysund/Eastgreenland, and after a one year record the gravimeter was moved to Narsarsuaq at the southern end of Greenland. Since the transport conditions are fairly rough we used a G-meter to check the calibration of the ET 18.

The first results show that the calibration can be checked on the 0.3 % level by parallel recording over three to five days at each station. The analyses of the tidal loading vectors give rise to the estimation of systematic errors in time depending station height of more than 5 cm if standard ocean tidal charts are used.

1. Introduction

Space born and aircraft based observations of the earth esp. concerning the changes of the Greenland ice cap are related to kinematic GPS measurements connected to fiducial sites. With regard to the accuracy of these measurements the time variation of the coordinates of the reference stations must be determined.

From August 1993 to August 1994 a LaCoste & Romberg earthtide meter recorded at the Seismological Observatory / Tele Station at Scoresbysund/Eastgreenland. This station is part of the NATURE[3] project as proposed during the 12th International Symposium on Earth Tides, Beijing, 1993, and the first of three on Greenland (Engen et al., 1993). The aim of these measurements is to determine true earthtide parameters influenced by the loading of the ocean nearby. By modelling the elastic response of the crust we want to derive real height variations due to the loading tides for the correction of air-borne measurements.

Compared to the Greenland Aerogeophysics Project (GAP) launched in 1991 (Brozena, 1992) and completed in summer 1992 this air-borne survey still yielded accuracies in altitude and acceleration in the range of meter and milligal, resp. ('first-

1: Institut für Geophysik, TU Clausthal,
Arnold-Sommerfeld-Str. 1, D-38678 Clausthal-Zellerfeld

2: Kort- og Matrikelstyrelsen, Geodesiavd., Rentemestervej,
DK-2400 København NV

3: NATURE: North Atlantic Tides Under REsearch

cut' navigation solution dicussed by Colombo & Peters, 1992). But these results are so promising that after the whole GPS constellation is in orbit decimeter-level positioning and submilligal acceleration precision should be achievable.

Colombo & Peters (1992) demonstrated that the vertical error achievable up to now is surprisingly small: Using two fixed stations as a reference they obtain 8 centimeters. Thus, GPS measurements have to be corrected for time variations applying the well known tidal potential and ocean loading vectors obtained up to now from global ocean tidal charts provided by Schwiderski (1979a/b) and others.

Global climate changes are assumed to induce global sea level changes. As pointed out by Carter & Robertson (1991), the increase of the sea level of only 1 millimeter world wide would correspond to a uniform decrease of the surface of the Greenland ice cap by about 16 centimeters. Keeping in mind the difficulties in geodetic datum realization for the detection of a 1 millimeter sea level change this suggests that it may prove easier to detect changes in the ice masses than in the sea level. Therefore, the monitoring of the Greenland ice cap (and other ice sheets) will be an important task for the future.

2. Gravimeter, data acquisition and calibration

The LaCoste & Romberg Earthtide Meter ET 18 is available for our measurements. In preparation of the recording in Scoresbysund a new data acquisition system was developed based on the existing program developed by G. Asch (Asch & Jentzsch, 1987), but modified for the use with a standard PC. It was also extended to a GPS time receiver and a telefon modem. In parallel we record air pressure and temperature. The data is stored on the hard disk as well as on a removable hard disk. The operating system is OS/2 for multi-tasking purposes. Tab. 2.1 gives the technical specifications.

Fig. 2.1 containes a sketch of the station. We use three PREMA A/D-converters for the data. The box 'shaker' indicates the so-called 'earthquake-shaker' which consists of a small motor with an excenter to vibrate the gravimeter if the beam is sticking to one plate. Another box is called 'spind. driver'; this denotes the readjustment device of the range adjusting screw. The 'heater box' denotes the power supply of the gravimeter, whereas the 'heater' below indicates the room heater consisting of the convector and three lamps which are switched on and off by a relais.

There is an additional chart recorder. In order to save battery power this recorder as well as the PC-monitor is not buffered by the UPS.

The gravimeter was installed on a concrete block in the basement of the observatory building in Scoresbysund. To stabilize recording conditions a wooden hut was built around the pillar. For the data acquisition system and the UPS we used a corner of a room in the story above. It is possible to check the station by telefon, even to change the recording program if necessary.

The gravimeter was serviced and carefully calibrated before the start of the record. Before the termination of the record at Scoresbysund a parallel record with the LCR gravimeter G 979 was carried out as well as at the beginning of the recording period at Narsarsuaq in the south of Greenland in August 1994. This check of the calibration shows that there was no change due to the rough

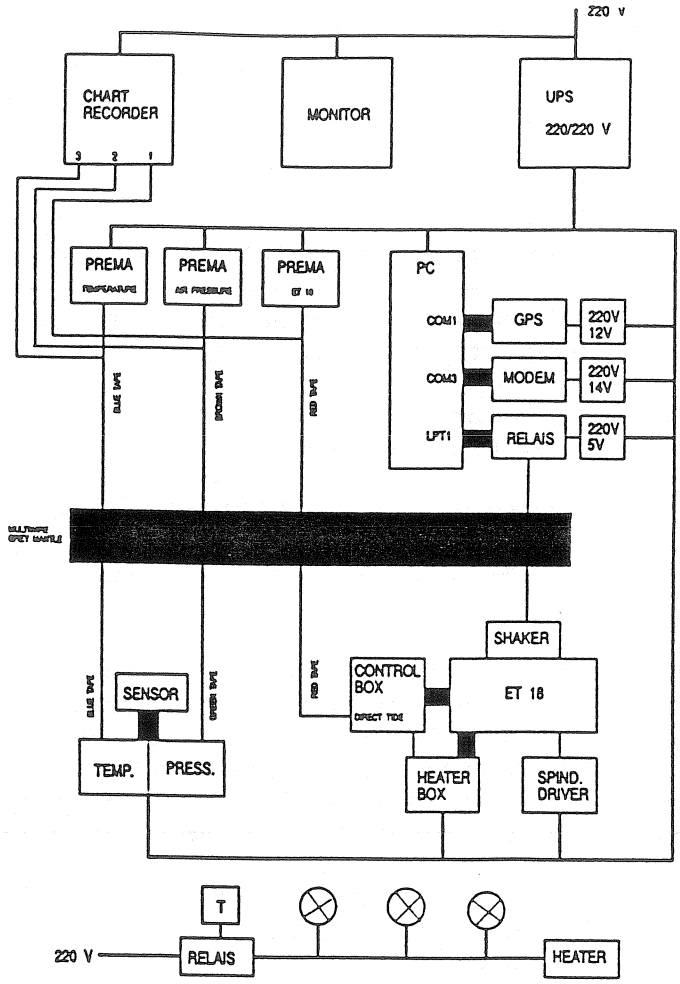

Figure 2.1: Sketch of the gravimeter station; note power supply and data links.

transport. Fig. 2.2 gives the parallel records at Narsarsuaq over about four days. After the separation of the instrumental drift the regression and correlation between both gravimeters was calculated. A cross-plot is given in fig. 2.3. The comparison shows that the calibration of the gravimeter ET 18 was within the 0.3 % accuracy obtained for the calibrations carried out before (comp. Jentzsch & Melzer, 1989; Ramatschi et al., 1993).

3. Data from Scoresbysund

Up to now about half a year of data was ready for the analysis. As can be seen from Fig. 3.1 the data look quite good: The data presented are filtered to hourly values. The drift of the gravimeter is very small which is a prove of the stable recording conditions. There is only one strong disturbance around hour 1000: There, after a power fail our UPS (battery) did not switch back to the mains. Thus, after the battery was empty the gravimeter

Table 2.1: Technical specifications of the gravimeter recording equipment.

PC	486, 50 MHz; operating system OS/2 2.0
modem	Hayes Smart-Modem V14400
time base	GPS-time (1 satellite modus)
A/D-converters	PREMA 4000 (6½ digits) via IEEE 488
air-pressure	selfmade; based on IC KP101 A resolution: 0.01 hPa
indoor temperature	selfmade; based on IC KPY 10 resolution: 0.01°C
sampling rates	gravity: 1 sec filtered to 20 sec temp./pressure: 20 sec filtered to 10 min

cooled down. The restart of the system caused the running-in curve. The other smaller gaps are mainly due to earthquakes.

Air pressure and room temperature are recorded inparallel. The air pressure covers quite a wide range (950 to 1030 hPa), esp. in autumn there is a strong drop which also strongly affects the gravity residuals. The temperature changes of about 1.3°C over the whole period look more dramatic than they are: Looking at periods of one week only the usual changes are within 0.1°C. All the experiences with our gravimeter reveal that this small saisonal variation does not influence the tidal results. Due to a good insulation the temperature stability of the gravimeter is not affected and thus the long-term drift is stable.

4. Results

Up to now for the analysis about 156 days of data were used. The data treatment is not yet finished and the corrections applied still have to be improved after the termination of the measurements. But already now the results of the data analysis contained in Tab. 4.1 are quite satisfying: The noise levels in the tidal bands are comparable to our earlier results, and the mean square error of 0.643 μGal is acceptable for this present stage of data treatment.

As can be expected from the theoretical tides the amplitudes are quite small according to the high latitude. Therefore the signal-to-noise ratios are also small compared to those obtained earlier with this gravimeter in Europe.

In Tab. 4.2 the residual vectors are given for waves O1 and M2 assuming a standard earth tidal model. These vectors are mainly related to the effect of ocean tidal loading and can be compared to the computed effect using the Schwiderski and Flather models. Up to now we only computed the theoretical loading effect for the waves O1 and M2 for the Schwiderski grid worldwide and the

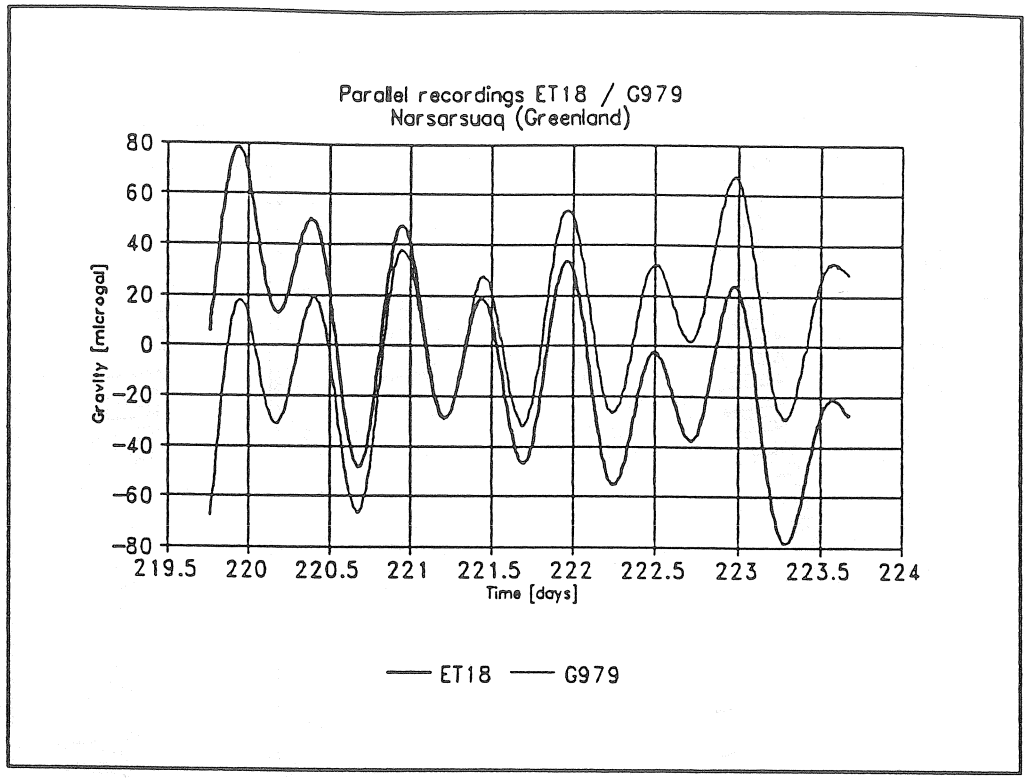

Figure 2.2: Parallel recordings of the gravimeter ET 18 (bold lines) and the gravimeter G 979 at Narsarsuaq.

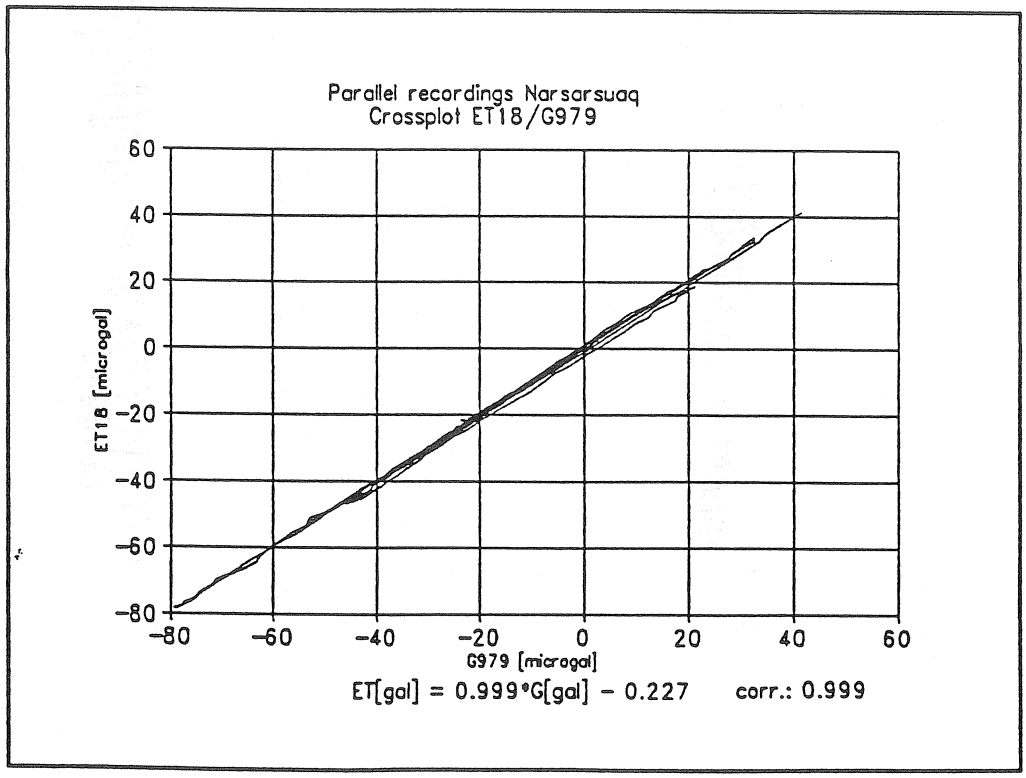

Figure 2.3: Cross plots of the records of both gravimeters at Narsarsuaq; note regression function and correlation coefficient.

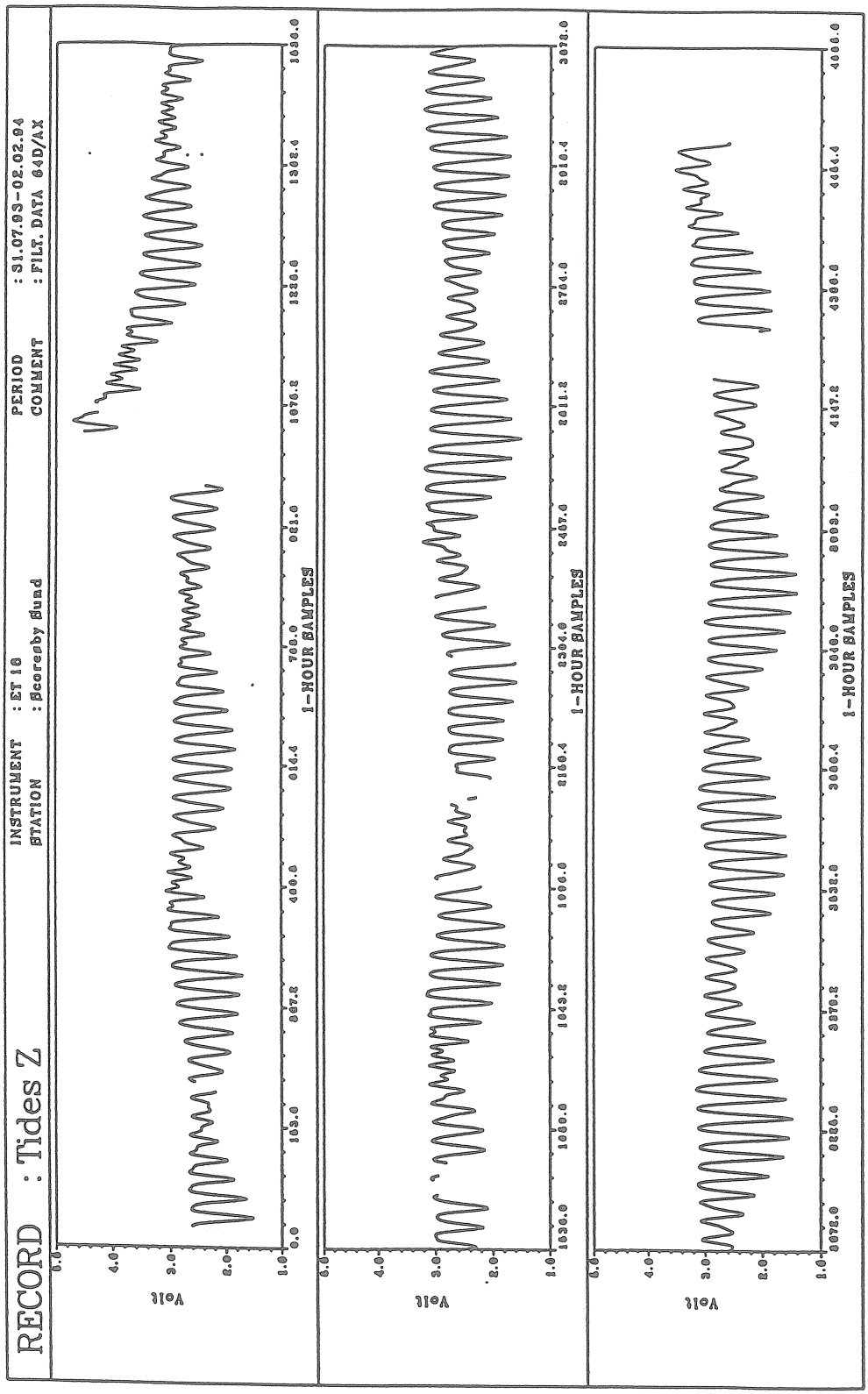

Figure 3.1: Gravity data from Scoresbysund filtered to hourly values; the period is July 31, 1993 until Feb. 2, 1994;

Table 4.1: Tidal analysis of the gravity record from Scoresbysund, Greenland; the number of days is 155.9, period July 31, 1993 to February 2, 1994. The coordinates of the station are: Latitude 70.485° N, 21.953° W, altitude 64.8 m.

NUMBER OF DAYS: 155.9
INERTIAL CORRECTION APPLIED

ESTIMATION OF NOISE BY FOURIER SPECTRUM OF RESIDUALS

NOISE LEVELS:		
DAILY WAVES	0.0770	MYGAL
HALF DAILY WAVES	0.0254	MYGAL
THIRD-DAILY WAVES	0.0158	MYGAL

ADJUSTED TIDAL PARAMETERS:

NR.	FROM	TO	WAVE		AMPL. MYGAL	SIGNAL/ NOISE	AMPLI.FAC.	PHASE LAG DEG	
1	129	163	SIG1		0.7409	10.	1.2368	-9.3427	SIG1
				±	0.0770		0.1286	5.9578	
2	164	193	Q1		4.0838	53.	1.0898	-0.4499	Q1
				±	0.0770		0.0206	1.0808	
3	194	219	O1		21.7507	282.	1.1112	1.6336	O1
				±	0.0770		0.0039	0.2029	
4	220	241	M1		1.7129	22.	1.1128	2.7069	M1
				±	0.0770		0.0500	2.5768	
5	242	274	P1K1S1		31.4376	408.	1.1420	1.7909	P1K1S1
				±	0.0770		0.0028	0.1404	
6	275	296	J1		1.8012	23.	1.1706	-3.1320	J1
				±	0.0770		0.0501	2.4505	
7	297	333	OO1		0.9449	12.	1.1210	0.8384	OO1
				±	0.0770		0.0914	4.6713	
8	334	374	2N2		0.3008	12.	1.1740	-13.5005	2N2
				±	0.0254		0.0990	4.8312	
9	375	398	N2		1.7602	69.	1.0968	-14.1555	N2
				±	0.0254		0.0158	0.8256	
10	399	424	M2		7.9622	314.	0.9499	-9.4514	M2
				±	0.0254		0.0030	0.1825	
11	425	441	L2		0.2434	10.	1.0275	-3.4586	L2
				±	0.0254		0.1071	5.9694	
12	442	488	S2K2		3.7736	149.	0.9677	5.1926	S2K2
				±	0.0254		0.0065	0.3851	
13	489	505	M3		0.1064	7.	1.9326	-11.6937	M3
				±	0.0158		0.2861	8.4817	

MEAN SQUARE ERROR	0.643	MYGAL
DEGREE OF FREEDOM	3716	

Flather grid in the North Atlantic applying Farrell's (1972) algorithm. These values are also given. Here, we used the same procedure as applied by the International Center for Earth Tides, Brussels; but in future we will digitize the coast lines carefully to reduce systematic errors.

Tab. 4.2: Tidal residual vectors compared to ocean loading computed for O1 and M2 on the basis of Schwiderski's and Flather's maps; upper table: observation results; lower table: computed, seperated into Newtonian and elastic effects.

WAVE	AMPLITUDE [μGal]	ERROR [μGal]	PHASE [°]	ERROR [°]
O1	1.1461	0.0770	147.2475	3.8541
M2	2.2809	0.0254	-145.0250	0.6371

	Newtonian		elastic		total	
	[μGal]	[°]	[μGal]	[°]	[μGal]	[°]
O1	.042	58.1	.183	-121.0	.141	-120.7
M2	.559	81.6	.826	105.8	1.355	96.1

5. Discussion

All the existing and planned fiducial sites on Greenland for monitoring global change are close to the ocean. Therefore, deformations of the crust by ocean tidal loading provide a strong time dependent part of the station coordinates. This disturbing signal cannot be corrected applying existing models because these models are global rather than local ones.

Therefore it is not astonishing that the parameters of the main tidal waves obtained for Scoresbysund vary considerably from the theoretical value of about 1.16. This leads to tidal residuals which can be allocated to the influence of ocean tidal loading. The observed residuals summed up show amplitudes in the order of up to 7 μGal. The comparison to the computed values reveals that due to the strong phase differences the usually applied correction on the basis of the available maps would be wrong by more than 10 μGal. Since close to the station the elastic part of the loading effect covers about 90% of the total load of the local seas the resulting systematic error for the elevation is at least between 1 and 5 centimeters. Thus, the errors in the loading model would cause differences which are in the order of the accuracy of the kinematic GPS as anticipated by several authors.

After the completion of the record at Scoresbysund in July 1994 we started to compute realistic tidal corrections for this station.

Generally, the ocean loading effect near the coast may reach 10% to 30% of the body tidal amplitude. In addition the phase shift also contributes to the resultant tidal vector. In terms of height changes this may provide an effect in the order of one decimeter (or even more) depending on the area and the local loading amplitudes.

Scherneck (1991) discussed this problem and concluded that loading effects close to the coasts cannot reliably be interpolated from global ocean tide models. This is in accordance to the earlier findings of Baker (1980) for the British Isles, Asch et al. (1986; 1987) and Jahr et al. (1991) for the Norwegian and Danish coasts, resp. Thus, the required accuracy for the vertical displacements in the sub-centimeter range cannot be achieved at such stations applying global models.

Recent investigations show that even the application of regional ocean tide models is not sufficient: Thomas & Woodworth (1990) found residual ocean tide signals in satellite altimeter data for the northeast Atlantic region which may affect the estimates of the mean sea level and the sea surface height variability. These variabilities could be reduced by applying Flather's models instead Schwiderski's (Flather, 1976; Schwiderski, 1979a/b). Knudsen (1992) reports about variability estimates averaging 10 centimeters, but reaching 15 to 20 centimeters betwen Iceland and Faeroe Islands. He used a collinear analysis to improve the ocean tide input.

6. Acknowledgements

Dr. Niels Andersen of KMS was responsible for the reconnaissance of the station in Scoresbysund and all the necessary preparations. Dr. Per Knudsen prepared the place at Narsarsuaq. The measurements fully depended on the careful maintenance of the gravimeter and the recording system by the local staff Ib Lorentzen and Tore Andreassen in Scoresbysund and Ulrik Poulsen in Narsarsuaq. The development of the recording system was carried out in cooperation with M. Liebing, who also took part in the installation work. D. Banka carried out the first routine analysis of the data. All this is gratefully acknowledged.

7. References

Asch, G., and G. Jentzsch, 1987. High sampling of tidal data. Bull. d'Inf. Marees Terr., 99, 6779 - 6785.

Asch, G. T. Jahr, G. Jentzsch, A. Kiviniemi, and J. Kääriäinen, 1987: Measurements of gravity tides along the 'Blue Road Geotra-verse' in Fennoscandia. Publ. Finn. Geod. Inst., No. 104, 55 p.

Asch, G., T. Jahr, G. Jentzsch, A. Kiviniemi, J. Kääriäinen, H.-P. Plag, and W. Thiel, 1986. Loading tides along the 'Blue Road Geotraverse'. Proc. 10th Int. Symp. Earth Tides, Madrid, 1985, Consejo Sup. de Invest. Cientificas, 707 - 717.

Baker, T.F., 1980. Tidal gravity in Britain; tidal loading and the spatial distribution of the marine tide. Geophys. J. R. Astr. Soc., 62, 249-267.

Brozena, 1992. The Greenland Aerogeophysics Project: Airborne gravity, Topographic and magnetic mapping of an entire continent. 6th Int. Symp. on Satellite Pos., Columbus, OH, March 1992.

Carter, W.E., and D.S. Robertson, 1991. Geodetic VLBI: Monitoring global change. AGU Chapman Conference on Geodetic VLBI: Monitoring Global Change, Washington, D.C., April 1991.

Colombo, O.L., and M.F. Peters, 1992. Precision long-range DGPS for airborne surveys. GPS World, April 1992.

Engen, B., G. Jentzsch, F. Madsen, and P. Schwintzer, 1993. NATURE: North Atlantic Tides Under Research - Tidal gravity measurements around the Norwegian Greenland Sea -. Proc. 12th Int. Symp. Earth Tides, Beijing, August 1993 (in press).

Farrell, W.E., 1972. Deformation of the earth by surface loads. Rev. Geophys. Space Phys., 10, 761-797.

Flather, R.A., 1976. A tidal model of the north-west European continental shelf. Mem. Soc. roy. des Sci. Liege, 6th series, 10, 141-164.

Jahr, T., G. Jentzsch, N. Andersen, and O. Remmer, 1991. Ocean tidal loading on the shelf areas araound Denmark. Proc. 11th Int. Symp. Earth Tides, Helsinki, 1989, Schweitzerbart, Stuttgart, 309 - 319.

Jentzsch, G., and J. Melzer, 1989. Calibration and stability of the gravimeter LCR ET 18. Bull. d'Inf. Marees Terr., 104, 7283 - 7289.

Knudsen, P., 1992. Separation of residual ocean tide signals in a collinear analysis of Geosat altimetry. EGS XVII General Assembly, Session G5, Edinburgh, April 1992.

Ramatschi, M., M. Liebing, and G. Jentzsch, 1993: Instrumental tests and calibration of the Gravimeter LaCoste & Romberg ET 18. Bulletin d'Information Marees Terrestres, 115, 8472 - 8477.

Scherneck, H.G., 1991. A parametrized solid earth tide model and ocean tide loading effects for global geodetic baseline measurements. Geophys. J. Int., 106, 677-694.

Schwiderski, E.W., 1979a. Ocean tides, part I: Global tidal equations. Marine Geodesy, 3, 161.

Schwiderski, E.W., 1979b. Ocean tides, part II: A hydrographical interpolation model. Marine Geodesy, 3, 219.

Thomas, J.P., and P.L. Woodworth, 1990. The influence of ocean tide model corrections on Geosat mesoscale variability maps of the North East Atlantic. Geophys. Res. Lett., Vol. 17, No. 13, 2389-2392.

Earth and Ocean Tides Parameters Recovered from SLR Data to Lageos

B. B. Pen, B. Wu, H. T. Hsu

(*Inst. of Geodesy and Geophysics, CAS 54 Xu Dong Road, 430077 Wuhan, China*)

1. Introduction

As wellknown to all, Lageos is strongly affected by the longwave length geopotential and longwave length manifestations of the earth and ocean tides. In early analysis of the recovery of the tide parameters from SLR data to Lageos, usually it is needed to analyse the orbit evolution over one or more years, and to focus on the pertubations in orbit elements. Following the progress of orbit dynamic models and the improvement of observation accuracy, recent solutions, such as Christodoulides, Dow et al., permitted the study of the tides through a direct analysis of the tracking data themselves. This kind of simultaneous solution explicitly accounts for many geodynamic effects, including the correlations of the tide parameters with the orbit parameters. The advantages of the new algorithm lie that: (1) it can solve the different geodynamic parameters simultaneously, such as: ERP, tides, station coordinates, earth gravity model; (2) it has no coupling of the errors from other geodynanic models into ocean tides parameters; (3) it can obtain the covariances of different parameters and estimate the reality of the solution.

In this paper, we firstly use the Helmert — Wolf algorithm and the developped software ISAS to estimate the global earth and ocean tides parameters based on 5 years normal point SLR data to Lageos, secondly, give the Love numbers h_2, l_2, secondly the 2nd, 4th degree ocean tides parameters for 12 major constituents. Finally, we discuss the effect of some facts, for example, the sideband minor ocean tides and the nutation model on the solution.

2. Modelling

Assume that the observation distance between the satellite and observation station is ρ_o, the corresponding computed distance is ρ_c, besides the observation error, the difference $\rho_o - \rho_c$ implies a planty of geodynamic informations, such as the adopted theoretical models, incorrect values of initial vector, station coordinates and adopted constants. In this respect, the observation equation can be linerized as follows

$$\rho_o - \rho_c = \sum_{j=1}^{L} \frac{\partial \rho}{\partial x_j} \Delta x_j + \sum_{i=1}^{M} \frac{\partial \rho}{\partial p} \Delta p_i + \sum_{k=1}^{N} \frac{\partial \rho}{\partial E_k} \Delta E_k + \sum_{l=1}^{N} \sum_{m=1}^{3} \frac{\partial \rho}{\partial X_{lm}} \Delta X_{lm} + v \qquad (1)$$

where

Δx_j: corrections to initial positions and velocity vectors of satellite

Δp_i: corrections to parameters of adopted models and constants, including tides parameters

ΔE_k: corrections to the earth rotation parameters

ΔX_{lm}: corrections to station coordinates

v: residuals

If the abovementioned corrections are independent each other, it is easily to solve by least square adjustment.

We know that the precision of satellite orbit determination becomes lower as the orbit arc trends longer. For this reason, the long arc solution is not avialable for precision orbit determination. Some parameters which vary quickly should be recovered in short arc, on the other hand, the parameters which change slowly can be found by long arc. For example, K_1 ocean tide parameter must be recovered in 3 years arc at least for Lageos observation data. To meet this reguirement we introduce the Helmert -- Wolf algorithm here, we divid the whole data set month by month, use each one month arc to solve for the local parameters which depend on the short arc only and use the whole data set to find the common parameters which is corelated with the long arc. In this case, a set of linear equations can be expressed as:

$$[A_i\ B_i]\begin{bmatrix}X_i\\Y\end{bmatrix}=[b_i]+[v_i] \tag{2}$$

where

X_i: local parameter matrix

Y: common parameter matrix

b_i: observation matrix

v_i: residual

i: the index of short arcs

The local parameters X_i can easily be recovered for each short arc as follows:

$$X_i=(A_i^TW_iA_i)^{-1}(A_i^TW_ib_i-A_i^TW_iB_iY) \tag{3}$$

W_i is the weight matrix, and the common parameters Y is obtained when combining all the short arcs:

$$\begin{aligned}Y&=N^{-1}d\\N&=\sum_{i=1}^{m}[B_i^TW_iB_i-B_i^TW_iA_i(A_i^TW_iA_i)^{-1}A_i^TW_iB_i]\\d&=\sum_{i=1}^{m}[B_i^TW_ib_i-B_i^TW_iA_i(A_i^TW_iA_i)^{-1}A_i^TW_ib_i]\end{aligned} \tag{4}$$

here m is the number of short arcs.

Another important point we have to consider in our modellng is the effect of the tide sidebands. As wellknown, if the observation data set is rather short, it's impossible to distinguish two ocean tide wavies which have

the nearly same frequencies. But in our case many major tides have the tide sidebands, for example, besides 165.555(K_1), we have tides 165.545, 165.565, 165.575, if the effects of sidebands are obscured, the recovered values of ocean tide parameters would be unreliable, especially for the solutions which are corrections to the initial ocean tide parameters.

For considering this effect we assume the response of the ocean to the tide-generating force is linear with the driving frequencies which close each other. For example, for two tide constituents β and β', their ocean tide heights can be written as

$$\left.\begin{aligned}\xi_\beta(\theta,\lambda,t) &= \sum_{l,m} D^{\pm}_{\beta,lm}\overline{P}_{lm}(\cos\theta)\cos(A_{\beta\pm m\lambda} + \varepsilon^{\pm}_{\beta,lm}) \\ \xi_{\beta'}(\theta,\lambda,t) &= \sum_{l,m} D^{\pm}_{\beta',lm}\overline{P}_{lm}(\cos\theta)\cos(A_{\beta'\pm m\lambda} + \varepsilon^{\pm}_{\beta',lm})\end{aligned}\right\} \qquad (5)$$

If the driving frequencies of these two constituents are very close, like the case of major tides and their sidebands, we have

$$D^{\pm}_{\beta',lm} = \frac{n_{\beta'}}{n_\beta} D^{\pm}_{\beta,lm}, \qquad \varepsilon^{\pm}_{\beta,lm} = \varepsilon^{\pm}_{\beta',lm} \qquad (6)$$

where

$D^{\pm}_{\beta,lm}$, $D^{\pm}_{\beta',lm}$: the amplitudes of constituents β and β'

$\varepsilon^{\pm}_{\beta,lm}$, $\varepsilon^{\pm}_{\beta',lm}$: the phases of constituents β and β'

n_β, $n_{\beta'}$: the theoretical amplitudes of constituents β and β'

In our model, we adopte this prediction method of the point linear admittence of the major tide constituents to calculate 23 minor ocean tide constituents for minimizing the sideband effects.

3. Data and Software

For the recovery of tide parameters, total 208910 three—minute normal points of 59 months global Lageos SLR data are used, and a software ISAS (IGG SLR analysis software) is developped. Table 1,2,3 list the collected data, adopted models and constants, and adjusted parameters used in our software respectively.

4. Result and Discusion

The results of ocean tide parameters of 12 major constituents obtained are listed in table 4, in order to compare with other author's studies, the results derived from GEM — T2 solution, Schwiderski cotidal maps, Starlette data by M. Cheng [1990] and TS4 solation by J. Dow [1988] are also given. In addition, the results of Love numbers h_2 and l_2 are listed in table 5 with some other solutions.

From table 4 we can see that our solutions are generally in good agreement with the results from other authors, except for the annual tide Sa, our Sa amplitude is obviously smaller than others. On the other hand, it is shown that the results of second-degree tide constituents and the third-degree major tide constituents O_1, K_1, M_2, K_2 coincide quite well between all the solutions, but still large discrepancies exist in the results for other third -- degree tide constituents. The phase of Mm tide in our solution has substancial difference to other studies, but rather well when compared with the result obtained by Willimson and Mash [1. 99/312. 7, 1985]. Love numbers h_2, l_2 given in table 5 are compared rather well with other solutions.

In order to analyze the effect of the different adopted nutation models on the solution, we select 14 months data from Nov. 1984 to Dec. 1985 to test the discrepancy between corrected nutation model and Wahr model. Six ocean tide constituents which have the periods shorter than one year and can be separated each other are taken into consideration. Table 6 lists the second -degree tide results.

It may be recognized that zonal tide parameters are strongly affected by nutation model, especially for the annual tide Sa, the value got from new model is nearly twice of the old value, this is just what we expected, the adoption of corrected model would change much more on the long period terms than the short period terms because of the difference of long period terms between corrected nutation model and wahr model. Our results given in table 4 correspond on the corrected nutation model and VLBI UT1 values, therefore this maybe one reason of our Sa values different from others.

Reference

[1] Melbourne, W. et al. MERIT STANDARD. Third Draft. 1983.

[2] J. G. Marsh and F. J. Lerch. Geodynamic and Geodetic Parameter Estimation from Starlette Laser Tracking Data. 1983.

[3] R. G. Williamson and J. G. Marsh. G. J. R., 90, 934. 1985.

[4] P. Moore. Bull. Geod., 60, 297. 1986.

[5] Dow, J. M., DGK. Reihe C. Nr. 344, 1988.

[6] Christodoulidis. D. C. et al., On the prediction of ocean tides for minor constituents. in Preoceedings of the 10th international symposium on earth tides. 659-678, 1985.

[7] Sinclair. A. T., Appleby. G. M., SLR Technical Note. No. 9. Royal Greenwich OBS., 1986.

[8] Merson, R. H., Odell. A. W., Technical Report 75093. Royal aircraft Establishment.

[9] D. C. Christodoulidis et al., J. G. R., 93, No. B6, 6216-6235. 1988.

[10] S. C. Cohen. and D. E. Smith. J. G. R., 90. No. B11. 9217-9220. 1985.

[11] Cheng. M. K. et al., J. G. R., 95. No. B6, 8723-8736. 1990.

[12] Marsh. J. G. et al., J. G. R., 95. N0. B13. 22043-22071. 1990.

[13] Schwiclerski. E. W., Rev. Geophys., 18. 243. 1980.

[14] Carter. W. et al., BIH Annual report for 1987. correction to the IAU 1980 nutation series.

[15] Smith. D. E. et al., J. G. R., 95. N0. B13. 22013--22041. 1990

Table 1. Normal Points Data

M\Y	1984	1985	1986	1987	1988
1		2249	5002	2651	2252
2	2431	2231	3587	3008	3063
3	2398	2464	3406	3506	2419
4	3751	3515	3817	4404	1626
5	4605	3921	3124	3355	1828
6	4499	5092	3409	3784	1972
7	3669	5595	2570	4100	2826
8	4409	5282	2924	4240	4000
9	4121	5635	2694	3947	3807
10	4370	4918	3673	4370	4223
11	3287	3837	3147	3635	3633
12	2772	3752	3663	3064	3379

Table 2. Models and Constants

model	description
Earth gravityal field	GEM－T1
Solid earth tides	Wahr model
Ocean tides	GEM－T1 with 23 minor tides
Luni－solar attraction	JPL DE－200
Tropsphere	Marini－Murray model
Station tidal displacement	Wahr model
Station ocean tidal loading displacement	MERIT standards
Precession	IAU 1976
Nutation	IAU plus Carter correction
Plate motion	AMO－2
C	299,792.485 m/s
GM	298,600,440 km^3/s^2
a	6,378,137 m
1/f	298.257

Table 3. Adjusted parameters

Long—arc parameters
• GM • Station coordinates • Velocities of stations • 12 major ocean tides with 50 coefficients • Love number h_2、l_2
Short—arc parameters (for each 30days arc)
• Solar rediation pressure • Along—track acceleration • Orbit state vector • ERP

Table 5. Love Number Values

h_2	l_2	Description
0.594 0.003	0.102 0.004	Our solution
0.6135 0.0054	0.0768 0.0191	VLBI, 1980—1984, Carter et al. (1985)
0.608 0.003	0.093 0.002	LAGEOS, 1980—1983, Christodoulidis et al. (1985)

Table 6. Comparison of values under corrected nutation and Wahr model

	New	Wahr
Ssa	2.06/227.5	1.92/232.9
Mm	1.69/313.2	1.67/306.8
Sa	0.78/117.9	0.39/198.8
O_1	3.60/317.9	3.55/314.2
M_2	3.28/323.8	3.32/322.4
S_2	0.81/292.5	0.81/288.3
(unit=cm/deg)		

Table 4. Ocean Parameters and Comparition With Other Results

Tide	l	m	Our results	GEM－T_2	Schwideski	Starlette	TS4
Sa	2	0	1.04/13.72	3.033/28.771		2.83/39.0	2.37/49.5
Ssa	2	0	1.45/247.34	1.276/249.472	1.24/221.7	1.59/253.3	2.01/257.1
	3	0	0.80/147.80	0.866/89.398	0.03/1.8		
Mm	2	0	1.29/316.07	0.740/256.318	1.06/258.9	1.42/245.5	1.33/269.0
	3	0	2.31/270.91	0.814/16.653	0.03/94.3		
Mf	2	0	2.24/231.64	2.069/237.076	1.71/252.0	2.84/242.1	1.81/222.2
	3	0	1.92/78.19	1.032/354.630	0.10/148.2		
Q_1	2	1	0.66/318.91		0.54/313.7	0.72/294.6	0.69/322.7
	3	1	0.59/135.32		0.31/107.3		
O_1	2	1	3.09/320.70	2.717/315.443	2.42/313.7	0.72/294.6	3.16/324.1
	3	1	1.84/80.97	1.390/83.019	1.73/77.6	1.05/63.3	2.01/84.7
P_1	2	1	0.88/308.70	1.105/313.188	0.90/313.9	0.99/331.0	0.81/321.1
	3	1	0.18/49.52	1.344/259.467	0.33/2.1	0.86/0.9	0.47/50.4
K_1	2	1	3.00/327.35	2.845/325.513	2.82/315.1	2.68/324.9	3.55/328.9
	3	1	0/97/29.08	0.903/14.513	0.57/59.0	141/346.0	1.40/35.8
N_2	2	2	0.69/333.05	0.678/334.416	0.65/321.8	0.92/329.3	0.65/331.4
	3	2	0.14/192.55	0.090/155.802	0.10/85.0		0.08/237.6
M_2	2	2	3.19/320.34	3.320/321.257	2.96/310.6	3.22/319.3	3.27/322.1
	3	2	0.28/168.32	0.304/156.469	0.20/152.4	0.12/160.6	0.29/164.4
S_2	2	2	0.80/302.17	0.831/300.412	0.93/314.0	0.83/301.6	0.83/307.3
	3	2	0.19/240.05	0.328/211.479	0.38/237.4	0.23/191.6	0.33/217.0
	4	2	0.27/119.45	0.333/87.229	0.41/86.5	0.32/89.1	0.35/29.9
K_2	2	2	0.27/316.63	0.319/313.503	0.26/315.1	0.29/315.9	0.14/319.7
	3	2	0.29/186.55	0.231/189.953	0.51/206.4	0.08/242.8	0.53/183.0
	4	2	0.15/147.48	0.169/112.652	0.19/76.0	0.10/97.0	0.21/41.1

(unit=cm/dcg)

New Ocean Tide Models for Loading Computations.

Ole Baltazar Andersen

National Survey and Cadastre (KMS), 2400 Copenhagen NV, Denmark
E-mail: ole@kms.min.dk, Fax: +45 3587 5052.

Abstract. During 1994 eight new ocean tide models have become available, that are valid for ocean tide loading computations. Most of these models are based on the high precision altimetry obtained from the TOPEX/POSEIDON satellite mission, and all of the models are superior to both the Cartwright & Ray 1991 model as well as to the Schwiderski 1980 model when compared to tide gauges in both the open ocean as well as in the Northwest European shelf region.

From a comparison to a common set of tide gauge data set compiled by C. Le Provost and others, the general result is that the TOPEX/POSEIDON based models are generally better that the best pure hydrodynamic model by C. Le Provost, (1994) except for shelf areas. Most of the TOPEX/-POSEIDON models are limited by the orbital inclination of the satellite (66° latitude), which means that they have to be extended in order to cover all oceans of the world before being usable for ocean tide loading calculations.

Presently only three of the new models are global. This is the Grenoble model, the adjusted Grenoble model by Andersen and the CSR 2.0 model from Center of Space Research in Texas. The global ocean tide model by Andersen have been derived by twisting the Grenoble model as to fit TOPEX/POSEIDON altimetry and shows very good agreement when comparing to tide gauge readings both in the open ocean and in the Northwest European shelf region.

Differences on the Northeest European shelf between loading calculated with the Cartwright & Ray 1991 model and the Grenoble 1994 model reaches 1.5 centimeters for the M_2 constituent and indicates the importance of these new models for ocean tide loading computations.

Introduction.

Presently around 12 new ocean tide model are available, with more or less global coverage. Furthermore most of the new ocean tide models already exists in several versions as they have been updated using more and more data. Virtually all of these models are based on early results from the TOPEX/POSEIDON satellite mission (hereafter T/P), which, among other purposes, has been designed specifically to enable the development of new global tide models. Early data from the T/P mission has shown remarkable accuracy, and with an alias period of only 62 days for the M_2 constituent, errors in existing models when applied to the T/P data have been very easily recognised. As the S_2 constituent has an alias period of 59 days, this implies that at least three years of data is needed in order to separate these two constituents using a normal harmonic approach at each observation point. However, by using response analysis or other methods this problem can be dealt with and ocean tide solutions can be obtained from as little as one year of data.

The aim of this investigation is to present new ocean tide models for ocean tide loading calculations, and to investigate how they compare to a common set of "ground truth" stations. This comparison to ground truth will be performed to a global set of 95 tide gauges as well as to a set of 65 tide gauges on the Northwest European Shelf, where also high resolution non-linear hydrodynamic models developed at the Proudman Oceanographic Laboratory (hereafter PAL) will be included in the comparison. It is important to be aware of, that in a comparison with tide gauge readings, errors in both models as well as derived harmonic constants at the tide gauge site are bound to limit the obtainable agreement.

Recent ocean tide models.

An overview of recent global ocean tide models which can be used for ocean tide loading computations is given in Table 1, where the 10 most recent models are listed.. Except for the

	Year	Hydro-dynamic assumption	Contributes to data		Number of constituents	Area (Latitude)	Resolution	Remarks
			Altimetry	Tide Gauges				
Schwiderski	1980	Linear	No	Yes	11+5[4]	Global	1° x 1°	-
Cartwright & Ray	1990	None	GEOSAT	No	60[1]	+/- 69°	1° x 1.5°	Orthotides
Grenoble	1994	Non-linear	No	Yes[2]	13[4]	Global	0.5° x 0.5°	Finite Elements
Mazzega	1994	None	T/P	No	?	?	?	Inversion
OSU	1994	Linear	T/P	No[3]	8+9[4]	-80°,70°	0.58° x 0.70°	Global Inversion
Ray, et al.	1994	None	T/P	No	60[1]	+/- 65°	1° x 1°	Orthotides, Proudman Functions
Texas	1994	None	T/P	No	60[1]	+/- 66°	1° x 1°	Orthotides
Andersen[ERS1]	1994	None	T/P,ERS-1	No	60[1]	-80°,80°	0.75° x 0.75°	Orthotides
Andersen	1994	"Nonlinear"	T/P	Yes[2]	13	Global	0.5° x 0.5°	Orthotides
Desai & Wahr	1994	None	T/P	No	60[1]	+/- 66°	1° x 1°	Othotides

[1] Number of constituents included in the tide generating potential for the orthotide formulation.
[2] The Grenoble model does not use tide gauges through the whole domain, only at the interfaces of sub-domain areas,
[3] The OSU model does not use tide gauge data in the present form but is prepared to use this type of information,
[4] Additional constituents have been induced by admittance,

Table 1. Recent ocean tide models recommended for ocean tide loading calculations.

hydrodynamic model by Schwiderski (Schwiderski, 1980a, 1980b), that of Cartwright and Ray based on GEOSAT altimetry (Cartwright and Ray, 1990), and the Grenoble model, all of these new models are based on data from the T/P mission.

The model referred to as the *Grenoble* model has been produced by C. Le Provost, M. L. Genco, F. Lyard, P. Vincent and P. Canceill (C. Le Provost et al. 1994), and is based on a finite element hydrodynamic scheme. This model along with that by Schwiderski are the only two that do not include satellite altimetry in their solution. The design of the model is based on a non-linear formulation of the shallow water equations, and the model covers the global ocean (including the Arctic) except for some minor areas such as the Bay of Fundy. The model is a global 0.5° x 0.5° resolution version with eight constituents M_2, S_2, N_2, K_2, $2N_2$, K_1, O_1 and Q_1. Five secondary constituents Mu_2, Nu_2, L_2, T_2 and P_1 have subsequently been deduced by admittance interpolation.

The *Oregon State University* (OSU) model by G. Egbert, A. Bennett and M. Foreman (Egbert et al., 1994) is constructed from a global inverse solution that best fits dynamics and data. The solution used in this analysis is the TPXO-2 model. This model uses a homogenous selection of T/P crossover data, and contains the eight major constituents M_2, S_2, N_2, K_2, K_1 O_1, P_1 and Q_1 and nine minor constituents deduced from an assumption of a linear admittance function. The solution is based on the first 40 repeats of T/P data, has a resolution of 0.58° x 0.70° and covers all ocean areas to 70°N.

The model by R. D. Ray, B. Sanchez and D. E. Cartwright is referred to as the *Ray et al.* model (Ray et al., 1994) and is also derived at NASA Goddard. The model uses an orthotides formulation in order to separate the M_2 and S_2 constituents, and includes the major 30 diurnal and semidiurnal constituents in the solution. The ocean tide signal has been expanded into Proudman functions with a resolution of 1° x 1°. As for the following other models derived from T/P altimetry, coverage is limited to 66°N to 66°S due to the inclination of the T/P satellite. For this investigation the most recent model of December, 30th, 1994 have been used.

The model derived by *P. Mazzega* (Mazzega, 1994) are derived using global inversion technique. Presently the author have not obtained information on the model.

From the Center for Space Research, University of Texas at Austin, a number of different ocean tides have recently been made available. The model included here is constructed by *R. J. Eanes.* (Eanes, 1994). This model also captures the sea surface height in the form of normal point measurements within 3° x 3° bins but uses an orthotide technique in order to separate the tide constituents. For this investigation the most recent version (2.0) has been used. This model is the only

model with orbits based on the JGM-3 geopotential model. The resolution of the model is 1° x 1° and the model is extended to global coverage outside the coverage of the T/P satellite with partly the Cartwright & Ray (1991) model and partly the Schwiderski (1980) model.

At the University of Colorado a model has been produced by *Desai & Wahr* (1994). Their model the orthotide technique in order to separate the tide constituents, but they also include the Mf, Mm, M9, Sa and Ssa constituents. For this investigation the version (2.69), which includes almost two years of T/P altimetry, has been used

The ERS-1 model by O.B. *Andersen* (Andersen, 1994) has constructed from ERS-1 and T/P data with the use of orthotides in order to separate the tide constituents. The resolution of this model is 0.75° x 0.75° and the coverage is limited by the presence of sea ice to the north (80°).

The new Andersen model is a long spatial wavelength adjustment of the M_2 and S_2 constituents of the Grenoble model using 2 years of T/P crossover data corresponding to 70 repeat cycles. As the model from Grenoble this model has a resolution of 0.5° and covers the global ocean. The model has been derived by first correction the T/P data using the Grenoble model and subsequently modelling the ocean tide residuals using an modified orthotide approach, where the orthotide technique has been modified as to account for the radiational potential. Subsequently the adjustment to the M_2 and S_2 constituents have been interpolated onto regular grids using collocation with a half width of 3500 km as to assure that the corrections only give almost basin scale adjustments. This is extremely important as to keep the fine structures of the Grenoble model unaltered, which is important for modelling tides in shelf regions. Finally, as the Grenoble model does not include the Mediterrenian sel, the model has been complemented with a 0.5° re-interpolated verion of the *Canceill et al* (1994) model covering the Mediterranean sea. The adjusted model is hence a global model with a resolution of 0.5° x 0.5° corrected within +/- 65° latitude using T/P altimetry. Between latitudes 65° and 75° the adjustment is gradually tapered towards zero, so that the model becomes identical to the Grenoble model above 75° latitude. In order to avoid misunderstandings, this model will in the following be called the Andersen model, while the older Andersen model using ERS-1 altimetry will be called the Andersen^{ERS1} model.

Presently four other global models are available, but as these models are either limited to the deep ocean or limited to four or fewer constituents these models have been discarded in this analysis. These models are the *B. Sanchez and N. Pavlis* model (Pavlis and Sanchez, 1994) and *Schrama & Ray* model (Schrama & Ray, 1994) which are limited by the 250 m bathymetry level and the *P. Knudsen* model (Knudsen, 1994) and R. Rapp model (Ohio State University) which only have four constituents.

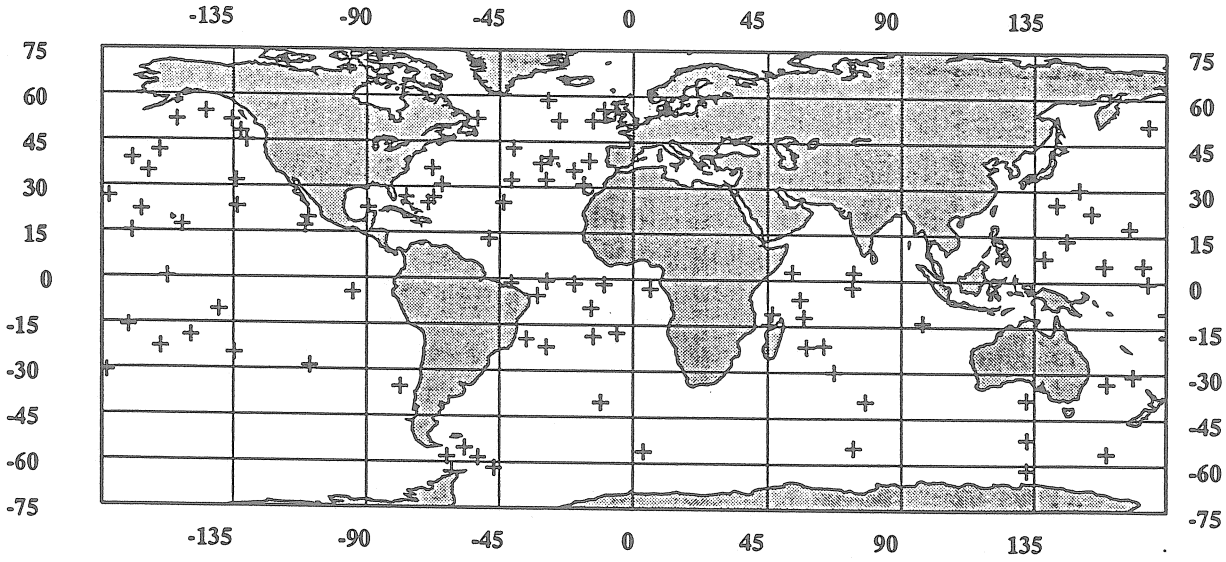

Figure 1. Location of the 95 selected common tide gauge available to all models.

COMPARISON TO TIDE GAUGE READINGS.

A new global set of tide gauge readings has been defined by C. Le Provost and other members of the T/P Tide Gauge Subcommittee to provide a common basis for comparing ocean tide models. This set,referred to as the '104 Standard Tide Gauge Set', has been constructed from the original 80 tide gauge set selected by Cartwright & Ray (1991) by various additions, corrections and updates. It has a reasonable spatial distribution with 42 tide gauges in the Atlantic Ocean, 19 readings in the Indian Ocean and 43 in the Pacific Ocean. Before a comparison to tide gauge readings could be made in the present work, a smaller selection of 95 of the 104 (39 Atlantic Ocean, 15 Indian Ocean, 40 Pacific Ocean) was made due to different coverage of the individual models. No quality selection was made on the selected tide gauges - the set was simply chosen as the subset of tide gauge readings available to all models. The locations of the 95 tide gauges are shown with crosses in Figure 1.

The real and imaginary parts of the major tide constituents were compared to the tide gauges readings by means of bi-linear interpolation within the global ocean tide model grids. Even though more sophisticated interpolation methods (e.g. optimal interpolation using collocation or krieging) might give better comparisons to the tide gauge readings, the somewhat simpler bi-linear interpolation method was chosen, as this method is generally recommended for interpolation in ocean tide models.

The vectorial RMS differences for a given constituent to be used subsequently is defined as follows:

$$RMS = [\frac{1}{N}\sum_{N}[\frac{1}{T}\int_{0}^{T}[H_1\cos(wt-G_1)-H_2\cos(wt-G_2)]^2+[H_1\sin(wt-G_1)-H_2\sin(wt-G_2)]^2\,dt\,]\,]^{1/2}$$

$$= [\frac{1}{N}\sum_{N}[\frac{1}{2}[H_1\cos(G_1)-H_2\cos(G)]^2+[H_1\sin(G_1)-H_2\sin(G_2)]^2\,]^{1/2}$$

where H_1 and G_1 are the interpolated model amplitude and Greenwich phaselag, H_2 and G_2 are the observed amplitude and Greenwich phaselag measured by the tide gauge, and T is the period of the observed constituent with frequency w.

	M_2	S_2	K_1	O_1	$M_2+S_2+K_1+O_1$
Schwiderski, 1980, (1° x 1°)	3.98	1.84	1.50	1.25	4.76
Cartwright & Ray, 1991 (1° x 1.5°)	3.25	2.29	1.97	1.27	4.61
Grenoble, 1994 (0.5° x 0.5°)	2.96	1.63	1.17[1]	1.05	3.72
Mazzega, 1994 (0.5° x 0.5°)	3.06	2.00	1.72	1.28	4.23
OSU, 1994, TPXO-2 (0.58° x 0.70°)	2.19	1.15[1]	1.37	1.00[1]	3.00
Ray et. al, DEC94 (1° x 1°)	1.98	1.28	1.30[2]	1.03[3]	2.88[2]
Texas, 1994, CSR 2.0 (1° x 1°)	2.00[3]	1.24[3]	1.33	1.03[3]	2.90
Andersen[ERS1], 1994 (0.75° x 0.75°)	2.69	1.65	1.61	1.21	3.82
Andersen, 1994 (0.5° x 0.5°)	1.86[1]	1.27	1.17[1]	1.05	2.73[1]
Desai & Wahr, 2.69, 1994 (1° x 1°)	1.96[2]	1.16[2]	1.31[2]	1.01[2]	2.83[2]

Table 2. RMS differences with 95 global tide gauge readings (centimetres). The three models that compare the best with tide gauge readings are indicated in supscript with 1,2 and 3 for each constituent.

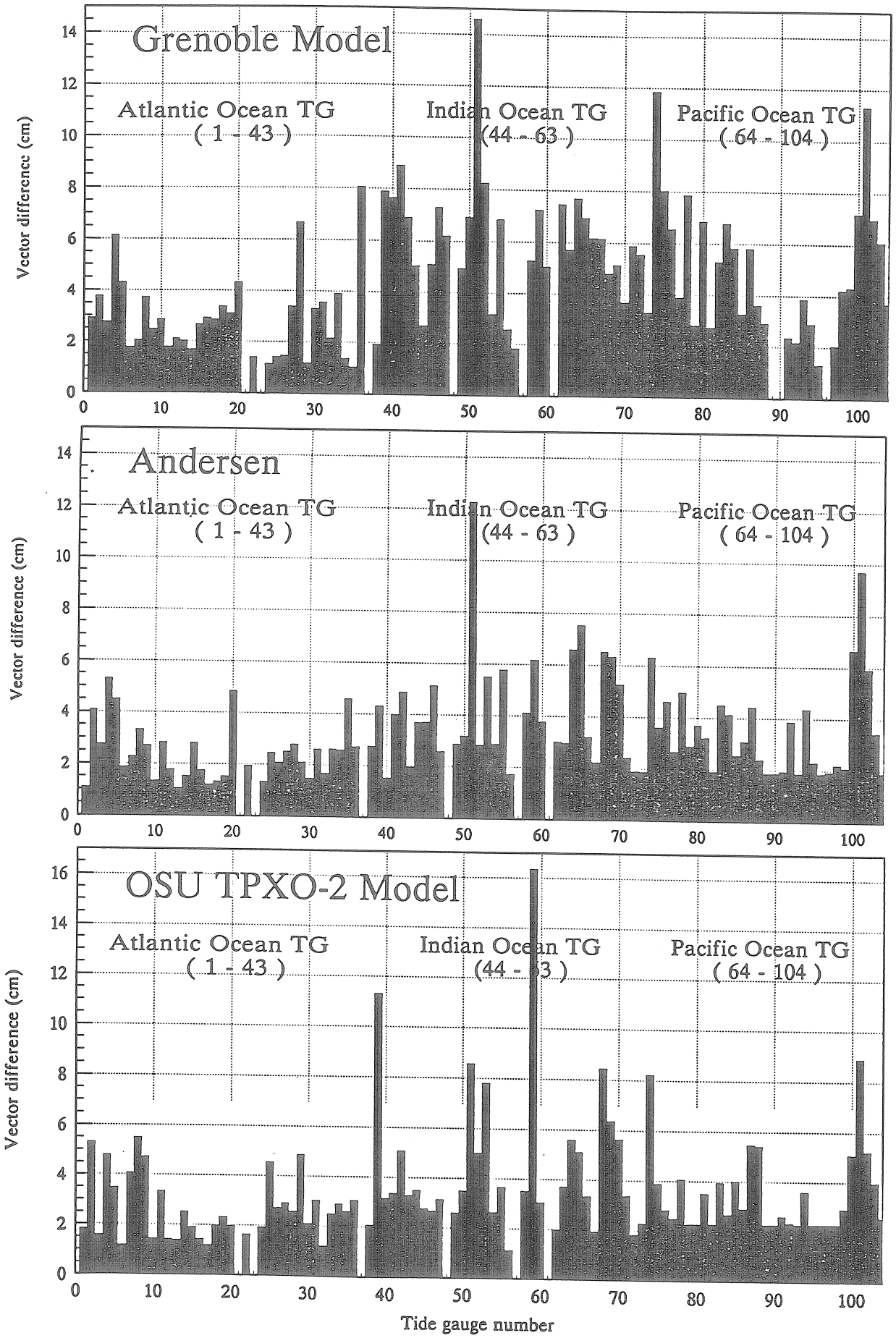

Figure 2. Direct comparison with the 95 tide gauge set. Top: The Grenoble model, Middle: The Andersen model, Bottom: the OSU TPXO-2 model from Oregaon State University.

Comparisons to the global set of 95 selected tide gauges is presented in Table 2 which displays RMS differences between the global ocean tide models, interpolated to the locations of the tide gauges, and the tide gauge readings themselves for the major four components and also for the total discrepancy of the $M_2+S_2+K_1+O_1$ constituents. The relatively good agreement of the model by Schwiderski is partly due to the fact that this model assimilated tide gauge data into it.

In Figure 2 the comparison to all the individual tide gauges has been plotted for the Grenoble model, the Andersen model and the OSU model. In Figure 2 it is evidently, that the Grenoble model performs substantially better in the Atlantic Ocean than in the Indian and Pacific Oceans. The T/P derived models in Figure 2 does on the other hand show a much more consistent RMS difference throughout the world ocean, with only a few bad tide gauge comparisons. An interesting tide gauge station is the station with number 59 (Heard Island - in the southern Indian Ocean). This compares very poorly to the OSU model, but much better for the Grenoble model. On the other hand station 51 (Name : Dzaoudzi - to the north of Madagascar in the Indian Ocean) compares much better for the OSU model than both the Grenoble and Andersen models. This indicates, that the major uncertanties is still associated with the ocean tide models, rather than the tide gauges.

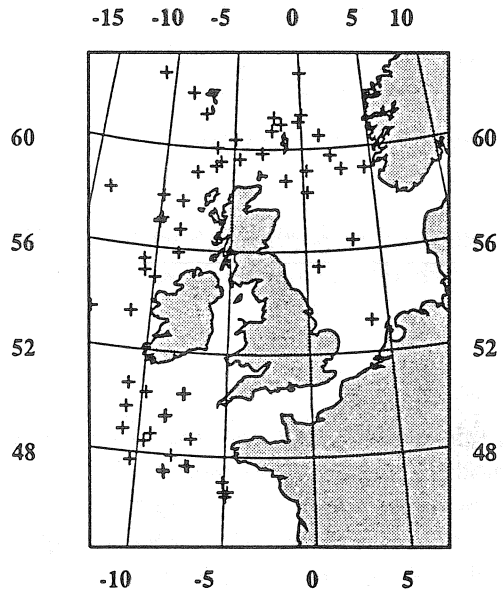

Figure 3. Location of selected tide gauge readings on the northwest European shelf.

The northwest European Shelf region was noted by *Woodworth and Thomas* (1990) to be a perfect test area to determine the ability to extract tide information from altimetry in general. In Figure 4 the locations of 65 selected pelagic tide gauge readings are shown with circles. The 65 selected tide gauge readings consist of 58 tide gauges published by IAPSO (M. Smithson, 1992) supplemented with 7 pelagic tide stations in the North Sea as obtained from the data banks at the Proudman Oceanographic Laboratory, Bidston Observatory.

The comparisons towards this set of 65 tide gauge station are shown in Table 3. Two additional "local" models have been added for the comparison. The 36km resolution Flather NEA model is the non-linear hydrodynamic finite difference model described by *Flather* (1981). This model uses a regular (0.33° by 0.5°) latitude - longitude grid covering approximately $37° < \phi < 72°$, $-30° < \lambda < 25°$ with open boundary forcing based on Schwiderski and some tide gauges. The 12km Flather model (0.11° by 0.16°) covers the NW European shelf ($48° < \phi < 62°$, $-12° < \lambda < 13°$), is that used operationally for coastal flood forecasting in the UK, and is optimised to predict water levels on UK coasts. Open boundary forcing for this model is based on NEA model results and tide gauges.

A surprising feature from the comparison to tide gauges in this area is, how poorly the older model of Cartwright and Ray (1991) fits tide gauge readings. It is evident that the Grenoble model and especially the Andersen model performs even better than the two widely used non-linear high resolution hydrodynamic models derived at POL by R. Flather. However, recent tests indicate, that the Flather model fits coastal tide gauges better than the Grenoble model. I must be noted, however, that one of the domain boundaries for the Grenoble model is around the Northwest European shelf region, which partly explains the good comparison to tide gauges.

Surprisingly, a number of the T/P derived models have severe problems in this region. This is the Texas CSR 2.0 model, the Desai & Wahr model and especially the OSU models. These model are only marginally better than the old Cartwright & Ray model.

	M_2	S_2	K_1	O_1	$M_2+S_2+K_1+O_1$
Schwiderski (1° x 1°)	5.79	1.92[2]	1.15[1]	0.78[2]	6.26
Cartwright & Ray (1° x 1.5°)	8.25	3.74	2.46	0.94[3]	12.16
Grenoble (0.5° x 0.5°)	3.99[3]	2.12	1.29[2]	0.70[1]	4.74[3]
Mazzega (0.5° x 0.5°)	4.40	1.95[3]	1.39[3]	1.32	5.18
OSU, TPXO-2 (0.58° x 0.70°)	9.34	8.55	1.45	1.14	12.80
Ray et al., DEC94 (1° x 1°)	4.65	3.31	1.62	1.27	6.07
Texas, CSR 2.0 (1° x 1°)	9.04	3.44	1.55	1.00	9.85
Andersen[ERS1] (0.75° x 0.75°)	5.78	4.32	2.15	1.68	7.57
Andersen (0.5° x 0.5°)	3.23[1]	2.23	1.29[2]	0.70[1]	4.21[1]
Desai & Wahr, 2.69, 1994 (1° x 1°)	9.43	4.00	2.18	1.30	10.55
Flather NEA, 1981 (0.33° x 0.5°)	5.08	2.74	1.59	1.12	6.09
Flather shelf, 1994 (0.16° x 0.11°)*	3.84[2]	1.57[1]	2.11	0.82	4.73[2]

*The comparison towards the Flather shelf model was limited to 47 tide gauges located within the coverage of the model.

Table 3. RMS differences with 65 selected tide gauge readings in the northwest European shelf region (centimetres). The three models that compare the best with tide gauge readings are indicated in supscript with 1,2 and 3 for each constituent.

LOADING COMPUTATIONS.

As to illustrate the impact of different ocean tide models on ocean tide loading estimates loading was calculated using more or less the "best" model - the Grenoble model, and the "worse" model for the Northwest European shelf region. Loading have been calculated using the wavenumber approach as described in Ray & Sanchez (1989) for the M_2 constituents of the above models. The Cartwright & Ray model has a resolution of 1.0 x 1.5 while the Grenoble model has a resolution of 0.5 x 0.5 . Amplitude differences was subsequently estimated by interpolating in the Grenoble model to the positions of the Cartwright & Ray grid points and the subtracting the Cartwright & Ray estimated loading from the Grenoble model estimated loading. The loading differences are shown in Figure 4. The range of differences ranges between -1.6 cm and 1.2 cm with some very large amplitudes in and around the Irish Sea and in the areas around the English Channel.

CONCLUSIONS.

Presently only the Andersen model combines high accuracy in the global open ocean including the Arctic Ocean with high accuracy in shelf regions which makes it the obvious choice for ocean tide loading calculations. If any of the other global ocean tide models are to be used, it is important carefully to chose different ocean tide models depending on the location of the calculation of the ocean tide loading.

For calculations in the north Atlantic ocean there is not doubt about that one should chose the Andersen or the Grenoble model due to the high resolution and accuracy when compared to tide gauges. These models compares favorable to the other coarser models based on T/P altimetry. It is also important to note, that the Grenoble model seems more questionably to use when calculating ocean tide loading in the Southern Atlantic, the Pacific and Indian Oceans, due so some basin-scale errors, that becomes present in the Grenoble model when compared to T/P derived models (Andersen et al., 1994).

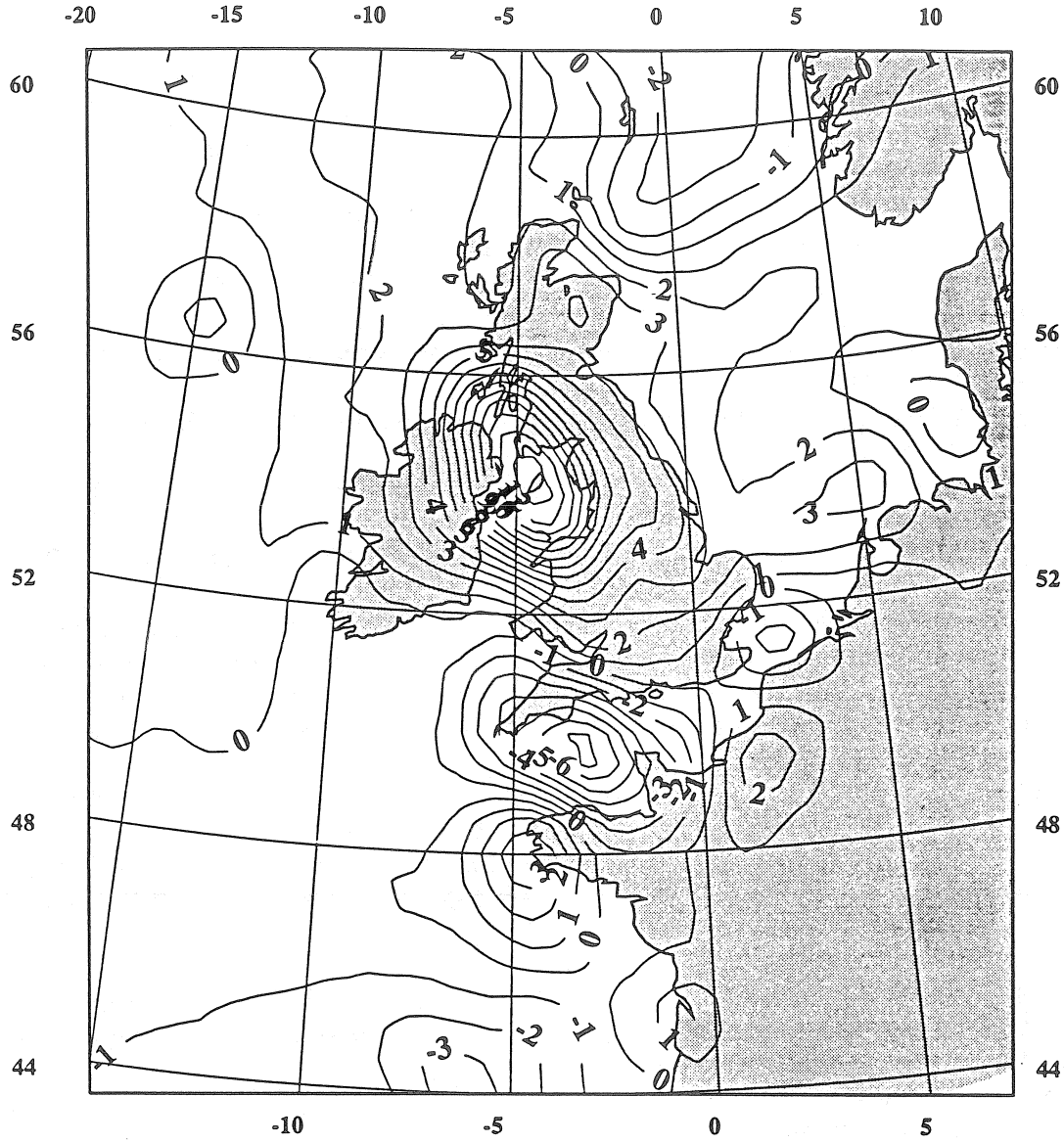

Figure 4. Loading differences using differenc ocean tide model. Differences are the Grenoble 1994 model minus the Cartwright & Ray 1991 model for the M_2 constituent. Contour interval is 1 mm.

In these regions the T/P derived model should be recommended. However it does not seem to be of major importance which T/P model that is chosen. In the deep ocean most T/P derived models compare on the centimeter level (Andersen et al., 1994), which would lead to insignificant differences in the calculation of ocean tide loading.

The impact on ocean tide loading calculations using different ocean tide models has been studied in the Northwest European shelf region. In this region differences between loading calculated with the Cartwright & Ray 1991 model and the Grenoble 1994 model reaches 2 centimeters which indicates the importance of these new models for ocean tide loading computations.

The general recommendation would therefor be to use the Andersen model, that has been corrected for the basin-scale errors present in the Grenoble model. It is also important to note that the Ocean tides for the Arctic Ocean seems to be much more accurate modelled in the Grenoble model (and therefor also in the Andersen model), than in the older model by Schwiderski. It should therefor be recommended to extend the limited ocean tide model derived from the T/P satellite using the Grenoble model outside the region covered by the T/P satellite when calculating ocean tide loading.

Acknowledgement. The authors are thankful to P. Vincent and all authors mentioned in this analysis for providing models at an early stage in the study over FTP. Thanks are also due to R. Ray (NASA Goddard) and the staff at POL for providing local models, loading grids and tide gauge data.

REFERENCES

Andersen, O.B.: Global Ocean Tides from ERS-1 and TOPEX/POSEIDON altimetry. In press *J. Geophys. Res.*, TOPEX/POSEIDON special issue 2, 1994.

Andersen, O.B., P. L. Woodworth and R. A. Flather: Intercomparisons of recent Ocean Tides Models. Submitted *J. Geophys. Res.*, TOPEX/POSEIDON special issue 2, 1994.

Canceill, P., R. Agelou and P. Vincent: Barotropic tides in the Mediterranean sea from a finite element numerical model, *J. Geophys Res.*, in press, 1994.

Cartwright, D. E.: Detection of tides from artificial satellites (Review). In Parker, B.B (Ed): *Tide Hydrodynamics*, 547-568, John Wiley, New York, 1991.

Cartwright, D. E. and R. D. Ray: Oceanic tides from Geosat Altimetry. *J. Geophys. Res.* 95 (C3), 3069-3090, 1990.

Cartwright, D. E. and R. D. Ray: Energetics of global ocean tides from Geosat altimetry, *J. Geophys. Res.*, 96, 16897-16912, 1991

Desai, S. D. & J. M. Wahr: Another Ocean tide model derived from TOPEX/POSEIDON altimetry, EOS, 75 (46), 57, 1994

Eanes, R. J.: Diurnal and semidiurnal tides from TOPEX/POSEIDON altimetry, EOS, 75(16), 108, 1994.

Egbert, G. D., A. F. Bennett and M. G. G. Foreman: TOPEX/POSEIDON Tides estimated using a global inverse model, In Press, *J. Geophys. Res.* TOPEX/POSEIDON special issue, 1994.

Flather, R. A.: Results from a model of the northeast Atlantic relating to the Norwegian Coastal Current. In R. Saetre and M. Mork (Eds): *The Norwegian Coastal Current.* Vol 2, 427-458, Bergen, Norway, 1981.

Flather, R. A.: A numerical model investigation of tides and diurnal-period continental shelf wave along Vancouver Island. *J. Phys. Oceanog., 18*, 115-139, 1988.

Genco, M. L.: *The tides in the Atlantic ocean: Modelisation and energetic budget* (In french). Ph.d thesis from the Joseph Fourier University, B.P. 53X - 38041 Grenoble CEDEX, France, 1993.

Glorioso, P. D. & R. A. Flather: A barotropic model of the currents off southeastern South America. Submitted to *J. Geophys Res.*, june, 1994

Knudsen, P.: Global Low Harmonic Degree Models of the Seasonal Variability and Residual Ocean Tides from TOPEX/POSEIDON altimeter data, In press *J. Geophys. Res*, TOPEX/-POSEIDON special issue I, 1994.

Pavlis, N. and B. Sanchez: Expansion of the worlds ocean tides in Proudman functions. In Press, *J. Geophys. Res.* TOPEX/POSEIDON special issue I, 1994.

Provost, C. Le, M. L. Genco, F. Lyard, P. Vincent, P. Canceil: Spectroscopy of the world ocean tides from a finite-element hydrodynamic model. In Press: *J. Geophys Res.* TOPEX/POSEIDON special issue. 1994

Ray, R. D. and B. Sanchez: Radial deformation of the Earth by oceanic tide loading, *NASA Tech. Memorandum, 100743*, Goddard Space Flight center, Greenbelt, Maryland, 1989.

Ray, R. D., B. Sanchez, and D. E. Cartwright: Some extensions to the response method of tide analysis applied to TOPEX/POSEIDON (abstract), *EOS, 75(16)* 108, 1994.

Schrama E.J.O., R. D. Ray; A preliminary tide analysis of TOPEX/POSEIDON altimetry, In Press, *J. Geophys. Res.* TOPEX/POSEIDON special issue, 1994.

Schwiderski, E. W.: Ocean Tides, Part 1: Global Ocean Tide Equations. *Marine Geodesy,* Vol 3, 161 - 217, 1980a.

Schwiderski, E. W.: Ocean Tides, Part 2: A Hydrodynamical interpolations model. *Marine Geodesy,* Vol 3, 218 - 257, 1980b.

Smithson, M. J.: *Pelagic Tide Constants 3*, IAPSO Publication Scientifique No 35, Published by IAPSO, 1992.

Wagner, C. A.: How well do we know deep ocean tides ? - An intercomparison of altimetric, hydrodynamic and gage data. *Manus Geod., 16*, 118-140, 1991.

Woodworth, P. L. and J. P. Thomas: Determination of the Major Semidiurnal Tides of the Northwest European Continental Shelf from Geosat Altimetry. *J. Geophys. Res.*, 95 (C3), 3061-3068, 1990.

Validation of ocean tide models by comparison to gravity loading measurements

O. Francis

Observatoire Royal de Belgique, Avenue Circulaire 3, B-1180 Bruxelles, Belgique
E-mail: francis@astro.oma.be

Introduction

Thanks to the TOPEX/POSEIDON satellite mission, a lot of new ocean tide models are now available. They are claimed to be superior to the Schwiderski model (1980) on the basis of a comparison with 95 selected tides gauges. The Earth Tides community found one's hopes on these new ocean models for improving the loading computations. Nevertheless, most of the new models are not well suited to loading computations because they do not cover the whole oceans and generally they are less reliable over the continental shelves due to the non-linearity of the tides in these areas.

In this short note, we compare the loading computations from two new global ocean tide models with those computed with the Schwiderski model which had been adopted by the Earth Tides community as the working standards. We used the pure hydrodynamic model of Le Provost et al. (1994) so-called the Grenoble model and the adjusted Grenoble model by Andersen (1994) which is an optimal combination of the Grenoble model and TOPEX/POSEIDON altimeter data. As these new models are still subject to improvement, only preliminary versions are available. A main new feature of these models favourable for loading computations is that their resolution is 0.5°x0.5° instead of 1°x1° for the Schwiderski model.

A more detailed comparison with more new ocean tide models will be presented at the IUGG General Assembly in Boulder by Llubes et al. (1995).

Mass conservation.

One of the main grievance of the people concerned by the gravity loading computation against the ocean tide models lies in the fact that they do not generally conserve the mass (Francis, 1992). From Table 1, it is comforting to note that the tidal mass is better conserved in the new models. We can also observe that the models have not only a higher resolution but also they cover more and more oceanic area. For instance, the Andersen includes the Mediterranean. The mean amplitude for the M2 wave is practically unchanged from one model to the other.

In the rest of the computation, I have applied a correction for mass conservation proportional to the tidal amplitude.

Loading computations

In order to calculate the gravity loading effect, the well-known Farrell's method has been used. It consists in evaluating numerically the following convolution integral over the oceans with a kernel, so-called Green's function, which is the response of the earth to a point-like mass load:

$$L(\phi,\lambda) = \rho_w \iint_{oceans} G(\phi,\lambda;\phi',\lambda')\, h(\phi',\lambda')\, dS'$$

where L is the gravity loading effect at the geographical location (ϕ,λ), ρ_w is the mean density of the sea water, G the Green's function for the gravitational effect of the load, h ocean tide vector and dS' the surface area. We used the Green's function for an elastic earth using PREM tabulated in Francis and Dehant (1987).

The observed tidal gravity parameters have been taken from the ICET Data Bank containing 352 permanent and temporary stations all around the world which have been recently revised by Melchior (1994). The time series have been analysed using a standard least square adjustment with Venedikov filters. A computed earth model giving the response of the earth to the luni-solar potential is then subtracted from these observations giving the first residue vector $\mathbb{B}(B,\beta)$ (I use the notation introduced in several papers by Melchior). This vector $\mathbb{B}$ contains mainly the oceanic tides contribution to gravity variations. The vector $L(L,\lambda)$ is the oceanic load vector as calculated from co-range and co-tidal maps. The difference $\mathbb{B}$-L gives the final residue vector which is the observation noise plus non-modelled contribution.

Comparison between observed residual vector $\mathbb{B}$ and oceanic tidal load L

The coastal stations (distance to the sea less than 10 km) have been discarded because there is disagreement in the computed load vectors when using algorithms from different authors due to the different way of discretizing the convolution integral. My present goal consists in assessing the difference in the ocean tide models and not in the difference in the loading computations in areas where this estimation of the loading is still problematic. I then retain 281 continental tidal gravity stations whose locations are shown in Figure 1.

To compare the observed residual vectors $\mathbb{B}$ with the computed tidal loading vectors L, their cosine and sine components for the M_2 wave are plotted on the same graphs (Figures 2 A-B). The best fit lines are then estimated with the constant values a, the slopes b and the associated mean-square errors (Table 2). The slopes are always higher or equal to 1 for the Grenoble and Andersen models and always lower than 1 for the Schwiderski model. The slope of the sine component for the Grenoble model and of the cosine component for the Andersen model is nearly 1 but this nice correlation is not preserved on the other component. Moreover, I do not observe significant changes in the correlation coefficients which is better for the sine component for all the models as observed previously. The mean-square errors are nearly the same for the cosine components being of the order of 0.56 microgal whereas the mean square errors for the sine components are of the order of 0.35 microgal for the new models i.e. 0.1 microgal less than for the Schwiderski model.

Final Residues X

Histograms of the cosine and sine components for the residual vectors X are shown in Figures 3 A-B. The Gaussian-like distributions of the residues for the new models are clearly shifted with respect to those calculated with the Schwiderski model. Looking at the standard deviation (Table 3), we observe that there is no improvement

for the cosine component whereas for the sine component there is a decrease from 0.7 microgal for the Schwiderski model to 0.6 microgal for the Grenoble and the Andersen models. Nevertheless, there is an anomaly for these models related to the fact that the maxima of the Gaussian-like distributions do not correspond to the average values.

Conclusion

The tidal gravity measurements from the ICET Data Bank contain 'integrated' information on the ocean tides which is independent of the models and then useful for their validation. This work shows slight improvement on gravity loading computations owing to the new global ocean tide models of Grenoble and Andersen: only the standard deviation of the sine component of final residues X for the M_2 wave is slightly reduced. We hoped to improve both components. Before going into further investigations, we will wait for updated solutions of the ocean tide models which should be available soon.

Acknowledgements

I am grateful to Lyard of the Grenoble team and to Andersen for providing me with their ocean tide models. Thanks are also due to Prof. Melchior for reading the manuscript.

References

Andersen, O.B., New Ocean Tide Models for Loading Computations, Bull. Inf. Mar. Terr., this issue, 1995.

Francis, O., Interactions between Earth and Ocean Tides, Bull. Inf. Marées Terrestres, 122, 8131-8144, 1992.

Francis O. and Mazzega P., Global charts of ocean tide loading effects, Journal of Geophysical Research, 95(C7), 11411-11424, 1990.

Le Provost, C. , M.L. Genco, F. Lyard, P. Vincent and P. Canceill, Spectroscopy of the world ocean tides from a finite element hydrodynamical model, J. Geophys. Res., Vol 99, N0. C12, 24777-24797, 1994.

Llubes M., P. Melchior, O. Francis and P. Mazzega, TOPEX/POSEIDON Ocean Tide Models as Compared to the ICET Gravity Data Bank, in preparation, 1995.

Melchior, P., A New data bank for tidal gravity measurements (DB92), Phys. Earth Planet. Inter., 82, 125-155, 1994.

Schwiderski, E.W., Ocean Tides, I, Global ocean tidal equations, Mar. Geod., 3, 161-217, 1980a.

Schwiderski, E.W., Ocean Tides, II; A hydrodynamical interpolation model, Mar. Geod., 3, 219-255, 1980b.

Table 1: Some statistics on the ocean tide models used in this study for the M_2 Wave.

Parameter	Schwiderski	Grenoble	Andersen
Number of grid points	41236	170497	171504
Total surface (m^2)	$3.50\ 10^{+14}$	$3.57\ 10^{+14}$	$3.59\ 10^{+14}$
Mean amplitude (cm)	32.6	33.1	33.2
Residual amplitude (cm)	0.73	0.38	0.07
Ratio Residual /Mean Amplitude	2.2%	1.1%	0.2%

Table 2: Coefficients of the best fit lines ($y = a + b\ x$) between observed and computed gravity loading and attraction effects for the M_2 wave.

Parameter	Schwiderski	Grenoble	Andersen
Cosine component			
a (microgal)	-0.03	+0.03	+0.05
b	0.99	1.09	1.00
correlation coefficient	0.71	0.69	0.71
Mean-square error (microgal)	0.56	0.59	0.55
Sine component			
a (microgal)	-0.16	-0.21	-0.22
b	0.95	1.00	1.06
correlation coefficient	0.91	0.91	0.91
Mean-square error	0.49	0.35	0.36

Table 3: Estimated parameters for the histograms of Figures 3.

Parameter	Schwiderski		Grenoble		Andersen	
	Cosine	Sine	Cosine	Sine	Cosine	Sine
Average (microgal)	-0.04	-0.22	-0.08	-0.21	0.05	-0.15
Standard deviation (microgal)	0.75	0.71	0.77	0.59	0.74	0.61
Mimimun value (microgal)	-2.68	-6.27	-3.41	-2.70	-3.24	-2.98
Maximun value (microgal)	4.06	1.74	4.54	2.05	3.85	2.17

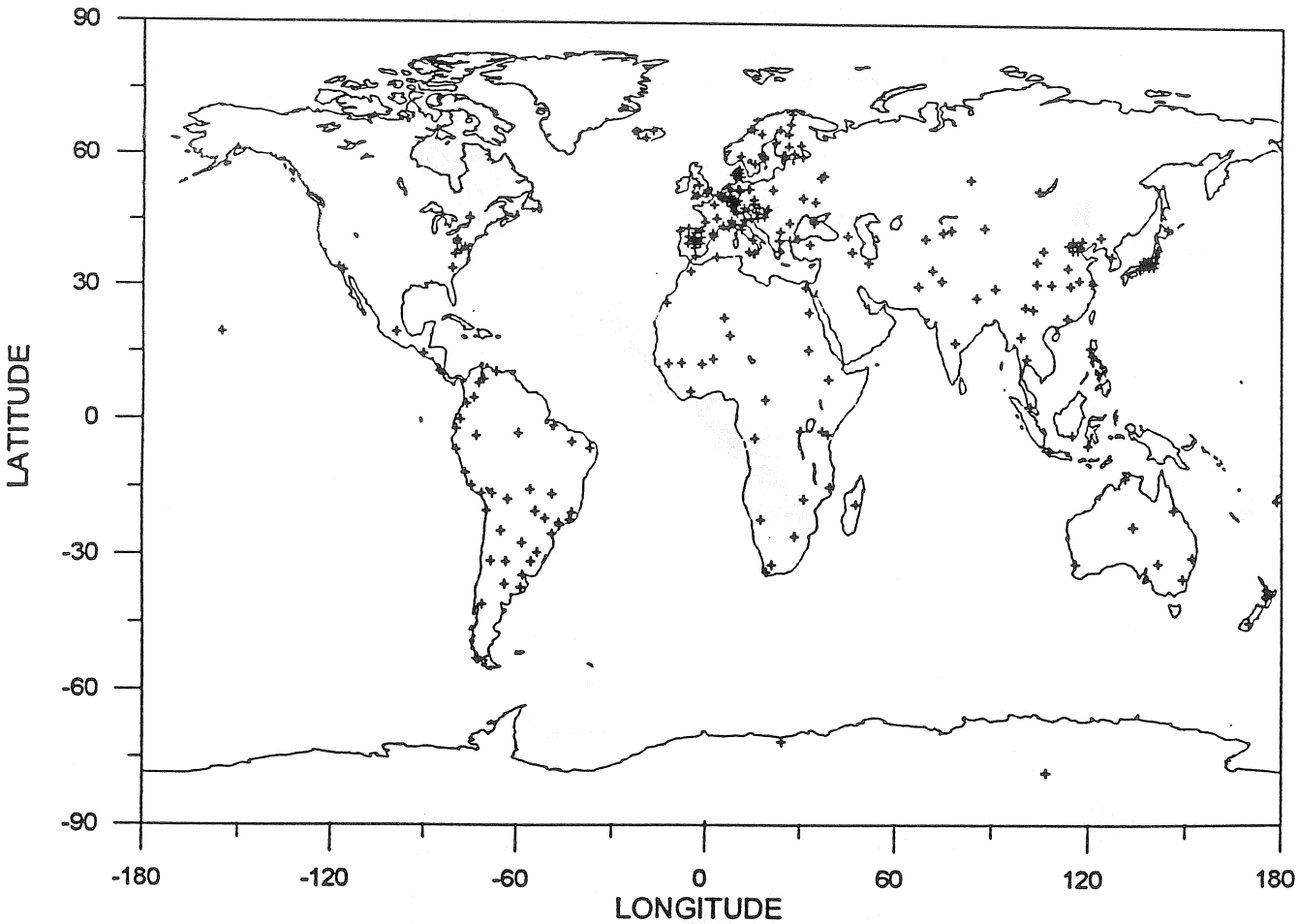

Figure 1: Location of the 281 tidal gravity stations of the ICET Data Bank used for comparison between observed and computed gravity loading effects.

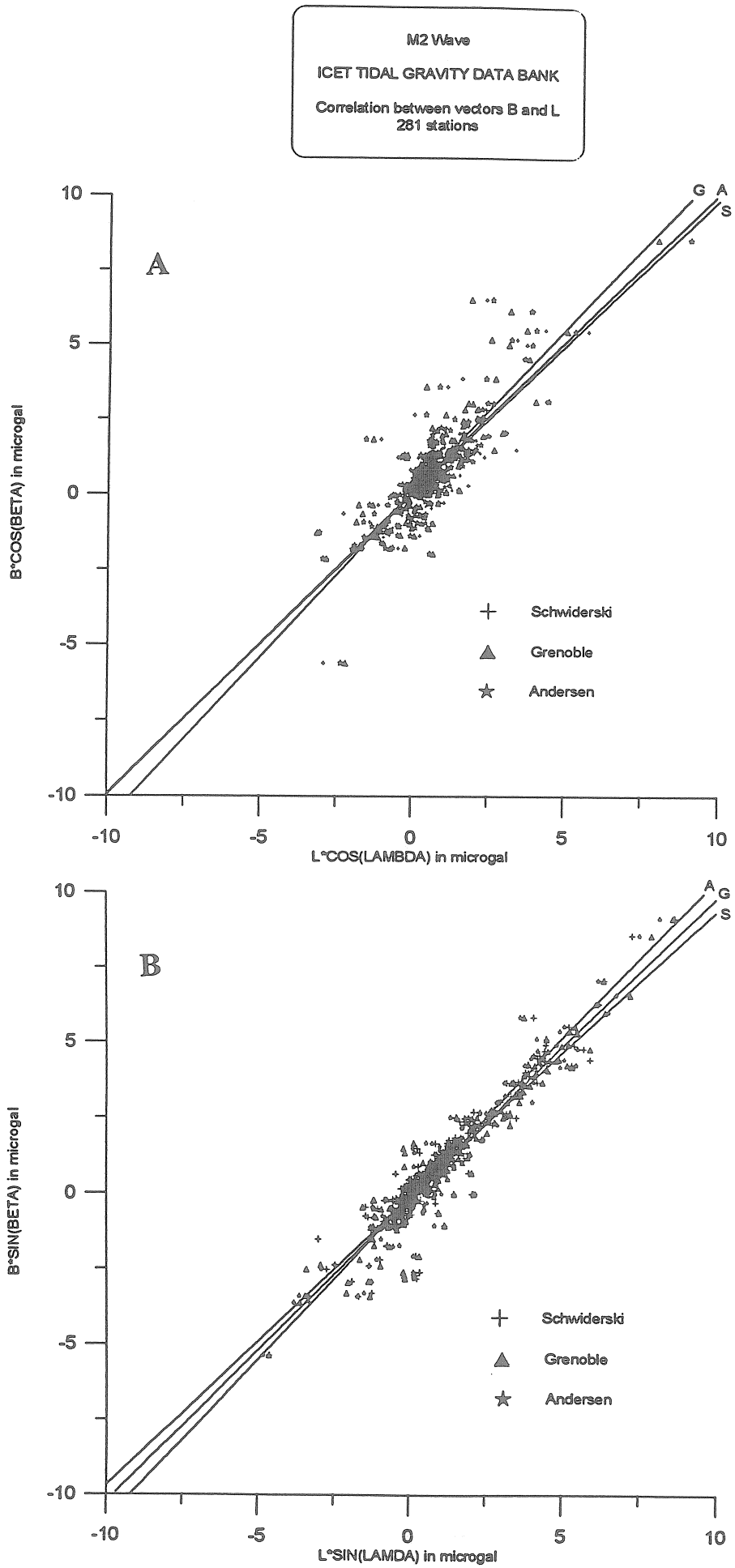

Figures 2: Comparison between observed residual vectors B and computed oceanic loading vectors L for the M_2 wave. (A) Cosine component, (B) Sine component.

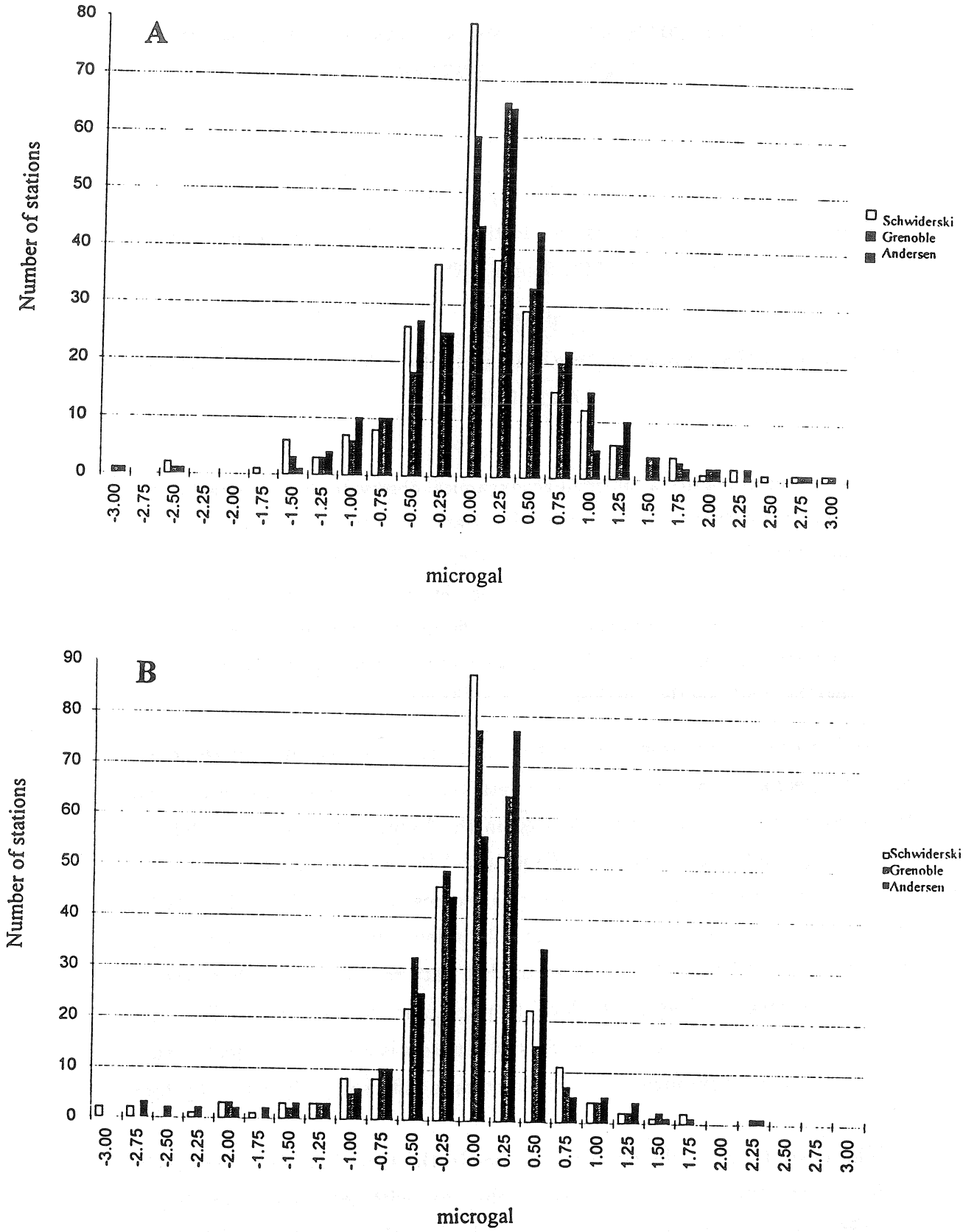

Figures 3: Histograms of the final residues X for the M_2 wave. (A) Cosine component, (B) Sine component.

HORIZONTAL DEFORMATIONS RECORDED WITH THE EXTENSOMETERS

P. Varga
Geodetic and Geophysical Research Institute of the Hungarian Academy of Sciences, H-9401 Sopron, POB 5, Hungary

T. Varga
Eötvös Loránd Geophysical Institute of Hungary, H-1145 Budapest, Columbus u. 17–23, Hungary

Results obtained at different geodynamical observatories with quartz tube extensometers in the Pannonian Basin are shown. Deformation data recorded with strainmeters are useful in seismology, in earth tide research and they can be used for the intepretation of recent tectonics in local and possibly in regional scale. It was found that local extensometric observations can be used in interpretation of recent geological processes together with another methods of earth sciences.

High precision extensometric (strain) data are in use recently for the study of recent geological processes. A more detailed description of this subject authors summarised in a paper published in the Volume 29, No. 1-2 (1994) of the Acta Geodetica et Geophysica Hungarica (*Varga et al.*, 1994).

High precision strainmeters have relative resolution $10^{-9} - 10^{-11}$ (what means an absolute resolution in case of a 20 m long extensometer ($10^{-2} - 10^{-4}$ micron). It must be mentioned however that data recorded with these instruments are strongly influenced by local (topographic, cavity) effects. Therefore the interpretation of data recorded by strainmeters is a very complicated task, because each site equipped with strainmeters is differently disturbed by local effects.

The importance of the strainmeters lies in the fact that phenomena with periods from some 10 s to years can be observed with them corresponding to the wide spectrum of movements taking place in the solid Earth (Table 1). Therefore it can be concluded that the strainmeters connect the frequency bands of seismic waves and of phenomena studied usually by means of geodetic methods. It worth to mention — even if according to authors knowledge it has not been studied in detail earlier — that the amplification of the extensometers at different frequencies is practically constant. With this prominent feature these devices stand alone within the instruments used in geodesy and geophysics.

Table 1. Geodynamical phenomena of the Earth

Type of phenomena	Period (in s)	Relative strain
Waves of distant earthquakes	10^{-1}–10^{-2}	10^{-6}–10^{-9}
Microseisms	1–20	10^{-9}–10^{-11}
Free oscillations	10^{2}–10^{3}	10^{-8}–10^{-11}
Tides	$2 \cdot 10^{4}$–$1 \cdot 10^{6}$	10^{-7}–10^{-8}
Seasonal processes (meteo – and hydrogeological)	$3 \cdot 10^{7}$	10^{-5}–10^{-7}
Annual variation of axial rotation speed	$3 \cdot 10^{7}$	10^{-9}–10^{-10}
Annual speed of tectonic phenomena	$3 \cdot 10^{7}$	10^{-5}–10^{-7}

From the visual point of view the most characteristic phenomena on strainmeter records are the earth tides. The diurnal and semidiurnal waves can be detected with a signal to noise ratio 10 or higher and the phase delay of the tidal waves can be obtained with a considerable accuracy too. Another conspicuous phenomenon on the strain records are the earthquakes. Of course, with extensometers only long-periodic seismic waves can be recorded but the accuracy of these part of the seismic spectrum can be recorded with high accuracy comparable with the resolution and reliability of the very broad band seismographs (*Varga et al.*, 1994).

At the stations of the Pannonian Basin quartz tube rod extensometers were used, the basic idea of which was developed at the Shmidt Institute of Earth Physics of the Russian Academy of Sciences, Moscow (*Latynina et al.*, 1978). To increase the sensitivity a specially high quality capacitive transducer system was constructed in the Geodetic and Geophysical Research Institute, Sopron (*Mentes*, 1981) which is able to work for long time in sites with extremely high humidity. For the strainmeters suspended on stainless wire silica glass tubes of 45 mm diameter and 2–3 mm thickness were used (with a linear thermal extension coefficient $0.45 \cdot 10^{-6}$). The length of the individual tube pieces are (2.0–2.5) m. The suspended quartz rod is held by supports with levelling screws. The quartz tubes assembled by means of adhesive and invar profile pieces (linear thermal expension coefficient $0.7 \cdot 10^{-6}$).

The fixed end of the extensometer is connected to the rock by a metallic rod which adjoined to the quartz tube by a magnetostrictive calibration unit which allows a calibration accuracy better as 5 percent. In order to reach high accuracy and resolution optical and capacitve sensors were used simultaneously in the first working period. Both transducers were installed at the free end of the extensometer system and show excellent agreement (*Latynina et al*, 1984, *Mentes*, 1991).

The displacement at the free and of the measuring system can be recorded with an resolving power which enables observations with an relative sensitivity of $10^{-10} - 10^{-11}$ if the external — natural and artificial – noise conditions are favourable. A study of the calibrating unit showed that the scale value of the record can be determined with an inner accuracy of 1.5 percent at the stability of 1.0 percent of the calibration current.

A detailed study of the mechanical part was given by *Latynina et al.* (1978), who concluded:

- forces hampering the free motion of the quartz rod espcially dangerous when the fitting of the individual tubes is not perfect
- forces acting again the motion of the rod at the suspension wires are proportional to the strain and they take not important role in the work of the instrument
- elastic deformations of the quartz tubes are not significant.

The extensometric network consists at this time 4 stations and 6 strainmeters. The Budapest Geodynamical Observatory is situated in a cave formed in limestone. There are two strainmeters at a distance 30–35 m both from the entrance and from the surface. The Sopron Geodynamical Observatory is in West-Hungary in an artificial tunnel driven in gneiss. The distance of the extensometer from the entrance is about 30 m, the overlaying of the gallery is 60 m thick. Station Beregovo (Ukraine) (*Latynina et al.*, 1992) is 10 km of Beregovo in a tunnel driven in tuff. Station Vyhné (Slovakia) (*Brimich et al.*, 1988) is a gallery driven in granite. The instrument is installed 130 m from the entrance.

The main parameters of the above listed stations and instruments can be found in Table 2.

Table 2. Quartz tube extensometric stations in the Pannonian Basin

Station	Latitutde	Longitude	Azimuth	Length of the instrument (in m)	Reference
Beregovo I	48.2°	22.7°	73°	27.5	Latynina et al., 1992
Beregovo II	48.2°	22.7°	37°	11.4	Latynina et al., 1992
Vyhné	48.5°	18.5°	55°	20.5	Brimich et al., 1988
Budapest I	47.6°	19.0°	114°	21.3	Varga et al., 1991
Budapest II	47.6°	19.0°	38°	13.8	Varga et al., 1993
Sopron	47.7°	16.5°	116°	22.0	Mentes, 1993

The network of extensometers were installed during the eighties. In case of all six strainmeters hourly values expressed in micrometer were used. The scale of the record was determined on the basis of the magnetostrictive calibration device mounted into each instrument. The intercalibration of the individual strainmeters using the calibration device developed by *Mentes* (1993) is the task of the nearest future.

It should be mentioned that during the studied time intervals there were no important changes in the recording conditions.

From long-periodic variations y are mainly composed from a quasi-annual component and from a monotonous, almost linear component and they can be modelled as

$$y = a + b \cdot t + c\sin(\omega t + e)\,,$$

where a, b, c and e are the arbitrary constants to be determined, t is the time in hours, ω is the circular frequency (i.e $\omega = \frac{2\pi}{T}$; $T = 8766$ hours $= 1$ year). b is the "secular" strain partly related to tectonic activity, c is the amplitude of the annual wave and e describes the phase shift between the observed and astronomical annual wave. All these data are collected together in Table 3.

Table 3. Long-periodic (secular) and yearly variations of the strainmeters

Station	Epoch	Annual drift in micron $\cdot y^{-1}$ (and in relative units $\cdot y^{-1}$)	Annual wave's amplitude (microns) (and in relative unit)	Phase shift in y
Beregovo	1986–1991	-4.27 $(-1.55 \cdot 10^{-7})$	13.90 $(5.05 \cdot 10^{-7})$	0.26
Beregovo II	1986–1991	27.56 $(-2.41 \cdot 10^{-6})$	4.35 $(3.82 \cdot 10^{-7})$	0.26
Vyhné	1984 – 1987 1989 – 1991	-0.90 $(4.39 \cdot 10^{-8})$	0.45 $(2.10 \cdot 10^{-8})$	0.32
Budapest I	1990–1992	-1.69 $(7.93 \cdot 10^{-8})$	10.4 $(4.88 \cdot 10^{-7})$	0.36
Budapest II	1990–1992	-31.42 $(-2.27 \cdot 10^{-6})$	1.2 $(8.69 \cdot 10^{-8})$	0.26
Sopron	1991–1993	1.51 $(6.81 \cdot 10^{-8})$	0.4 $(1.82 \cdot 10^{-8})$	0.12

It can be concluded on the basis of Table 3, that:

- phase values are of about 0.3 years. Only exception is Sopron with his 0.12 year phase shift.

- The annual drifts are somewhat bigger as 10^{-7} the values which can be connected to tectonical origin (*Agnew*, 1986) but even this data are not bigger as the mean annual drift in planetary scale obtained by *Varga* (1984) as $2.1 \cdot 10^{-6}$ y^{-1} for 28 stations.

- From strainmeter measurements the corresponding stress rates are $6(10^4 - 10)$ Pa much smaller as *Becker* (1993) obtained from in situ stress measurements (*Varga et al.*, 1994).

References

Agnew D C, 1986: Reviews of Geophysics, 29, No. 3, 579-624.

Brimich L, Latynina L A, 1988: J. Phys. Earth, No. 12, 3-9 (in Russian)

Latynina L A, Karmaleeva R M, 1978: Deformografic measurements. Nauka, Moscow (in Russian)

Latynina L A, Szabó Gy, Varga P, 1984: Acta Geod. Geoph. Mont. Hung., 19, 197-205.

Latynina L A, Jurkevics O I, Bajsarovits I M, 1992: Geoph. J., 12, No. 2, 63-67.

Mentes Gy, 1981: Acta Geod. Geoph. Mont. Hung., 16, 269-280.

Mentes Gy, 1991: Mareés Terrestres, Bull. d'Information, 110, 7936-7939.

Mentes Gy, 1993: Mareés Terrestres, Bull. d'Information, 115, 8467-8471.

Varga T, Latynina L A, Brimich L, Mentes Gy, Katona Gy, Varga P, 1993: Mareés Terrestres, Bull. d'Information, 116, 8537-8545.

Varga P, Varga T, 1994: Recent horizontal deformation of the Pannonian Basin measured with extensometers. Acta Geod. Geoph. Hung., 29 (in print)